



Norwegian University of  
Science and Technology

# Load Deflection Characteristics of Guide Vane End Seals

**Hans Kristian Hofsrud**

Mechanical Engineering

Submission date: June 2017

Supervisor: Bjørn Haugen, MTP

Norwegian University of Science and Technology  
Department of Mechanical and Industrial Engineering



# Abstract

This Master Thesis consider the load deflection characteristics of end seals incorporated in guide vanes used in hydropower turbines. The force response of the end seals is critical in order to prevent leakage and thus increase the efficiency of the turbine. The guide vanes is located in front of the turbine runner in order to regulate the flow of water. At present time, either one or two O-rings, cut into mouldings, is used as these aforementioned end seals. Rainpower, which have proposed this master thesis only have a selection of experimental measurements of the load characteristics for a limited amount of geometries and material parameters of the end seals.

By use of two dimensional modelling and Finite Element Analysis focusing on groove tolerances, cross-sectional dimensions, and material properties, a parameter study of situations including both one and two sealing elements is assessed. ABAQUS 6.14-1 is used for construction of two dimensional models and conducting Finite Element Analysis of the sealing elements. Interaction properties such as contact algorithm and frictional behaviour are taken into consideration. In addition, procedure notes, additional results, proposed test data guide lines for experimental material testing of elastomers and early model development is presented in appendices.

It was concluded that; using a linear-elastic material approach is sufficient to recreate the trends of the material behaviour in highly confined environments. Several load deflection curves were carried out and compared, the results indicated distinctive material trends depending on the aforementioned factors. However, experimental test data of different material batches are required to implement numerical analysis with hyperelastic properties in ABAQUS. Relevant theory, methodology and results is considered in addition to evaluation and discussion of results. Recommendations for any further work have also been proposed.





# Sammendrag

Denne masteroppgaven er utarbeidet med hensyn på å vurdere belastningsegenskapene til endetetningene som er plassert i ledeskovelene foran vannkraftturbiner. Kraftsresponsen endetetningene er kritisk i forhold til å kunne forhindre lekkasje og dermed øke effektiviteten til turbinen. Ledeskovlene er plassert foran turbinens løpehjul for å regulere strømmen av vann inn på hjulet. Per dags dato brukes enten én eller to O-ringer, kuttet som lister, til endetetninger. Rainpower, som har kommet opp med denne masteroppgaven, har kun et lite utvalg av eksperimentelle målinger av belastningsegenskapene for en begrenset mengde av geometriske og materielle parametere i endetetningene.

Ved bruk av todimensjonal modellering og elementanalyse med fokus på sporstoleranser, tverrsnittsdimensjoner og materialeegenskaper, er det utarbeidet en parameterstudie av situasjoner som inkluderer både én og to tetningselementer. Programvaren ABAQUS 6.14-1 er brukt til konstruksjon av todimensjonale modeller og analysering av tetningene. Kontaktegenskaper som kontaktalgoritme og friksjonsoppførsel er tatt med i betraktning. I tillegg er prosedyrenotater, tilleggsresultater, testveiledning for eksperimentell materialtesting av elastomerer og tidlig modellutvikling presentert i vedlegg.

Opgaven konkluderer med at; ved hjelp av en lineær-elastisk materialtilnærming er det mulig å gjenskape trendene i kraftresponsen til materialet i svært begrensede omgivelser. Forskellige belastingskurver er utarbeidet og sammenlignet. Avhengig av de ovennevnte faktorene som eksempelvis antall tetningselementer gir resultatene ulike materialtrender. Det konkluderes videre med at eksperimentelle testdata av forskjellige materialprøver er nødvendig for å implementere numerisk analyse med hyperelastiske materialeegenskaper i ABAQUS. Relevant teori, metodikk og resultater vurderes i tillegg til evaluering og diskusjon av resultater. Anbefalinger til videre arbeid er også foreslått.



# Acknowledgements

This master thesis would not have been possible without the support and guidance from my academic supervisor. I would like to thank Associated Professor Bjørn Haugen, my supervisor at NTNU and PhD candidate Petter Østby at Rainpower for their guidance.

I would like to acknowledge the suggestions, discussions and feedback provided by Trelleborg Sealing Solutions and Ebbe Smith, PLM Technology. I would also like to thank my friend Álvaro Fernández for spending a valuable amount of time helping with preparation of the report.

Finally, I would like to thank all my friends and family for their accompanying and help during my two years taking master degree.

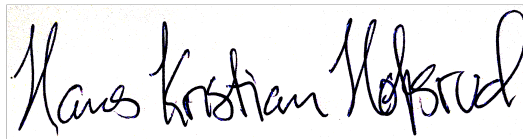


# Preface

This master thesis is submitted in partial fulfilment of the requirements for the degree of Master of Science (MSc) at the Norwegian University of Science and Technology (NTNU). The work has been performed at the Department of Mechanical and Industrial Engineering (MTP), NTNU, Trondheim, during the spring semester of 2017 with Associate Professor Bjørn Haugen as main supervisor.

No preliminary work was carried out during fall semester of 2016. The author of this master thesis had unfavorable prerequisites in relation to what is desirable, this was due to the choice of writing project thesis within product development. However, this turned out to be less interesting than expected. Fortunately, there was an opportunity writing this master thesis. Despite a low level of prerequisites in terms of minimal experience using ABAQUS, and missing opportunity to attend the course, TMM4250 - Advanced Product Simulation (which would have been preferable) during the fall semester, the choice of writing another master thesis has been satisfying. This master thesis has been very interesting, but also very frustrating at times. Learning ABAQUS demands considerable time, conducting non-linear analyses requires an important amount of expertise and a careful understanding of what you want to accomplish and also a awareness of the analysis capabilities of the software at use. In the end the learning curve has been very steep and the final results satisfy the objective.

Trondheim, 2017-06-11

A handwritten signature in black ink, reading "Hans Kristian Hofsrud". The signature is written in a cursive style with a large initial 'H' and 'K'.

Hans Kristian Hofsrud

# Contents

<b>Abstract</b>	<b>i</b>
<b>Sammendrag</b>	<b>iii</b>
<b>Acknowledgements</b>	<b>v</b>
<b>Preface</b>	<b>vii</b>
<b>List of Figures</b>	<b>xiv</b>
<b>List of Tables</b>	<b>xv</b>
<b>List of Equations</b>	<b>xvi</b>
<b>Abbrevations</b>	<b>xvii</b>
<b>1 Introduction</b>	<b>1</b>
1.1 Background . . . . .	1
1.2 Problem description . . . . .	2
1.3 Problem scope . . . . .	2
1.3.1 Objectives . . . . .	2
1.3.2 Limitations . . . . .	3
1.3.3 Outline . . . . .	3
<b>2 Theoretical background</b>	<b>5</b>
2.1 Hydropower turbines . . . . .	5
2.1.1 Turbines . . . . .	5
2.1.2 Guide vanes . . . . .	7
2.2 The O-ring as sealing element . . . . .	8
2.3 Material . . . . .	9
2.3.1 Elastomers . . . . .	9
2.3.2 Material Behaviour . . . . .	12
2.3.3 Viscoelastic behaviour of Nitrile Butadiene Rubber . . . . .	13
2.3.4 Poisson 's Ratio . . . . .	15

2.4	Tribology of Elastomers . . . . .	15
2.4.1	Friction . . . . .	16
2.5	FEM Analysis . . . . .	16
2.5.1	Implicit and Explicit methods . . . . .	18
2.5.2	Contact algorithms . . . . .	20
2.5.3	Plane stress and plane strain . . . . .	23
<b>3</b>	<b>Methodology</b>	<b>25</b>
3.1	Finite Element Analysis configuration . . . . .	26
3.1.1	Modelling . . . . .	27
3.2	Implicit or Explicit analysis . . . . .	29
3.3	Contact and Interaction . . . . .	30
3.3.1	General contact . . . . .	30
3.3.2	Contact pair algorithm . . . . .	31
3.3.3	Hard contact . . . . .	31
3.3.4	Subsequent steps . . . . .	32
3.3.5	Friction . . . . .	32
3.4	Boundary conditions . . . . .	34
3.4.1	Amplitude . . . . .	36
3.5	Material Approach . . . . .	36
3.6	Mesh and elements . . . . .	38
3.7	Final models . . . . .	40
3.7.1	One O-ring . . . . .	40
3.7.2	Two O-rings . . . . .	42
3.8	Triangular Groove . . . . .	44
3.8.1	Numerical calculations . . . . .	44
3.8.2	Analytical calculations . . . . .	45
<b>4</b>	<b>Results</b>	<b>49</b>
4.1	Description . . . . .	50
4.2	Experimental test result . . . . .	51
4.3	One O-ring results . . . . .	53
4.3.1	One O-ring compared to experimental tests . . . . .	54
4.4	Two O-rings results . . . . .	57
4.4.1	Two sealing elements compared to experimental tests . . . . .	58
4.5	Comparison of curves . . . . .	60
4.5.1	Groove dimensions comparison . . . . .	60
4.5.2	Material hardness comparison . . . . .	62
4.5.3	Cross-sectional diameter compared - One seal . . . . .	64
4.5.4	Cross-sectional diameter compared - Two seals . . . . .	66

4.5.5	One ring compared to two rings . . . . .	68
4.6	Hysteresis . . . . .	72
4.6.1	Groove too small . . . . .	72
4.6.2	Groove tangential . . . . .	73
4.6.3	Groove too wide . . . . .	74
4.7	Three positions . . . . .	75
4.7.1	Hysteresis . . . . .	76
4.7.2	Slip through . . . . .	80
4.8	Triangular groove . . . . .	83
4.8.1	Analytical results . . . . .	83
4.8.2	Numerical results . . . . .	84
<b>5</b>	<b>Discussion</b>	<b>85</b>
5.1	Analysis configuration . . . . .	85
5.1.1	Equilibrium solver . . . . .	85
5.1.2	Early attempts . . . . .	86
5.1.3	Material approach considerations . . . . .	86
5.1.4	Plane stress and plane strain . . . . .	87
5.1.5	Influence of Poisson ´s Ratio . . . . .	89
5.1.6	Mesh comparison . . . . .	90
5.2	Interactions . . . . .	92
5.2.1	Contact algorithm . . . . .	92
5.2.2	Friction . . . . .	93
5.3	Assessment of experimental tests . . . . .	95
5.4	Assesment of results . . . . .	96
5.4.1	Comparison curves . . . . .	96
5.4.2	Material . . . . .	97
5.4.3	Slip through . . . . .	99
5.4.4	Hysteresis loops . . . . .	100
5.4.5	Triangular groove . . . . .	100
<b>6</b>	<b>Concluding remarks</b>	<b>103</b>
<b>7</b>	<b>Recommendations for Further work</b>	<b>105</b>
	<b>Litterature</b>	<b>110</b>
	<b>Appendix</b>	<b>111</b>
<b>A</b>	<b>Technical description of guide vanes end seals</b>	<b>A-1</b>



## CONTENTS

---

<b>B</b>	<b>Original experimental tests sheet</b>	<b>B-1</b>
<b>C</b>	<b>Procedure notes</b>	<b>C-1</b>
<b>D</b>	<b>Dassault Systèmes - ABAQUS 6.14-1</b>	<b>D-1</b>
<b>E</b>	<b>Stress and strain</b>	<b>E-1</b>
<b>F</b>	<b>Material</b>	<b>F-1</b>
<b>G</b>	<b>Experimental tests</b>	<b>G-1</b>
<b>H</b>	<b>Implicit results</b>	<b>H-1</b>
<b>I</b>	<b>Plane strain results</b>	<b>I-1</b>
<b>J</b>	<b>Plane stress results</b>	<b>J-1</b>
<b>K</b>	<b>Model development</b>	<b>K-1</b>
<b>L</b>	<b>Risk analysis</b>	<b>L-1</b>

# List of Figures

- 1.1 Guide vane [29] . . . . . 1
- 2.1 Francis turbine . . . . . 6
- 2.2 Guide vanes [29] . . . . . 7
- 2.3 O-rings incorporated in sealing groove [44] . . . . . 9
- 2.4 Stress-Strain curve for NBR 70A [38] . . . . . 11
- 2.5 Stress-Strain curve for a typical linear-elastic material . . . . . 12
- 2.6 Linear FEA and Non-Linear FEA regions . . . . . 17
- 2.7 Implicit or Explicit depending on simulation [31] . . . . . 19
- 2.8 Six element bar[11] . . . . . 20
- 2.9 Fictitious bar, element 7 is introduced with axial stiffness,  $\omega$ . [12] . . . . . 21
- 2.10 Introducing force pair  $(-\lambda, \lambda)$  [12] . . . . . 22
- 2.11 Default penalty stiffness and scaled penalty stiffness [20] . . . . . 22
- 3.1 Circular area equal to rectangular groove area . . . . . 27
- 3.2 Wire part definition . . . . . 28
- 3.3 O-ring part definition . . . . . 28
- 3.4 Dimensions . . . . . 29
- 3.5 General contact definition [20] . . . . . 30
- 3.6 Contact pairs definition [20] . . . . . 31
- 3.7 Example: Boundary Condition manager . . . . . 34
- 3.8 Boundary conditions . . . . . 35
- 3.9 Editing amplitude . . . . . 36
- 3.10 Mesh of the O-ring . . . . . 39
- 3.11 Inital step . . . . . 40
- 3.12 Pre-tensioned step . . . . . 41
- 3.13 Final compression . . . . . 41
- 3.14 Position 1 . . . . . 42
- 3.15 Position 2 . . . . . 43
- 3.16 Position 3 . . . . . 43
- 3.17 Triangular groove . . . . . 44
- 3.18 Triangular groove model used for numerical calculations . . . . . 45
- 3.19 Triangular angle . . . . . 46

3.20	Symmetric model . . . . .	46
3.21	Simplified model . . . . .	46
3.22	Friction forces . . . . .	47
4.1	Direction explanation . . . . .	50
4.2	Experimental tests [44] . . . . .	51
4.3	Compression steps - A single sealing element . . . . .	53
4.4	Experimental test compared to numerical test - Shore 70A - 6 mm - One sealing element . . . . .	54
4.5	Experimental test compared to numerical test - Shore 90A - 6 mm - One sealing element . . . . .	55
4.6	Experimental test compared to numerical test - Shore 70A - 5 mm - One sealing element . . . . .	56
4.7	Compression steps for two sealing elements . . . . .	57
4.8	Experimental test compared to numerical test - Shore 70A - 6 mm - Two rings . . . . .	58
4.9	Experimental test compared to numerical test - Shore 90A - 6 mm - Two sealing elements . . . . .	59
4.10	Shore 70A - 6 mm - One seals - Groove varying . . . . .	60
4.11	Shore 70A - 6 mm - Two seals - Varying groove dimensions . . . . .	61
4.12	Shore 70A and 90A - 6 mm - One seal - Groove too small . . . . .	62
4.13	Shore 70A and 90A - 6 mm - Two seals - Groove too small . . . . .	63
4.14	Shore 70A - 5 mm and 6 mm - One seal - Groove too small . . . . .	64
4.15	Shore 70A - 5 mm and 6 mm - One seal - Groove too wide . . . . .	65
4.16	Shore 70A - 5 mm and 6 mm - Two seals - Groove too small . . . . .	66
4.17	Shore 70A - 5 mm and 6 mm - Two seals - Groove too wide . . . . .	67
4.18	Shore 70A - 6 mm - One and two compared - Groove too small . . . . .	68
4.19	Shore 90A - 6 mm - One and two compared - Groove too small . . . . .	69
4.20	Shore 70A - 6 mm - One and two compared - Groove too wide . . . . .	70
4.21	Shore 90A - 6 mm - One and two compared - Groove too wide . . . . .	71
4.22	Multiple steps - Hysteresis - Shore 70A - $\mu=0.5$ - 6 mm . . . . .	72
4.23	Multiple steps - Hysteresis - Shore 70A - $\mu=0.5$ - 6 mm . . . . .	73
4.24	Multiple steps - Hysteresis - Shore 70A - $\mu=0.5$ - 6 mm . . . . .	74
4.25	6 mm - $\mu=0.5$ - No pre-tension - 3 positions . . . . .	75
4.26	Position 1 - Two steps - 6 mm . . . . .	76
4.27	Position 2 - Two steps - 6 mm . . . . .	76
4.28	Position 3 - Two steps - 6 mm . . . . .	77
4.29	Hysteresis - 6 mm - $\mu=0.5$ . . . . .	77
4.30	Position 1 - Two steps - 5 mm . . . . .	78

## LIST OF FIGURES

---

4.31	Position 2 - Two steps - 5 mm . . . . .	78
4.32	Position 2 - Three steps - 5 mm . . . . .	78
4.33	Position 3 - Two steps - 5 mm . . . . .	79
4.35	Slip Through - Illustrated - $\mu=0.5$ - 6 mm . . . . .	80
4.36	Slip Through - $\mu=0.5$ - 6 mm . . . . .	81
4.37	Slip Through - Illustrated - $\mu=0.2$ - 6 mm . . . . .	81
4.38	Slip Through - $\mu=0.2$ - 6 mm . . . . .	82
4.39	Triangular groove - $\alpha=55^\circ$ - 6 mm . . . . .	84
4.40	Triangular groove - $\alpha=50^\circ$ - 6 mm . . . . .	84
5.1	Comparison of plane stress and plane strain . . . . .	89
5.2	Comparison of Poisson 's Ratio - Shore 70A - $\text{Ø}6$ . . . . .	90
5.3	Shore 70A - $\text{Ø}6$ - Mesh comparison . . . . .	91
5.4	Mesh of two O-rings in Shore 70A hardness . . . . .	91
5.5	$\text{Ø}6$ - Shore 70 - Friction comparison . . . . .	93
5.6	$\text{Ø}6$ - Shore 70 - Friction comparison - $F=0.2$ . . . . .	94
5.7	$\text{Ø}6$ - Shore 70 - Friction comparison - $F=0.5$ . . . . .	94
5.8	Assumed implementation of experimental tests . . . . .	95
5.9	Angle $\beta$ , between the seal centers . . . . .	99

# List of Tables

- 4.1 Parameters - Shore 70A - 6 mm - One sealing element . . . . . 54
- 4.2 Parameters - Shore 90A - 6 mm - One ring . . . . . 55
- 4.3 Parameters - Shore 70A - 5 mm - One sealing element . . . . . 56
- 4.4 Parameters - Shore 70A - 6 mm - Two sealing elements . . . . . 58
- 4.5 Parameters - Shore 90A - 6 mm - Two sealing elements . . . . . 59
- 4.6 Parameters - Shore 70A - 6 mm - One seal - Groove varying . . . . . 60
- 4.7 Parameters - Shore 70A - 6 mm - Two seals - Varying groove dimensions . . 61
- 4.8 Parameters - Shore 70A and 90A - 6 mm - One seal - Groove too small . . 62
- 4.9 Parameters - Shore 70A and 90A - 6 mm - Two rings - Groove too small . . 63
- 4.10 Parameters - Shore 70A - 5 mm and 6 mm - One seal - Groove too small . . 64
- 4.11 Parameters - Shore 70A - 5 mm and 6 mm - One seal - Groove too wide . . 65
- 4.12 Parameters - Shore 70A - 5 mm and 6 mm - Two seals compared - Groove  
too small . . . . . 66
- 4.13 Parameters - Shore 70A - 5 mm and 6 mm - Two seals compared - Groove  
too wide . . . . . 67
- 4.14 Parameters - Shore 70A - 6 mm - One and two compared - Groove too small 68
- 4.15 Parameters - Shore 90A - 6 mm - One and two compared - Groove too small 69
- 4.16 Parameters - Shore 70A - 6 mm - One and two compared - Groove too wide 70
- 4.17 Parameters - Shore 90A - 6 mm - One and two compared - Groove too wide 71
- 4.18 Parameters - Shore 70A - 6 mm - Two seals - 3 positions . . . . . 75
  
- 5.1 Poisson´s Ratio - Shore 70A - Ø6 - One ring . . . . . 90
- 5.2 Parameters - Mesh of one O-ring in Shore 70A hardness . . . . . 90
- 5.3 Parameters - Mesh of two O-rings in Shore 70A hardness . . . . . 91

# List of Equations

2.1 Hookes law . . . . .	13
2.2 Strain energy potential - polynomial form [1] . . . . .	13
2.3 Poisson´s Ratio . . . . .	15
2.4 Linear FEA . . . . .	18
2.5 Non-linear FEA . . . . .	18
2.6 Master-Slave method stiffness matrix [11] . . . . .	20
2.7 Penalty method stiffness matrix [12] . . . . .	21
2.8 Lagrange multiplier method stiffness matrix . . . . .	22
2.9 Hydrostatic pressure . . . . .	23
3.1 Circular area equal to rectangular groove area . . . . .	27
3.2 Coulomb friction equation . . . . .	33
3.3 Gent´s equation . . . . .	37
3.4 E-modulus for Shore 70A . . . . .	37
3.5 Shore 70A . . . . .	37
3.6 E-modulus for Shore 90A . . . . .	37
3.7 Shore 90A . . . . .	37
3.8 Slip angle formula . . . . .	47
4.1 Calculations of slip angle when $\mu=0.5$ . . . . .	83

# Abbreviations

CAD Computer Aided Design

DOF Degree of Freedom

FEA Finite Element Analysis

FEM Finite Element Method

LFEA Linear Finite Element Analysis

MFC Multifreedom constraint

NBR Nitrile Butadiene Rubber

NFEA Non-linear Finite Element Analysis





# Chapter 1

## Introduction

### 1.1 Background

Hydropower is a widely used source of energy in Norway. Utilizing the potential of running water is important in terms of contribution to a sustainable development. As a result, minimize the loss of water into the hydropower turbine runner is essential. Guide vanes are located in front of hydropower turbines to regulate the flow of water into the runner, and adjust the flow when needed. End seals made of elastomeric material, are incorporated in the guide vanes with the intention to reduce the amount of leakage, a low level of leakage provides high turbine efficiency which is critical for harnessing the potential. In general, high head francis turbines have an efficiency of approximately  $\eta = 0.96$ , meaning the utilization is high. The end seals are either pre-fabricated mouldings or O-rings cut into mouldings as shown in Figure 1.1.

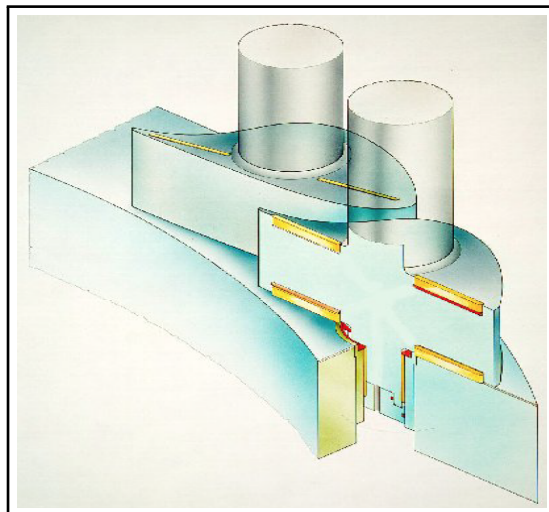


Figure 1.1: Guide vane [29]

O-ring as sealing elements are widely used for different mechanical applications, often surrounding pipes with pressure or without pressure, in order to prevent leakage.

Due to the fact that the O-rings as sealing elements are relatively cheap and have high reliability, the range of applications are wide. As a result; it is important to predict the materials response to load.

## 1.2 Problem description

The problem formulation is given by PhD candidate Petter Østby at Rainpower<sup>1</sup>. End seals are incorporated in the guide vanes in order to minimize leakage water between guide vane ends and the mating surfaces on head and bottom covers. This is especially important on high head units, where the leakage will reduce turbine efficiency and may contribute to increased sand erosion and/or galling. In order to better predict the proper function of the seals, a parameter study of the load deflection curves is necessary. Sensitivity with respect to geometry, number of sealing elements and material properties are of particular interest.

Particularly, this thesis aims at answering the following question: How does the end seals behave in terms of load-characteristic, during changes in geometry of the groove in terms of tolerances relative to the size of the O-ring? This master thesis is needed for better predicting, by numerical simulations, the reliability of guide vane end seals in high head francis turbines. By answering the aforementioned question, a better prediction of the influence of the different aforementioned properties on the end seal performance can be considered.

## 1.3 Problem scope

### 1.3.1 Objectives

The objective of this thesis is to better predict the performance of the end seals by means of conducting a parameter study of the load deflection curves. In order to do this, it is necessary to survey force response behaviour of the sealing material during compression. At present time, Rainpower does not have any load deflection curves as result of numerical analyses. A parameter study of the end seals is performed in order to compare different load characteristics to uncover the force response when parameters are changed. The main steps to successfully establish a parameter study for elastomeric sealing elements are:

- Examine previous research
- Identify which parameters that should be taken into account

---

<sup>1</sup>Rainpower is a company which provides solutions within hydropower including new power plants, electromechanical systems, service and upgrading [30]

- Prepare material approach
- Prepare models with different parameters
- Conduct analysis with different parameters which will be presented in Chapter 4
- Comparison of results obtained from analysis
- Assessing results

### 1.3.2 Limitations

In the hydropower industry there are several different designs of turbines, and the use of end seals for the guide vanes is limited due to both the size of the guide vanes (in terms of head height) as well as the turbine type. Please note that this master thesis will target the use of end seals in high head Francis turbines.

Due to limited information regarding how the experimental load deflection tests (found in Appendix B), which serve as basis for this parameter study is conducted, several assumptions are made. Usually, Finite Element Analysis (FEA) of elastomeric materials requires definition of hyperelastic properties in the software used. Due to the limited access to experimental test results for the material properties, a simplification in terms of a linear-elastic material approach is implemented. The results from the analyses may not be representative, as a hyperelastic approach usually is recommended for the material considered in this master thesis. A prominent part of this thesis in addition to carry out load deflections curves, is the consideration of using a linear-elastic material approach for a hyperelastic material.

As a result of the material hardness numbers used for the experimental tests in which provide the basis for this study, only two material hardness numbers will be considered; Nitrile Butadiene Rubber (NBR) Shore 70A and Shore 90A. Additionally, due to the fact that it is the cross section of the end seal which is of particular interest, modelling is restricted to the two dimensional working environment and the frictional behaviour is assumed to be equal between all mating surfaces, and independent of the environment.

### 1.3.3 Outline

This master thesis is structured as an research report with the following contents:

- Preface
- Abstract
- Chapter 1 - Introduction

- Chapter 2 - Theoretical background
- Chapter 3 - Methodology
- Chapter 4 - Results
- Chapter 5 - Discussion
- Chapter 6 - Conclusion
- Chapter 7 - Recommendations for Further Work
- Appendices

The software used for conducting analysis is ABAQUS 6.14.1 provided by Dassault Systemés. To simplify for any following research, and/or redoing of the project; how FEA is conducted are described in method section with additional information from experiences in the appendices.

During the report, pages which is half-written will occur. These pages are left intentionally blank due to readability. It is also worth mentioning that the terms; "sealing elements", "O-rings" and "seals" is used interchangeably throughout this thesis.

# Chapter 2

## Theoretical background

This chapter will present a Francis turbine and the function of guide vanes in a Francis turbine, as well as the theory behind the O-ring as a sealing element and the material used for the incorporated end seals. To gain insight to the most suitable approach to analyse an elastomeric O-ring, it is important to provide an overview of previous work. In addition, it is also capital to present the theory behind the set-up of the analyses. Finite Element Method (FEM) of elastomeric materials are known to be challenging and a variety of approaches to the analyses have been proposed. Several papers and books retrieved from <https://ntnu.oria.no> and <https://scholar.google.no> are used to acquire fundamental knowledge and theory.

As mentioned, the objective in this master thesis is obtaining load-displacement curves from compression sequence of elastomeric sealing elements. Commonly, in previous literature the objective of analysing incompressible material is to obtain stress-strain curves. This makes previous research relevant in the context of how materials are defined, and which properties are similar to the material analysed here, but the obtained results may not be directly applicable to this document. In addition to literature retrieved from the internet, papers and books, a very valuable amount of information have been given by my supervisor at NTNU, Bjørn Haugen and by PhD candidate at Rainpower, Petter Østby. Additional information has also been provided through e-mail correspondance with Trelleborg Sealing Solutions, PLM Technology, and Dassault Systèmes.

### 2.1 Hydropower turbines

#### 2.1.1 Turbines

Hydropower turbines are used to transform the energy of water into mechanical work, mostly to generate electric power. As a result of alternating conditions in terms of the environment where the turbine is installed, the turbine type may vary. However, the most common turbines are the Francis turbine, Pelton turbine, Pump turbine and the Kaplan

turbine. The Kaplan turbine is used at low heads and the design can be compared to the design of a wind turbine. The Pelton turbine is used for high heads, while the Francis Turbine is used for heads that are in between the high heads suited for the Pelton turbine and the low heads for the Kaplan turbine [43]. Figure 2.1 illustrates a typical vertical Francis turbine:

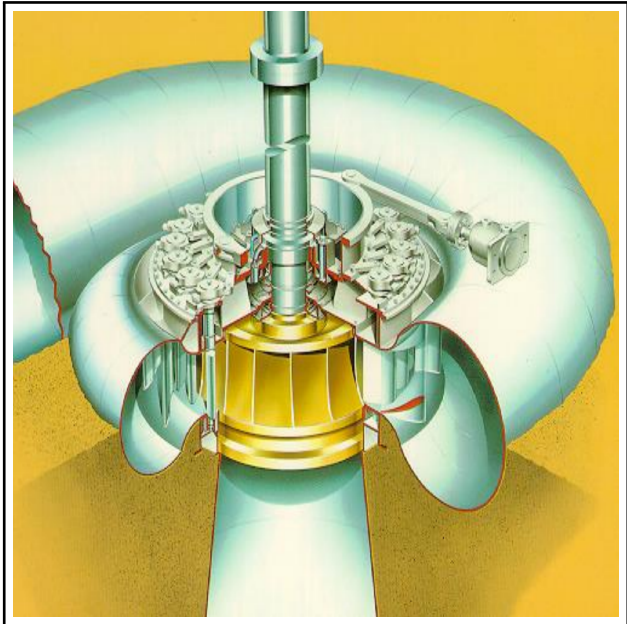


Figure 2.1: Francis turbine

### 2.1.2 Guide vanes

The guide vanes are located in front of the Francis runner with the intention to regulate the flow of water into the runner. They can be adjusted to either increase or reduce the flow rate of water through the turbine. As seen from Figure 2.2, the guide vanes are arranged between two parallel covers, which are positioned normal to the turbine shaft [27].

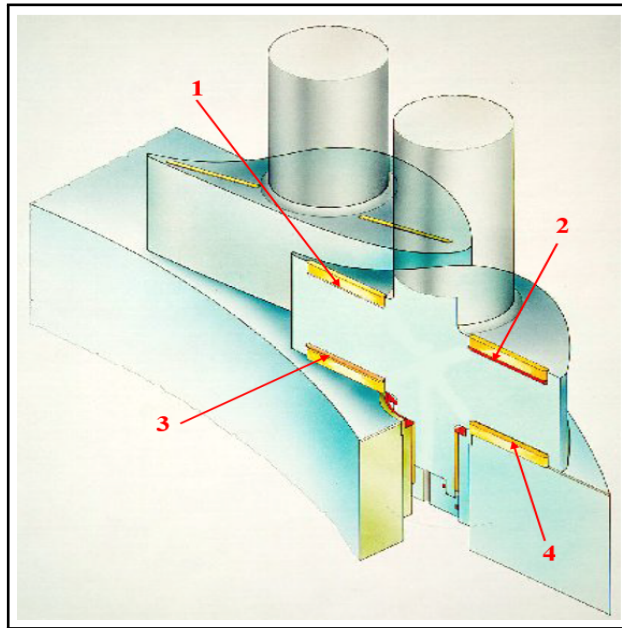


Figure 2.2: Guide vanes [29]

Incorporated in each of the guide vanes there are four mouldings, two above the center axis and two below (highlighted by numbers in Figure 2.2). The reason why the same material properties can be used for both the upper and the lower mouldings, even though the lower mouldings have to support the full weight of the guide vane (i.e. approximately 200 kg.), is that the water pressure equalizes the pressure from the guide vane on the moulding. The main function of the sealing elements is to minimize the leakage of water between the upper and lower surfaces to maximize the efficiency of the turbine. The sealing elements are especially important in high head turbines to increase the turbine efficiency, while in turbines where the head is below a certain height the seals are rarely used [44]. This is because the contribution from the end seals to increase turbine efficiency is considered as negligible for low heads. Furthermore, other advantages related to the use of end seals in the guide vanes are reduction of sand erosion and the fact that the spring characteristics of the O-rings contribute in centering the guide vanes, which is preferable in order to reduce the risk of galling<sup>1</sup> [29].

<sup>1</sup>Galling can be defined as "surface deformation and adhesive interaction in metal-to-metal wear" [5]

## 2.2 The O-ring as sealing element

The sealing of the guide vanes uses either a pre-fabricated moulding or an O-ring which is cut to be used as a moulding. The O-ring as a sealing element for guide vanes is installed into a rectangular groove, often as two O-rings (one above the other) preventing leakage as illustrated in Figure 2.3. This is the situation seen from straight ahead. The cross sectional diameter of the sealing elements is usually either 5 mm or 6 mm. An elastomeric O-ring is one of the most general components in mechanical systems. It is widely used for several different applications, as for instance surrounding axles, couplings and cylinders. The reason O-rings are so widely used for sealing applications is because it is both economical, reliable and effective [41].

Due to the fact that O-rings are widely used as sealing elements, failure analysis is important and meaningful for economical concern as well as functionality, capability and reliability [23]. This capability depends upon different parameters such as tolerances of the groove, O-ring dimensions and contact conditions between the surface of the sealing element and the groove [16]. Analyzing and representing different load characteristics can provide important information about these concerns. However, conducting FEA of elastomeric O-ring seals is challenging due to hyperelasticity, non-linear material, complex geometry and variations in material parameters for the exact same material [16]. When installed in the groove and pressure is applied, the O-ring experiences a compression against the walls of the groove. The elastomer material used in the O-rings have a very low elastic modulus and thus the O-rings are highly deformable. The amount of transversal expansion over the axial compression is represented by the Poission's ratio, and since this coefficient is close to 0.5 they maintain a constant volume despite being exposed to high deformation [13].

Both the O-ring and the groove have tolerances, as a sufficient free space in design criteria is required to permit a variation in the expansion when compressed. The amount of compression varies, depending on the force/pressure acting on the O-ring. Tolerances for the free space in which the O-ring can expand are thus necessary. Recommended tolerances can be found in British Standard 1806 [13]. In addition to the expansion from the compression, the elastomer material experiences a thermal expansion. The thermal expansion coefficient is usually an order of magnitude higher that of surrounding metalwork.



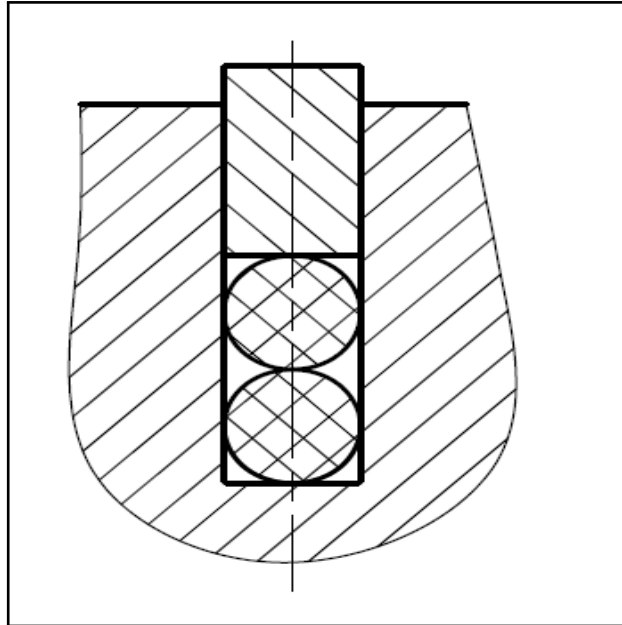


Figure 2.3: O-rings incorporated in sealing groove [44]

Due to the properties, O-rings of elastomeric materials elastomer experience expansion, or swell in the range of 5% - 10%, which usually increase the sealing capability. Hence, a tolerance space for this expansion have to be accounted for when designing the sealing groove [13]. Elastomers have properties that allow for both large deformations and large strains, as well as non-linear elastic behaviour [15]. The reason why elastomer materials have these properties is the process of vulcanization and cross-linking structure which is described in section 2.3.

The O-ring is one of the most reliable seals, and can be used for sealing up to several hundred bars. If the seal is correctly implemented, there are four main reasons for potential failure [13]:

- Movement of the faces that compress the seal
- Displacement of the seal out of the groove
- Loss of elastomeric properties due to ageing
- Variation in temperature can cause loss of either compression or the elastic properties

## 2.3 Material

### 2.3.1 Elastomers

The O-ring in the guide vane end seals analysed in this master thesis is made of the elastomeric material, NBR, Nitrile Butadiene Rubber. Elastomer is a group of materials

including silicon, rubber and other rubber-like materials in which sustain elastic deformations greater than 200 %. As a results of the fact that molecule chains of elastomers consists of coil-like molecules, the deformation is reversible when applying a force. The flexibility of the material exists because of the geometry of the aforementioned structure. Upon loading, these coils unwind between the cross-link attachment points, and after removal of the stress, the coils recover, resulting in the effect of recovery of most of the deformation [2].

As a result of the molecular structure of rubber-like materials is made of entangled chains of polymer molecules, it can be compared to a bowl of spaghetti. Unprocessed rubber has limited areas of use, but by material processing, cross linkage occur; providing strength and durability. Elastomer is a polymer and the term is used to identify the group of polymers with the same material properties such as viscoelasticity, high elasticity and glass transition temperature below room temperature [42].

Fillers can be added to modify the chemical properties, improve the mechanical behaviour, or to introduce micro-structural changes in the material. Adding sulfur and subjecting the rubber to pressure and temperature causes cross-links to form. Cross-links are chemical bonds between the molecules which is produced during the process of vulcanization. Vulcanization involves heat and addition of curatives, for instance sulphate. When vulcanization is performed on the material, the material becomes a elastic polymeric material and as a result vulcanization cannot be reversed [37]. A greater degree of cross-linking results in a harder rubber. Vulcanization is a method for material processing, but for elastomeric materials to obtain the wanted mechanical properties, filler materials are added [18]. Although cross-linking results in the rigid network structure of thermosetting plastics, typical elastomers behave in a very different manner because the cross-links occur much less frequently along the chains.

Regarding filler materials, acrylonitrile is added to NBR (approximately 18 % to 51 %) in the form of polyacrylonitrile with the objective of increasing the oil and gasoline resistance and allowing for low temperature flexibility. Yet, NBR also contains polybutadiene, a material which presents a very different glass transition temperature ( $-0^{\circ}$ ) from polyacrylonitrile ( $+90^{\circ}\text{C}$ ). Hence, increasing the amount of acrylonitrile in the polymer leads to an increase in the glass transition temperature ( $T_g$ )<sup>2</sup> of NBR, together with an increase in its brittleness temperature. Additionally, the elastic behavior of NBR vulcanizates also becomes poorer as the concentration of bound acrylonitrile in the NBR increases, but at the same time the copolymer becomes more thermoplastic, which is advantageous regarding the processibility of compounds [18].

NBR is a synthetic type of rubber with good oil-resistancy, high elasticity, good deformation capacity and low compression set. Compression set describes the materials

---

<sup>2</sup> $T_g$  is the glass transition temperature, which means the temperature where the material exhibit a transition from a hard, glassy state into a viscous rubbery state.

ability to restore its original thickness after undergoing compressive stresses. NBR has complicated material characteristics as a result of absorbing energy like viscous liquid and isotropic properties. Non-linear problems with complicated boundary conditions, are very common and the description of the O-rings mechanical behaviour requires complex procedures in the analysis [6]. Even though NBR have a relatively high price, it is used in applications where, besides good mechanical properties, there is also the requirement for good resistance to swelling in oils and gasoline, and a good resistance to heat ageing and abrasion. Typically, areas of use are in static seals, O-rings, and packings for crank shafts and valves and in membranes [18].

In many materials the stress-strain curve consists of a linear part which is the elastic region, and a plastic region in which is not linear. The elastic stress and the elastic strain are linear related for materials such as steel. The elastic modulus can be calculated from the slope of the stress-strain curve in the linear region. In elastomer, where large elastic deformations are present, the relationship between the elastic stress and the elastic strain is non-linear, hence the elastic strain can be compared to the behaviour of a spring. Accompanying spring characteristics is critical in the situation considered involving incorporated guide vanes end seals. When dealing with elastomeric materials and other non-linear materials, the stress-strain relationship is defined by a strain density function ( $W$ ) instead of the elastic-plastic response curve used for common materials such as steel and aluminium [6].

Figure 2.4 illustrate a arbitrary, but representative stress-strain curve emphasizing the fact of no specific linear-elastic region.

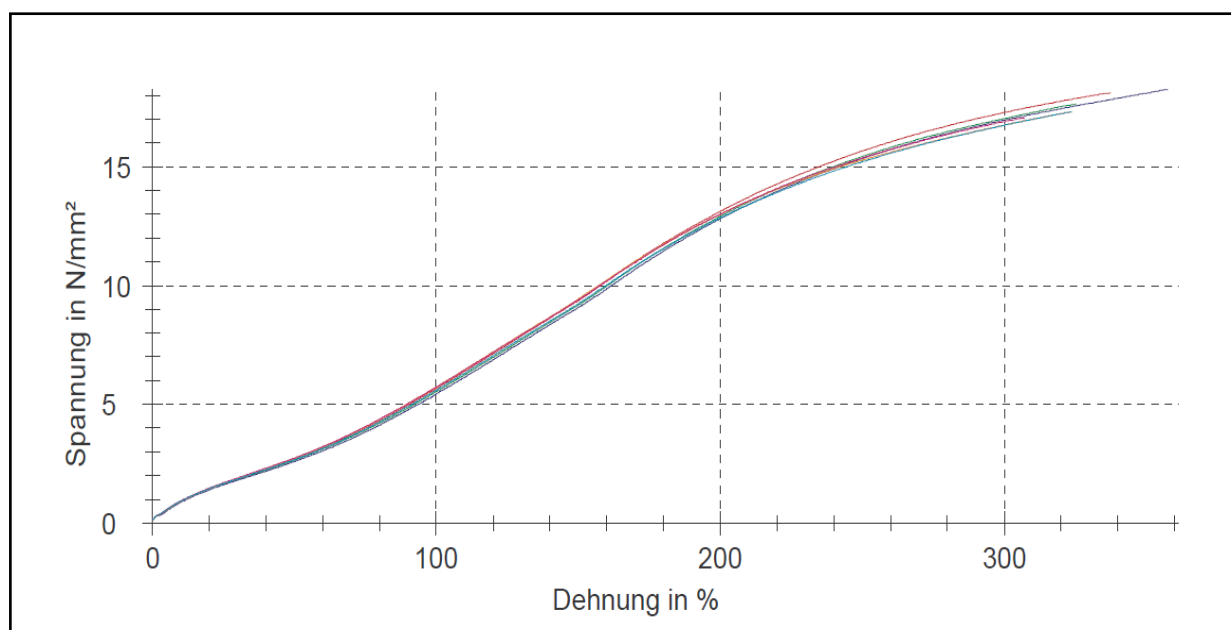


Figure 2.4: Stress-Strain curve for NBR 70A [38]

Figure 2.5 shows a typical stress-strain curve for a linear-elastic material such as steel.

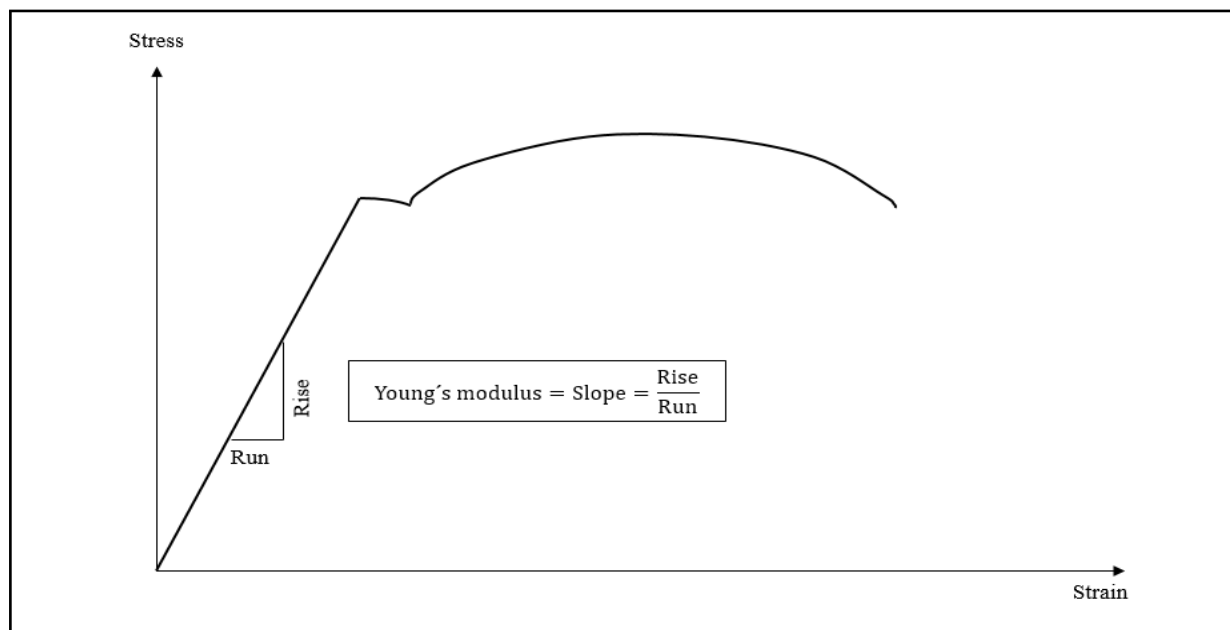


Figure 2.5: Stress-Strain curve for a typical linear-elastic material

One of the characteristics of elastomeric materials is that they present very little compressibility compared to their shear flexibility. When O-rings are used as a seal, the material is highly confined. To get accurate results when the material are elastomeric and confined it have to be modelled correctly with respect to the compressibility [34]. Seal elements are often made of elastomer due to its material properties: the unique function of the elastomeric material makes it special because at working temperature it is both incompressible and has a low elastic modulus. As presented in [13], the elastomer material is incompressible, so when it is compressed on the axis of the seal interference it is necessary to let it expand on the perpendicular axis. Even though the Poisson's Ratio is close to 0.5, the elastomer material maintains constant volume and is highly deformable.

### 2.3.2 Material Behaviour

The behaviour of materials differs depending on which fillers are added during processing. When finished, materials attain properties that are intended to be perfect for the specific area of use. For an elastomeric material which is going to be employed as an O-ring in guide vane end seals, the most common material behaviour approach is hyperelastic. Hyperelasticity is essential to obtain the most correct strain-stress behaviour of elastomeric materials. Due to non-linear large strains, the general Hooke's law (Equation 2.1) is not sufficient to describe the material behaviour of elastomeric materials. Essentially, the primary difference between a linear elastic material and non-linear hyperelastic material is the derivation of the strain-stress relationship. Strain-stress relationship for a hyperelastic

material derives from a strain density function and not a constant factor, e.g, Young's modulus for a linear elastic material [1].

Usually, when loading a test specimen, or a batch in the elastic region, it restores the original size and no permanent changes is imposed after unloading. The property of this reversible feature is the elastic property of the deformation process. Common for most materials is that elastic behavior can be observed, and thus represented by Equation 2.1, Hooke's Law. Here, strain is a linear function of stress [28].

$$\sigma = E\epsilon \quad (2.1)$$

A **linear elastic** material model is valid for materials which exhibit small strains. This material model is commonly used for materials such as steel, aluminium, copper and cast iron. It can be either isotropic, orthotropic or fully anisotropic material. For materials which undergo elastic strain normally less than 5 %, the linear elastic approach are used [34]. Elastic strains can be very high for hyperelastic materials. Because of this, the linear elastic material approach is normally not recommended used because it is not appropriate for elastic strains greater than approximately 5%.

A **hyperelastic** material behaviour is one way of describing a material that is highly elastic. Regarding the description of the strain energy density,  $W$ , is significantly more complex compared to linear elastic material, where the stress is normally a linear function of strain. Defining hyperelasticity strictly depends on experimental test data of the material properties. There are several hyperelastic material models which can be derived. Usually, the strain energy potentials have a polynomial form with basis in Equation 2.2 [1]. A selection of hyperelastic models are described in Appendix F. These models are based on experimental test data such as uniaxial tension/compression, biaxial tension/compression, planar tension/compression and volumetric data.

$$W = \sum_{i+j=1}^N C_{ij}(I_1 - 3)^i(I_2 - 3)^j + \sum_{i=1}^N \frac{1}{D_i}(J - 1)^{2i} \quad (2.2)$$

$W$  is the strain energy potential,  $J$  is the elastic volume ratio,  $I_1$ ,  $I_2$  is stretch invariants, while  $N$ ,  $C_{ij}$  and  $D_i$  is material constant from experimental test data.

### 2.3.3 Viscoelastic behaviour of Nitrile Butadiene Rubber

The hyperelasticity criteria can be expanded to include viscoelasticity requiring additional tests values such as constant stress with time-varying strain, constant strain with time-varying stress and time-varying loading [37]. Elastomers like NBR have time-dependent material behaviour. Time-dependent properties are often associated with viscoelasticity,

i.e. viscoelastic material behaviour. Viscosity is a measure of the ability of a material or fluid to resist flowing. For example, water flows more easily than oil because it has a lower viscosity. High viscosity materials generally resist flow. Viscoelasticity is the property of materials that exhibit both viscous and elastic characteristics when undergoing deformation. Elastomers display significant viscoelastic effects at high temperatures resulting in reduced viscosity. Because viscoelastic materials have the viscosity factor, they have a strain rate which is time dependent. Purely elastic materials do not dissipate energy, heat, such as for instance elastomeric materials when a cyclic loading is applied.

In general elastomeric materials as well as polymers experiences effects of viscoelasticity when they are exposed to force over time. For an elastic seal, the pressure remains constant over time. Due to the remaining pressure, elastomers exhibit time-dependent, or viscoelastic behavior. The sealing pressure will tend to decay over time [37]. Viscoelastic materials creep over time, and creep of polymers is significant at low temperatures, typically ( $\geq -20^\circ$ ) [37]. The viscoelastic behaviour as function of temperature 0-10 °C variation.

The basic hyperelastic material definition can be expanded to include viscoelasticity, whereas it builds upon the hyperelastic behaviour. Mechanical properties of certain materials are history-dependent but behave nearly elastically. When unloaded, they return to their undeformed state. An important terms when talking associated with viscoelasticity is, hysteresis <sup>3</sup>. Viscoelastic materials exhibit hysteresis under repeated loading, and energy typically in form of heat, is dissipated. This heat contribute to significant changes in the behaviour of the material which affect the response. Energy dissipation through hysteresis is represented by the region between the loading and unloading curves in a load-deformation cycle, and occurs with all rubbers [37]. In the case of cyclic loadings, hysteresis arises from the frictional sliding of the long molecules across one another. Another term associated with viscoelasticity is damping, due to the fact that the stress/strain response of a viscoelastic material is rate-dependent, i.e, the material exhibits damping behavior [37].

Hyperelasticity only approximates the elastomeric materials' mechanical response. Viscoelastic materials exhibit stress relaxation and creep behavior [37]. To define the time-dependent, or viscoelastic behavior part of the material behavior additional tests are required. The following tests is required to describe the viscoelastic material behaviour: [37].

- Creep test, where the stress is constant and the strain is time-varying.
- Stress relaxation test, where the strain is constant and the stress is time-varying.
- Dynamic test where the loading is time-varying.

---

<sup>3</sup>For elastomers it is not uncommon to exhibit elasticity damage (softening) and hysteresis during the cyclic loading. Cycles of loading results in decrease in stiffness, this is termed Mullins Effect [4]

### 2.3.4 Poisson 's Ratio

Compression of materials depend on the ratio between the transverse strain and the axial strain. When compressing on a component in any given direction, e.g. y-direction it elongates in both x and y direction in addition to the direction of the acting load. The Poisson 's ratio,  $\nu$ , define the transversal expansion divided by the axial compression [28].

$$\nu = \frac{\varepsilon_y}{\varepsilon_x} \quad (2.3)$$

$\varepsilon_y$  is defined as the strain in y-direction, while  $\varepsilon_x$  is the strain in the x-direction. The Poisson 's ratio varies in relation to material properties. Typically,  $\nu$  is approximately 0.5 for incompressible materials such as elastomers [1].

## 2.4 Tribology of Elastomers

Tribology is a concept that refers to the science and technology of interaction surfaces in relative motion and the practices related. The definition of tribology for elastomers is: "the science and technology for investigating the regularities of the emergence, change and developing of various tribological phenomena in rubber and rubber-like materials and their tribological applications" [42]. Tribology of elastomers have according to the increase in use of elastomeric, rubber and rubber-like materials become more and more important. Interactions of the elastomeric materials with a rigid surface on a sliding interface is essentially different from that of the metals, considering this interaction to contain adhesion and hysteresis [42].

The contact stresses is important in terms of the seals ability to actually seal and how effective the sealing properties are. The contact stress together with the friction coefficient between the surfaces affect the total sealing ability. The coefficient of friction strictly depends on a several factors, being the most important ones:

- Material
  
- Surface roughness
  
- Temperature dependency
  
- Lubrication
  
- Static friction or dynamic friction

### 2.4.1 Friction

Friction does not depend on the amount of surface area in contact between the moving bodies or, within certain limits, on the relative speed of the bodies. It does, however, depend on the magnitude of the forces holding the bodies together. The velocity gradient are also an important parameter and should be considered. There are mainly three states of friction we are taking into consideration when talking about the phenomena:

- Static friction
- Dynamic friction
- Run-in friction

Experimental data show that the friction coefficient that opposes the initiation of slipping from a sticking condition, i.e static friction, is different from the friction coefficient that opposes established slipping, i.e. kinetic friction. **Static friction** is often characterized with a static friction coefficient. This parameter describes how "connected" the mating surfaces are, in terms of how much force are needed to provide movement of a component? **Dynamic friction** is often characterized with a dynamic friction coefficient which describes how much resistance two surfaces in contact are exposed during movement. Typically, the static friction coefficient is higher than the kinetic friction coefficient due to the fact that a higher force is needed to *make* the object move than *keep* it moving. The static friction coefficient corresponds to the value given at zero slip rate, and the kinetic friction coefficient corresponds to the value given at the highest slip rate. The static and kinetic friction coefficients can be functions of contact pressure, temperature, and field variables. The transition between static and kinetic friction is defined by the values given at intermediate slip rates [34]. **Run-in friction** is the unsteady state of friction, due to the fact that energy between the surfaces changes with time, even though environmental and operational conditions are kept constant [42].

## 2.5 FEM Analysis

The finite element method can be used for a various of challenges and are widely used within structural analysis and analysis of mechanical components , e.g. an O-ring end seal. The approach is based on conservative structural mechanical principles, but development of FEM follows that of digital computer technology. The software implements a series of numerical operations to produce results [3]. FEM approaches the challenge by dividing the whole assembly, whole part or parts of the part into elements. The geometry and properties such as the size of the elements are defined by the mesh. FEM calculate the stiffness of each of these elements and which forces required to provide deformations. The



elements are connected in nodes until they represent the whole assembly or part. It is possible to calculate the displacement of each of the nodes by combining the stiffness of each the elements by solving the equilibrium equations for each node. When the deformation of each element are known, it is possible to calculate the stress and forces acting [40].

Structural analysis are based on the principle of equilibrium, kinematic compatibility and stress-strain relationship. FEA can be both linear and non-linear. Linear FEA (LFEA) meaning linear correlation between force and displacement, meaning that if the applied force is doubled the displacement and associated internal stresses is also doubled, while this correlation is not linear in non-linear FEA (NFEA) [10]. As for instance, if the strain-stress curve presents a linear region (elastic region) at the beginning when load is applied to the material, if the material go back to the original shape, the relationship is linear and the material is within its elastic region. In linear FEA the displacement are assumed to be small and the material linear and within the elastic region. The equilibrium equations is established assuming the displacements are small and that the stress and strain are linear functions of the displacement<sup>4</sup> [26]. If the deformation is permanent, the material is in its plasticity region where non-linear FEA should be applied as shown in Figure 2.6. In addition, non-linearity is present in analysis where boundary conditions, e.g. large enforced displacement leads to contact. Friction, displacement and stresses of contacting bodies are usually not linear dependent on the applied load, which add non-linear complexity to the analysis [26].

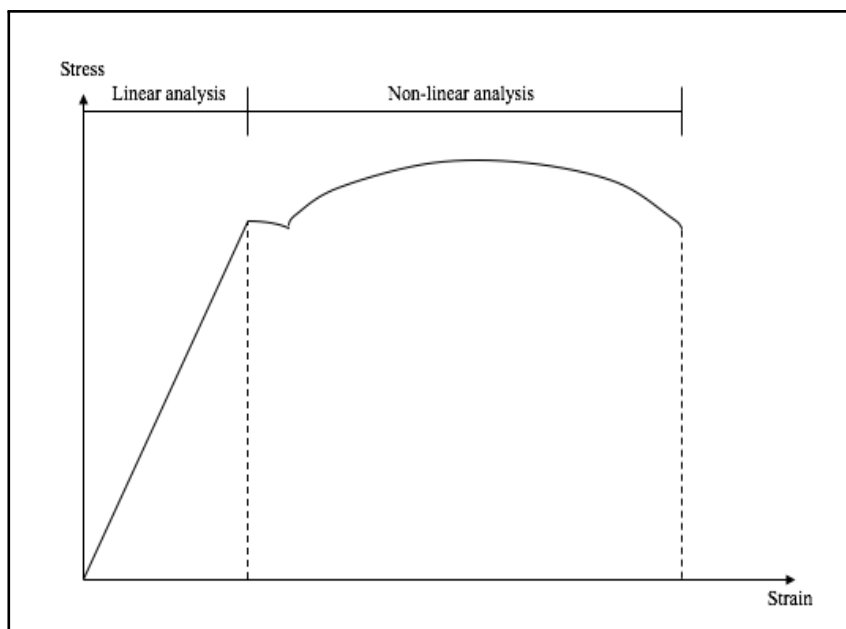


Figure 2.6: Linear FEA and Non-Linear FEA regions

<sup>4</sup>The internal shear force is achieved by integrating the external force. The moment is achieved by intergrating the internal shear force. Integrating moment over axial stiffness gives the angular deflection and displacement is achived by integrating the angular deflection.

Equation 2.4 presents the linear relationship for linear FEA:

$$[K]D = F \quad (2.4)$$

In non-linear FEA, as seen for Equation 2.5, both the stiffness,  $K$  and the force,  $F$  is a function of the displacement  $D$ .

$$[K(D)]D = F(D) \quad (2.5)$$

### 2.5.1 Implicit and Explicit methods

The equilibrium equations in a FEA is solved either implicitly or explicitly. The Implicit method the solver iterates for each time increment and does not move on before the convergence criterion is satisfied for each increment. The implicit analysis does Newton-Raphson<sup>5</sup> iterations to enforce equilibrium of the internal structure forces with the externally applied loads. This type of analysis is usually more accurate than the alternative explicit solver. Challenges with the implicit solver is, normally it may undergo difficulties when analysing problems with large deformations, non-linearity or contact definitions. How this challenges are experienced throughout this master thesis is described in section 3.2. The size of the increments can in a greater extent be controlled by the user and it take bigger increment steps. This type of analysis can handle problems such as cyclic loading, snap through, and snap back better as long as control methods such as arc length control or generalized displacement control are used. To clarify, there are different approaches to how Newton-Raphson iterations are conducted for the implicit solver. Alternatively, in the Appendix C will be presented. The challenge with the implicit solver is that during the Newton-Raphson iterations one must update and reconstruct the stiffness matrix for each iteration, which can be computationally costly.

The explicit solver produces a large number of small time steps efficiently [34]. According to Harewood [17] the implicit approach with its iterative solver undergo problems when trying to converge when analysing highly non-linear material behaviour. By reformulation of the equations, they can be solved directly to determine the solution at the end of the increment without iterations [17]. The explicit solver does an incremental procedure updating the stiffness matrix at the end of each increment based on geometry changes, material changes or both. A new stiffness matrix is constructed and the next increment of load or displacement is applied to the system. If the increments are small enough, the result from the explicit solver will be accurate. As a matter of fact, this is

---

<sup>5</sup>The most widely used iterative procedure. Uses linear approximations to solve equations.

also the challenge with explicit solver, because it is necessary with several small increments for obtaining high accuracy. If the number of increments are not sufficient the solution tends deviate from the correct solution. An explicit, dynamic analysis is computationally efficient for the analysis of large models with relatively short dynamic response times and for the analysis of extremely discontinuous events or processes. This type of analysis allows for the definition of very general contact conditions and uses a consistent, large-deformation theory [36].

Whereas ABAQUS/Standard must iterate to determine the solution to a non-linear problem, ABAQUS/Explicit determines the solution without iterating by explicitly advancing the kinematic state from the previous increment. However, the choice of solver may be dependent on different parameters, such as material properties. A large scope of different stress analysis problems can be solved by use of ABAQUS/Standard and/or ABAQUS/Explicit. Such problems are often divided either into static or dynamic response problems. Dynamic problems are in which inertia effects are significant, while in static problems the inertia are negligible. Additionally, there exists a middle point situation in which when a force is applied, it is applied so slowly that the deformation is slow as well, meaning a low strain rate. In this case, quasi-static analyses can be performed. Because of low strain rate, the inertial forces is very small and thus negligible [10]. Figure 2.7 shows when to consider the different solvers.

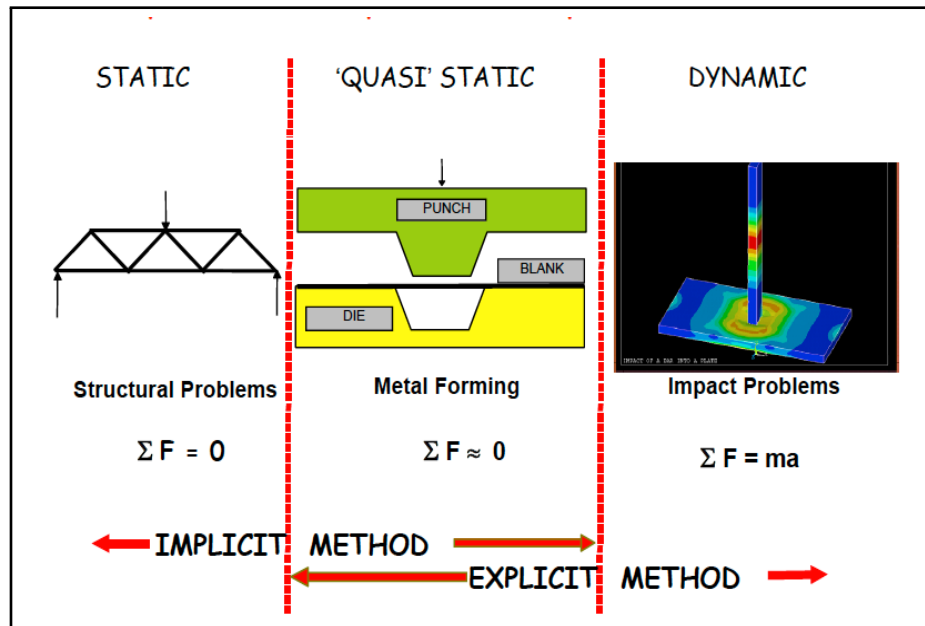


Figure 2.7: Implicit or Explicit depending on simulation [31]

ABAQUS/Standard (implicit) is usually more efficient when solving smooth non-linear problems, while ABAQUS/Explicit considered as favorable for wave propagation analysis. However, a selection of static or quasi-static problems can be simulated well with either solver. Typically, these are problems that usually would be solved implicitly, but

may experience trouble converging due to contact interactions or material complexities, resulting a large number of iterations. with ABAQUS/Standard but may have difficulty converging because of contact or material complexities, resulting in a large number of iterations. Such analyses requires a large set of linear equations to be solved which is computately expensive using the implicit approach [31].

## 2.5.2 Contact algorithms

For a variety of mechanical situations, interactions between parts and their respective surfaces is present. Parameters affecting contact interactions is for instance; separation, penetration, sliding or sliding with resistance. There are several contact algorithms depending on the properties of the parts and the simulation. When contact theory is discussed, a highly relevant term is; multifreedom constraint (MFC). MFC is equations connecting two or more displacement components at different nodes. Three methods for defining contact will be presented; master-slave elimination method, the penalty method and the Lagrange multiplier adjunction [11].

The master-slave elimination remove all slave freedoms in purpose of creating a new set of degrees of freedom (DOFs). A slave degree of freedom is chosen for each constraint. For the following example,  $u_2$  is chosen as master and  $u_6$  is chosen as slave node indicating these two nodes move by the same amount [11]. Figure 2.8 illustrate a six element bar with seven nodes.

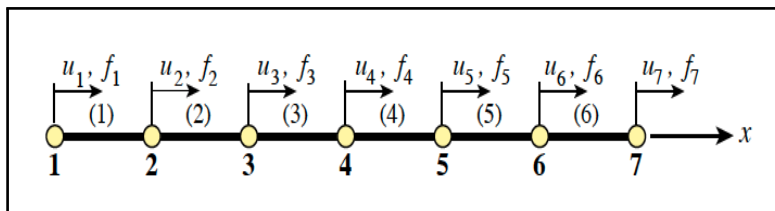


Figure 2.8: Six element bar[11]

$$\begin{bmatrix} K_{11} & K_{12} & 0 & 0 & 0 & 0 \\ K_{21} & K_{22} + K_{66} & K_{23} & 0 & K_{56} & K_{67} \\ 0 & K_{32} & K_{33} & K_{34} & 0 & 0 \\ 0 & 0 & K_{43} & K_{44} & K_{45} & 0 \\ 0 & K_{56} & 0 & K_{45} & K_{55} & 0 \\ 0 & K_{67} & 0 & 0 & 0 & K_{77} \end{bmatrix} \begin{bmatrix} u_1 \\ u_2 \\ u_3 \\ u_4 \\ u_5 \\ u_7 \end{bmatrix} = \begin{bmatrix} f_1 \\ f_2 + f_6 \\ f_3 \\ f_4 \\ f_5 \\ f_7 \end{bmatrix} \quad (2.6)$$

The Penalty Method introduce a penalty element with a certain penalty weight as shown in Figure 2.9.

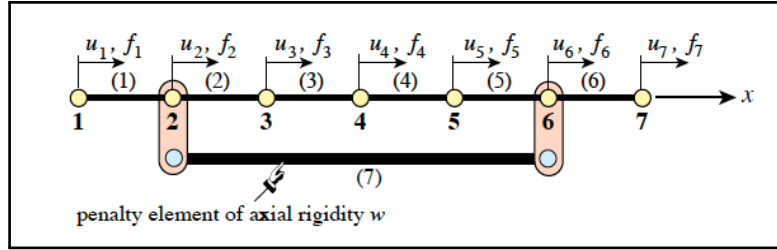


Figure 2.9: Fictitious bar, element 7 is introduced with axial stiffness,  $\omega$ . [12]

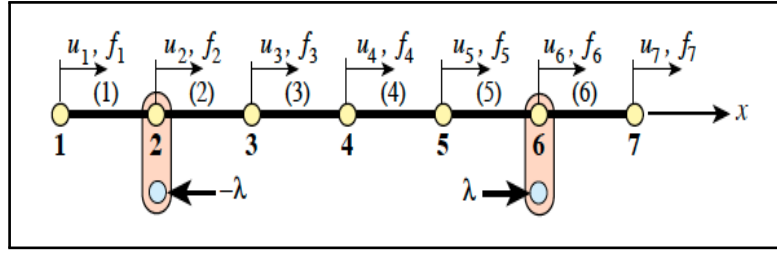
The penalty element is a bar with axial stiffness,  $\omega$ . This element is treated like any other arbitrary bar, but requires a penalty weight which is introduced into the stiffness matrix as indicated in Equation 2.7. The penalty weight is added between the two involved nodes. In the example from [12], one can see that the axial bar is added between node 2 and node 6, introducing  $\omega$  for the corresponding stiffness in the stiffness matrix:

$$\begin{bmatrix}
 K_{11} & K_{12} & 0 & 0 & 0 & 0 & 0 \\
 K_{21} & K_{22} + \omega & K_{23} & 0 & 0 & -\omega & 0 \\
 0 & K_{32} & K_{33} & K_{34} & 0 & 0 & 0 \\
 0 & 0 & K_{43} & K_{44} & K_{45} & 0 & 0 \\
 0 & 0 & 0 & K_{54} & K_{55} & K_{56} & 0 \\
 0 & -\omega & 0 & 0 & K_{65} & K_{66} + \omega & K_{67} \\
 0 & 0 & 0 & 0 & 0 & K_{76} & K_{77}
 \end{bmatrix}
 \begin{bmatrix}
 u_1 \\
 u_2 \\
 u_3 \\
 u_4 \\
 u_5 \\
 u_6 \\
 u_7
 \end{bmatrix}
 =
 \begin{bmatrix}
 f_1 \\
 f_2 \\
 f_3 \\
 f_4 \\
 f_5 \\
 f_6 \\
 f_7
 \end{bmatrix}
 \quad (2.7)$$

The assessment of the penalty weight is important to get the correct balance accuracy, but this part is considered as the challenge since it requires calculation by the square root rule<sup>6</sup> or by numerical experimentation. Using the Square Root Rule to determine the penalty weight requires knowledge of both stiffness magnitudes and properties of the floating-point for the hardware of the computer, as well the precision selected by the software.

Another contact approach is the Lagrange Multiplier adjunction. This approach does add a unknown value called, Lagrange multiplier;  $\lambda$ . While the penalty method added a value into the stiffness matrix, the Lagrange multiplier adjunction add a force pair into the force matrix. By adding a force pair for each node, the stiffness matrix needs to be expanded with a new row and a new column [12]. If there are several nodes, the stiffness matrix becomes very large and the computational time for the solver increases. Figure 2.10 shows the interpretation of the Lagrange multiplier force pair.

<sup>6</sup>Square Root Rule states that  $\omega$  is in fact  $10^k \sqrt{10^p}$ , where  $k$  is stiffness magnitude and  $p$  is the floating-point precision in terms of decimal places


 Figure 2.10: Introducing force pair  $(-\lambda, \lambda)$  [12]

The Lagrange introduce a rigid link for node 2 and 6 instead of a axial stiffness bar between the nodes.

$$\begin{bmatrix} K_{11} & K_{12} & 0 & 0 & 0 & 0 & 0 \\ K_{21} & K_{22} & K_{23} & 0 & 0 & 0 & \\ 0 & K_{32} & K_{33} & K_{34} & 0 & 0 & 0 \\ 0 & 0 & K_{43} & K_{44} & K_{45} & 0 & 0 \\ 0 & 0 & 0 & K_{54} & K_{55} & K_{56} & 0 \\ 0 & 0 & 0 & 0 & K_{65} & K_{66} & K_{67} \\ 0 & 0 & 0 & 0 & 0 & K_{76} & K_{77} \end{bmatrix} \begin{bmatrix} u_1 \\ u_2 \\ u_3 \\ u_4 \\ u_5 \\ u_6 \\ u_7 \end{bmatrix} = \begin{bmatrix} f_1 \\ f_2 - \lambda \\ f_3 \\ f_4 \\ f_5 \\ f_6 + \lambda \\ f_7 \end{bmatrix} \quad (2.8)$$

The advantage with the Lagrange multiplier adjunction is the precision of the results, since this contact algorithm provides exact results, which in most cases are of particular interest. The main advantage with the penalty method is, as mentioned, it decreases the computational time for the computer solver. The Penalty Method allows the surfaces to penetrate, while the Lagrange is, as mentioned, exact and does not include any artificial stiffness. The level of penetration using the penalty method are controlled by the aforementioned penalty weight. Figure 2.11 illustrate the effect of adjusting the penalty stiffness:

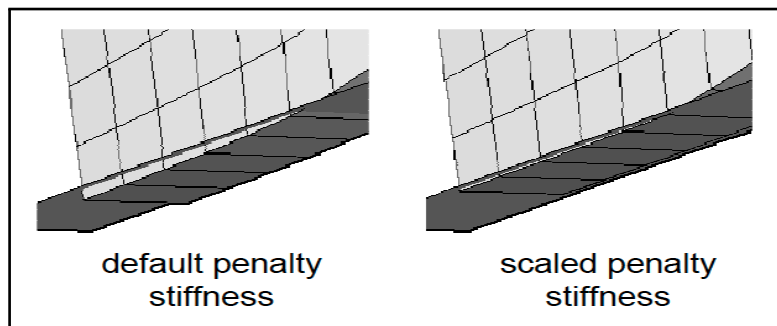


Figure 2.11: Default penalty stiffness and scaled penalty stiffness [20]

The penalty method and the Lagrange multiplier adjunction are two separate methods to approach the contact between elements. The augmented Lagrangian method<sup>7</sup>

<sup>7</sup>Iterative procedures where  $\omega$  is kept constant trying to improve the accuracy of the penalty method [9].

is established as a connection between these two approaches [12].

### 2.5.3 Plane stress and plane strain

The theoretical background for plane stress and plane strain is highly relevant to this master thesis due to two dimensional modelling. When considering problems in plane analysis, plane stress and plane strain designate certain limitations and assumptions associated with the field of displacement and stress. Plane stress is defined to be the state of stress in which the normal stress  $\sigma_z$  and the shear stress,  $\sigma_{xy}$  and  $\sigma_{yz}$ , directed perpendicular to the x-y plane are assumed to be zero [32]. Plane strain is defined to be a state of strain in which the strain normal to the x-y plane,  $\varepsilon_z$ , and the shear strain  $\gamma_{xz}$  and  $\gamma_{yz}$ , are assumed to be zero. In plane strain, one deals with the situation in which dimensions of the structure in one direction, e.g. z-direction, is considerably larger in comparison to the dimensions of the structure in the other two directions, x and y [32].

To sum up, in plane stress, the stress reaction is limited to the x-y plane while the strain is allowed to act in x, y and z. For plane strain, the strain reaction is limited to the x-y plane, while the stress is allowed to act in x, y and z direction. Additionally, the influence of the hydrostatic pressure is significant in compression of materials and can be applied to any uniaxial deformation [28]. Hydrostatic pressure is a natural force, and is the pressure created at static state.

$$p = \rho gh \tag{2.9}$$





# Chapter 3

## Methodology

The configuration of the simulations from modelling, through step definition, contact interactions, and elements will be covered in chronological order. Considerations including justification of assessments made to achieve functional simulation models will be presented throughout this chapter and in chapter 5. Furthermore, definitions of the associated boundary conditions and material properties assigned to the models will be described in detail.

Numerical analyses are performed using ABAQUS 6.14-1 with a linear-elastic approach to the material behaviour, meaning the properties of the O-ring seals mainly refer to Young's modulus, material density and Poisson's Ratio (without defining a plasticity criteria with the intention of recreating fully elastic deformation). Normally, hyperelastic material approach is recommended since linear and non-linear FEA methods for metal compounds lack precision for elastomers and rubber-like materials. However, rubber-like materials and elastomers, such as NBR, are assigned a hardness number which can be used to calculate an approximate Young's modulus. In general, hardness is a material property in which indicates the ability to resist plastic deformation, usually by penetration [28]. Several given equations can be used for converting hardness number into Young's modulus, but the most commonly used is the Gent equation presented in section 3.5.

Setting up analyses including contact, large deformations and boundary conditions was quite challenging due to restrictions in ABAQUS. Several assumptions were made to be able to set up the model with associated the features correctly. In the following list, the full set of assumptions is presented:

- Linear elastic approach
- Isotropic material
- Quasi-static analysis
- Friction coefficient varying between 0.2, 0.5 and 1.0
- Friction coefficient equal between all surfaces

- Using partition on the O-ring to achieve a refined, structured mesh
- Using analytical rigid on the wires as a result of two dimensional problem and contact analysis
- Temperature dependency is neglected
- General state of the Shore 70A and Shore 90A NBR rubber material
- The thickness in Z-direction is assumed to be 1 mm for the two dimensional models.
- Poisson 's ratio equals 0.4995
- SI units (mm) are used: millimetre (mm), Mega Pascals (MPa) and tons.

### 3.1 Finite Element Analysis configuration

Normally, if complex mechanical problems are analysed, modelling is conducted in Computer Aided Design (CAD) programs such as Siemens NX, SolidWorks or Autodesk Inventor. Alternatively, ABAQUS provide a modelling module thus can be used for simple models. An important aspect when defining a FEA is the properties of the modelled parts. For instance if the material properties are unique, it is important to define the material properties correctly to obtain the correct results from the analysis. In general, the property of the different parts define which analysis, and how the analysis can and should be conducted.

Simplifying is usually preferable when conducting FEA for a variety of mechanical problems. In this master thesis an approach of two dimensional modelling is chosen to simplify the modelling process and to decrease the computational time for the solvers. Using two dimensional parts is considered sufficient to represent the compressed O-ring mouldings. Primarily, the difference between three dimensional and two dimensional modelling for the considered situation is that the force is applied as a uniform load along the length in three dimensions. As a consequence, it is necessary to divide the force over the length of the O-ring to compare the three dimensions experimental results with the two dimensional numerical results. The length, or depth, in the z-direction in the two dimensional model is assumed to be 1 mm.

Particularly, it is the O-ring and associated properties which is of interest when conducting a parameter study of the load deflection characteristics of guide vanes end seals. Approaching the situation when the O-ring fill as much as the rectangular groove. Figure 3.1 illustrate the desired situation:

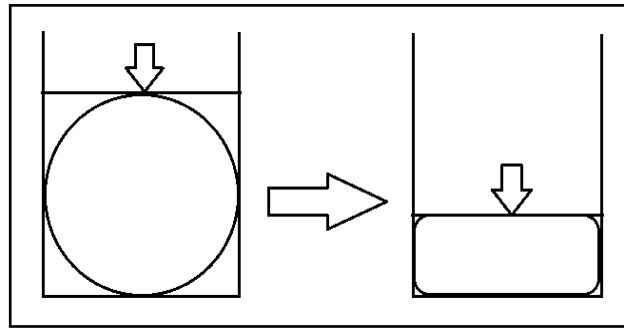


Figure 3.1: Circular area equal to rectangular groove area

The aim of the compression is to fulfill Equation 3.1:

$$hb = \pi r^2 \quad (3.1)$$

The analysis conducted is defined as non-linear as the boundary conditions results in large displacements. Additionally, non-linearity often occurs in contact problems, and since the compressed O-ring is incorporated in a highly confined area, it is defined as a non-linear analysis.

### 3.1.1 Modelling

ABAQUS provides three different possibilities of describing parts, deformable, discrete rigid or analytical rigid. Rigid parts are usually used to represent very stiff or infinite stiff components [34] (2.4.1). The impact of surfaces representing the rectangular groove walls was considered negligible and assumed to be infinitely stiff. Supported by the ABAQUS/-CAE User's Guide [36] section 11.7.1, analytical rigid wires seems to be the preferred alternative;

*"An analytical rigid part is similar to a discrete rigid part in that it is used to represent a rigid part in a contact analysis. If possible, an analytical rigid should be the used part when describing a rigid part because it is computationally less expensive than a discrete rigid part".*

As a results of using analytical rigid parts; it does not require mesh in two dimensional planar, resulting in fewer elements which decrease the computational time of the analysis. Figure 3.2 depicts the interface for defining the analytical wires in ABAQUS:

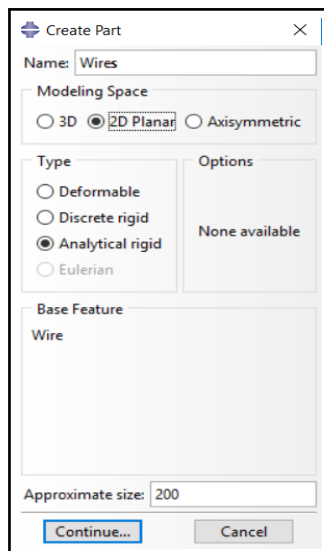


Figure 3.2: Wire part definition

The O-rings are modelled as a deformable shell in 2D planar and the assigned section is solid and homogeneous. Thickness of the shell is, as mentioned, assumed to be 1 mm. The length of the O-ring mouldings used in the experimental tests is 100 mm. Figure 3.3 illustrate the interface of defining the O-rings in ABAQUS.

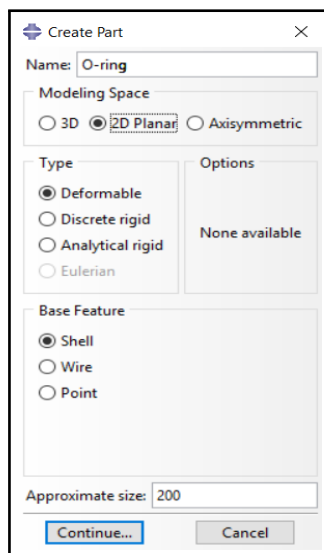


Figure 3.3: O-ring part definition

In summary, the surfaces representing the groove are modelled as four analytical rigid wires with dimensions as shown in Figure 3.4. The O-ring rubber seal is modelled as a two-dimensional deformable shell. Reference points are added to each of the analytical rigid wires, where boundary conditions are assigned. The O-rings typically has a cross sectional diameter of either 5 mm or 6 mm.

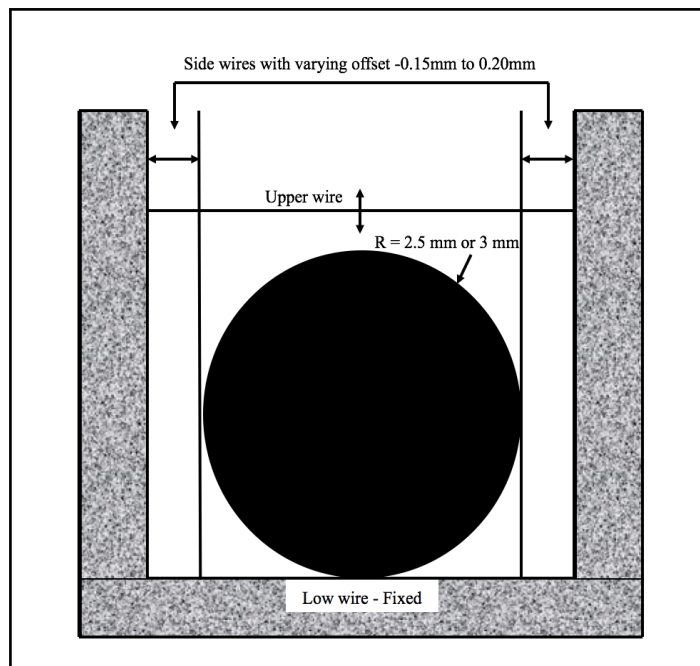


Figure 3.4: Dimensions

## 3.2 Implicit or Explicit analysis

Usually, the explicit solver is recommended for crash-tests, simulations with large deformation, complex contact conditions and/or non-linear material behaviour as mentioned in section 2.5.1. The implicit solver can encounter numerical difficulties in converging to a correct solution during an analysis involving large element deformation, highly non-linear plasticity or contact between surfaces. The explicit solver appears to be more robust and efficient for analyses where contact conditions are present [17]. It was questionable which of the solvers would work for better this approach. Especially, the implicit solver faced challenges converging due to the interaction definitions in combination with 2D modelling, analytical rigid surfaces and large deformations.

To sum up, according to section 2.5.1 and the previous paragraph, the implicit solver seems preferable in static and quasi-static problems which do not involve complicated contact between mating surfaces. For the implicit solver to work properly, very small time increments must be employed to solve the equilibrium equations. Particularly, aforementioned challenges with the implicit solver were experienced repeatedly throughout this Master Thesis. Guide vanes end seals are incorporated in highly confined environments resulting in both large deformations and contact interactions. Personal experience supported by a selection of literature and ABAQUS User Manuals clarified that the dynamic, explicit solver should be chosen in this context.

### 3.3 Contact and Interaction

The contact conditions depends on several different factors which makes interaction modelling challenging in analysis software. In some cases it is necessary to model every part as close to the reality as possible, while in other situations, some instances can be represented by rigid parts. The definition of parts affect the definition of interactions properties. Parts inserted in highly confined environments such as for instance an O-ring in a rectangular or triangular groove is exposed for complex contact theory between the surfaces involved. Contact between mating surfaces in ABAQUS 6.14-1 is defined in the interaction module, while in which step they are active is defined in the interaction manager. Defining contact interactions is challenging and several parameters need to be considered, e.g. defining the appropriate contact algorithm. ABAQUS/Standard and ABAQUS/Explicit provides two contact algorithms for interaction problems [34]:

- General contact algorithm
- Contact pair algorithm - Surface-to-surface

#### 3.3.1 General contact

Usually, the general contact algorithm is recommended because it detects all surfaces and defines the points of contact. This simplifies the interaction definitions for the user compared to the contact pair algorithm. The general contact algorithm uses the Lagrange multiplier adjunction by default. Figure 3.5 illustrate the definition of the general contact:

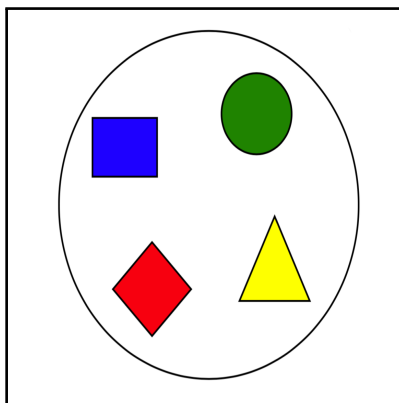


Figure 3.5: General contact definition [20]

Unfortunately, there are restrictions using the recommended general contact algorithm in ABAQUS/Explicit which led to challenges in this master thesis. Since the simulation models are made in two dimensions including contact with analytical rigid parts, general contact cannot be used. This is supported by ABAQUS Analysis User's Guide [34] section 36.4.1: General contact can only be used for three dimensional surfaces in ABAQUS/Explicit. The general contact algorithm is unavailable since it does not

consider contact using analytical rigid parts in two dimensional environments, although these surface types can be included in contact pair. Hence, the other contact algorithm, contact pairs, has to be used. Generally, part definition has significant influence of the preferable contact algorithm in ABAQUS.

### 3.3.2 Contact pair algorithm

Using contact pair, or surface-to-surface contact, requires remarkable caution when defining the respective surfaces in contact. In this algorithm, the user needs to define which surfaces are in contact while the general contact algorithm figures this out by itself. Figure 3.6 illustrate the definition of this method:

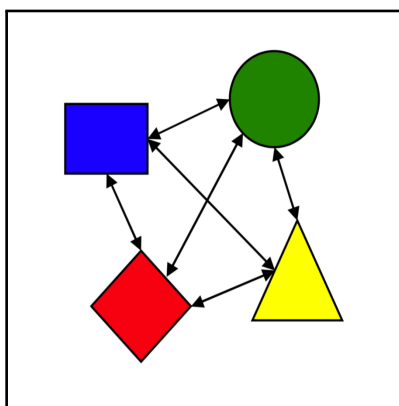


Figure 3.6: Contact pairs definition [20]

As a consequence of using contact pair algorithm in ABAQUS /Explicit there are two mechanical constraint formulations that need to be considered: **kinematic contact method** and **penalty contact method**, (please note that the theory behind these two models was described in section 2.5.2). The kinematic contact algorithm is described by master-slave contact pair. "The kinematic contact algorithm uses a kinematic predictor/corrector contact algorithm to strictly enforce contact constraints (for example, no penetrations are allowed). The kinematic contact algorithm has no influence on the stable time increment" [34]. The contact pair algorithm uses the kinematic contact method by default, which is the chosen one for the simulations in this master thesis. However, it is possible to use the penalty method as an alternative [34].

### 3.3.3 Hard contact

Furthermore, the solver should account for "hard contact". By use of hard kinematic contact, penetration of surfaces is limited. "However, after the initial weighted correction is applied, it is possible to still have some penetration of the surfaces. Therefore, Abaqus/Explicit uses a second contact correction to resolve any remaining overclosure

in a balanced master-slave contact pair that uses hard kinematic contact” [34]. Apparently, this turned out to be an essential part of interaction modelling, especially during simulations containing multi-steps analyses creating hysteresis curves. If the command, ”allow separation after contact” is toggled on, the O-rings will separate through the rigid wires when loading. If toggled off, the surfaces are not allowed when load is applied. If separation is not allowed during unloading, the surface areas of the components which have been in contact will remain touching to each other and the possibility of distorted elements occurring is high, leading to wave speed propagation error<sup>1</sup>. This significantly improved the representation of the O-ring simulation and contact interactions. Summarizing, the solver should **not** allow separation during loading, and allow separation during unloading.

### 3.3.4 Subsequent steps

For analyses conducted in this master thesis the contact and interactions conditions differ from model to model depending on the number of loading steps, how many O-rings are present, if there are side walls and whether the side walls contribute to pre-tension. If the same contact condition is valid for two or more subsequent steps, it only needs to be defined in the first step as ABAQUS automatically propagate for the next steps. If it is desirable to change the interaction properties from one step to the next, it is necessary to assign the properties to each step in the interaction manager. The contact definition as well as the boundary conditions require careful consideration for each step they are active.

### 3.3.5 Friction

Regarding contact properties, it is necessary to consider frictional behaviour either if there is no friction, i.e. frictionless, or specify a coefficient of friction. For the simulations conducted, the coefficient of friction is assumed to be 0.5 between all mating surfaces. This is a rough approximation with basis in a selection of internet searches. There is a considerable uncertainty related to this assumptions in which will be discussed in section 5.2.2. Still, for some cases 0.0, 0.2 and 1.0 is used to emphasize a phenomenon. For simplicity, there will be no distinction between static, run-in or dynamic friction during the analysis which theory is presented in section 2.4.1.

Mechanical challenges does often have a certain level of friction between mating surfaces in an assembly. It can be useful to analyse the situation or the challenges both with and without friction. ”The friction coefficient can depend on slip rate, contact

---

<sup>1</sup>Wave speed describe at which speed a wave travels, while wave speed propagation describe how fast a wave propagates. If the wave speed propagation is to high in one or more elements, the analysis become unstable and will be aborted.



pressure, temperature and field variables. By default, it is assumed that the friction coefficients do not depend on field variables” [34]. The friction model available in ABAQUS is the Coulomb friction model which in its general form allows the friction coefficient to be defined in terms of slip rate, contact pressure, average surface temperature at the contact point, and field variables. The Coulomb friction model is one of the most commonly used frictiona Equation 3.2:

$$F_f = \mu N \tag{3.2}$$

$F_f$  represent the frictional force,  $N$  represent the normal force and  $\mu$  is the friction coefficient. The friction coefficient strongly depend on the surface of the parts in contact. The roughness, lubrication and the geometry of the parts have influence on the coefficient. The basic Coulomb friction model represent the maximum allowable shear stress across the contact area to the contact pressure between the surfaces involved for the connecting bodies [34].

### 3.4 Boundary conditions

In general, boundary conditions define how the components are supposed to behave during the analysis. Boundary conditions are important as they define the behaviour of various components during a simulation. Several aspects are affected by boundary conditions, such as movement of parts in an assembly, parts fixed, where the load is applied and the magnitude of the applied load. Alternatively to applying a load, it is possible to define an enforced displacement, an approach which is followed in this master thesis. The sequence of boundary conditions, and in which step the respective ones are active, is defined in the boundary condition manager. As an example, the case in which the side walls are fixed, the bottom wire is fixed and the upper wire is allowed to move in vertical direction is defined for the initial step. The movement of the upper wire in the vertical direction is assigned to consecutive load step. If the side walls are contributing to a pre-tension state for the O-ring, the movement of the O-rings is defined in the particular load step. An example of how this is defined during an analysis where the loading and unloading are done in consecutive multiple steps to create the stable hysteresis loops are shown in Figure 3.7:

Name	Initial	Load_step_1	Load_step_2	Unloading_step_1	Load_step_3	Unloading_step_2	Load_step_4	Unloading_step_3
BC-1	Created	Propagated	Inactive	Inactive	Inactive	Inactive	Inactive	Inactive
BC-2			Created	Propagated	Propagated	Propagated	Propagated	Propagated
Fixed_Bottom	Created	Propagated	Propagated	Propagated	Propagated	Propagated	Propagated	Propagated
Fixed_Sides			Created	Propagated	Propagated	Propagated	Propagated	Propagated
Fixed_Top	Created	Propagated	Inactive	Inactive	Inactive	Inactive	Inactive	Inactive
Leftwall_displ		Created	Inactive	Inactive	Inactive	Inactive	Inactive	Inactive
Rightwall_displ		Created	Inactive	Inactive	Inactive	Inactive	Inactive	Inactive
Vertical_displ			Created	Inactive	Inactive	Inactive	Inactive	Inactive
Vertical_displ_2					Created	Inactive	Inactive	Inactive
Vertical_displ_3							Created	Inactive
Vertical_unloading							Created	Inactive
Vertical_unloading_2								
Vertical_unloading_3								

Figure 3.7: Example: Boundary Condition manager

The definition of boundary conditions varies from model to model. The lower wire represents the bottom of the groove and is fixed in all the models independently of how many, and which steps are active. For assemblies with side walls providing pre-tension, the wires have an enforced displacement varying from 0.00 mm to -0.20 mm in a load step before the vertical enforced displacement is active. When the side walls have moved

the given magnitude, the vertical displacement is active in the next loading step. The response from the vertical loading step is of particular interest and the force needed to compress the O-ring the given enforced displacement is retrieved from the reference point of the upper wire. This enforced displacement vary for most of the simulations models as a results of different size of the groove. For a smaller groove, the possible vertical displacement is less than for a wider groove, meaning that it was necessary to tune the enforced displacement to fint the point where Equation 3.1 were fulfilled. A enforced vertical displacement for the upper wire of approximately 2 mm was considered sufficient to recreate the experimental curves shown in Figure 4.2 (presented in section 4.2).

As a matter of fact, modelling with analytical rigid wires requires definition of a reference point(s) where mass and inertia are excluded. In addition to assigning boundary conditions, loads and movements; the force mangitude needed to obtain the enforced displacement can be retrieved from this paricular points. The reference point is used to indicate the rigid body reference point if the part is either a discrete or an analytical rigid part. The reference points will appear on each instance when creating an assembly. The interaction module can be used to apply contact conditions, while the load module can be used to either apply load or boundary conditions, such as an enforced displacement. Motion or constraints applied to the reference point are then applied to the entire rigid part [36]. Figure 3.8 shows the boundary conditions applied to the reference points.

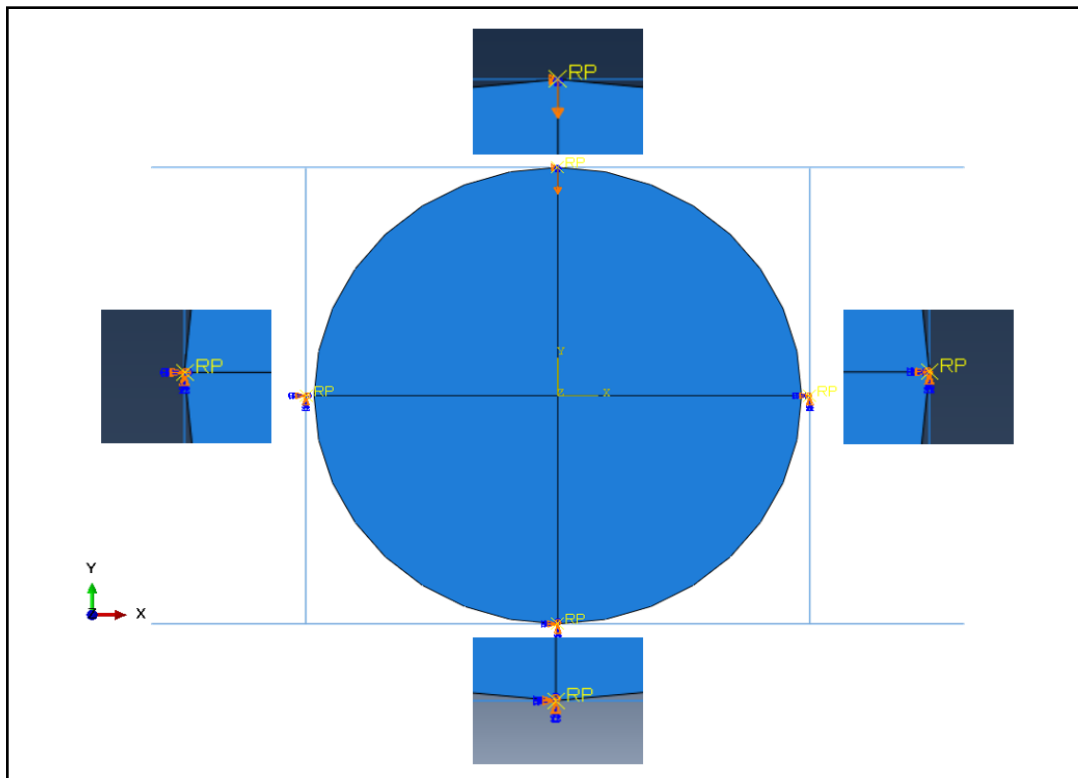


Figure 3.8: Boundary conditions

### 3.4.1 Amplitude

Boundary conditions applied during an explicit step require an amplitude to define the variation in time. Amplitude is used to control the enforced displacement sequence. In other words, it is necessary to define the time relative to the simulation step. Figure 3.9 shows how the amplitude is defined for the simulations:

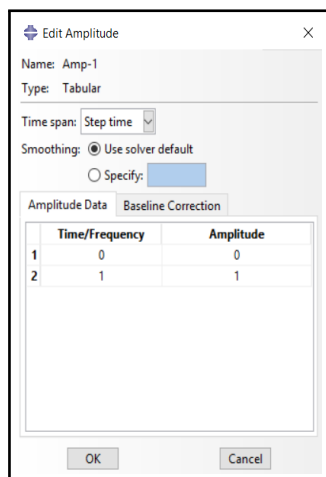


Figure 3.9: Editing amplitude

To clarify, when the time is 0, the simulation is at its initial step, while at time equal to 1 the simulation step is finished. The amplitude equal to one can be interpreted as 100 % of the simulation. For instance, if a simulation is significantly more complex than compression of O-rings in two dimensions, the simulation time is probably longer. It is then appropriate to write, for instance 20 in the time bracket and 1 in the amplitude bracket indicating a 20 seconds simulation.

## 3.5 Material Approach

Normally, incompressible materials such as NBR are assumed to have hyperelastic properties. Several studies, as for instance [21], [6], [7], [8] and [15] have presented their work analysing elastomeric materials using hyperelasticity. As mentioned in section 2.3.2, numerical analysis of hyperelasticity strictly depends on access to experimental tests data and information regarding how the tests are conducted to obtain the most correct hyperelastic material model.

If experimental data is unavailable, it is challenging to derive the hyperelastic model correctly because the material behaviour depends on how the material are processed [33]. As a result of limited experimental test data, it was decided to approach the material behaviour of elastomeric O-ring compression sequence as a linear-elastic problem. Considerations associated with this approach, and why it is reasonable to use it for this particular case, is covered in section 5.1.3.

Generally, NBR is described by a shore hardness number which is decided through a hardness test<sup>2</sup> instead of a modulus. Due to the fact that the linear-elastic material approach mainly refers to the Young's modulus and the Poisson's Ratio [41], it is necessary to use the hardness number to calculate an approximate modulus.

However, there is a direct correlation between the shore hardness number and the Young's modulus. There are certain ways to calculate the modulus from this hardness number. In 1958, Gent [14] presented his work where he derived a relationship between the ISO hardness and the Young's modulus. This relationship is perhaps the most widely known way of describing the relationship between the modulus and the hardness number [24]. Thus, the Gent equation is used to convert the shore hardness to the elasticity modulus in this master thesis:

$$E(MPa) = \frac{0.0981(56 + 7.66s)}{0.137505(254 - 2.54s)} \quad (3.3)$$

Where  $s$  is the Shore hardness number, which is 70 and 90 for the O-rings considered, and hence:

$$E(MPa) = \frac{0.0981(56 + 7.66 * 70)}{0.137505(254 - 2.54 * 70)} \quad (3.4)$$

Assuming Shore hardness number 70, the Young's modulus is calculated:

$$E_{Shore70A} \approx 6MPa \quad (3.5)$$

$$E(MPa) = \frac{0.0981(56 + 7.66 * 90)}{0.137505(254 - 2.54 * 90)} \quad (3.6)$$

Assuming Shore hardness number 90, the Young's modulus is calculated:

$$E_{Shore90A} \approx 21MPa \quad (3.7)$$

Regarding the linear-elastic approach; if the pure material behaviour was supposed to be described, this approach will probably not be appropriate since: "Viscoelasticity approximates the time-dependent behaviour and hyperelasticity only approximates the mechanical response for the elastomers" [37]. In general, most of the NBR in Shore 70A and Shore 90A hardness have an E-modulus within the range of 2 MPa and 30 MPa.

---

<sup>2</sup>The hardness testing are conducted as a durometer hardness test. This is a pretty simple, inexpensive and fast testing method for hardness of elastomers [24].

This is very low compared to materials such as steel which have an Youngs modulus of about 210 000 MPa. The low elastic modulus illustrates why a linear-elastic approach can be challenging to use for the analyses, because the linear region of the stress-strain curve is extremely short or negligible. The Poisson's Ratio is assumed to be close to 0.5 for incompressible materials. According to Trelleborg Sealing Solutions, the density for Shore 70A is  $1.25e - 9\text{tons}/\text{mm}^3$  and  $1.30e - 9\text{tons}/\text{mm}^3$  for Shore 90A. The values for elastomers actually vary but, for simplicity,  $1.30e - 9\text{tons}/\text{mm}^3$  is assumed for all the simulations.

In addition, two other models, the Reuss model and another model where G (shear modulus) is used for converting the hardness number to Young's modulus. These are presented in Appendix F. Nevertheless, the Reuss model tends to, in general, give higher modulus than the Gent equation. The Gent equation is widely used to describe the correlation between the elastic modulus and the durometer hardness and it tends to give a good approximation [24]. As a result of these calculations, a Young's modulus of 6MPa and 21MPa is used for Shore 70A and Shore 90A respectively in the performed analyses.

### 3.6 Mesh and elements

Consideration of mesh structure, element size and control of elements is essential in FEM analyses. However, independently of modelling space dimensions, this is more important in analyses where stresses are considered; because mesh refining can detect high local stresses which elements of large size would not be able to capture. In this master thesis where the force versus displacement behaviour is of particular interest. The element size and the elements are of capital importance and should be considered, but if stresses do not change dramatically when changing the element size from, e.g, 0.3 to 0.5; results will not be affected, irrespectively of which value is used.

Since analytical rigid surfaces in ABAQUS represent a theoretical rigid surface, no mesh is required. By using analytical rigid surfaces, the computational time are minimized and the potential element error is reduced since these surfaces have no elements. In comparison, the discrete rigid alternative requires mesh of the surfaces. The O-ring in this master thesis is represented as a two dimensional deformable shell and hence requires a mesh and a thoughtful consideration of the element geometry and size. Depending on which of the material behaviour approaches is chosen to analyse the material, different types elements are required. When doing hyperelastic material model analysis, where the material is incompressible, the use of hybrid elements is recommended by both PLM technology [33] and Dassault Systèmes [34]. This is just an alternative in ABAQUS/Standard and not in ABAQUS/Explicit [37]. Unfortunately, hybrid elements cannot be employed for two dimensional problems in ABAQUS/Explicit due to element definition not being

supported in this software version.

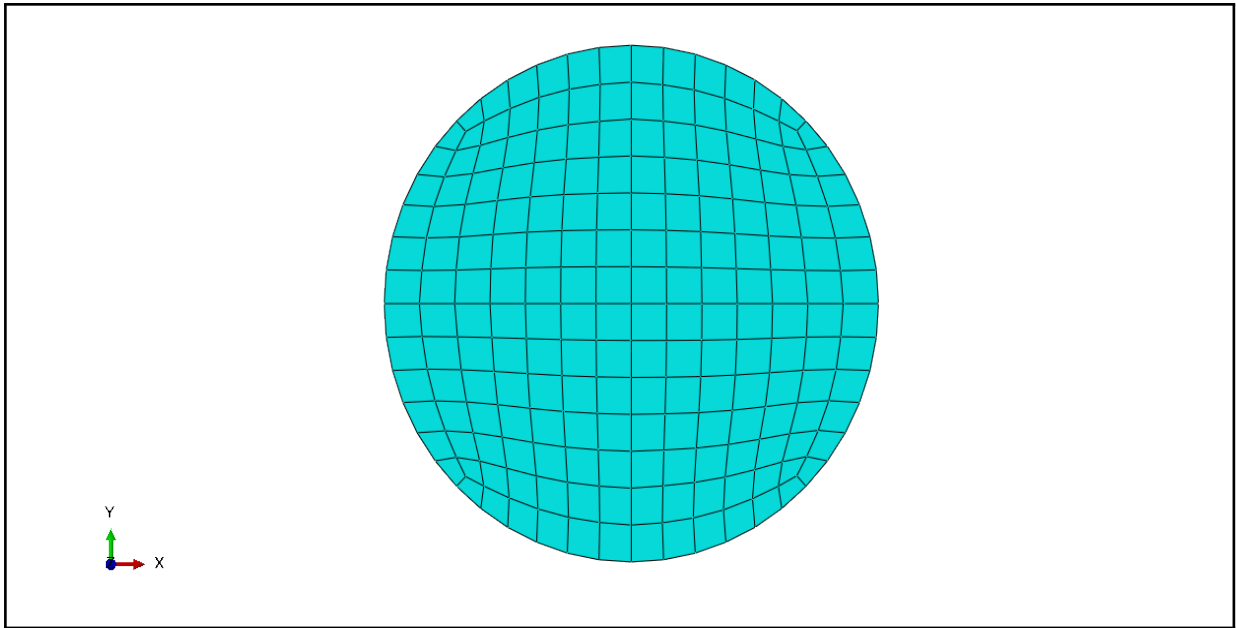


Figure 3.10: Mesh of the O-ring

Commonly, the element size is set to 0.3 in most cases when using a structured quadrilateral mesh. Partitioning the O-ring into four equal parts helps refining the structured mesh. Additionally, attempts with smaller elements have also been tried, but introduced negligible changes in stress. In order to avoid difficulties with wave propagation speed and distorted elements, the largest element size with negligible deviation in stress were chosen. Additional considerations associated with the mesh is covered in section 5.1.6.

## 3.7 Final models

### 3.7.1 One O-ring

This subsection presents the final assemblies containing one O-ring used in the analyses obtaining the required load deflection curves. The rectangular groove is modelled with different offsets for the side walls of the groove, in order to observe trends in the force response of the end seal when tolerances between the size of the groove and the size of the O-ring vary. The offset of the side walls is given five different parameters; 0.00 mm offset (the walls are tangential to the O-ring), 0.05 mm, 0.10 mm, 0.15. and 0.20 mm for a groove wider than the ring diameter. For the tolerances where the rectangular groove are smaller than the O-ring; values of -0.025 mm, -0.05 mm, -0.10 mm and -0.15 mm in addition to 0.00 mm are chosen.

Figure 3.11 shows one O-ring with side walls and 0.00 mm offset. All of the four wires are analytical rigid while the O-ring is deformable a shell.

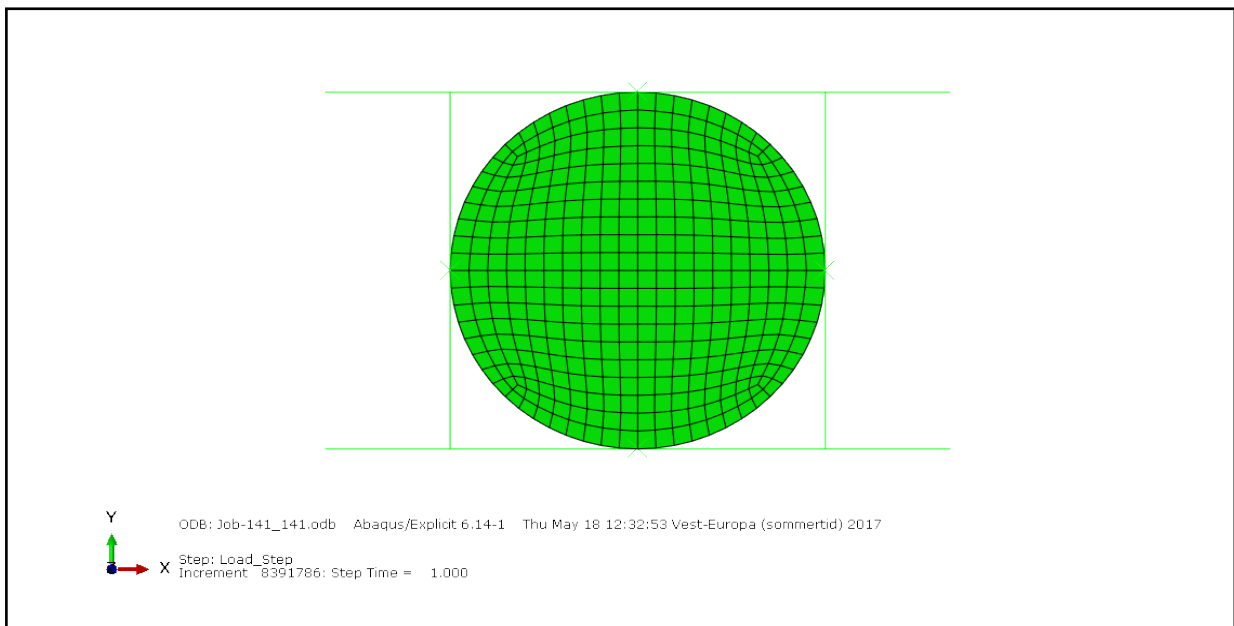


Figure 3.11: Inital step

In order to illustrate the situation where the groove is smaller than the diameter of the end seals, a load step where the side walls provides pre-tension is added ahead of the load step of the vertical wire. As shown in Figure 3.12, the tension increases at the sides of the O-ring when the side walls are moved a certain distance from both sides, towards the center, resulting in a groove smaller than the O-ring diameter. This is used selecting the models to obtain a theoretical tension representing the situation where the O-ring is larger than the groove. The tension is indicated by a slightly lighter blue colour at the regions in contact with the side walls.



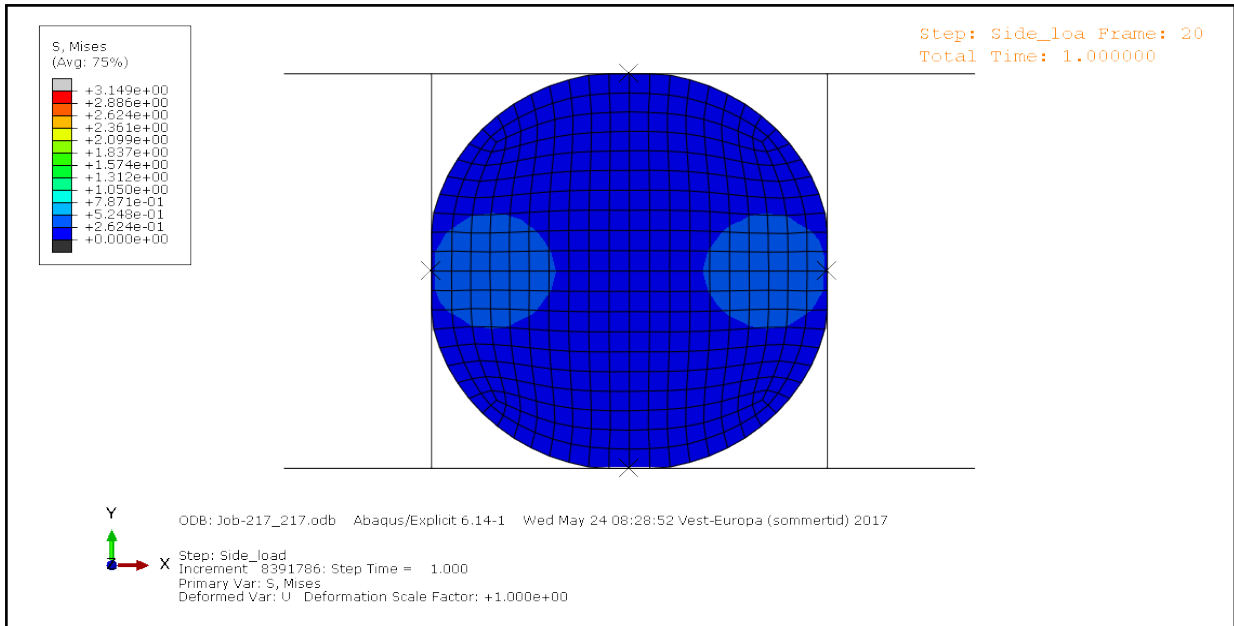


Figure 3.12: Pre-tensioned step

Figure 3.13 shows the O-ring after the vertical step. In this case, a pre-tensioned step is followed by a vertical displacement of the upper wire, compressing the O-ring down. This vertical displacement is the enforced displacement retrieved from the reference point of the upper wire.

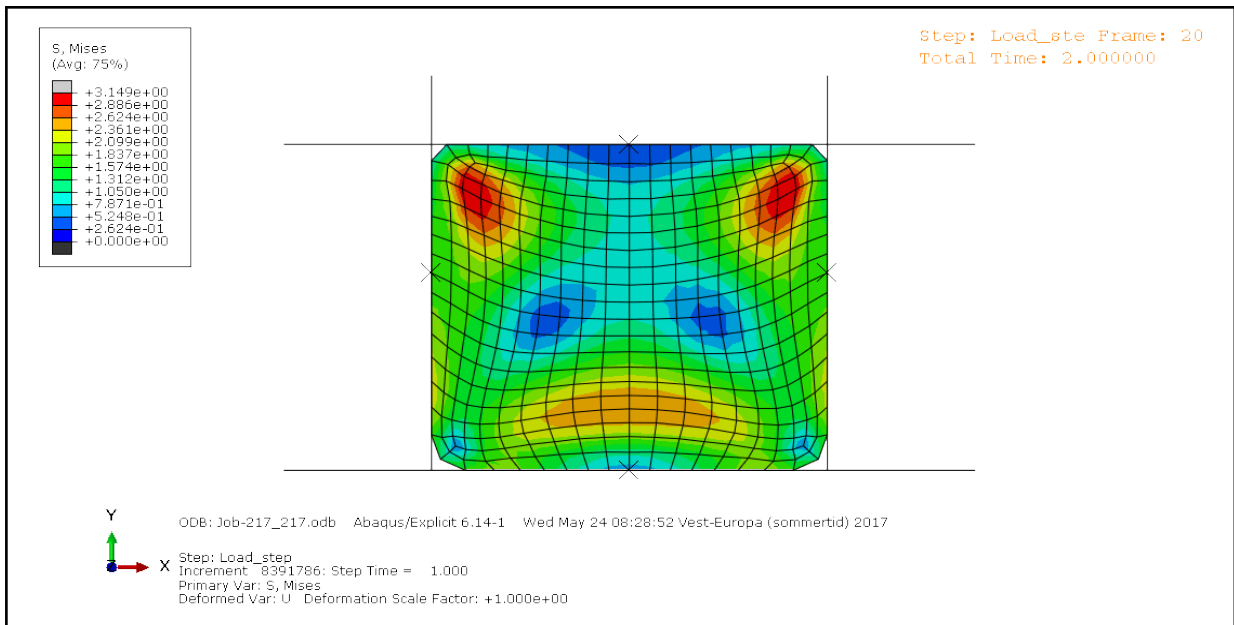


Figure 3.13: Final compression

### 3.7.2 Two O-rings

This subsection will present the final models used to obtain the load deflection characteristics for two O-rings in compression. It was of particular interest to observe how the O-rings behave when positioned differently according to one another. It is chosen to analyze three different positions, with different offsets for the side walls of the groove and with multiple steps to observe hysteresis effects. Similarly to the case for one O-ring, the offset for the side-walls varies from both sides.

The following models present three different positions. Position 1, in which the two O-rings are one above the other as illustrated in Figure 3.14 is the most common positioning:

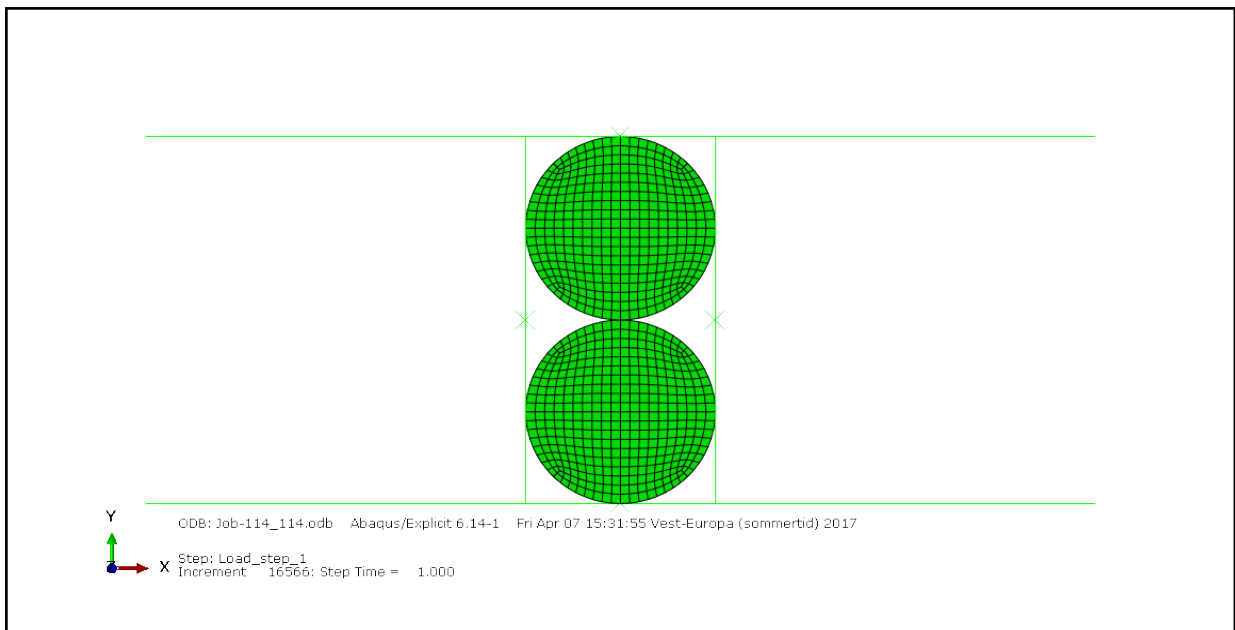


Figure 3.14: Position 1

Figure 3.15 shows position 2, where the center of the two O-rings are skewed an angle,  $\beta=45^\circ$  relative to one another.

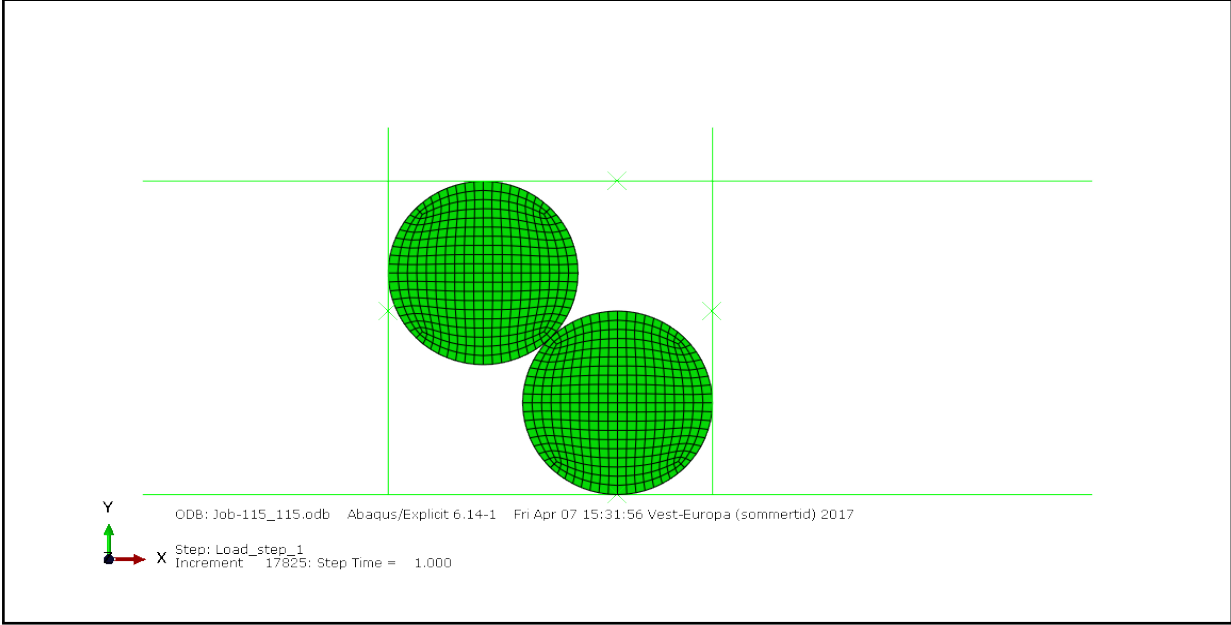


Figure 3.15: Position 2

Figure 3.16 shows position 3, where the two O-rings are skewed an angle,  $\beta=22.5^\circ$  relative to each other's center.

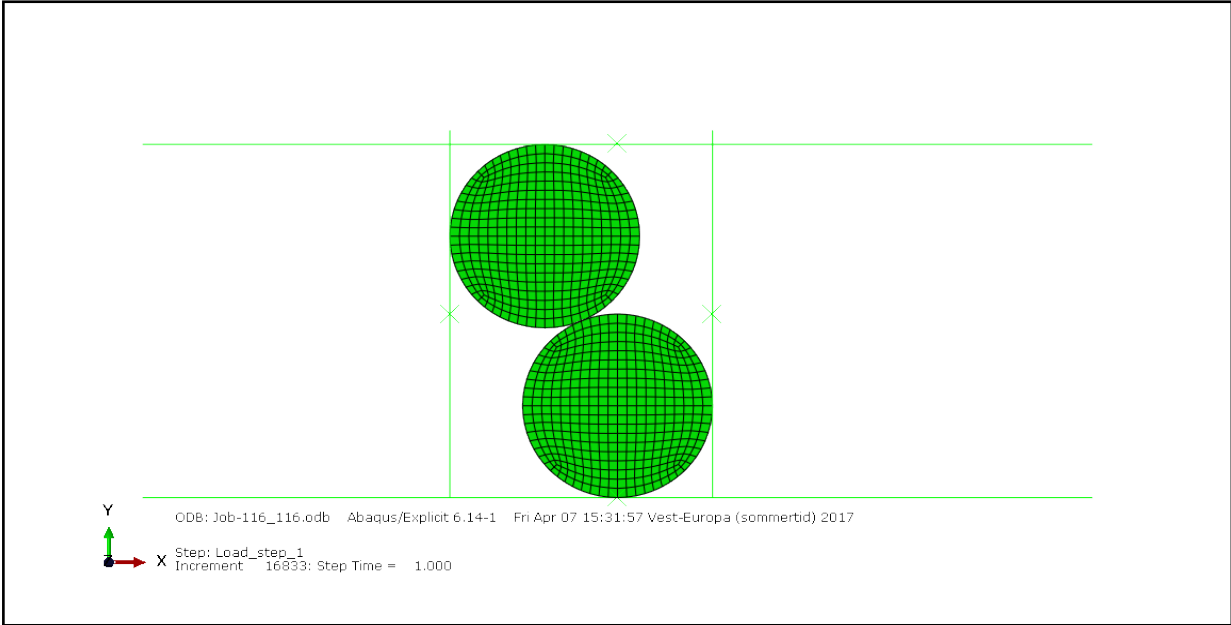


Figure 3.16: Position 3

The set-up of the models with two O-rings is very similar to the case for one, but since there are two rings, the need for additional boundary and interaction conditions is present. The definitions of the reference points are similar to the models with one O-ring.

### 3.8 Triangular Groove

The geometry of the sealing groove where the mouldings are incorporated is usually rectangularly shaped. For experimental reasons, it is also relevant to analyze how the seal behave if the geometry of the groove is changed. Different experiments where the surfaces form a triangular groove, by removing the lower wire is conducted. In this situation, the coefficient of friction is becoming essential. By what angle,  $\alpha$  between the two surfaces forming the triangular groove, does the O-ring stick with a consistent coefficient of friction? In the case of calculating  $\alpha$ , both analytical and numerical models are conducted for comparison. The coefficient of friction is set to be 0.5 between the triangular steel surfaces and the rubber O-ring for these particular analyses.

In Figure 3.17 the triangular case with varying angle between the side walls can be seen.

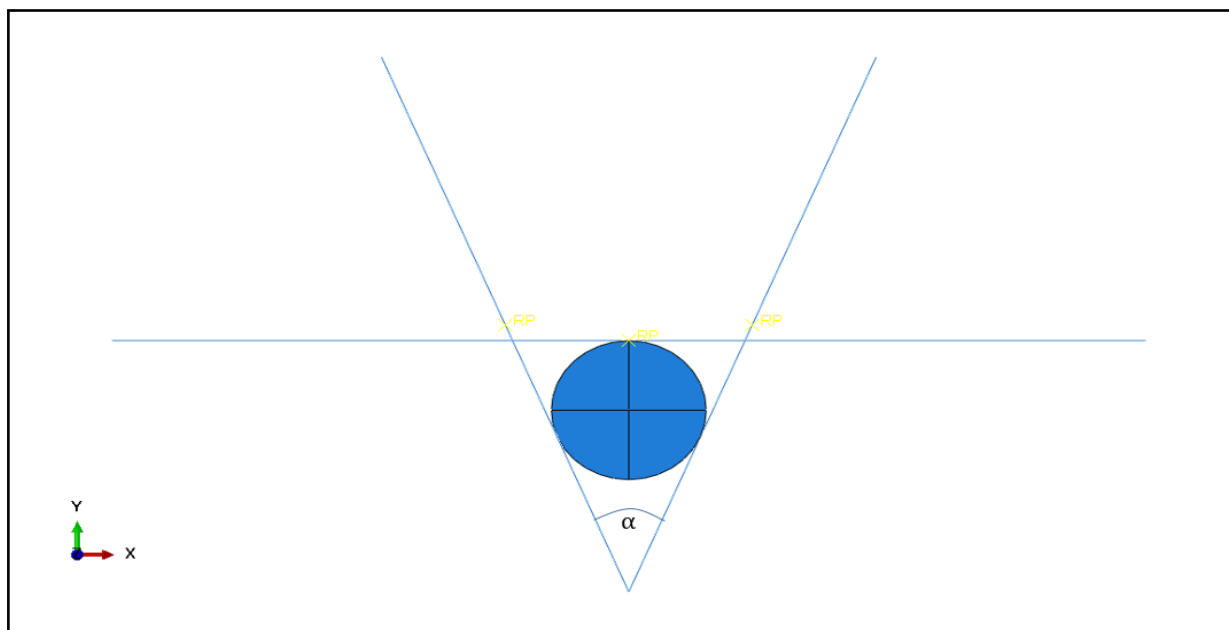


Figure 3.17: Triangular groove

#### 3.8.1 Numerical calculations

Using ABAQUS for calculating the critical angle,  $\alpha$  in Figure 3.17 for the triangular groove is done by conducting analyses where several values for the angle are chosen in order to approximate the one in which the O-ring will stick to the side walls. The model is constructed with varying angles between the surfaces. First, by performing simulations with  $\alpha$  equal to;  $30^\circ$ ,  $45^\circ$ ,  $60^\circ$ ,  $75^\circ$  and  $90^\circ$  it was possible to delimit the interval in which the boundary between slip and stick for the O-ring lies. In a second approach, several values within this interval was tested to find the exact limit of stick and slip. Please note that in these simulations, the upper wire was assumed to the O-ring with 2 mm in vertical direction. For the Shore 70A hardness with a friction coefficient of 0.5, the

stick/slip limit was found to be in between  $50^\circ$  and  $55^\circ$  interval. When comparing the numerical result with the analytical solution, the latter ( $50^\circ - 55^\circ$ ) resulted to be twice as big for the numerical result; because the situation were simplified for the analytical calculations.

It should be noticed that, as for the particularities of the components in terms of material properties, cross sectional diameter, part definitions and contact interactions; they are actually equal to those employed in the simulations with rectangular grooves. Hence, for the sake of brevity, the aforementioned particularities will not be repeated here. The results from the simulation will be presented in section 4.8. Figure 3.18 illustrate the model used for numerical calculations.

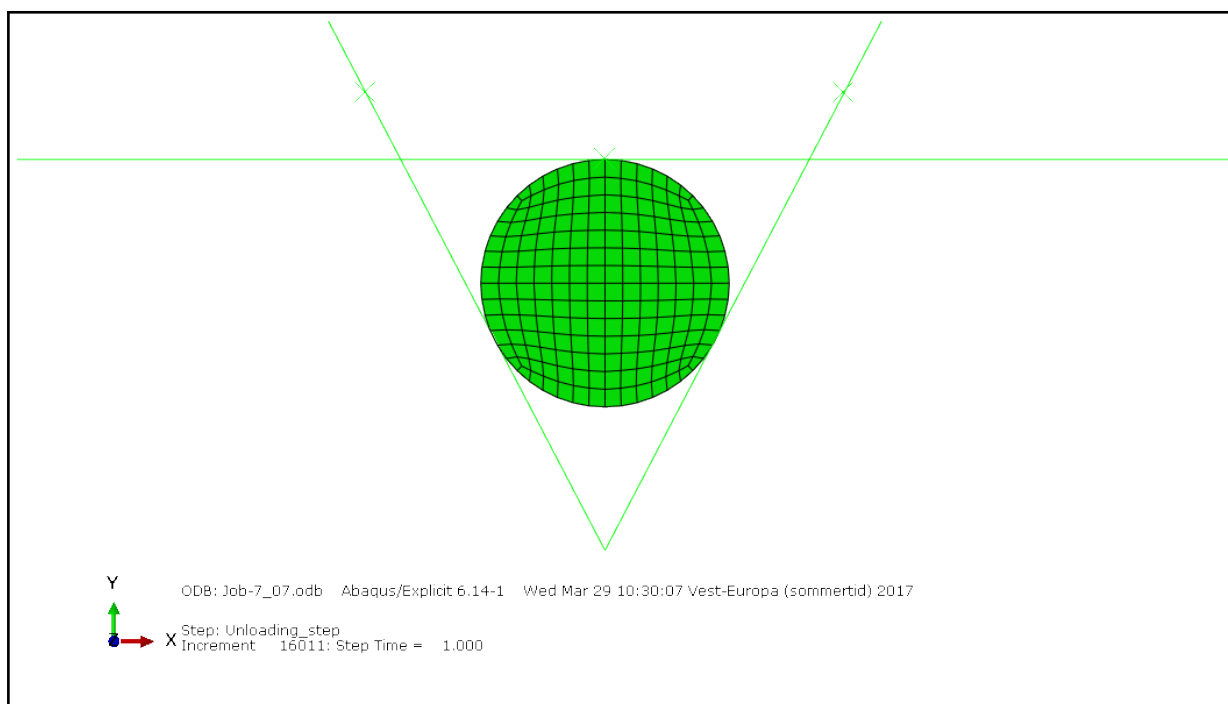


Figure 3.18: Triangular groove model used for numerical calculations

### 3.8.2 Analytical calculations

In order to validate the modelling and the numerical results obtained in ABAQUS for the rectangular groove, an analytical study of this simple cases has been performed. The material behaviour from the physical tests can be compared to numerical analysis done in ABAQUS. Yet, the analytical studies in this thesis work are simply limited to the frictional behaviour and specifically to the case where the geometry changes for the groove, from rectangular to triangular.

In order to solve the analytical calculations, the Coulomb friction equation is employed. The basic formula is shown in Equation 3.2, and by introducing a friction coefficient of 0.5 for rubber against steel, the slip angle between the O-ring and the surfaces can be calculated from Equation 3.8. Figure 3.19 shows the actual case of surfaces forming

a triangular groove, while Figure 3.21 show the simplified approach used for analytical calculations.

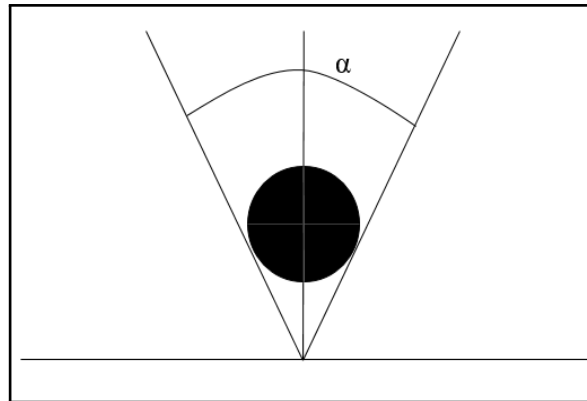


Figure 3.19: Triangular angle

In order to calculate the angle  $\alpha$  analytically both symmetri and conventional friction calculating; illustrated by a sliding box, is used for simplicity. Figure 3.20 shows the actual case of surfaces forming a triangular groove assuming symmetri:

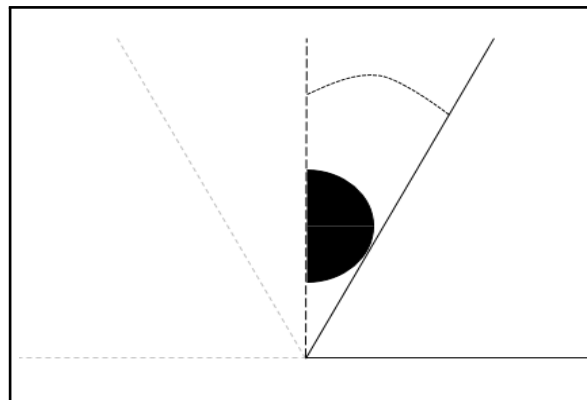


Figure 3.20: Symmetric model

Figure 3.21 shows the simplified case of surfaces forming a triangular groove:

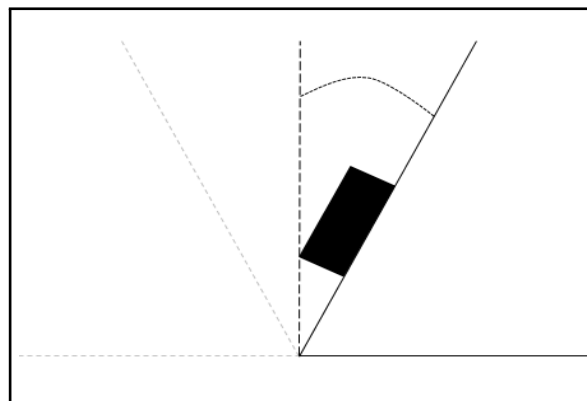


Figure 3.21: Simplified model

Figure 3.22 shows the resulting forces:

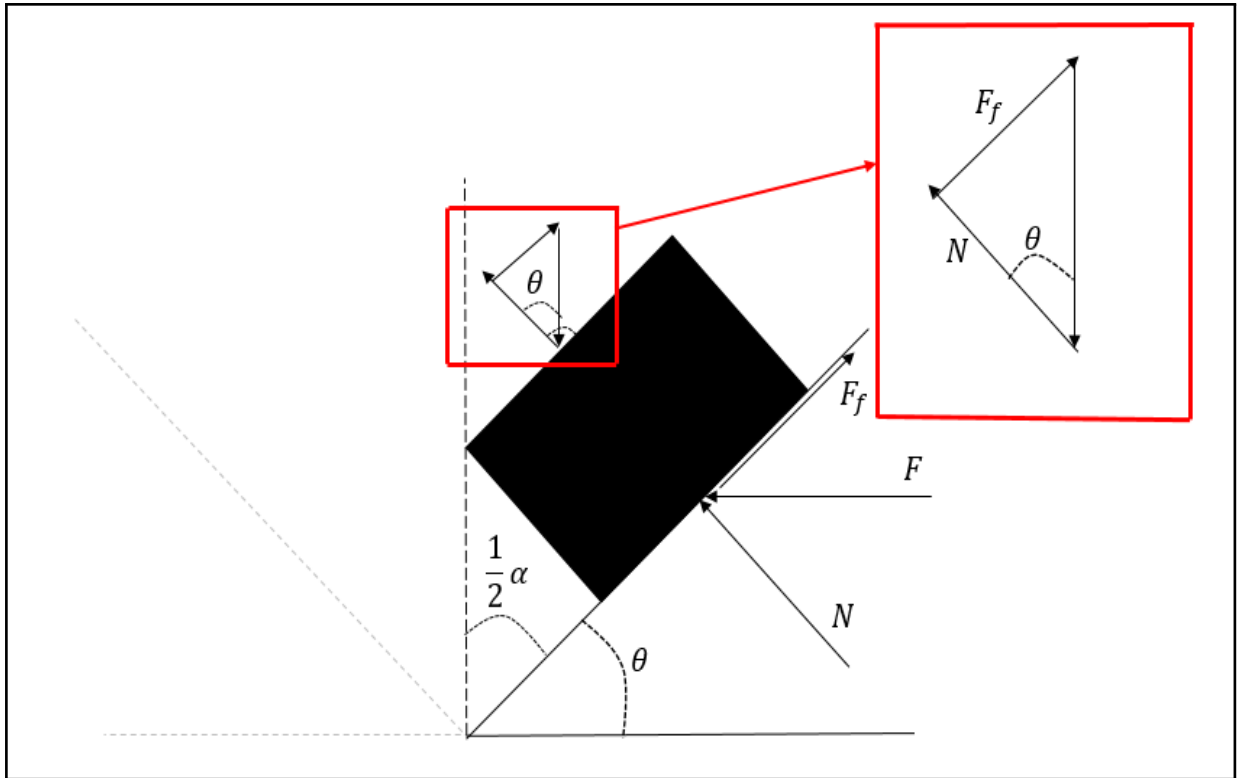


Figure 3.22: Friction forces

From trigonometric relationship it is derived that:

$$\tan\left(\frac{1}{2}\alpha\right) = \mu \quad (3.8)$$

Note that  $\frac{1}{2}\alpha = \theta$ . It is also important to notice the consequences due to the usage of symmetry. The angle  $\frac{1}{2}\alpha$ , have to be mutiplied with the factor 2 to obtain the correct result.





# Chapter 4

## Results

In this section, the results pertaining to the analyses discussed in previous sections are presented. The experimental tests results serve as reference curves for the numerical analysis. The results in this chapter are categorized as subsections depending on the following parameters:

- One or two sealing elements
- Shore 70A and Shore 90A material hardness
- Cross-sectional diameter 5 mm and/or 6 mm
- Side walls with or without a pre-tensioning step
- Side wall offset varying from (0.00 mm to -0.20 mm) and (0.00 mm to 0.20 mm)
- Hysteresis loops
- Two O-rings, one above the other in three different positions
- Slip through phenomenon
- Results from triangular groove experiment(both numerical and analytical)
- Comparisons of the aforementioned parameters

As mentioned in section 3.4, a reference point is assigned to each of the rigid wires. Boundary conditions are assigned to the reference point. The force response results from the applied enforced displacement is retrieved from this point.

In addition to the results of the numerical analyses for the rectangular groove, numerical and analytical results for triangular groove friction angle will be presented.

## 4.1 Description

For the purpose of readability, there is consistency related to a selection of the parameters presented throughout this chapter. In general, offset of side walls (-0.025 mm to -0.15 mm) indicates side wall displacement contributing to pre-tension in the material. Notice, pre-tension of for instance -0.05 mm by the side wires are from both sides resulting in a total groove 0.1 mm smaller than the O-ring ring diameter. Furthermore, offset of side walls (0.05 mm to 0.20 mm) indicates side walls contributing to the opposite of pre-tension in terms of a groove too wide for the incorporated O-ring.

The parameters for each of the resulting diagrams will be presented in tables ahead of the result figure. In the respective table; the coefficient of friction ( $\mu$ ), the offset of side walls, cross section diameter and material hardness is presented. The reason some curves may have a final force magnitude considerably higher than the curves compared, is the tuning of the enforced displacement. Some simulations converged to a higher force than the ones compared. As a result of using SI units(mm); mm, MPa and tons; the y-axis representing the force in Newton (N) and the x-axis representing the displacement in millimetre (mm). Additional results is presented in Appendix I.

To clarify, Figure 4.1 shows the direction used when referring to the positive and negative direction.

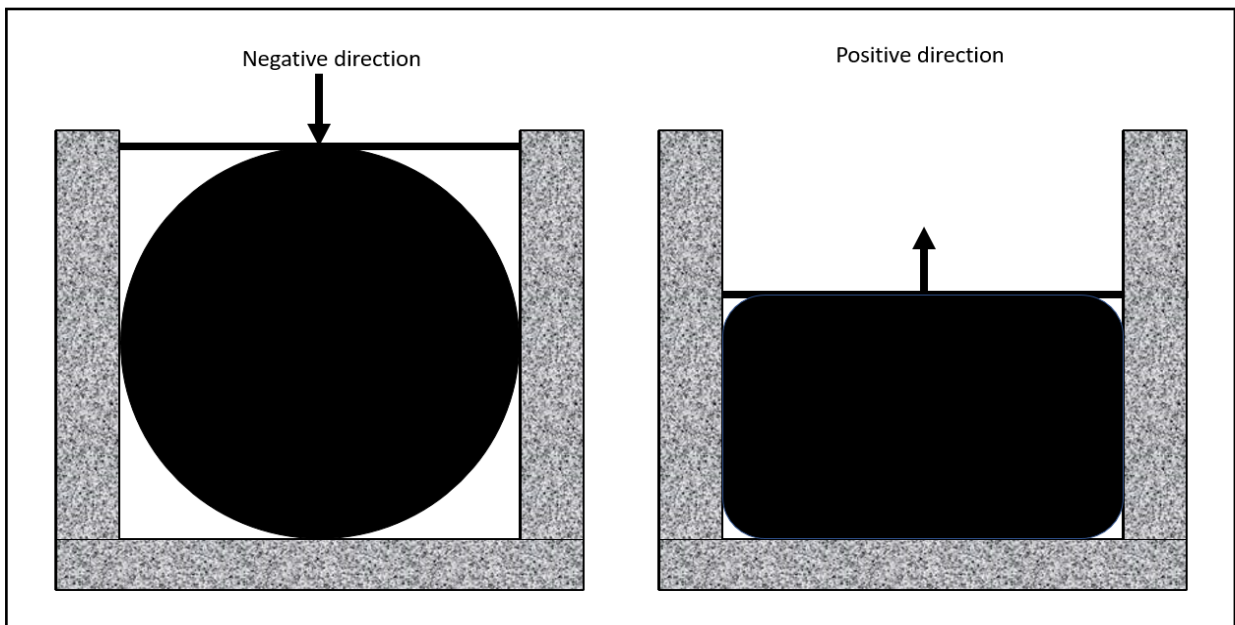


Figure 4.1: Direction explanation

## 4.2 Experimental test result

Figure 4.2 which is adapted from Appendix B illustrates the experimental test results in which serve as comparison basis for the numerical simulations conducted throughout this master thesis. The experimental test result sheet contains curves from the following parameters:

- One sealing element in Shore 70A hardness with cross-sectional diameter 6 mm.
- One sealing element in Shore 70A hardness with cross-sectional diameter 5 mm.
- One sealing element in Shore 90A hardness with cross-sectional diameter 6 mm.
- Two sealing elements in Shore 70A hardness with cross-sectional diameter 6 mm.
- Two sealing elements in Shore 90A hardness with cross-sectional diameter 6 mm.

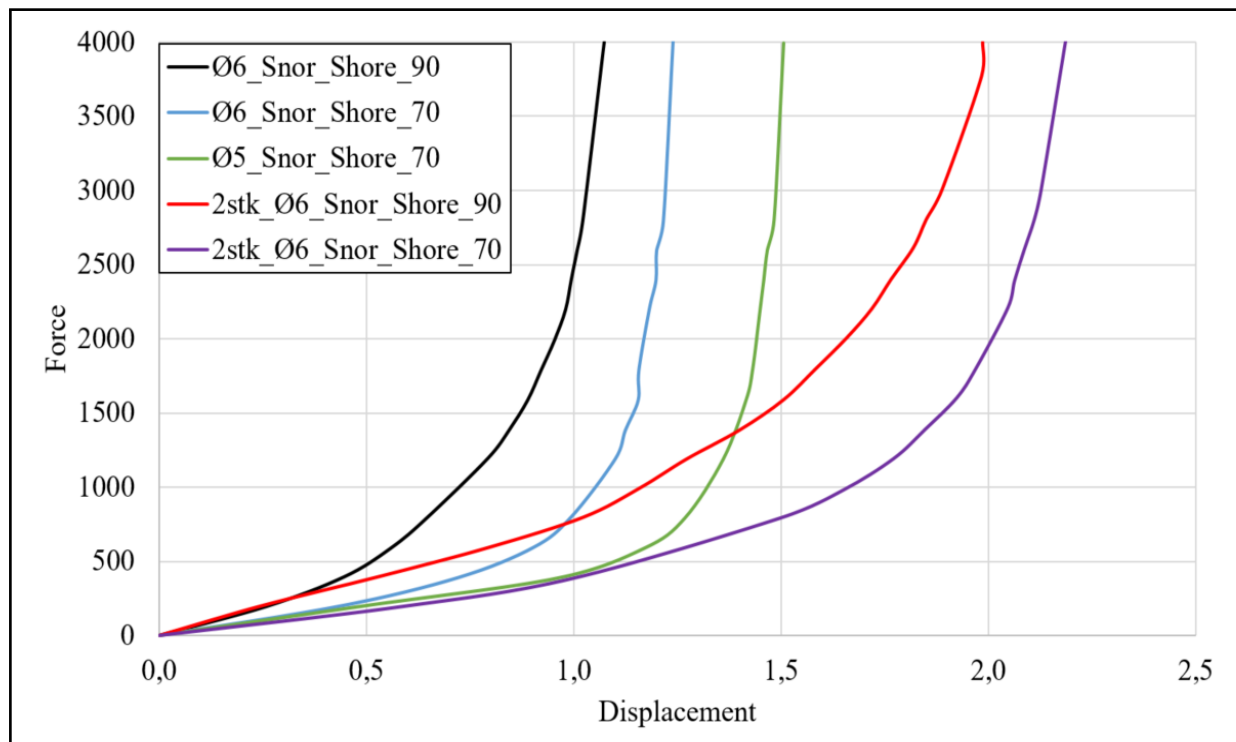


Figure 4.2: Experimental tests [44]

The length of the mouldings used for the experimental tests are 100 mm. To be able to compare these experimental tests to the two-dimensional numerical tests, it was necessary to divide the force over the length to achieve the force over 1 mm. As mentioned in section 3 is this one of the assumption made for the numerical analyses (a thickness 1 mm in z-direction). However, it is important to emphasize that it is unknown how the experimental tests are conducted and which environmental factors that are taken into account. Assumptions associated with the implementation of these tests

is covered in section 5.3. Please note that, for consistency; the experimental curve is the black line in Figure 4.4, 4.5, 4.6, 4.8 and 4.9. This experimental curve is compared to a selection of numerical curves. The parameters for these curves (i.e. numerical) are arbitrary chosen. Additionally, the original test results sheet provided by Rainpower can be found in Appendix B.

### 4.3 One O-ring results

In this section the results of analysis with one sealing element in compression will be presented. Analysis with the following parameters are conducted:

- One sealing element compared to experimental tests
- Sealing element with cross sectional diameter 5 mm or 6 mm
- Shore 70A and Shore 90A hardness
- Numerical results with side walls offset; 0.00 mm, -0.025 mm, -0.05 mm, -0.10 mm and -0.15 mm from both sides, illustrating the situation when the groove is too small compared to the diameter of the O-ring.
- Numerical results with side walls offset; 0.00 mm, 0.05 mm, 0.10 mm, 0.15 mm and 0.20 mm from both sides, illustrating the situation when the groove is too wide compared to the diameter of the O-ring.

Figure 4.3 illustrates the different steps of compression sequence according to the curve. In the last step, it is possible to see how the compressed sealing element fill the rectangular groove as mentioned in section 3.1.

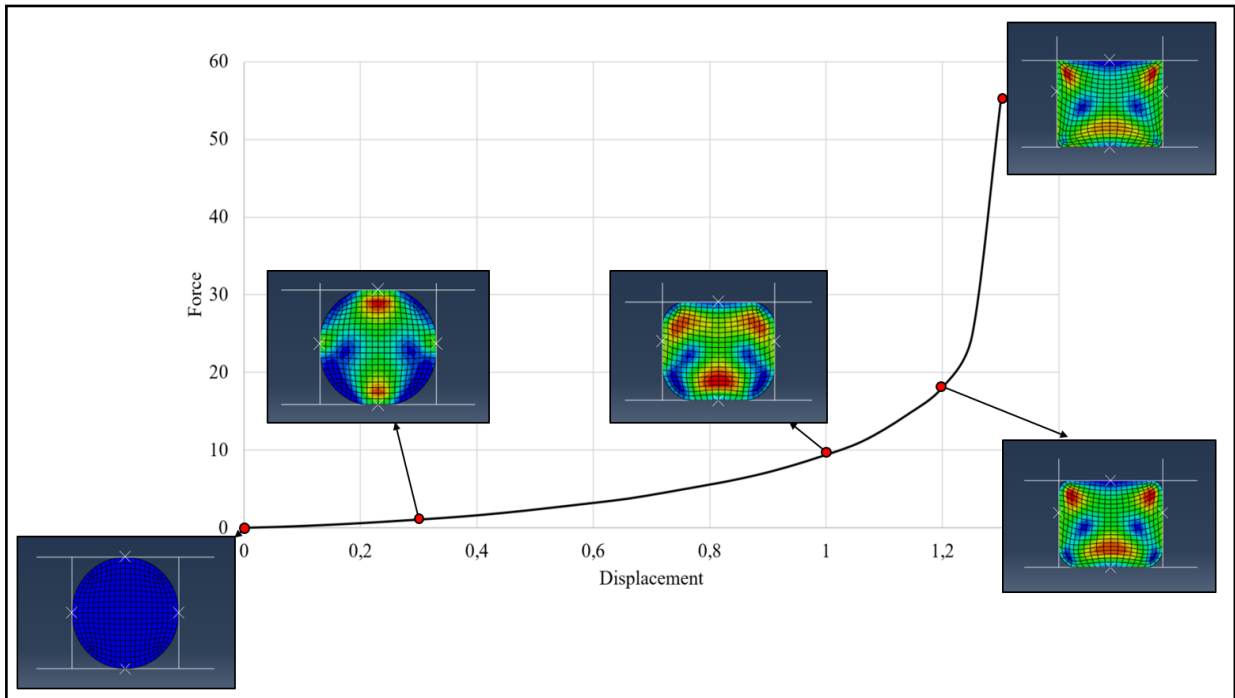


Figure 4.3: Compression steps - A single sealing element

### 4.3.1 One O-ring compared to experimental tests

Figure 4.4 compares a selection of the numerical tests to the experimental tests for a single Shore 70A sealing element with 6 mm as cross-sectional diameter. The parameters for the different tests are presented in Table 4.1.

Table 4.1: Parameters - Shore 70A - 6 mm - One sealing element

Hardness	Cross section	Offset side walls	$\mu$	Test
Shore 70A	6 mm	Unknown	Unknown	Experimental
Shore 70A	6 mm	0.00 mm	0.5	Numerical
Shore 70A	6 mm	-0.025 mm	0.5	Numerical
Shore 70A	6 mm	-0.05 mm	0.5	Numerical

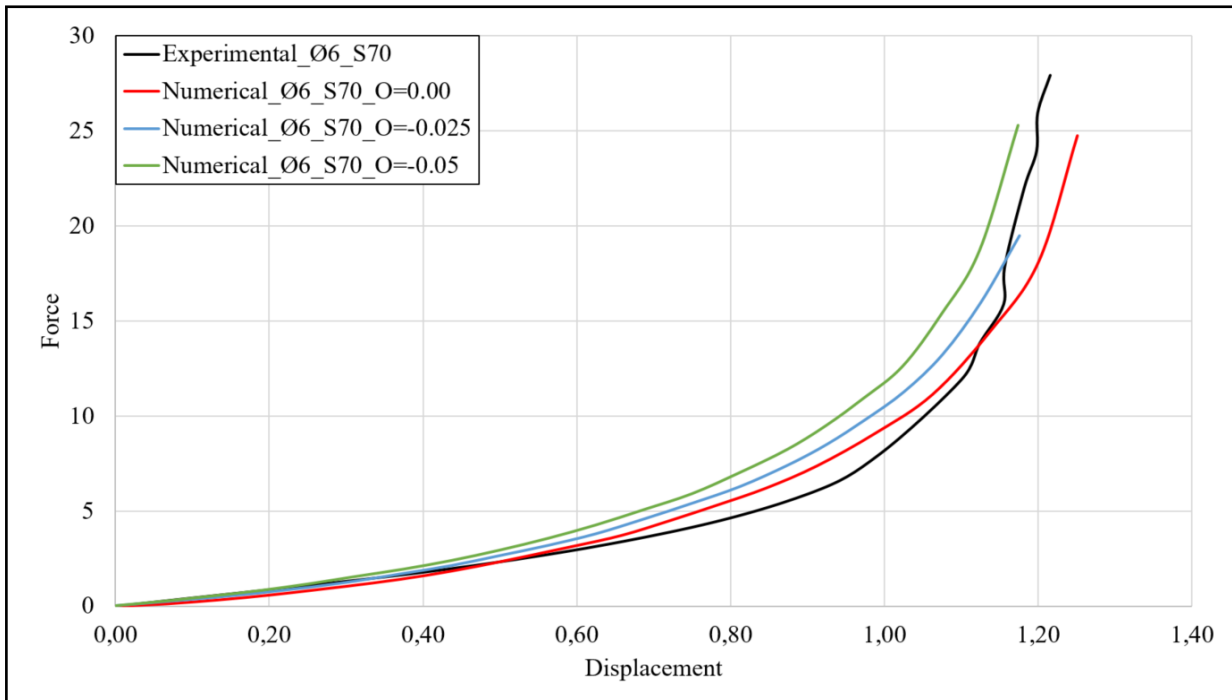


Figure 4.4: Experimental test compared to numerical test - Shore 70A - 6 mm - One sealing element

Figure 4.5 compares a selection of the numerical tests to the experimental tests for a single Shore 90A sealing element with 6 mm as cross-sectional diameter. The parameters for the different tests are found in Table 4.2.

Table 4.2: Parameters - Shore 90A - 6 mm - One ring

Hardness	Cross section	Offset side walls	$\mu$	Test
Shore 90A	6 mm	Unknown	Unknown	Experimental
Shore 90A	6 mm	0.00 mm	0.5	Numerical
Shore 90A	6 mm	-0.025 mm	0.5	Numerical
Shore 90A	6 mm	-0.05 mm	0.5	Numerical
Shore 90A	6 mm	0.05 mm	0.5	Numerical
Shore 90A	6 mm	0.10 mm	0.5	Numerical

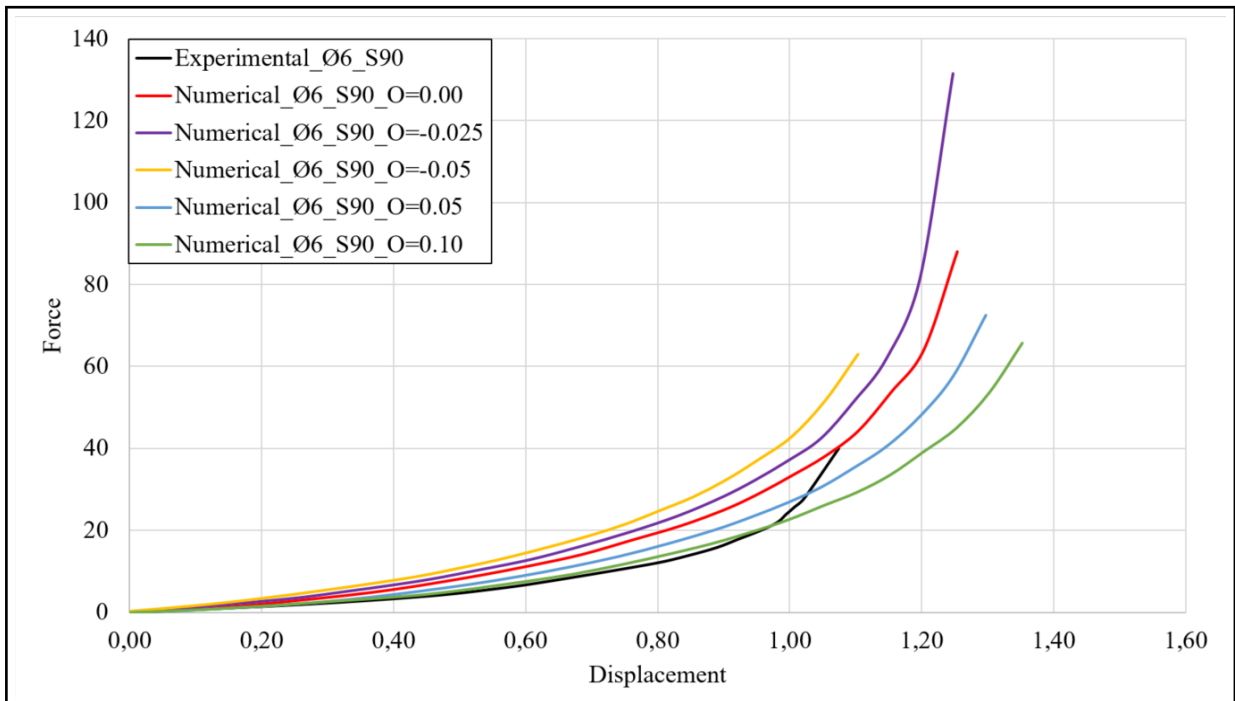


Figure 4.5: Experimental test compared to numerical test - Shore 90A - 6 mm - One sealing element

Figure 4.6 compares a selection of the numerical tests to the experimental tests for a single Shore 70A sealing element with 5 mm as cross-sectional diameter. The parameters for the different tests is presented in table 4.3.

Table 4.3: Parameters - Shore 70A - 5 mm - One sealing element

Hardness	Cross section	Offset side walls	$\mu$	Test
Shore 70A	5 mm	Unknown	Unknown	Experimental
Shore 70A	5 mm	0.00 mm	0.5	Numerical
Shore 70A	5 mm	0.05 mm	0.5	Numerical
Shore 70A	5 mm	0.10 mm	0.5	Numerical
Shore 70A	5 mm	0.15 mm	0.5	Numerical
Shore 70A	5 mm	0.20 mm	0.5	Numerical

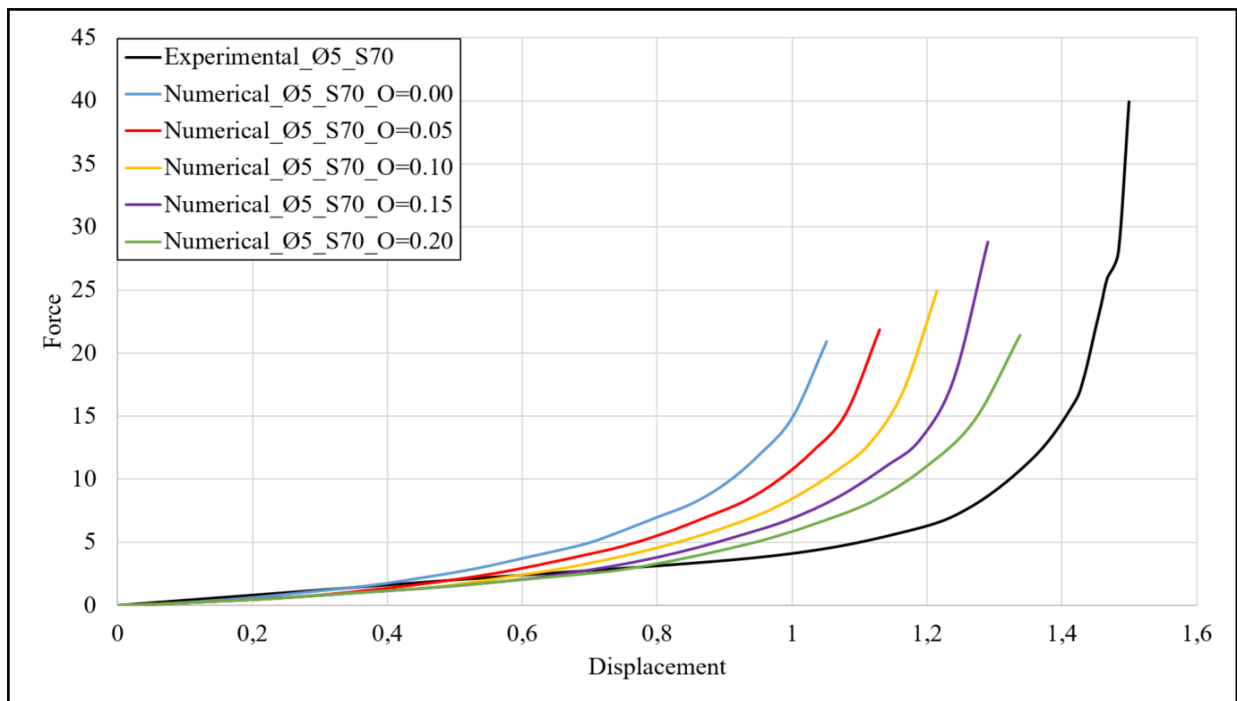


Figure 4.6: Experimental test compared to numerical test - Shore 70A - 5 mm - One sealing element



## 4.4 Two O-rings results

In this section the results of analysis with different parameters for two sealing elements in compression will be presented. The different parameters are:

- Sealing elements with cross-sectional diameter 5 mm or 6 mm
- Shore 70A and Shore 90A hardness
- Three different positions
- Numerical results with side walls offset; 0.00 mm, -0.025 mm, -0.05 mm, -0.10 mm and -0.15 mm from both sides, illustrating the situation when the groove is too small compared to the cross-sectional diameter of the sealing elements.
- Numerical results with side walls offset; 0.00 mm, 0.05 mm, 0.10 mm, 0.15 mm and 0.20 mm from both sides, illustrating the situation when the groove is too wide compared to the cross-sectional diameter of the sealing elements.

Figure 4.7 illustrates the different steps of the compression sequence for two sealing elements corresponding to the curve. In the last step it is possible to see how the compressed sealing elements almost fill the rectangular groove as mentioned in section 3.1. Due to frictional effects; numerical analysis of two sealing elements abort before the whole groove is filled. This is discussed extensively in section 5.2.2.

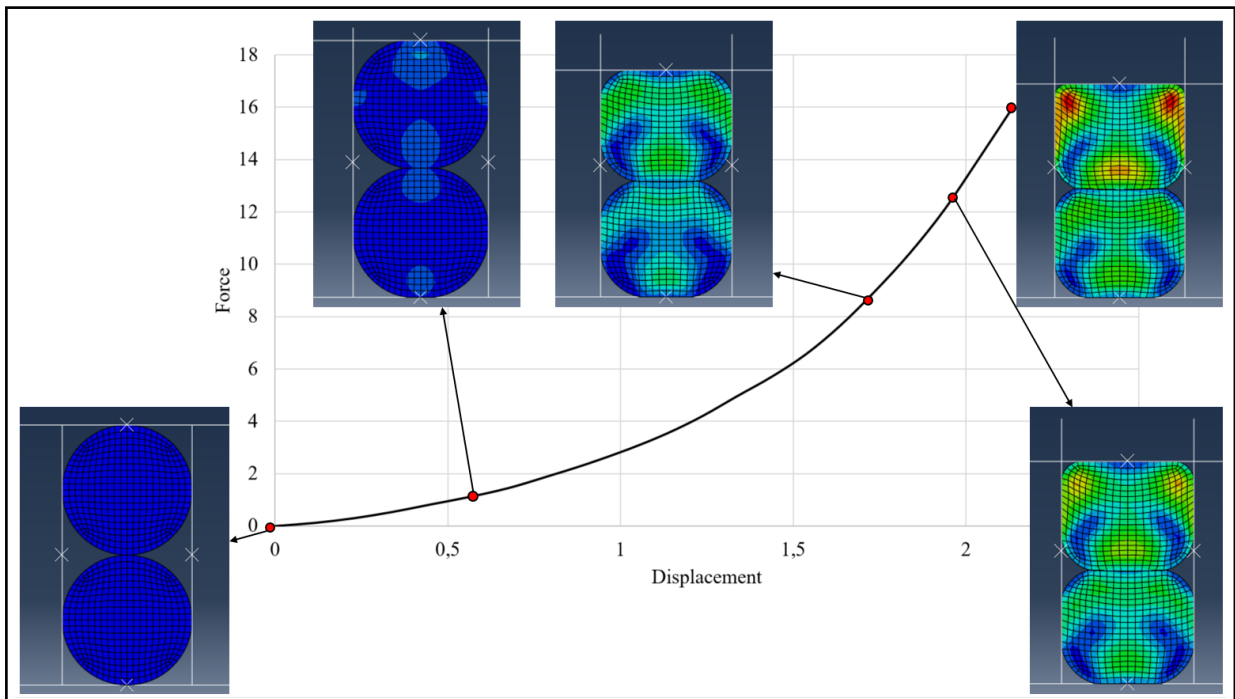


Figure 4.7: Compression steps for two sealing elements

#### 4.4.1 Two sealing elements compared to experimental tests

Table 4.4 presents the parameters for the analysis where the side walls are offset from two sealing elements above one another (in position 1) when the cross-sectional diameter of the seals is 6 mm.

Table 4.4: Parameters - Shore 70A - 6 mm - Two sealing elements

Hardness	Cross section	Offset side walls	$\mu$	Test
Shore 70A	6 mm	Unknown	Unknown	Experimental
Shore 70A	6 mm	0.00 mm	0.5	Numerical
Shore 70A	6 mm	-0.025 mm	0.5	Numerical
Shore 70A	6 mm	-0.05 mm	0.5	Numerical

In Figure 4.8 the experimental test for two Shore 70A sealing elements with 6 mm cross-sectional diameter is compared to numerical results with the parameters presented in Table 4.4.

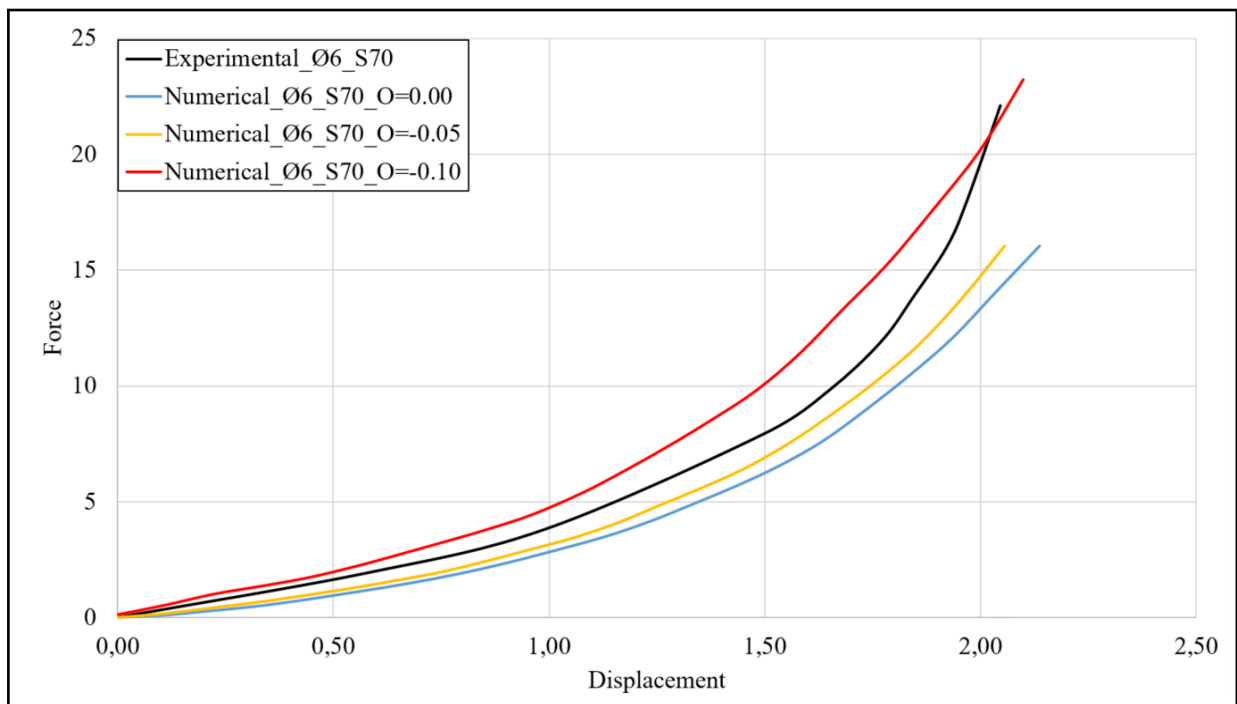


Figure 4.8: Experimental test compared to numerical test - Shore 70A - 6 mm - Two rings

Table 4.5 presents the parameters for the analysis where the side walls are offset from two Shore 90A sealing elements above one another when the cross-sectional diameter of the seals is 6 mm.

Table 4.5: Parameters - Shore 90A - 6 mm - Two sealing elements

Hardness	Cross section	Offset side walls	$\mu$	Test
Shore 90A	6 mm	Unknown	Unknown	Experimental
Shore 90A	6 mm	0.00 mm	0.5	Numerical
Shore 90A	6 mm	-0.10 mm	0.5	Numerical
Shore 90A	6 mm	0.05 mm	0.5	Numerical
Shore 90A	mm6	0.10 mm	0.5	Numerical

In Figure 4.9 the experimental test for two Shore 70A sealing elements with 6 cross-sectional diameter is compared to the numerical results with the parameters presented in Table 4.5.

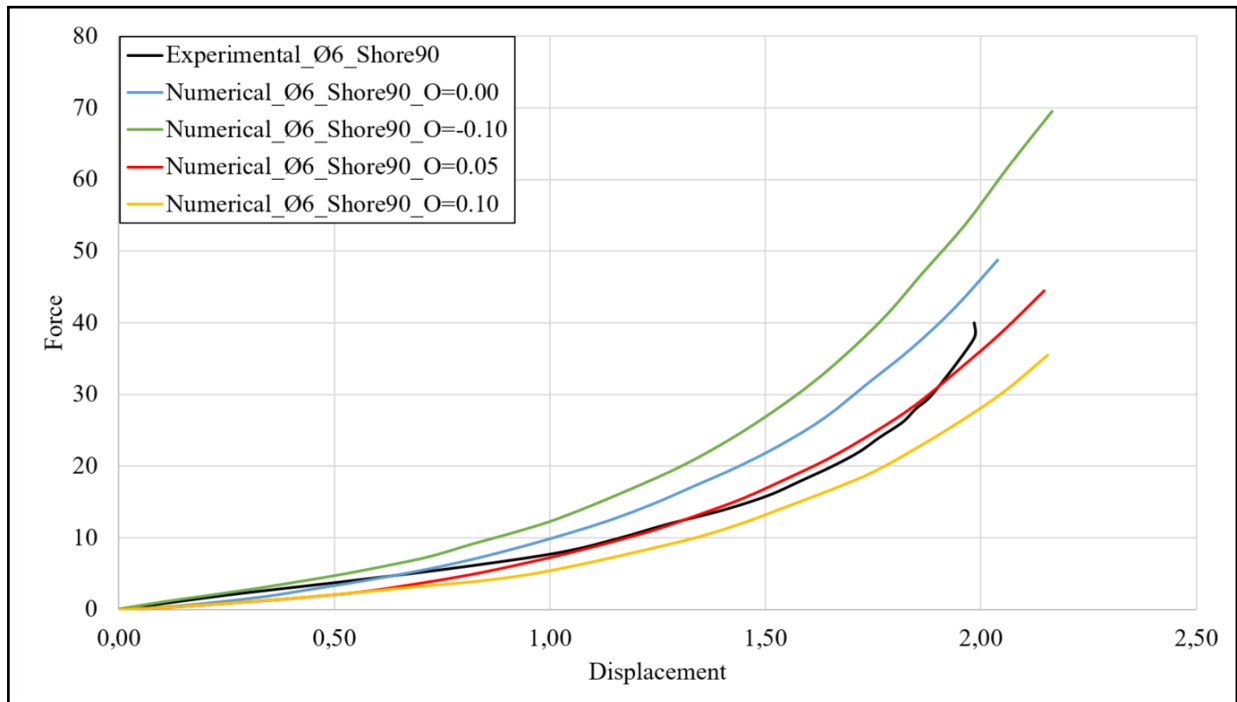


Figure 4.9: Experimental test compared to numerical test - Shore 90A - 6 mm - Two sealing elements

## 4.5 Comparison of curves

### 4.5.1 Groove dimensions comparison

Table 4.6 presents the parameters for the analysis for a single O-ring in Shore 70A material hardness. The side walls are varying from -0.15 mm (indicating a groove too small) to 0.20 mm (indicating a groove wider than the cross-sectional diameter of the seal).

Table 4.6: Parameters - Shore 70A - 6 mm - One seal - Groove varying

Hardness	Cross section	Offset side walls	$\mu$	Test
Shore 70A	6 mm	0.00 mm	0.5	Numerical
Shore 70A	6 mm	-0.025 mm and 0.05 mm	0.5	Numerical
Shore 70A	6 mm	-0.05 mm and 0.10 mm	0.5	Numerical
Shore 70A	6 mm	-0.10 mm and 0.15 mm	0.5	Numerical
Shore 70A	6 mm	-0.15 mm and 0.20 mm	0.5	Numerical

Figure 4.10 illustrates the numerical test results for one sealing element with the parameters presented in Table 4.6.

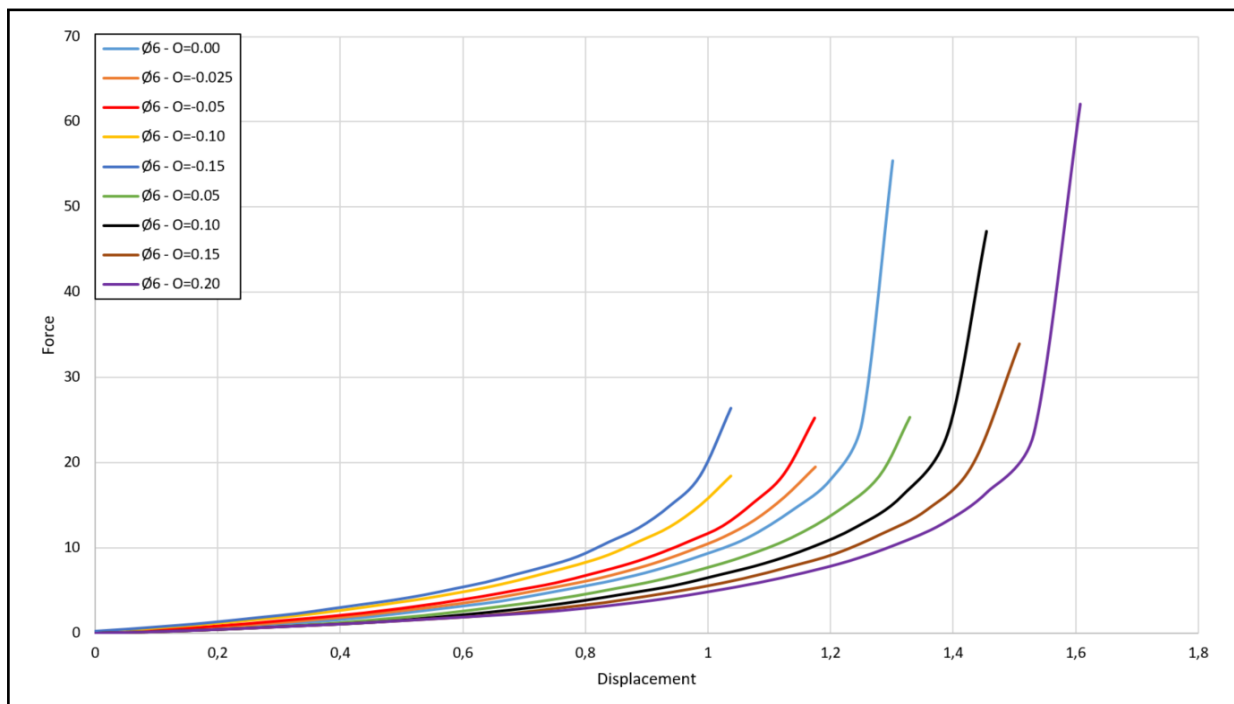


Figure 4.10: Shore 70A - 6 mm - One seals - Groove varying

Table 4.7 presents the parameters for the analysis for a two O-rings in Shore 70A material hardness. The side walls are varying from -0.15 mm (indicating a groove too small) to 0.20 mm (indicating a groove wider than the cross-sectional diameter of the seal).

Table 4.7: Parameters - Shore 70A - 6 mm - Two seals - Varying groove dimensions

Hardness	Cross section	Offset side walls	$\mu$	Test
Shore 70A	6 mm	0.00 mm	0.5	Numerical
Shore 70A	6 mm	-0.025 mm and 0.05 mm	0.5	Numerical
Shore 70A	6 mm	-0.05 mm and 0.10 mm	0.5	Numerical
Shore 70A	6 mm	-0.10 mm and 0.15 mm	0.5	Numerical
Shore 70A	6 mm	-0.15 mm and 0.20 mm	0.5	Numerical

Figure 4.11 illustrates the numerical test results for two sealing elements with the parameters presented in Table 4.7.

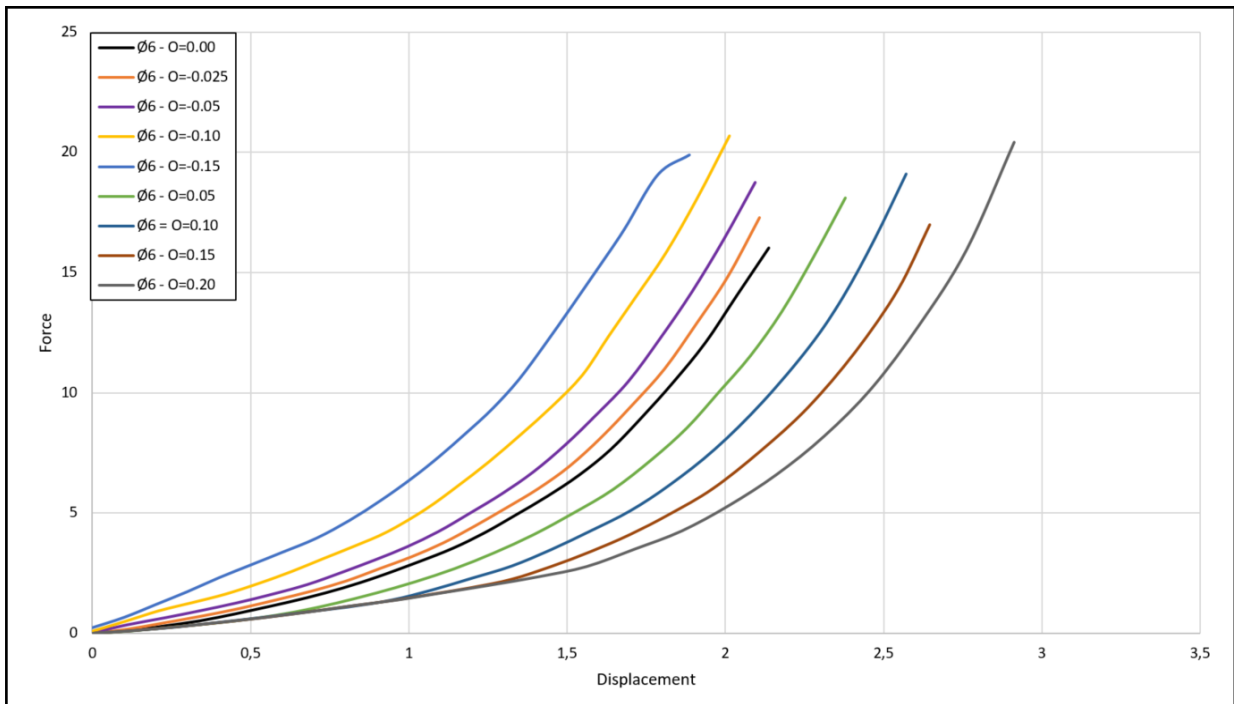


Figure 4.11: Shore 70A - 6 mm - Two seals - Varying groove dimensions

### 4.5.2 Material hardness comparison

Table 4.8 presents the parameters for the analysis for a single O-ring in both Shore 70A and Shore 90 A material hardness. The side walls contribute to pre-tension in the sealing element, illustrating a groove too small compared to the cross-sectional diameter of the seal.

Table 4.8: Parameters - Shore 70A and 90A - 6 mm - One seal - Groove too small

Hardness	Cross section	Offset side walls	$\mu$	Test
Shore 70A and 90A	6 mm	0.00 mm	0.5	Numerical
Shore 70A and 90A	6 mm	-0.025 mm	0.5	Numerical
Shore 70A and 90A	6 mm	-0.05 mm	0.5	Numerical
Shore 70A and 90A	6 mm	-0.10 mm	0.5	Numerical
Shore 70A and 90A	6 mm	-0.15 mm	0.5	Numerical

Figure 4.12 illustrates the numerical test results for one sealing element with the parameters presented in Table 4.8.

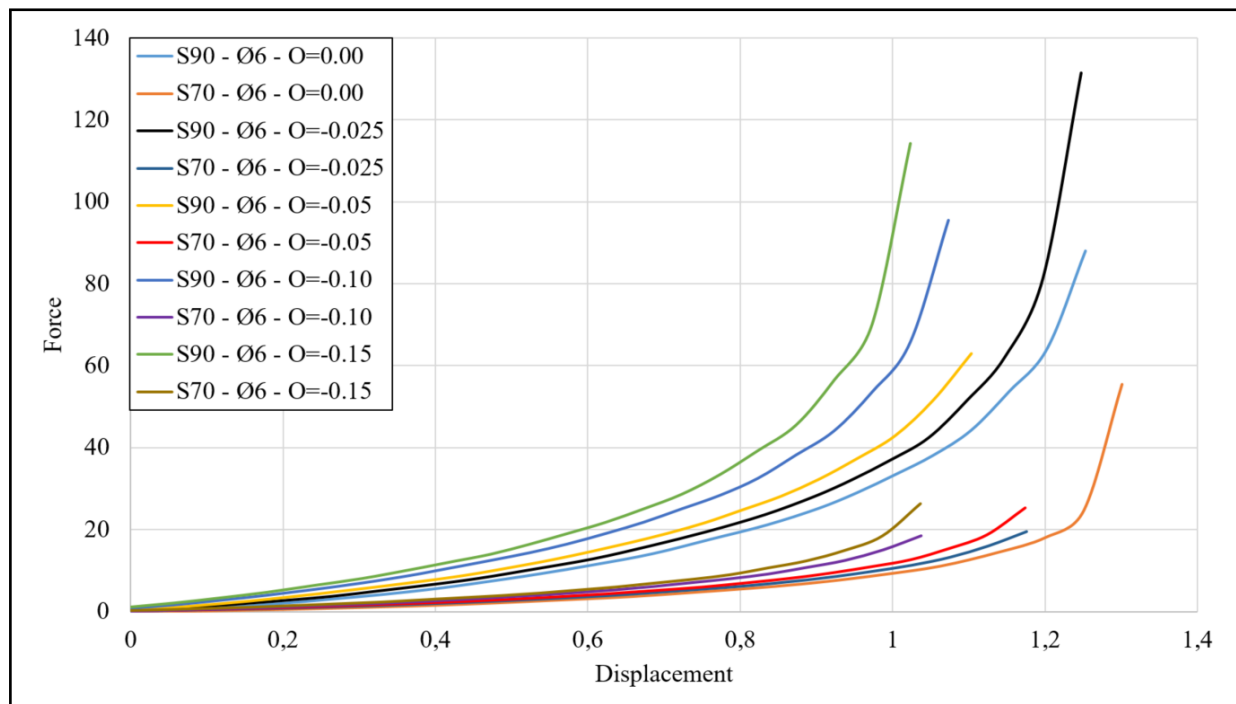


Figure 4.12: Shore 70A and 90A - 6 mm - One seal - Groove too small

Table 4.9 presents the parameters for the analysis for two O-rings in both Shore 70A and Shore 90 A material hardness. The side walls contribute to pre-tension in the sealing elements, illustrating a groove too small compared to the cross-sectional diameter of the seals.

Table 4.9: Parameters - Shore 70A and 90A - 6 mm - Two rings - Groove too small

Hardness	Cross section	Offset side walls	$\mu$	Test
Shore 70A and 90A	6 mm	0.00 mm	0.5	Numerical
Shore 70A and 90A	6 mm	-0.025 mm	0.5	Numerical
Shore 70A and 90A	6 mm	-0.05 mm	0.5	Numerical
Shore 70A and 90A	6 mm	-0.10 mm	0.5	Numerical
Shore 70A and 90A	6 mm	-0.15 mm	0.5	Numerical

Figure 4.13 illustrates the numerical test results for two sealing elements with the parameters presented in Table 4.9.

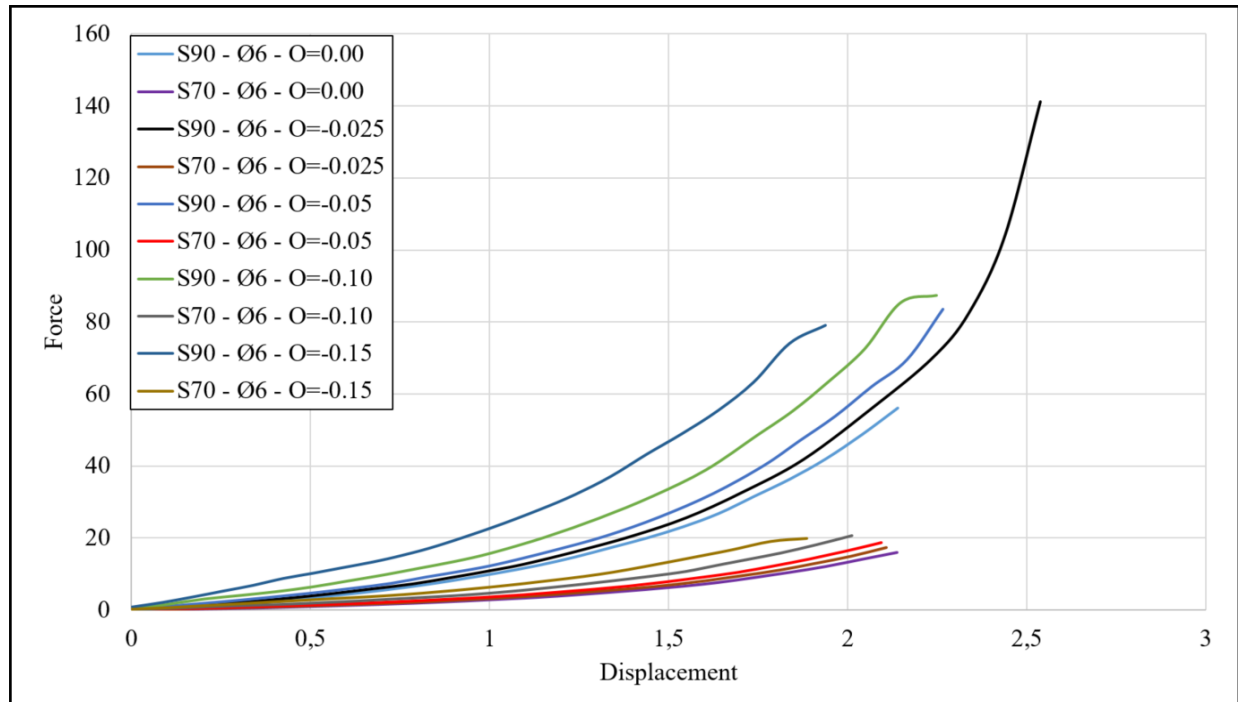


Figure 4.13: Shore 70A and 90A - 6 mm - Two seals - Groove too small

Note; simulation results with identical conditions as in Figure 4.12 and 4.13, but by use of a groove which is wider than the cross-sectional diameter of the seal can be found in Appendix I (Figure I.17 and Figure I.18).

### 4.5.3 Cross-sectional diameter compared - One seal

Table 4.10 presents the parameters for the analysis where the side walls contribute to pre-tension in a single sealing element, illustrating a groove too small compared to the cross-sectional diameter of the seal.

Table 4.10: Parameters - Shore 70A - 5 mm and 6 mm - One seal - Groove too small

Hardness	Cross section	Offset side walls	$\mu$	Test
Shore 70A	5 mm and 6 mm	0.00 mm	0.5	Numerical
Shore 70A	5 mm and 6 mm	-0.025 mm	0.5	Numerical
Shore 70A	5 mm and 6 mm	-0.05 mm	0.5	Numerical
Shore 70A	5 mm and 6 mm	-0.10 mm	0.5	Numerical
Shore 70A	5 mm and 6 mm	-0.15 mm	0.5	Numerical

Figure 4.14 illustrates the numerical test results for one sealing element with the parameters presented in Table 4.10.

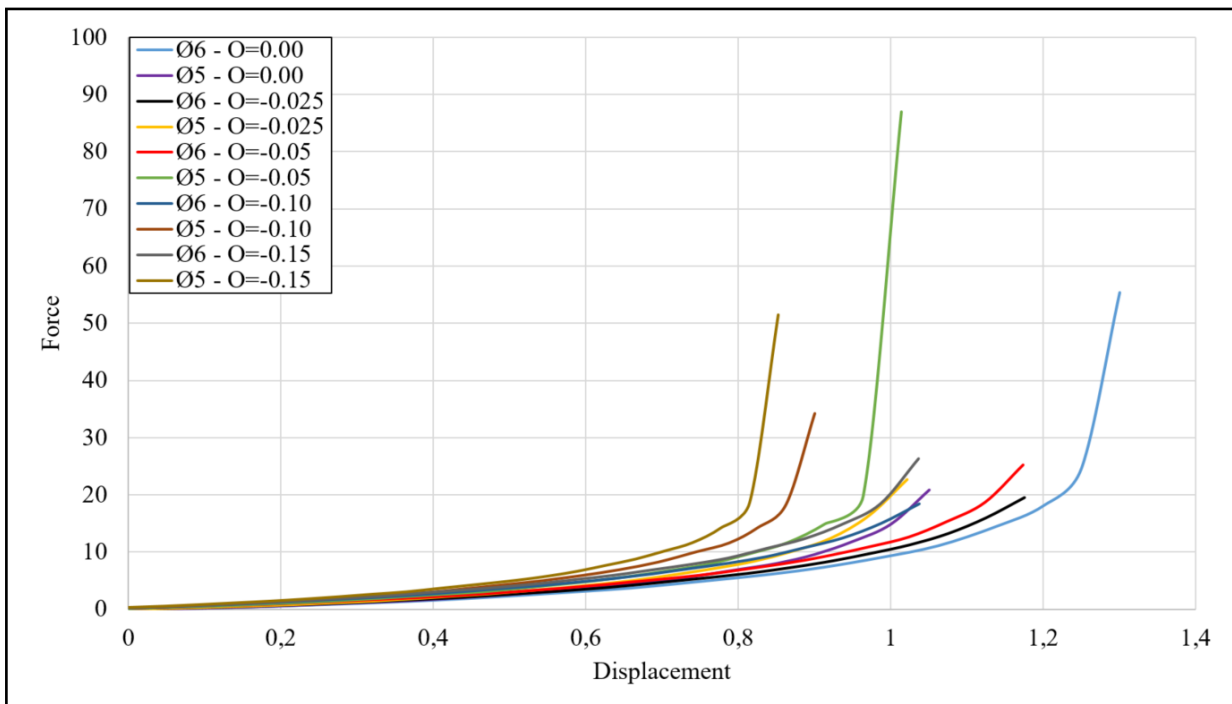


Figure 4.14: Shore 70A - 5 mm and 6 mm - One seal - Groove too small



Table 4.11 presents the parameters for the analysis where the offset of the side walls represent a groove too wide compared to the cross-sectional diameter of the sealing element.

Table 4.11: Parameters - Shore 70A - 5 mm and 6 mm - One seal - Groove too wide

Hardness	Cross section	Offset side walls	$\mu$	Test
Shore 70A	5 mm and 6 mm	0.00 mm	0.5	Numerical
Shore 70A	5 mm and 6 mm	0.05 mm	0.5	Numerical
Shore 70A	5 mm and 6 mm	0.10 mm	0.5	Numerical
Shore 70A	5 mm and 6 mm	0.15 mm	0.5	Numerical
Shore 70A	5 mm and 6 mm	0.20 mm	0.5	Numerical

Figure 4.15 illustrates the numerical test results for one sealing element with the parameters presented in Table 4.11.

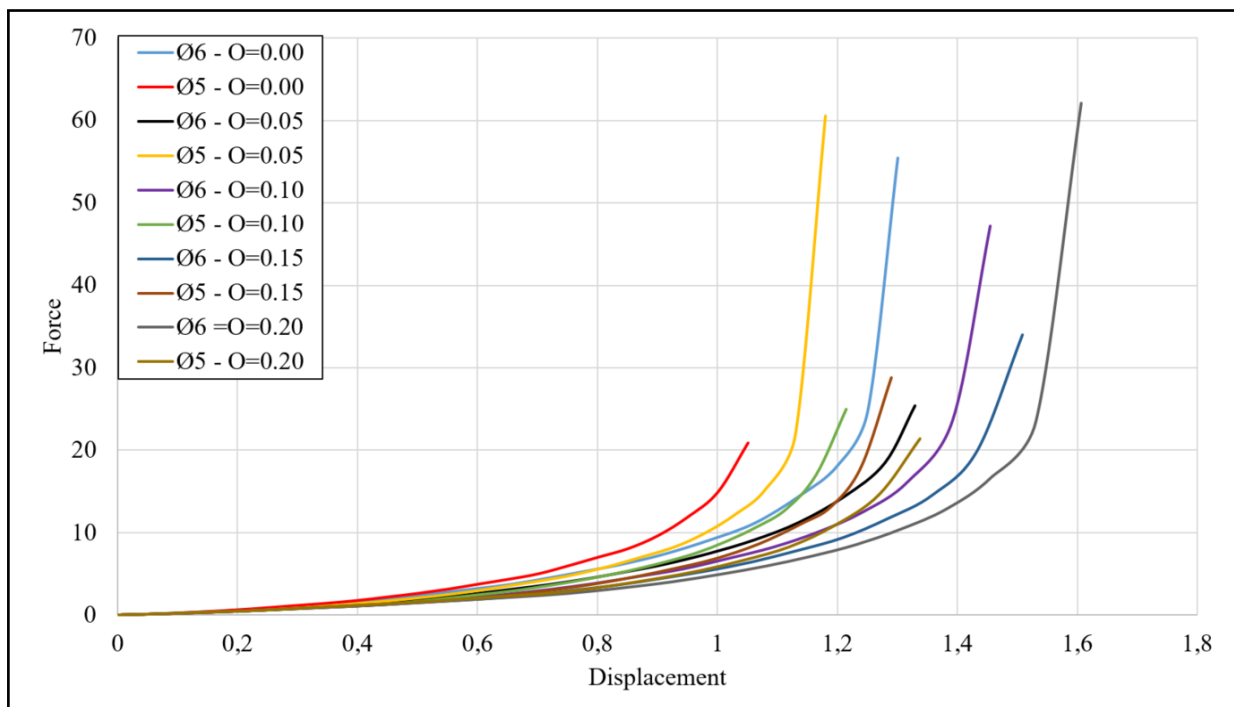


Figure 4.15: Shore 70A - 5 mm and 6 mm - One seal - Groove too wide

Note; simulation results with identical conditions as in Figure 4.14 and 4.15, but by use of Shore 90A material hardness can be found in Appendix I (Figure I.19 and Figure I.20).

#### 4.5.4 Cross-sectional diameter compared - Two seals

Table 4.12 presents the parameters for the analysis where the side walls contribute to pre-tension in the sealing elements, illustrating a groove too small compared to the cross-sectional diameter of the seals.

Table 4.12: Parameters - Shore 70A - 5 mm and 6 mm - Two seals compared - Groove too small

Hardness	Cross section	Offset side walls	$\mu$	Test
Shore 70A	5 mm and 6 mm	0.00 mm	0.5	Numerical
Shore 70A	5 mm and 6 mm	-0.025 mm	0.5	Numerical
Shore 70A	5 mm and 6 mm	-0.05 mm	0.5	Numerical
Shore 70A	5 mm and 6 mm	-0.10 mm	0.5	Numerical
Shore 70A	5 mm and 6 mm	-0.15 mm	0.5	Numerical

Figure 4.16 illustrate the numerical test results for two sealing elements with the parameters presented in Table 4.12.

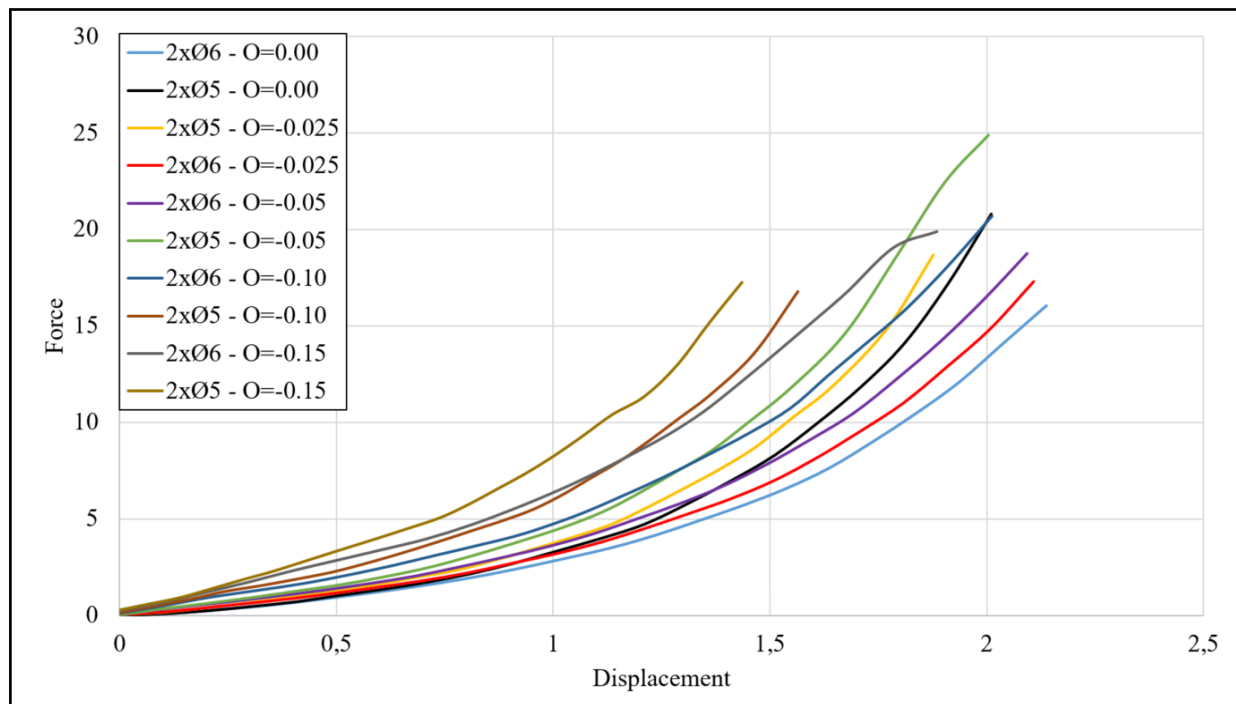


Figure 4.16: Shore 70A - 5 mm and 6 mm - Two seals - Groove too small

Table 4.13 present the parameters for the analysis where the side walls contribute to pre-tension in the sealing elements, illustrating a groove too small compared to the cross-sectional diameter of the seals.

Table 4.13: Parameters - Shore 70A - 5 mm and 6 mm - Two seals compared - Groove too wide

Hardness	Cross section	Offset side walls	$\mu$	Test
Shore 70A	5 mm and 6 mm	0.00 mm	0.5	Numerical
Shore 70A	5 mm and 6 mm	0.05 mm	0.5	Numerical
Shore 70A	5 mm and 6 mm	0.10 mm	0.5	Numerical
Shore 70A	5 mm and 6 mm	0.15 mm	0.5	Numerical
Shore 70A	5 mm and 6 mm	0.20 mm	0.5	Numerical

Figure 4.17 illustrate the numerical test results for two sealing elements with the parameters presented in Table 4.13.

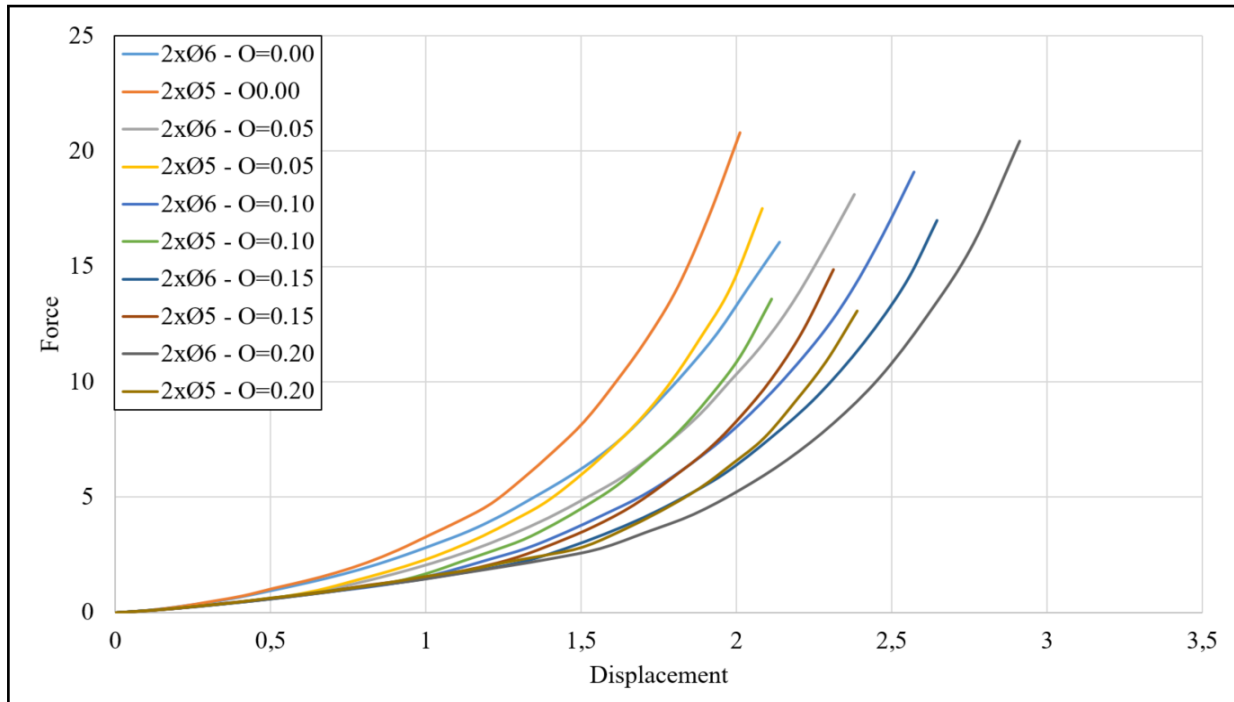


Figure 4.17: Shore 70A - 5 mm and 6 mm - Two seals - Groove too wide

Note; simulation results identical to Figure 4.16 and Figure 4.17 but by use of Shore 90A material hardness can be found in Appendix I (Figure I.25 and I.26).

### 4.5.5 One ring compared to two rings

Table 4.14 presents the parameters for the analysis where the side walls contribute to pre-tension in the sealing elements, illustrating a groove too small compared to the cross-sectional diameter of the seals.

Table 4.14: Parameters - Shore 70A - 6 mm - One and two compared - Groove too small

Hardness	Cross section	Offset side walls	$\mu$	Test
Shore 70A	6 mm	0.00 mm	0.5	Numerical
Shore 70A	6 mm	0.025 mm	0.5	Numerical
Shore 70A	6 mm	-0.05 mm	0.5	Numerical
Shore 70A	6 mm	-0.10 mm	0.5	Numerical
Shore 70A	6 mm	-0.15 mm	0.5	Numerical

Figure 4.18 illustrates the numerical test results for one and two sealing elements with the parameters presented in Table 4.14.

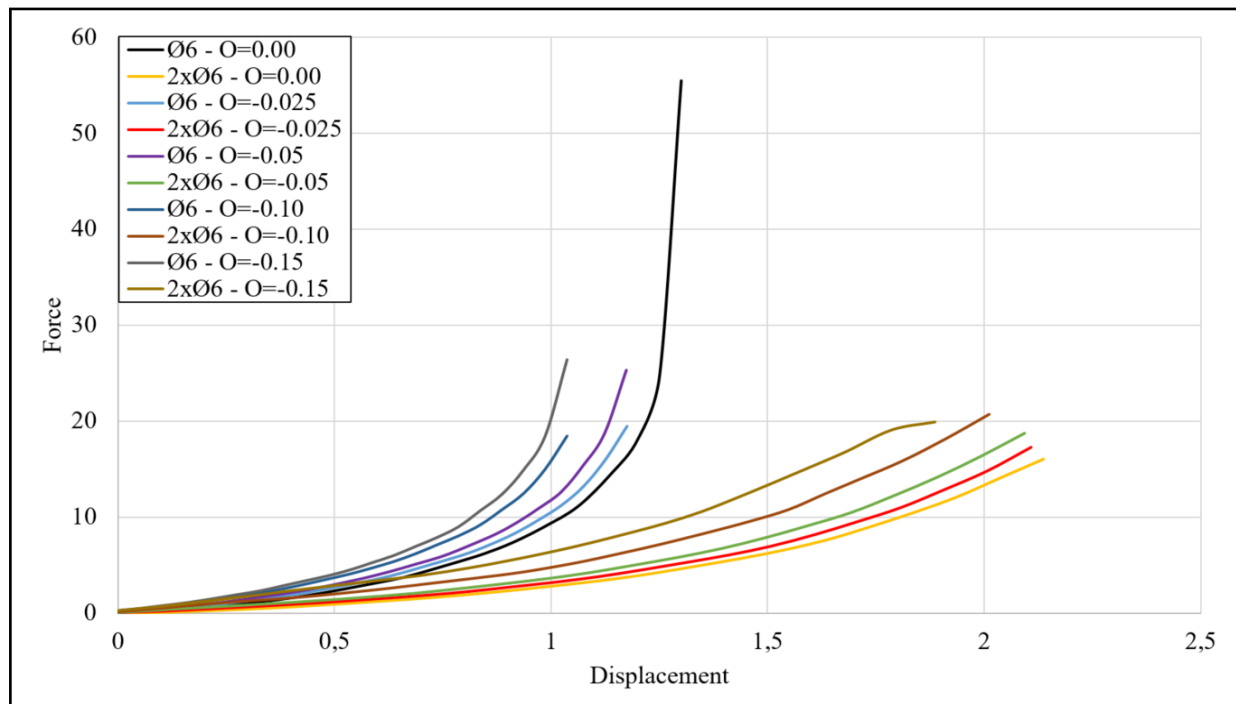


Figure 4.18: Shore 70A - 6 mm - One and two compared - Groove too small

Note; simulation results identical to Figure 4.18 but by use of cross-sectional diameter of 5 mm can be found in Appendix I (Figure I.21).

Table 4.15 presents the parameters for the analysis where the side walls contribute to pre-tension in the sealing elements, illustrating a groove too small compared to the cross-sectional diameter of the seals.

Table 4.15: Parameters - Shore 90A - 6 mm - One and two compared - Groove too small

Hardness	Cross section	Offset side walls	$\mu$	Test
Shore 90A	6 mm	0.00 mm	0.5	Numerical
Shore 90A	6 mm	-0.025 mm	0.5	Numerical
Shore 90A	6 mm	-0.05 mm	0.5	Numerical
Shore 90A	6 mm	-0.10 mm	0.5	Numerical
Shore 90A	6 mm	-0.15 mm	0.5	Numerical

Figure 4.19 illustrates the numerical test results for one and two sealing elements with the parameters presented in Table 4.15.

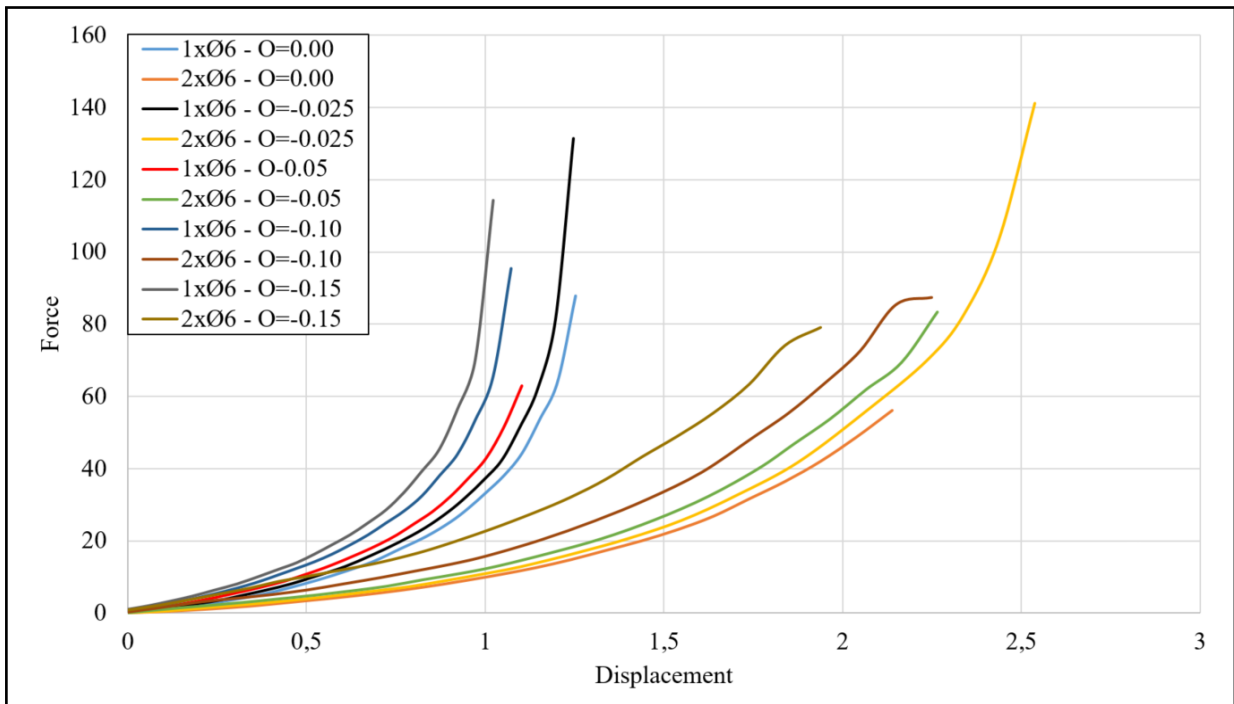


Figure 4.19: Shore 90A - 6 mm - One and two compared - Groove too small

Note; simulation results identical to Figure 4.19 but by use of cross-sectional diameter of 5 mm can be found in Appendix I (Figure I.22).

Table 4.16 presents the parameters for the analysis where the offset of the side walls represent a groove too wide compared to the cross-sectional diameter of the sealing elements.

Table 4.16: Parameters - Shore 70A - 6 mm - One and two compared - Groove too wide

Hardness	Cross section	Offset side walls	$\mu$	Test
Shore 70A	6 mm	0.00 mm	0.5	Numerical
Shore 70A	6 mm	0.05 mm	0.5	Numerical
Shore 70A	6 mm	0.10 mm	0.5	Numerical
Shore 70A	6 mm	0.15 mm	0.5	Numerical
Shore 70A	Ø6	0.20 mm	0.5	Numerical

Figure 4.20 illustrates the numerical test results for one and two sealing elements with the parameters presented in Table 4.16.

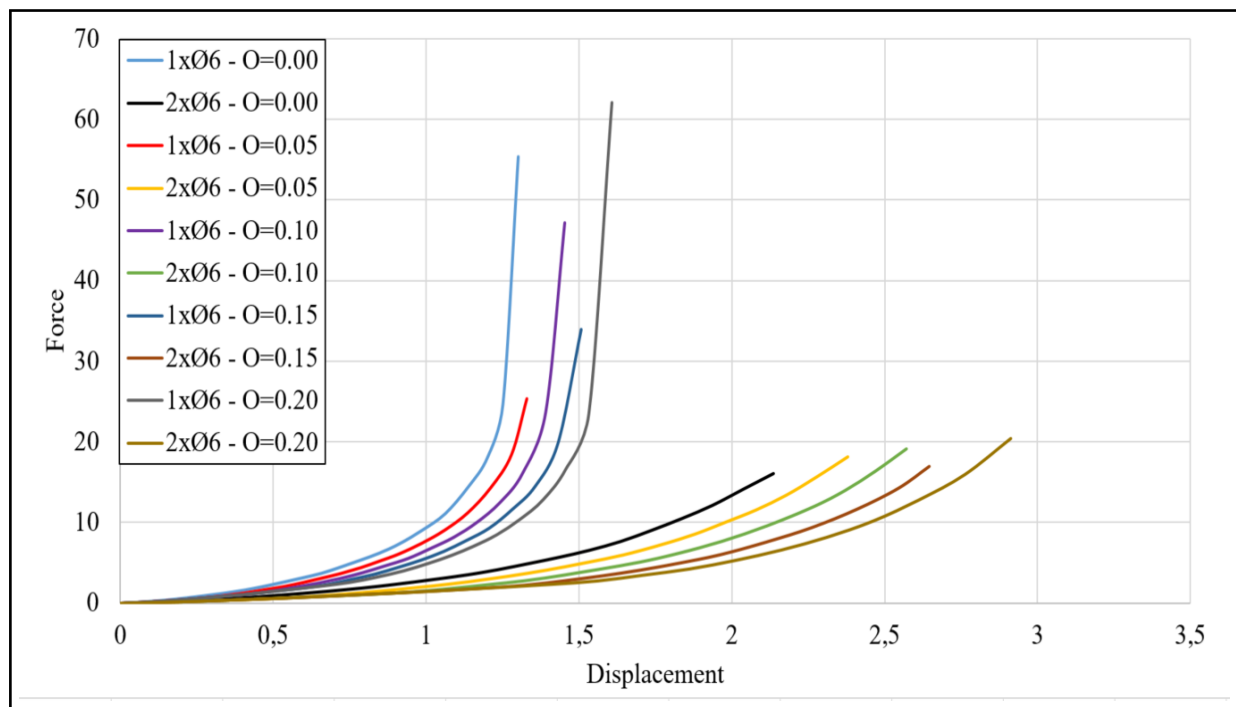


Figure 4.20: Shore 70A - 6 mm - One and two compared - Groove too wide

Note; simulation results identical to Figure 4.20 but by use of cross-sectional diameter of 5 mm can be found in Appendix I (Figure I.23).

Table 4.17 presents the parameters for the analysis where the offset of the side walls represent a groove too wide compared to the cross-sectional diameter of the sealing elements.

Table 4.17: Parameters - Shore 90A - 6 mm - One and two compared - Groove too wide

Hardness	Cross section	Offset side walls	$\mu$	Test
Shore 90A	6 mm	0.00 mm	0.5	Numerical
Shore 90A	6 mm	0.05 mm	0.5	Numerical
Shore 90A	6 mm	0.10 mm	0.5	Numerical
Shore 90A	6 mm	0.15 mm	0.5	Numerical
Shore 90A	6 mm	0.20 mm	0.5	Numerical

Figure 4.21 illustrates the numerical test results for one and two sealing elements with the parameters presented in Table 4.17 is presented.

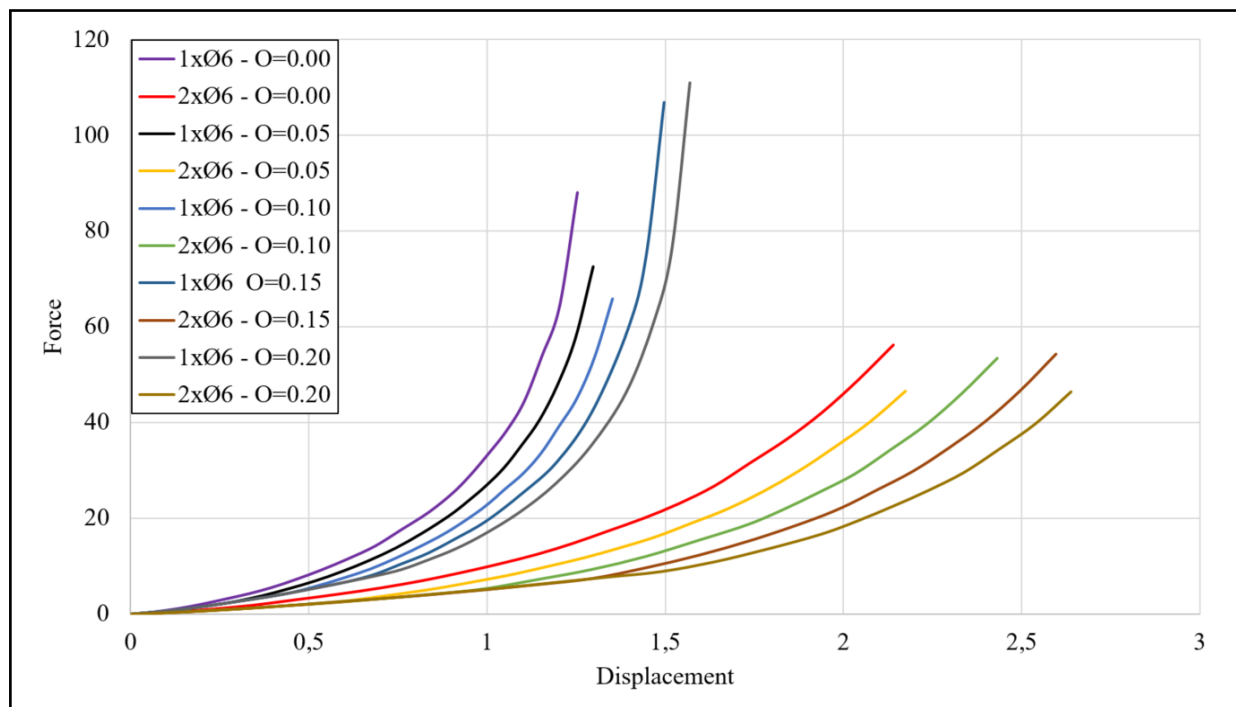


Figure 4.21: Shore 90A - 6 mm - One and two compared - Groove too wide

Note; simulation results identical to Figure 4.21 but by use of cross-sectional diameter of 5 mm can be found in Appendix I (Figure I.24).

## 4.6 Hysteresis

Hysteresis loops will be presented throughout this section to illustrate the effects of friction during cyclic loading.

### 4.6.1 Groove too small

Results with multiple loading and unloading step for two O-rings with shore 70A material hardness in position 1 is shown in Figure 4.22. The groove is too small compared to the cross-sectional diameter of the seal is analyzed. The sequence of steps are as follows:

1. The simulation starts with the required initial step
2. Load step of the side walls of -0.10 mm from both sides which gives a pre-tension
3. Load step from upper wire in negative vertical direction
4. Unload step from upper wire in positive vertical direction
5. Load step from upper wire in negative vertical direction
6. Unload step from upper wire in positive vertical direction
7. Load step from upper wire in negative vertical direction
8. Unload step from upper wire in positive vertical direction

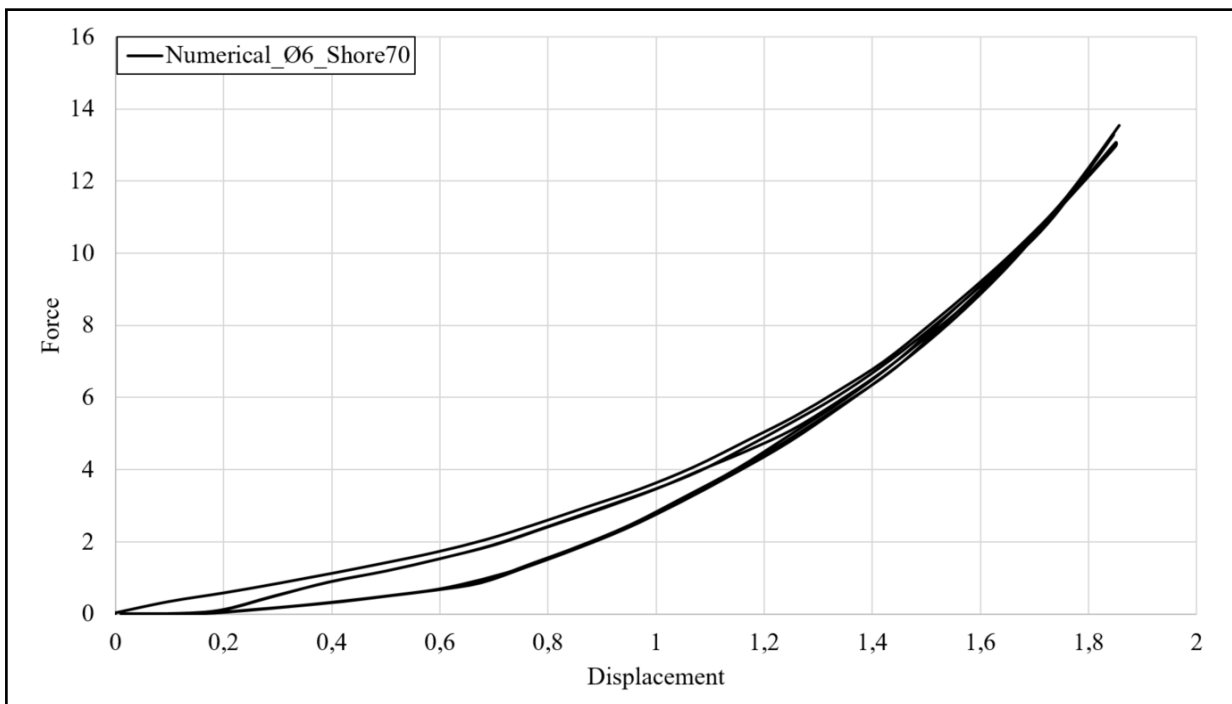


Figure 4.22: Multiple steps - Hysteresis - Shore 70A -  $\mu=0.5$  - 6 mm



### 4.6.2 Groove tangential

Analyses with multiple loading and unloading step is conducted. Two O-rings in position 1 with tangential side walls to the sealing element is analyzed. The sequence of steps are as follows:

1. The simulation starts with the required initial step
2. Load step from upper wire in negative vertical direction
3. Unload step from upper wire in positive vertical direction
4. Load step from upper wire in negative vertical direction
5. Unload step from upper wire in positive vertical direction
6. Load step from upper wire in negative vertical direction
7. Unload step from upper wire in positive vertical direction

The simulation are conducted with friction coefficient,  $\mu$ , 0.5. The shore 70A hardness is shown in Figure 4.23:

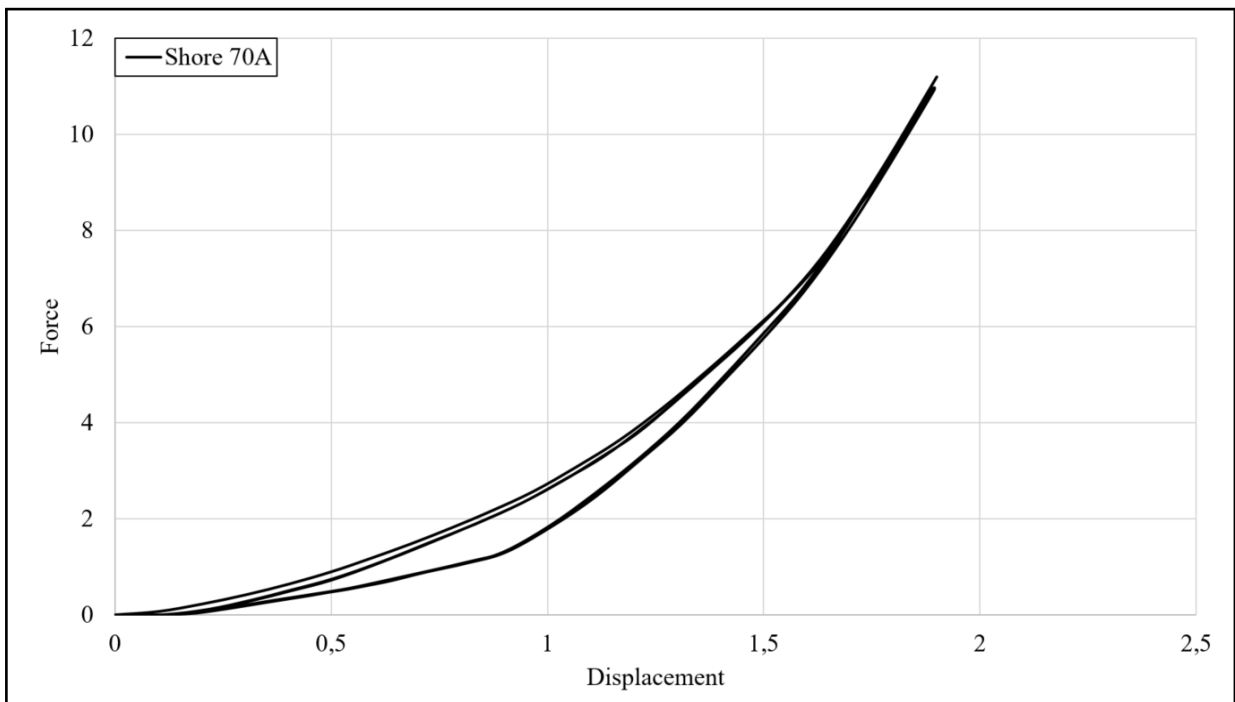


Figure 4.23: Multiple steps - Hysteresis - Shore 70A -  $\mu=0.5$  - 6 mm

### 4.6.3 Groove too wide

Analyses with multiple loading and unloading step is conducted. Two O-rings in position 1 with a groove too wide compared to the cross-sectional diameter of the sealing element is analyzed. The sequence of steps are as follows:

1. The simulation starts with the required initial step
2. Load step from upper wire in negative vertical direction
3. Unload step from upper wire in positive vertical direction
4. Load step from upper wire in negative vertical direction
5. Unload step from upper wire in positive vertical direction
6. Load step from upper wire in negative vertical direction
7. Unload step from upper wire in positive vertical direction

The next simulations are conducted with side walls 0.10 offset fra the tangent of the O-rings, using a coefficient of friction,  $\mu$ , equal to 0.5. The shore 70A hardness is shown in Figure 4.24:

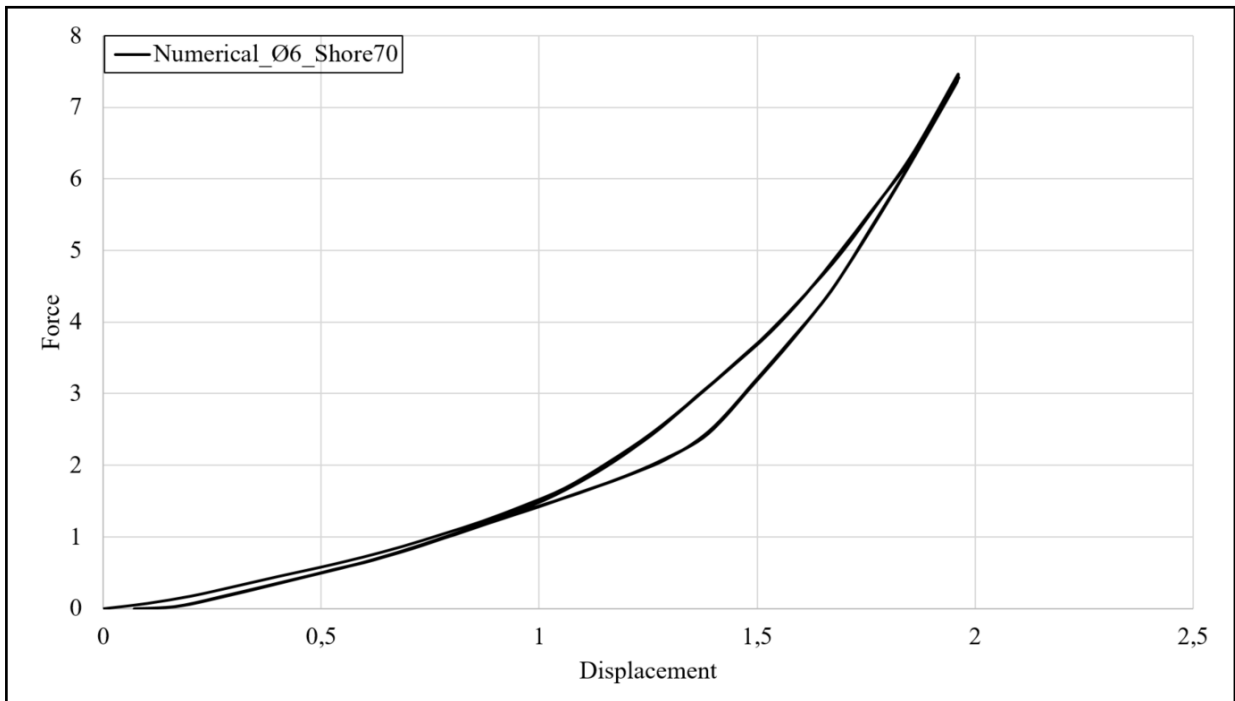


Figure 4.24: Multiple steps - Hysteresis - Shore 70A -  $\mu=0.5$  - 6 mm

Note; Hysteresis loops identical to Figure 4.22, 4.23 and 4.24, but by use of Shore 90A material hardness is presented in Appendix I (Figure I.28, I.29 and I.32).

## 4.7 Three positions

This section presents results obtained from the situations where two sealing elements are incorporated in the sealing groove as presented in section 3.7.2. Table 4.18 presents parameters used for one single compression for three different positions:

Table 4.18: Parameters - Shore 70A - 6 mm - Two seals - 3 positions

Hardness	Cross section	Offset side walls	$\mu$	Test	Position
Shore 70A	6 mm	0.00 mm	0.5	Numerical	1
Shore 70A	6 mm	0.00 mm	0.5	Numerical	2
Shore 70A	6 mm	0.00 mm	0.5	Numerical	3

Figure 4.25 illustrates the load deflection characteristics of two sealing elements with the parameters given in Table 4.18:

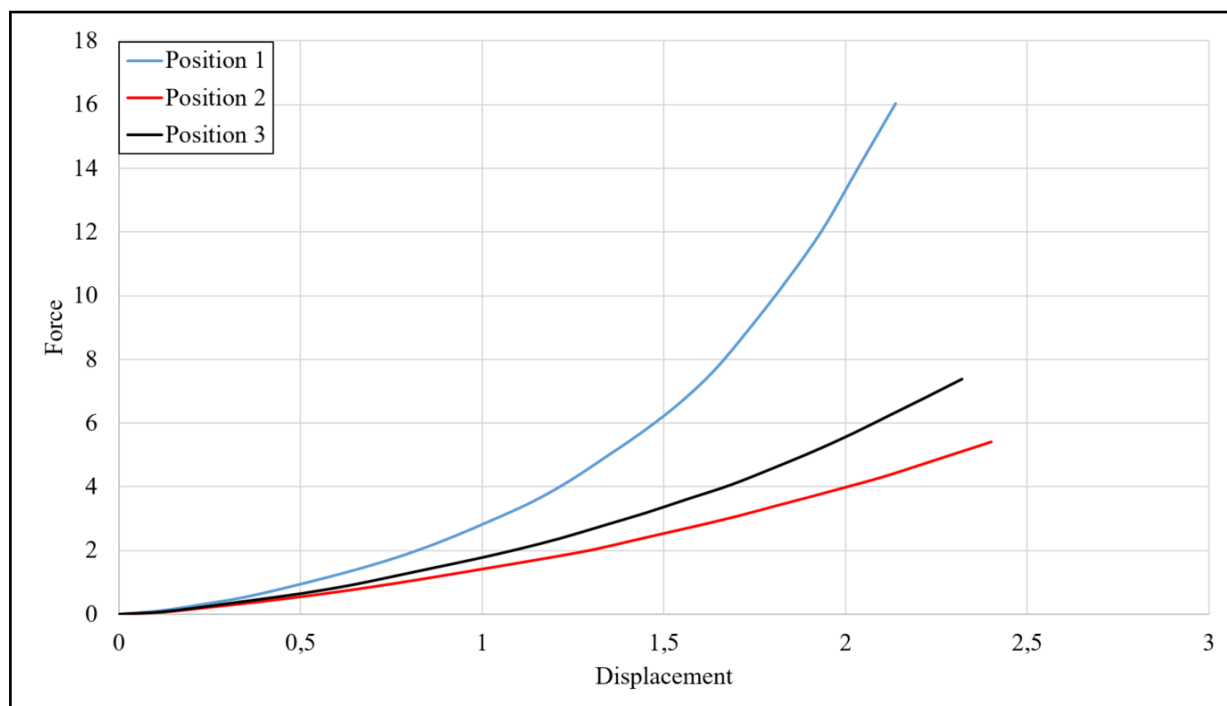


Figure 4.25: 6 mm -  $\mu=0.5$  - No pre-tension - 3 positions

Note; the identical comparison with side walls offset -0.10 mm representing when the rectangular groove is too small compared to the two O-rings, is presented in Appendix I by Figure I.27.

### 4.7.1 Hysteresis

The following curves illustrates the hysteresis behaviour(cyclic loading) for two sealing elements in position 1, 2 and 3 when only four steps are conducted:

1. The simulation starts with the required initial step
2. Load step from upper wire in negative vertical direction
3. Unload step from upper wire in positive vertical direction

Figure 4.26, 4.27 and 4.28 illustrates the compression sequence of two O-rings in Shore 70A with cross-sectional diameter 6 mm relative to each other in position 1,2 and 3 with no offset of the side walls.

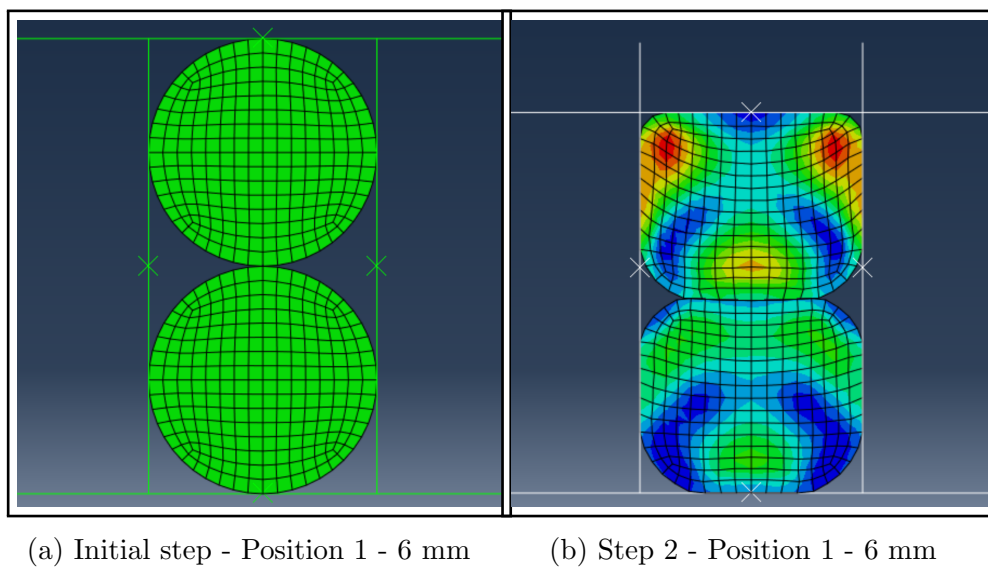


Figure 4.26: Position 1 - Two steps - 6 mm

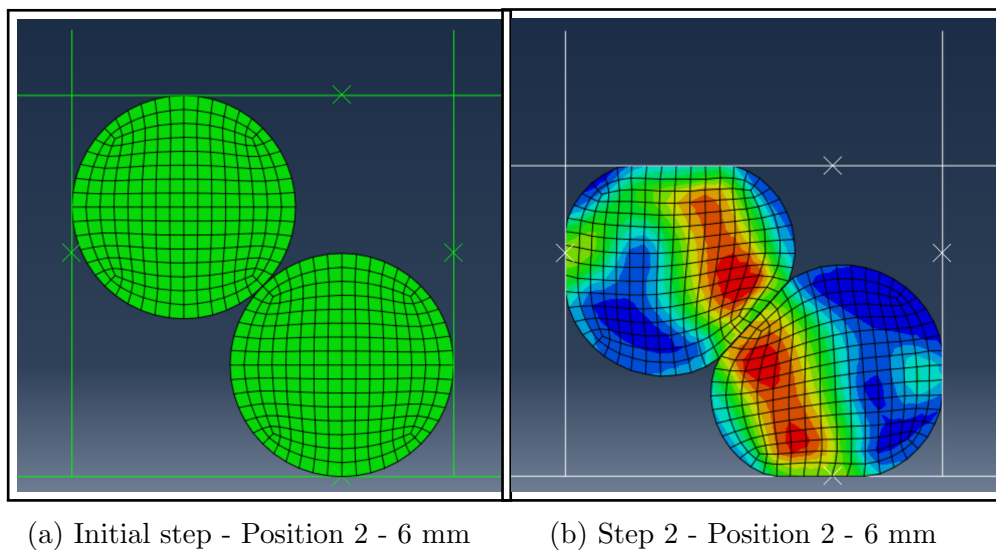


Figure 4.27: Position 2 - Two steps - 6 mm

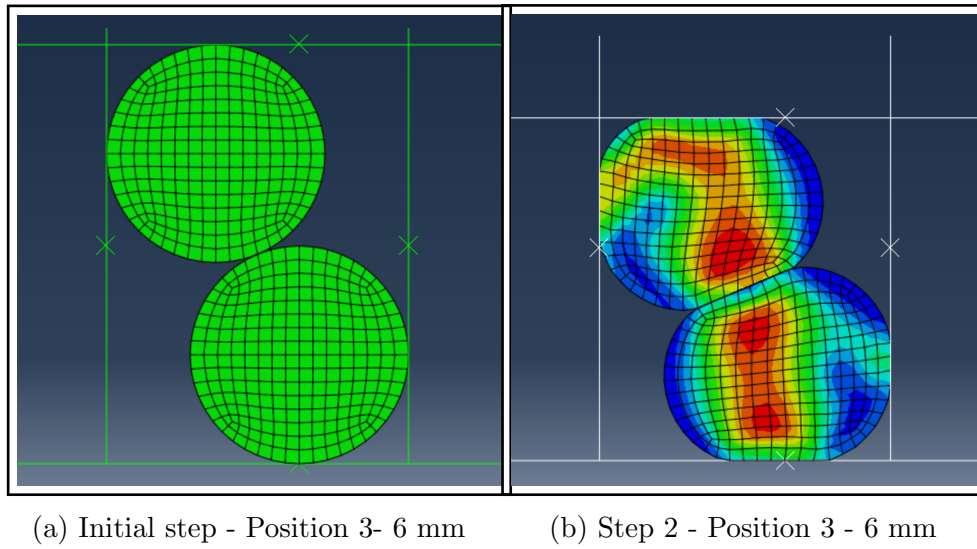


Figure 4.28: Position 3 - Two steps - 6 mm

Figure 4.29 illustrates hysteresis loops as a result of cyclic loading for Figure 4.26, 4.27 and 4.28.

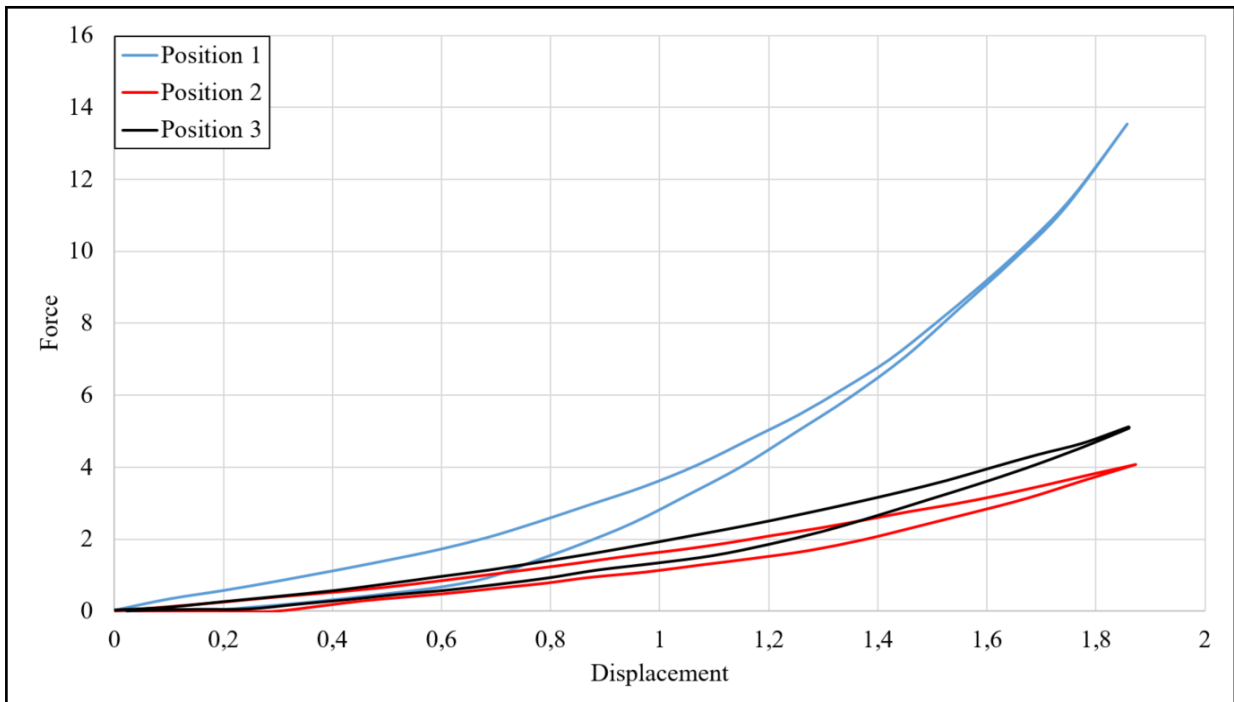
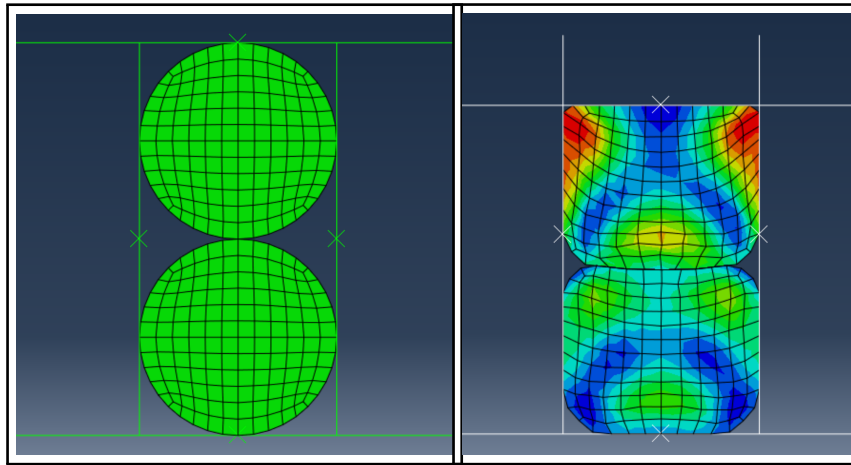


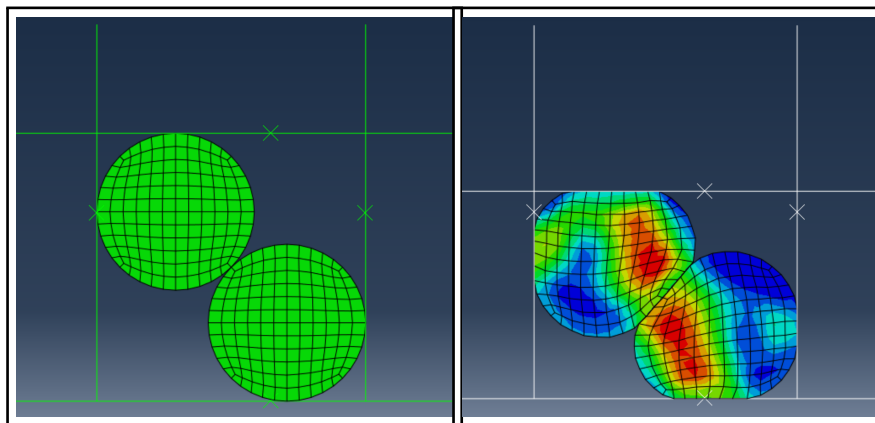
Figure 4.29: Hysteresis - 6 mm -  $\mu=0.5$

Figure 4.30, 4.32 and 4.33 illustrate the similar situation as Figure 4.26, 4.27 and 4.28, but with cross-sectional diameter of 5 mm:

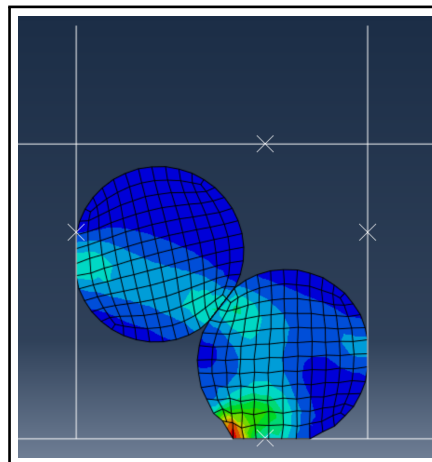


(a) Initial step - Position 1 - 5 mm (b) Step 2 - Position 1 - 5 mm

Figure 4.30: Position 1 - Two steps - 5 mm

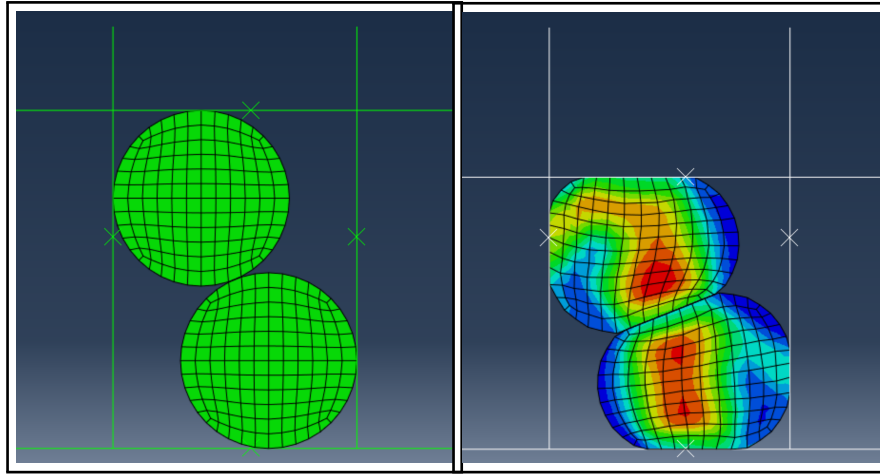


(a) Initial step - Position 2 - 5 mm (b) Step 2 - Position 2 - 5 mm



(a) Step 3 - Position 2 - 5 mm

Figure 4.32: Position 2 - Three steps - 5 mm



(a) Initial step - Position 3- 5 mm    (b) Step 2 - Position 3 - 5 mm

Figure 4.33: Position 3 - Two steps - 5 mm

Figure 4.34 illustrates hysteresis loops as a result of cyclic loading for Figure 4.30, 4.32 and 4.33.

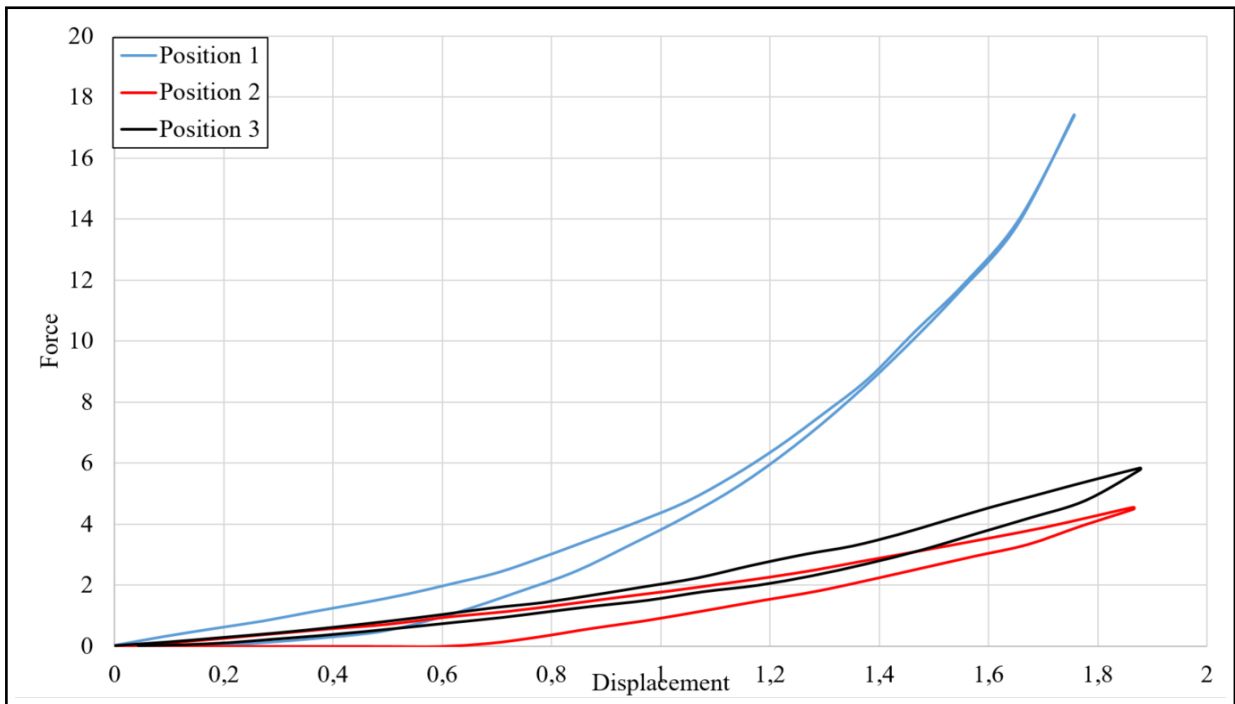


Figure 4.34: Hysteresis - 5 mm -  $\mu=0.5$

### 4.7.2 Slip through

Figure 4.38 and 4.36 illustrate the result of compression when two O-rings is incorporated in the rectangular groove in three different positions. The side walls do not contribute to pre-tension, meaning there is only one vertical load step present. During this step, the upper wire move have an enforced displacement i ngeative direction compressing the sealing element down. When in position 2 and 3, the center of the O-rings are respectively offset by  $45^\circ$  and  $22.5^\circ$  relative to one another. In Figure 4.38 the friction coefficient is 0.2, while in Figure 4.36 it is 0.5 between all surfaces.

Figure 4.35 illustrates the final step for compression of two O-rings in position 2 with coefficient of friction equal to 0.5:

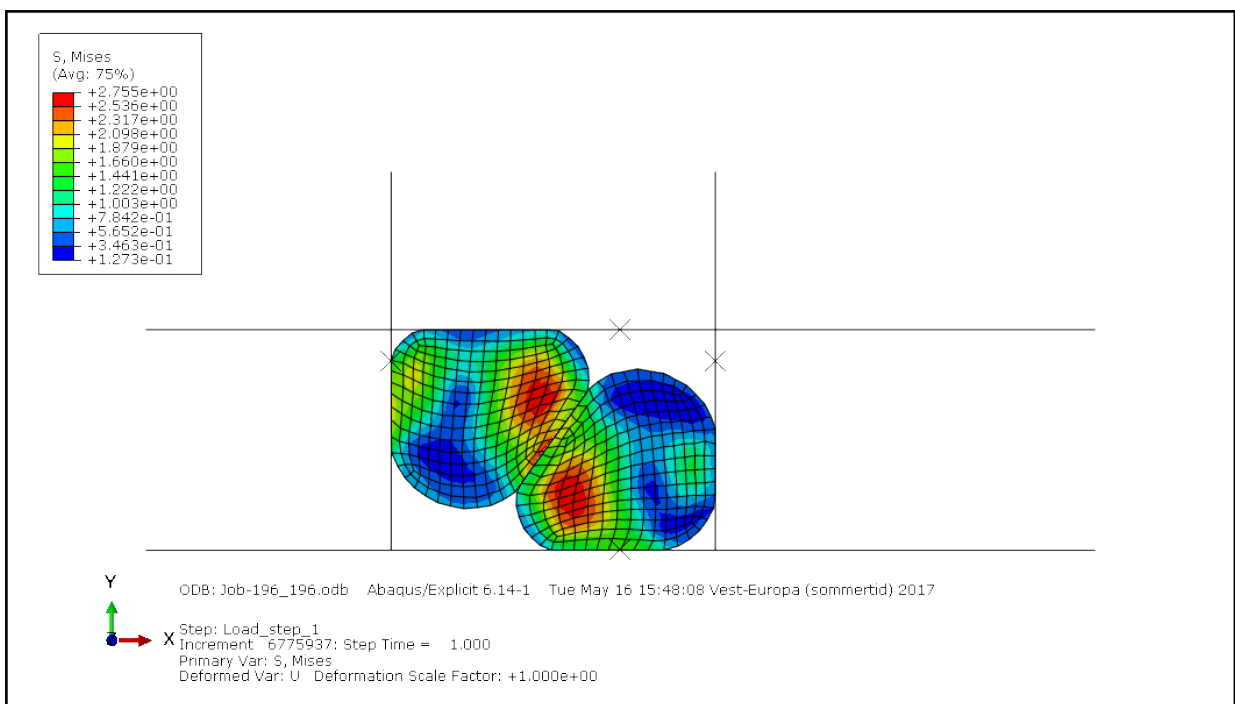


Figure 4.35: Slip Through - Illustrated -  $\mu=0.5$  - 6 mm



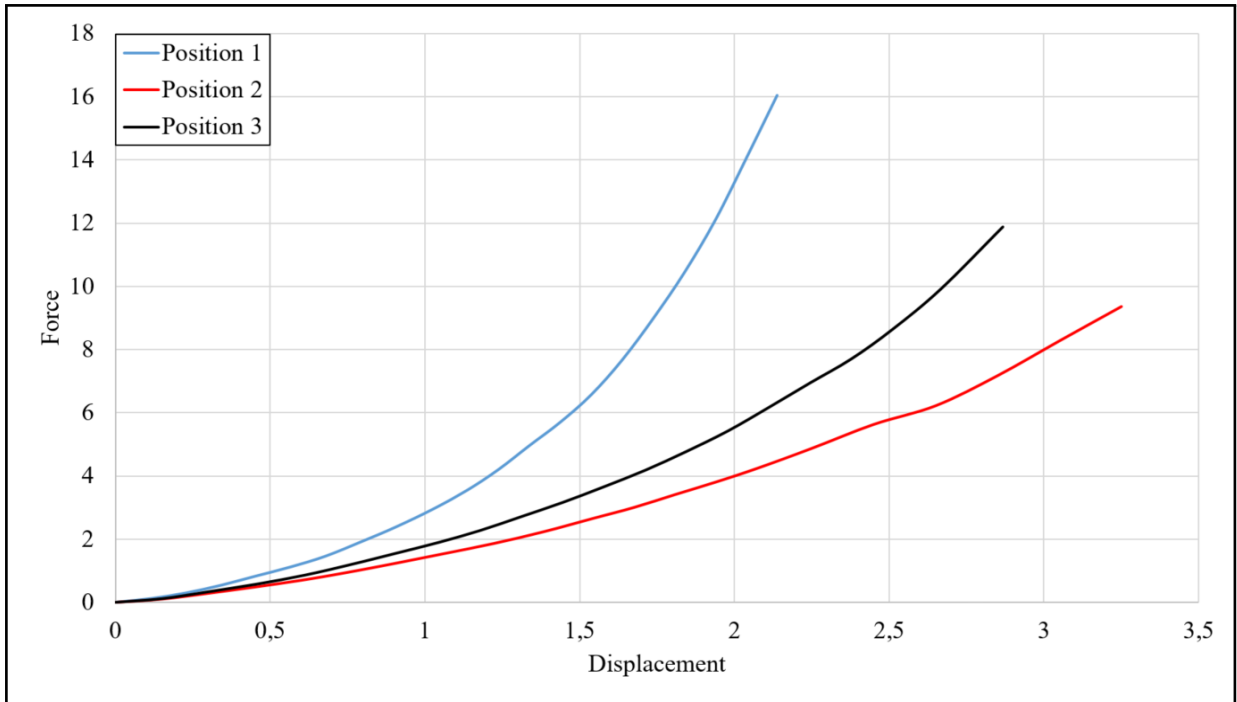


Figure 4.36: Slip Through -  $\mu=0.5$  - 6 mm

Figure 4.37 illustrates the final step for compression of two O-rings in position 2 with coefficient of friction equal to 0.2:

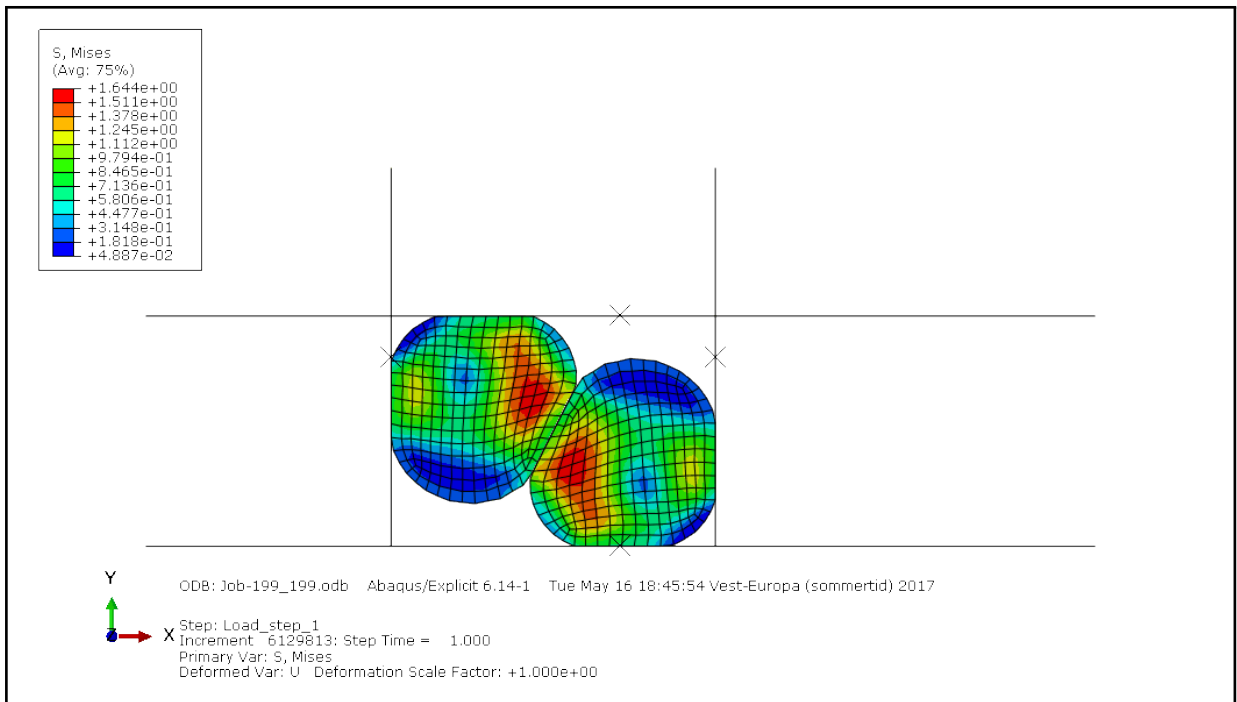


Figure 4.37: Slip Through - Illustrated -  $\mu=0.2$  - 6 mm

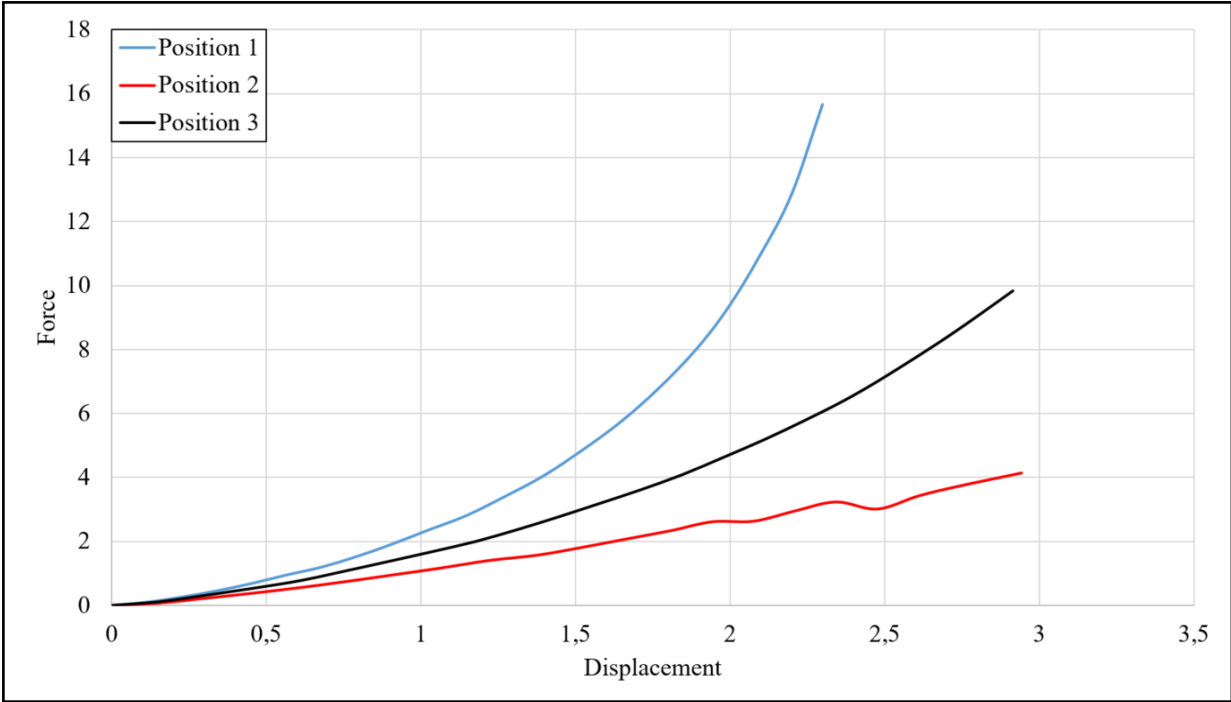


Figure 4.38: Slip Through -  $\mu=0.2$  - 6 mm

## 4.8 Triangular groove

As an experiment, simulation with a triangular groove instead of a rectangular groove were conducted. The objective of this approach is to identify how steep the angle between the two surfaces forming a triangular groove can be. When do the O-ring stick to the side walls due to the coefficient of friction? The results are carried out analytically by use of Coulomb friction Equation 3.2, and trigonometric relationships. Additionally, the result have been numerically calculated in ABAQUS.

### 4.8.1 Analytical results

By use of the simplification presented in section 3.8.2 and the Coulomb friction equation (Equation 3.2) the angle,  $\alpha$ , where the O-ring stick to the surfaces forming a triangular groove is calculated as follows:

The required angle for  $\mu=0.5$  is calculated in equation 4.1:

$$\tan^{-1}(0.5) = 26.56^\circ \tag{4.1}$$

With a friction coefficient of  $\mu = 0.5$ , the slip angle is calculated to be  $26.56^\circ$ . As a consequence by use of symmetri,  $26.56^\circ$  have to be multiplied by the factor 2 to obtain the total angle ( $\alpha$ ) between the surfaces. This means that the analytical  $\alpha$  equals  $53.12^\circ$ .

### 4.8.2 Numerical results

Figure 4.39 and 4.40 illustrate the limit for when the O-ring sticks to the wall depending on the angle,  $\alpha$ , between the surfaces forming a triangular groove. This simulation is conducted by one vertical load step of the upper wire followed by a unloading step (One loading cycle). The coefficient of friction,  $\mu$  is assumed to be 0.5.

Figure 4.39 illustrates that the O-ring **do not** get stuck due to friction and the angle ( $\alpha$ ) between the surfaces forming a triangular groove.

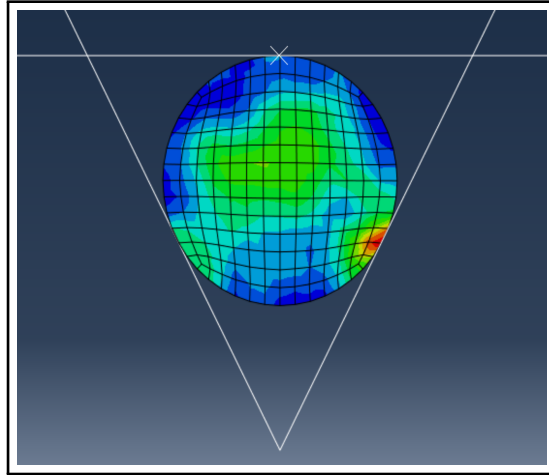


Figure 4.39: Triangular groove -  $\alpha=55^\circ$  - 6 mm

Figure 4.40 illustrates that the O-ring **do** get stuck due to friction and the angle ( $\alpha$ ) between the surfaces forming a triangular groove.

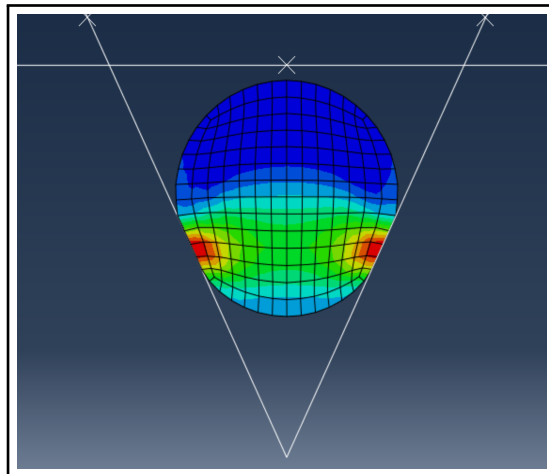


Figure 4.40: Triangular groove -  $\alpha=50^\circ$  - 6 mm

# Chapter 5

## Discussion

As mentioned in Chapter 3, several assumptions are made in this master thesis to recreate the approximate material deformation behaviour indicated by the experimental curves in Figure 4.2. When the simulations intended to give the correct representation, it was necessary to compare the numerical results to the experimental results. As seen from the final curves, deviation is present when comparing the aforementioned results. The deviation can be a result of several parameters, as for instance uncertainties related to the calculation of Young's modulus or the tolerances of the groove and temperature dependancy (which is neglected in the numerical simulations).

This chapter will critically examine assessments and considerations associated with the process, the influence of elements and Poisson's Ratio, contact definitions and the material approach. Finally, discussion of what the resulting curves might represent will be covered.

### 5.1 Analysis configuration

#### 5.1.1 Equilibrium solver

As a result of several attempts trying to represent the load characteristics of the guide vanes end seals in the best way possible, a considerably amount of time has been used configuring simulation models. The assessment of choosing the explicit instead of implicit solver is highly relevant as this simulation process is considered to be quasi-static. As mentioned in section 2.5.1, a selection of quasi-static simulations can be solved using either method. The implicit solver was tested and turned out to work well for a selection of the models, providing smoother curves than the explicit solver. Presumably, due to two dimensional modelling and the definition of contact interaction, the explicit solver did not work when contact pairs are defined in later steps than the initial. To clarify, the implicit solver works for the simulations where the contact is defined at the initial step (the surfaces involved are in contact from the beginning of the simulation). This

is the case when the groove is too small, indicated by a load step which moves the side walls either -0.15 mm, -0.10 mm, -0.05 mm, -0.025 mm or 0.00 mm towards the center of the O-ring to achieve pre-tension. Besides, the implicit solver only worked for the models containing one O-ring. A selection of analysis results with the implicit solver is attached in Appendix H. Further preparation of implicit analysis configuration is proposed as further work.

### 5.1.2 Early attempts

A challenge throughout this master thesis has been to construct models that represent the actual situation correctly considering the assumptions mentioned in section 3. The first attempts at modelling the plates were by constructing two dimensional plates with a higher Young's modulus compared to the rubber O-ring, which should depict plates much stiffer than the seal. A full description of assembly development can be found in Appendix K. However, this approach developed unwanted stresses in the plates, and contributed to consecutive challenges when modelling. ABAQUS Analysis User's Guide [34] suggested that parts whose function is to represent very stiff parts relative to other components, including contact interactions, should be modelled as rigid bodies. As mentioned, in section 3.1.1, ABAQUS provides two options when considering rigid parts; discrete or analytical. Attempts to model the wires as discrete rigid were conducted before noticing the user guide recommended analytical rigid parts when modelling involving contact. This supports the idea that the actual situation is represented.

### 5.1.3 Material approach considerations

Due to the fact that hyperelasticity is recommended when analysing elastomeric materials, a linear-elastic approach was chosen in this master thesis. In general, elastomeric materials usually have no distinct modulus, since the material properties are different from batch to batch. This is supported through e-mail correspondence with Trelleborg Sealing Solutions [38], which deliver the O-ring seals to Rainpower. They stated: "it is a significant difference between the compounds used for NBR. It is therefore almost impossible to give a general state of the versions of the Shore 70A and Shore 90A NBR material". Additionally, since Trelleborg test the material using a batch piece from the production and not the final O-ring, it is not possible to compare a batch test to a test of a finished O-ring [38].

In conjunction with the calculations of Young's modulus from the hardness number, it is assumed that the material properties are conservative in terms of a distinct modulus. Due to the strain density function and the dependency on experimental (material) test data to provide the most correct hyperelastic material model, the mechanical behaviour of elastomeric materials is complicated. Using a linear-elastic approach is con-

sidered difficult in terms of representing the exact material behaviour.

However, in this case, the linear-elastic approach intends to represent the trends of the curve correctly according to the magnitude of the displacement, and the curve path when compared to the experimental tests. For instance, Figure 4.4 shows that the trend of the curve is approximately correct, with curves presenting a slight displacement depending on the offset of the side walls. Please note that the results achieved by use of linear-elastic approach should be considered with great caution. Nevertheless, there are reasonable justifications of why this material approach seems to provide correct trends of the force-displacement curve for an incompressible, hyperelastic material. One such justification is presumably due to the environment. The mouldings analyzed in this master thesis are incorporated in a highly confined environment. As a consequence, the end seals have limited possibilities to move, expand or stretch. In other words, the deformation state of the material in terms of percentage (%)<sup>1</sup> is considered as restricted. Additionally, the dependency of hyperelastic material properties is probably more prominent during pure material testing such as tensile tests, than in for instance a compression sequence in a highly confined environment.

Viscoelasticity is given significant space in the theoretical background. This is due to the fact that elastomeric materials experience effects of viscoelasticity when they are exposed to load over time. Additionally, elastomers display significant viscoelastic effects at high temperatures resulting in reduced viscosity as mentioned in section 2.3.3. Both temperature dependency and viscoelasticity is neglected in this master thesis, but this will be effects for sealing elements in operation, and it is of great interest to survey the effects of these parameters as a part in further work (Chapter 7).

As mentioned in section 3.5, FEA of hyperelastic materials strictly depends on experimental test data. Furthermore, it is of great interest to conduct experimental material tests for implementation in for instance ABAQUS, and the results should be compared to the ones obtained from the linear-elastic approach.

#### 5.1.4 Plane stress and plane strain

The purpose of modelling in a two dimensional environment was to simplify the process, and decrease the computational time for numerical analyses. However, additional challenges are introduced in terms of element type definition when meshing. In general, it is necessary to consider the two types challenges in plane analysis; plane stress and plane strain conditions. The definition of plane stress or plane strain is critical. Respectively, the two types introduce certain restrictions and assumptions on the stress and displacement for the element type.

Plane stress is the default option for elements in two dimensional analyses in

---

<sup>1</sup>A elastic strain deformation greater than 200% was mentioned in section 2.3

ABAQUS. The first analyses using analytical rigid wires for the groove, and solid, homogeneous shell for the O-ring were conducted with element configuration as the default option (i.e. plane stress). Due to uncertainties about the linear-elastic approach and the fact that the curves of the plane stress approach followed the experimental curves for a certain time, it seemed as a correct decision. Additional simulations were conducted varying other parameters that the plane stress/strain definition, as for instance how the solvers iterate, interaction conditions and an attempt of defining bilinear material model<sup>2</sup>.

Eventually, when the results from plane stress were retrieved, the same trends were found in several curves but the curves deviate at some point near the end of the compression. Results did not represent the typical trends for incompressible materials (where the force increases towards infinity as the sealing element do not have the ability to be compressed any further) the plane stress/strain relation was discussed and noted.

The contribution of the hydrostatic pressure is highly relevant in addition to the contribution of transverse extraction (Poisson's Ratio). For plane stress conditions, the contribution from the hydrostatic pressure is significantly less than the deviatoric (shear stress) contribution. For plane strain conditions, it is the opposite situation: the hydrostatic pressure has great influence. To sum up, plane stress is considered as an unfavourable approach due to the fact that it allows for expansion in z-direction. Hence, plane strain conditions should be used instead.

However, changing the element definition from plane stress to plane strain definition gave immediate results for the trends of the curves, since the end seal becomes restricted to expand exclusively in the x-y plane. Figure 5.1 shows the resulting curve for plane stress compared to plane strain using the exact same model: a single O-ring with cross sectional diameter 6 mm in Shore 70A quality with 0.00 mm offset of the side walls, a Poisson's ratio of 0.4995 and a coefficient of friction equal to 0.5. Additionally, Figure 5.1 illustrates how plane strain follows an appropriate trend while plane stress undoubtedly deviates from the expected behaviour.

---

<sup>2</sup>Bilinear material curve is a curve where the stress-strain curve is assumed to be linear from the yield point to the point of necking



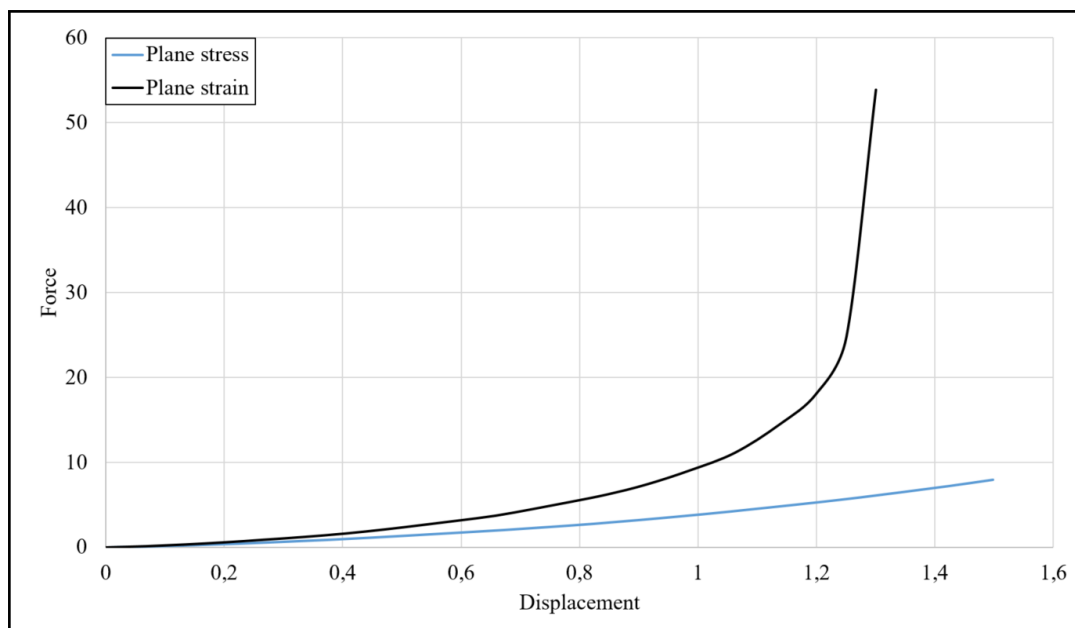


Figure 5.1: Comparison of plane stress and plane strain

Please note that the plane strain curve (black line) in Figure 5.1 is the same as the one used in Figure 4.4 (red line), but in this context it is independent of the results presented in Chapter 4. Figure 5.1 focuses on emphasizing the difference between plane stress and plane strain.

A selection of (incorrect) results from the plane stress analyses can be found in Appendix J. It is individually from test to test where the numerical curve deviate from the physical curve. A enforced vertical displacement in between 1 mm and 3 mm was assumed to be enough to recreate the path of the experimental curves, but the curve did not represent incompressibility in terms of a steep change in the force needed for compression, indicating that the representation is clearly not correct.

### 5.1.5 Influence of Poisson's Ratio

In addition to the hydrostatic pressure, the Poisson's Ratio tends to have noticeable influence in incompressible elastomeric materials. For the compression sequence of a material in a highly confined environment, the transverse extraction is presumed to be considerably more prominent than the hyperelastic properties. This is probably one of the reasons the trends of the curves intend to recreate the trends of the experimental curves which serve as basis. As mentioned in section 2.3.4, the Poisson's Ratio,  $\nu$ , of an incompressible material is close to 0.5.

To illustrate the impact of the Poisson's Ratio as it approaches 0.5, analyses with a single O-ring in Shore 70A material hardness with no offset of the side walls and a coefficient of friction,  $\mu$ , assumed to be 0.5 have been conducted and compared to the experimental test. Notice how the accuracy is increasing in Figure 5.2 as the Poisson's

Ratio approaches 0.5. Table 5.1 presents the parameters used in the models.

Table 5.1: Poisson's Ratio - Shore 70A - Ø6 - One ring

Hardness	Cross section	$\nu$	$\mu$	Test
Shore 70A	Ø6	0.45	0.5	Numerical
Shore 70A	Ø6	0.495	0.5	Numerical
Shore 70A	Ø6	0.4995	0.5	Numerical

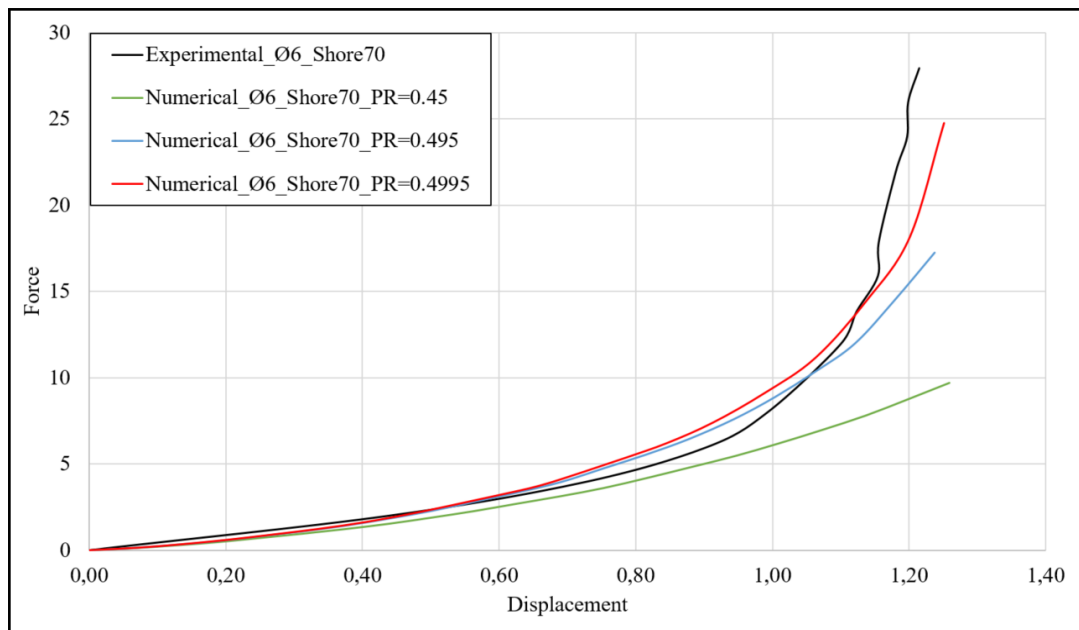


Figure 5.2: Comparison of Poisson's Ratio - Shore 70A - Ø6

### 5.1.6 Mesh comparison

The size of the mesh seeds has influence when analysing mechanical components. The importance of the size is essential when retrieving stress and strain, and also, to a certain extent; the force-displacement curve. Figure 5.3 illustrates the difference between the curves for a single O-ring with cross section diameter 6 mm in Shore 70 A hardness.

Table 5.2: Parameters - Mesh of one O-ring in Shore 70A hardness

Hardness	Cross section	Seed size	$\mu$	Test
Shore 70A	Ø6	0.3	0.5	Numerical
Shore 70A	Ø6	0.6	0.5	Numerical

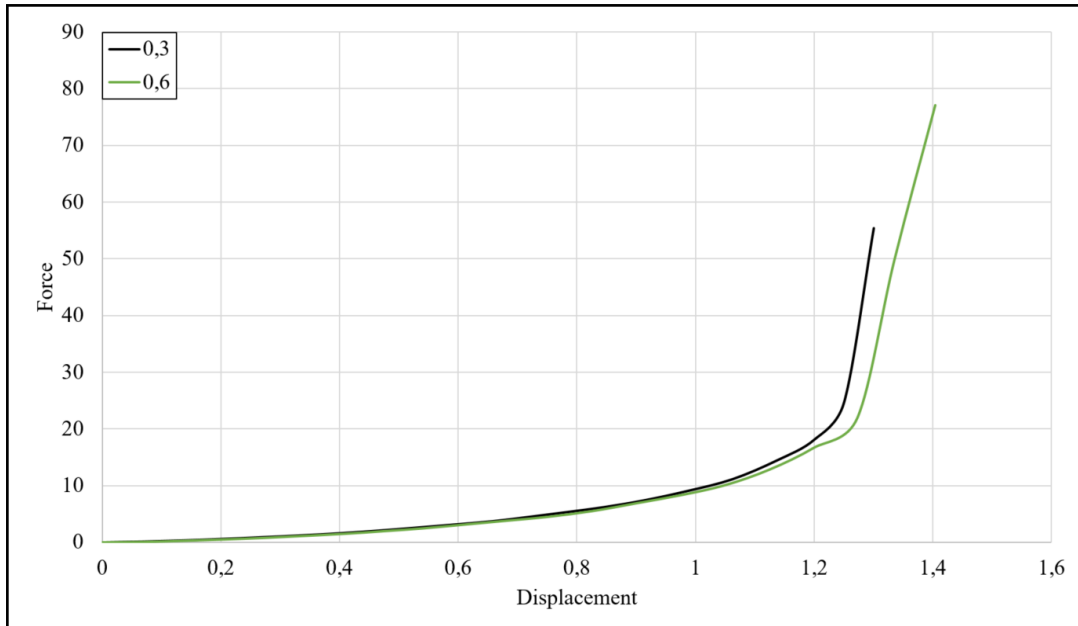


Figure 5.3: Shore 70A - Ø6 - Mesh comparison

Figure 5.3 illustrates the difference in the curves for two O-rings with cross section diameter 6 mm with Shore 70 A hardness.

Table 5.3: Parameters - Mesh of two O-rings in Shore 70A hardness

Hardness	Cross section	Seed size	$\mu$	Test
Shore 70A	Ø6	0.3	0.5	Numerical
Shore 70A	Ø6	0.6	0.5	Numerical

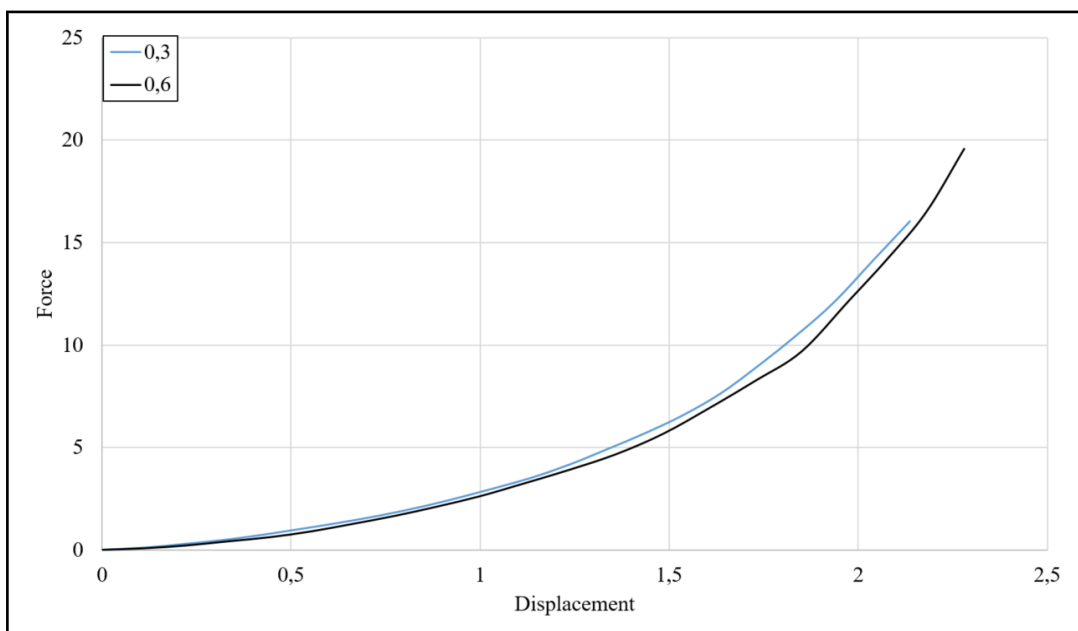


Figure 5.4: Mesh of two O-rings in Shore 70A hardness

As shown from the comparison of mesh effects for both one and two O-rings, the trends of the curves are similar and hence the effect of the mesh seeds is considered as negligible. Usually, hybrid elements <sup>3</sup> are recommended when analysing hyperelastic materials. This is not applicable for this master thesis due to the approach of using two dimensional planar with linear elastic material approach. Still, quadrilateral elements seem to provide desirable results. However, hybrid elements should be considered if similar analyses are conducted in a three dimensional environment using hyperelastic material models.

## 5.2 Interactions

### 5.2.1 Contact algorithm

Interaction properties have been given significant attention in this master thesis, even though they do not tend to have remarkable influence on the results. Defining contact interactions has been essential in setting up the simulation models correctly. Guide vane end seals are, as mentioned, incorporated in a highly confined environment making the definition of contact interactions highly relevant. Defining contact as a kinematic contact method was considered desirable because the penetration challenges using the penalty method may lead to problems. As mentioned in section 2.5.2, choosing the penalty weight is challenging and requires experience. If this value is chosen to be too high, the stiffness will be high resulting in a small amount of penetration. This can contribute to numerical instabilities.

By using the kinematic contact method, the pure master-slave algorithm is used by default. This algorithm defines the slave node to follow the master node, resulting in no penetration. The consideration of using kinematic contact method intends to be the most reasonable approach for the simulations of the end seals. However, it is unlikely that rubber material in any circumstances will penetrate surrounding metalwork. The situation of penetration between surfaces is assumed to be more likely to happen when, e.g, two surfaces of steel slide or interact. As for instance, if the end seals had not been incorporated, the guide vane and the mating steel surfaces would presumably have slid against each other, which may result in galling.

Additionally, it will be (as further work) of particular interest to carry out numerical simulations changing the contact definition from kinematic algorithm to the penalty algorithm including the coefficient of friction.

---

<sup>3</sup>In general the hybrid elements are used for incompressible materials to avoid volumetric locking

## 5.2.2 Friction

An important parameter when defining interaction properties is the coefficient of friction,  $\mu$ . The coefficient of friction may influence the load deflection curves in certain situations. Yet, as illustrated in Figure 5.5,  $\mu$  does not have any particular influence on the trends of the curves. It is reasonable to assume  $\mu$  is somewhat higher than 0.0, and 0.5 was considered a good approximation as a result of internet research. In addition, the coefficient is assumed to be similar between all mating surfaces, which is probably not the fact for rubber against steel, or rubber against rubber. Friction between rubber and steel is most likely around 0.5 and rubber versus rubber approximately 1.0, depending on the surface properties and environment.

However, using 0.5 as friction coefficient between all surfaces may not give a 100 % correct picture of the frictional conditions, but should not influence the trends of the load deflection curves. The coefficient of friction will probably alter due to changes in the environment; if the environment is lubricated (wet), it is doubtful that  $\mu$  exceeds 0.5.

For a single compression step, the influence of the friction coefficient is considered as minimal. This is illustrated in Figure 5.5. However, for certain situations, as for instance when the angle  $\beta$  between the O-ring centers is approximately  $45^\circ$ , the coefficient of friction may have greater influence (this is considered in depth in section 5.4.3).

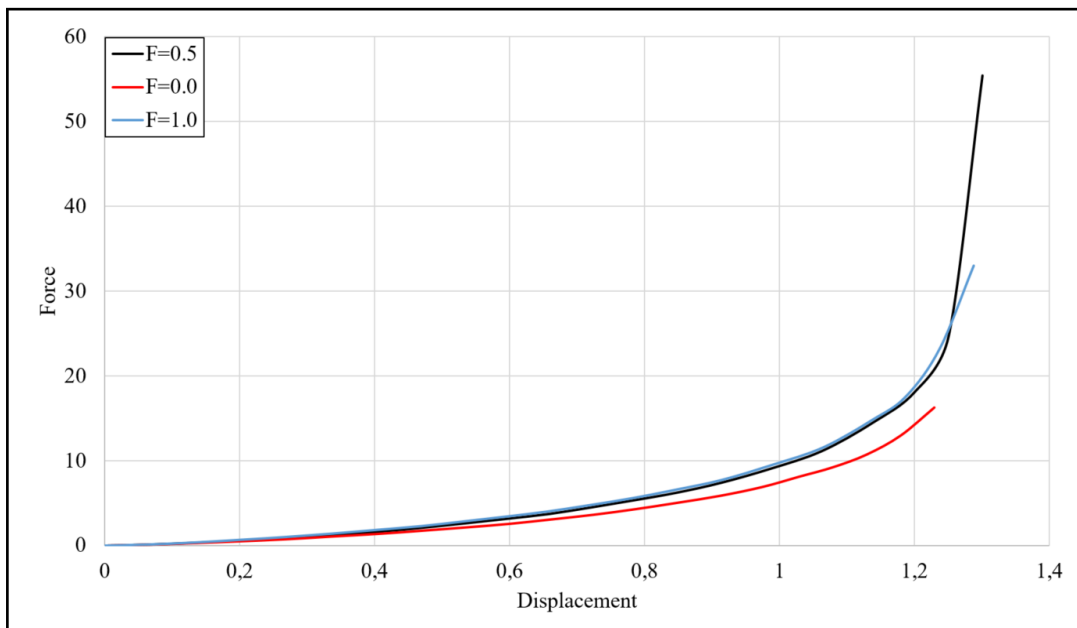


Figure 5.5: Ø6 - Shore 70 - Friction comparison

Please note that the plane strain curve (black line) in Figure 5.5 is the same as the one used in Figure 4.4 (red line), but in this context it is independent of the results presented in Chapter 4. Figure 5.5 focuses on emphasizing the difference between the respective friction coefficients.

When the compression sequence contains two O-rings instead of one, the frictional

effects are noticeably more prominent. If only one O-ring is compressed, the analysis experiences convergence problems when whole the rectangular groove is filled. When compressing two O-rings, the solver experiences convergence problems prior to the point where the whole groove is filled; due to the frictional effects of the upper O-ring towards the upper corners, ensuring element distortion in this area. In Figure 5.6 and 5.7 the effect of friction for compression of two O-rings is partially illustrated with the curvature of the horizontal grid lines.

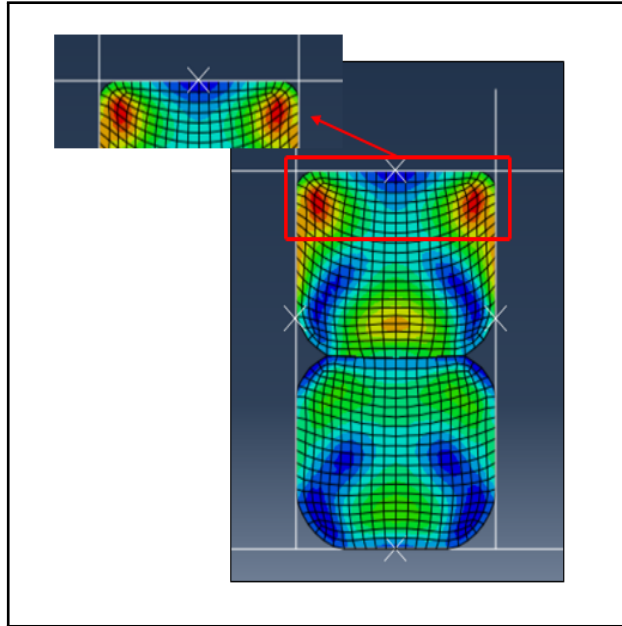


Figure 5.6:  $\text{Ø}6$  - Shore 70 - Friction comparison -  $F=0.2$

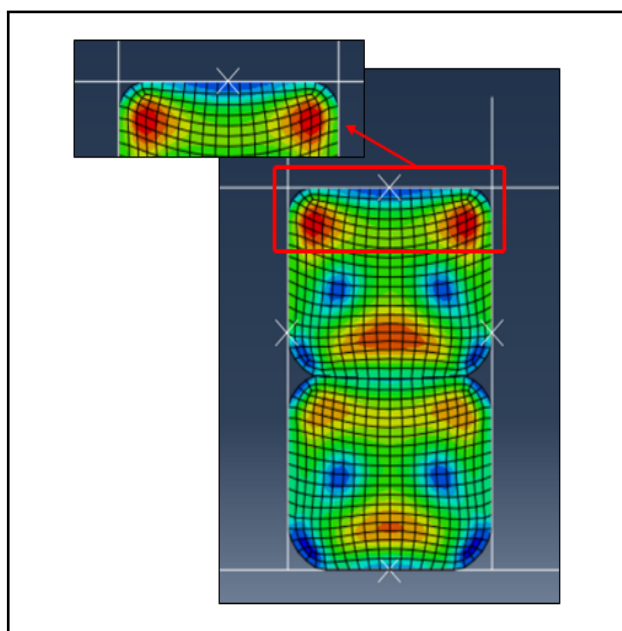


Figure 5.7:  $\text{Ø}6$  - Shore 70 - Friction comparison -  $F=0.5$

### 5.3 Assessment of experimental tests

The experimental results presented in section 4.2 provide the basis for the current parameter study. However, information about the implementation of the experimental tests were limited. As a result, several assumptions were made, presented in Chapter 3. Summarizing, the basis for the numerical simulations is an assumption of how the experimental tests have been completed and thus attempted to be recreated in the numerical simulations. Generally, the experimental tests are assumed to be conducted by using four surfaces (tangential to the seal) representing the groove with either one or two sealing elements incorporated, and compressing the O-ring down as shown in Figure 5.8:

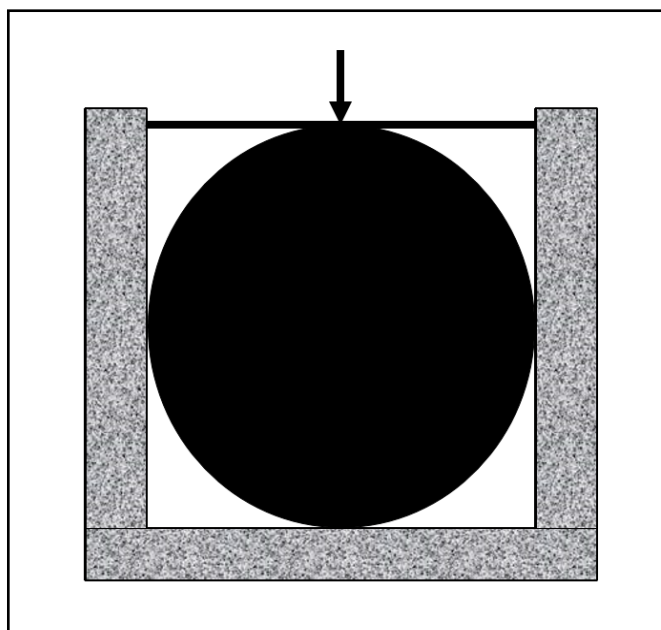


Figure 5.8: Assumed implementation of experimental tests

The force and displacement are measured during the compression sequence. Yet, despite reasonable assumptions being made; several questions remain unanswered. Are the experimental tests conducted with or without pre-tension of the O-ring? Which tolerances are used? Which properties does the tested O-ring have? Where there any changes in temperature for the material?(temperature dependency is unknown for the experimental tests). For further work, as mentioned in Chapter 7, it would have been preferable to conduct new experimental tests for comparison.

Usually, for numerical analyses it is necessary to define either the force applied or an enforced displacement for the simulation. For instance; if a 2 mm enforced displacement is applied, what is the force needed? For the experimental tests, it may be possible to install the seal between compressing surfaces and try to compress as hard as possible for maximum displacement. Since the experimental tests illustrate that the force increases towards infinity before reaching the given displacement, it would have been preferable

to treat both displacement and force as unknowns, but this is challenging to be implemented in numerical simulations. Related to this considerations, the arc length method is presented in Appendix C which is an iteration procedure mainly used for buckling and collapse analyses. For this method both displacement and load increments are controlled simultaneously. However, this requires functionality for the implicit solver.

## 5.4 Assessment of results

### 5.4.1 Comparison curves

Broadly speaking, the force response tends to be dependent on the dimensions of the groove, the number of sealing elements and their corresponding cross-sectional diameter. Illustrated by the comparison curves presented in section 4.5.3 (e.g. Figure 4.14 and 4.15), the choice of diameter or tolerances can be combined to a certain extent. As shown in Figure 4.14, a single O-ring with a diameter of 6 mm combined with a groove of -0.30 mm smaller than the sealing diameter, or a single O-ring with diameter 5 mm with a groove of -0.05 mm smaller tends to provide considerably similar load deflection curves. Additionally, as shown in Figure 4.15 a single O-ring in Shore 70A material hardness with cross sectional diameter 6 mm with a groove 0.10 mm wider than the sealing element, and one with diameter 5 mm with a groove 0.20 mm wider tends to provide approximately similar force response curves.

Figure 4.16 and 4.17 compare the cross-sectional diameter when the groove contains two sealing elements instead of one as in Figure 4.14 and Figure 4.15. There are a certain difference in cross-sectional diameter and tolerances of the groove when using two sealing elements instead of one, but the trends are similar.

Generally, the force and the vertical displacement vary relatively to the dimensions of the groove as shown in Figure 4.10 and Figure 4.11. A groove which is too small compared to the cross-section of the sealing element demands a higher force to achieve the equal value of displacement as in the case where the groove is tangential. The force needed to compress the O-ring a given vertical displacement is higher when the groove is smaller relative to the O-ring diameter. Additionally, a trend in which a given vertical displacement is higher in terms of a wider groove: meaning, a higher vertical displacement is obtained for wider grooves. As indicated by several of the resulting figures, the cases where the groove is bigger than the O-ring: the force needed to achieve the enforced vertical displacement decreases as the offset of the side walls increases from 0.00 mm to 0.20 mm. For the opposite case, where the O-ring is wider than the groove; it is possible to see that the force needed to achieve the enforced displacement increases as the width of the groove decreases.

Independent of the material hardness or the width of the groove, by employing



two sealing elements instead of one, it is possible to achieve a greater displacement for the same force magnitude. This is illustrated in Figure 4.18, 4.19, 4.20 and 4.21. Particularly, this trend insinuate to be reasonable due to the fact that the sealing elements do have significantly more space to fill using two elements instead of one.

Overall, due to the lack of consistency of how the numerical curves fit the experimental trends, the results can be characterized as arbitrary. The trends of the curves, especially for Shore 70A material hardness fits pretty well. However, Figure 4.4, 4.5, 4.6, 4.8 and 4.9 illustrate that the trend of the numerical curves fit the experimental test correctly. In general, it seems that it is the offset of side walls which describes how close the numerical curve is to the experimental, as shown for instance in Figure 4.6. This is unlikely to be the case as it is doubtful that the offset of side walls was changed during the experimental test. Assuming the walls were tangential to the side of the O-ring; the numerical simulations with offset equal to 0.00 mm should have been the curves with a better fit.

## 5.4.2 Material

As seen in Figure 4.4, the combination of parameters for the numerical simulations seems to be reasonable as it follows the trend of the experimental curve almost perfectly. As mentioned in section 5.3, one of the assumptions made for the implementation of the experimental tests that the walls are tangential to the seal. However, Figure 4.5 tends to be highly accurate (following the curve of a sealing element in a groove which is in total 0.2 mm wider than the O-ring diameter) until approximately 1 mm in displacement before it deviates from the numerical curve. The reasons for this discrepancy may be numerous, but the material trends for Shore 70A material are more accurate compared to Shore 90A for one sealing element.

Furthermore, several assumptions are made which can be considered as potential causes. A reasonable assumption considering the uncertainty of calculating the Young's modulus from the hardness number using Gent's equation, is that this is likely a too conservative approach. It would have been extremely useful to compare hyperelastic results to the linear elastic results presented in this master thesis to either conclude or declare this assumption. This is due to the fact that elastomeric materials are expected to have varying material properties batch to batch. The use of the Gent's equation should also be discussed, as it is usually considered as a good approximation between Shore 20A and Shore 80A [24]. This can be one of the reasons the numerical results for Shore 70A intends to provide better results compared to the experimental tests, than the Shore 90A numerical results. As a matter of fact, the calculation of 6 MPa for the Shore70A material can be considered (from the numerical analyses) to be a better approximation of the Young's modulus for the material in the experimental tests than the approximation

of 21 MPa for the Shore 90A material.

Generally, the resulting curves, as for instance Figure 4.12 and Figure 4.13 illustrate that the Shore 90A material is significantly harder compared to the Shore 70A material as a higher force is needed for the Shore 90A material to compress the similar displacement.

### 5.4.3 Slip through

When two O-rings are incorporated in the guide vanes, their positions relative to each other seem to have minimal influence for an angle,  $\beta$  (shown in Figure 5.9) less than  $45^\circ$ . In Figure 4.35, the friction coefficient is 0.5 and illustrated by the curves in Figure 4.36 one can see the above O-ring do not "slip through" on the left side of the lower O-ring. However, in Figure 4.37, the friction coefficient is 0.2 and illustrated by the corresponding curves in Figure 4.38 one can see that in position 2 (red line) the force do not increase as the two other curves do. This is presumably the point where the seals "slip through". The force necessary to push the O-ring further down do not increase because the upper O-ring have overcome the frictional resistance between the sealing elements.

This is probably due to the fact that the frictional force is not strong enough to prevent "slip through" which means that the above O-ring "slip" down in between the left side wall and the lower O-ring. Supported by the results from the "slip through" simulations, both the angles ( $\beta$ ) between the O-rings centers, and the friction coefficient contribute to for this failure to happen.

For the case of two O-rings, it is assumed that position 1 (one straight above the other as presented in Figure 3.14) is more likely to be present than the two other positions, due to the fact that there are tolerances for the geometry of the groove. Predominantly, situations where positions 2 or 3 (center of the O-rings  $45^\circ$  and  $22^\circ$  relative to one another) are present is considered as minimal.

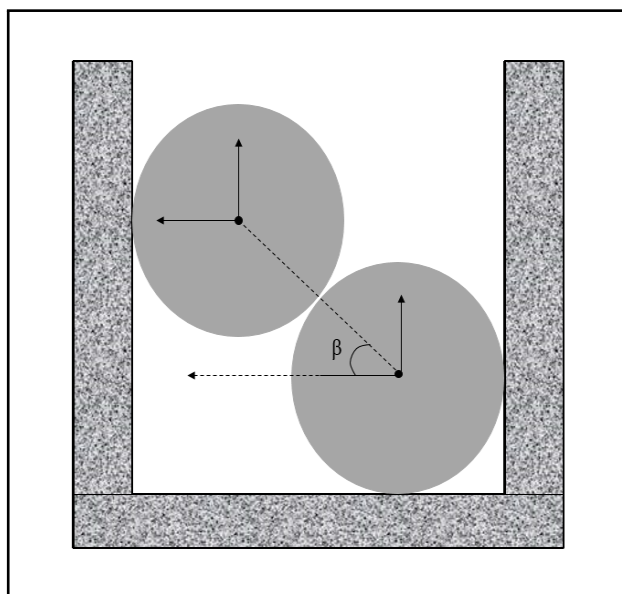


Figure 5.9: Angle  $\beta$ , between the seal centers

### 5.4.4 Hysteresis loops

As shown by the hysteresis loops, energy dissipation is present during cyclic loading. As a result of varying parameters for the groove, the phase where energy dissipates is different in terms of when the O-ring interacts with the surrounding surfaces. When the side walls are either tangential or contribute to pre-tensioning, the "gap" between the loading and unloading step (which indicates energy loss), of the curve is concentrated at the beginning of the simulation as shown in Figure 4.22 and Figure 4.23. This is probably due to contact occurring at this point. For situations in which the side walls are offset, indicating a groove too wide for the O-rings, the energy dissipation region occurs later (higher on the curve), in terms of the simulation step where the O-rings interact with the side walls. This is illustrated in Figure 4.24 and I.32. In this context, the representation seems to be reasonable according to the energy loss associated with contact interaction, i.e. friction.

However, considering the hysteresis loops from the simulation with two O-rings in three different positions as presented in section 4.7.1 the frictional force indicates to be "strong" enough to prevent slip through during cyclic loading (so the sealing element do not get fastened), and the O-rings are able to restore its initial position when unloading. For this to be a problem, the combination of frictional force and the angle,  $\beta$  between the O-ring centers have to be of magnitudes in which is considered as unrealistic (position 2). Due to the fact of machining tolerances for the groove (situation 2), where the O-ring centers are  $45^\circ$  offset from one another, this is probably unreasonable. Figure 4.29 illustrates by simulating one load cycle (loading + unloading step) that the sealing elements do not get stuck, but regain its original shape and position 2. However, Figure 4.34 illustrates by simulating one load cycle (loading + unloading step), that the sealing elements do get stuck (the red curve reaches the x-axis at approximately 0.6 and not 0.0) and do not regain its original shape and position 2. Meaning that this position is sensitive for changes in the cross-sectional diameter (from 6 mm down to 5 mm for this situation) with a constant coefficient of friction,  $\mu$  equal to 0.5. This is illustrated in Figure 4.32c, where the O-ring are locked between the left side wall and the lower O-ring.

### 5.4.5 Triangular groove

Considering the numerical results in section 4.8 for a triangular geometry of the groove; the angle  $\alpha$ , between the surfaces forming a triangular groove where the O-ring is stuck due to frictional effects seems to correspond well with the analytical calculations. From the analytical calculations, the angle,  $\alpha$  was found to be  $26.56^\circ$  times the factor 2 (due to symmetry), which equals  $53,13^\circ$ . As seen in Figure 4.39 and Figure 4.40 which represent the result from the numerical analyses; the limit when the O-ring sticks to the side walls is in between the calculated interval ( $50^\circ - 55^\circ$ ). Figure 4.39 illustrates the situation where

the angle  $\alpha$ , is  $55^\circ$  which is not steep enough to the O-ring to stick to the side walls after unloading. Figure 4.40 illustrates the situation where the angle  $\alpha$ , is  $50^\circ$ , which is steep enough for the O-ring to stick to the side walls after unloading. However, triangular grooves can be useful for saving space and can make assembly more convenient. However, associated challenges in terms of dimensions may be present.



# Chapter 6

## Concluding remarks

- Several load characteristics are carried out indicating the load sensitivity to geometry changes for either one or two sealing elements in material hardness Shore 70A and Shore 90A.
- The resulting curves of varying tolerances compared illustrate how the force increases as the rectangular groove dimensions decreases (smaller groove). And the other way around; the force decreases as the groove increases (wider groove).
- The number of sealing elements, the material hardness, cross-sectional diameter and the combination of these parameters should be considered prior to installation as they provide different load-deflection curves.
- If considering a triangular formed groove, the sealing element will probably get stuck if the angle  $\alpha$ , is in between the intervall  $50^\circ$  and  $55^\circ$  between the surfaces forming the groove, when the friction coefficient  $\mu$ , is 0.5.
- The purpose of modelling the sealing elements in a triangular groove was to see the effects of the friction, asking the question; how steep does the angle between the triangular walls have to be before the O-ring get stuck cause to friction? The slip angle were first calculated by conventional friction calculations by hand before simulated in ABAQUS. Numerical analyses were conducted with several values for the angle chosen in order to approximate the one in which the O-ring will stick to the side walls. Conclusively, both the numerical simulations and the analytical calculations gave approximately the same results depending on the coefficient of friction.
- Even though the information about the experimental tests were limited for the guide vanes end seals, simulations conducted in this master thesis represent the material trends in a satisfying way using a linear elastic approach. The majority of the curves from the numerical simulations follow the trends of the experimental tests results.

- The combination of a highly confined environment, Poisson's Ratio, Plane strain definition and contact algorithm have great influence on the results, and have provided the fundament for recreating the curve trends.
- Despite several uncertainties, it seems that using the linear elasticity with plane strain can recreate the trends of hyperelastic material behavior in highly confined environment. Due to recommendation of using hyperelasticity, the results obtained using linear-elastic approach should be treated with the great caution.
- The force needed to achieve the given displacement increased parallel with the increase in Poisson's Ratio. When using plane strain element definition, the Poisson's Ratio is beneficial. It is a remarkable difference between 0.45, 0.495 and 0.4995, concluding that the closer to 0.5 the better approximation of the curve trend. The increase in Poisson's Ratio increase the computational time for the solver as well.
- Hysteresis curves are carried out illustrate the fact of energy dissipation due to frictional sliding as mentioned in section 2.3.3. The cyclic loading sequence is not long enough to state the effects due to ageing, but it shows how the energy dissipation is present during loading and unloading.
- When analyzing two sealing elements relative to one another, the angle  $\beta$  between the centers have to be approximately  $45^\circ$  according to one another with a low friction coefficient for slip through to occur.
- The level of "slip through" depends on the positioning of the sealing elements relative to one another, the coefficient of friction,  $\mu$  and the cross-sectional diameter. When the coefficient of friction is 0.5, the friction force is "strong" enough to prevent slip through when the cross-sectional diameter is 6 mm.
- The test plan for the experimental tests should be similar for the numerical analysis for comparison. Test data guidelines in addition to relevant standards for experimental testing of elastomers is presented in Appendix G.



# Chapter 7

## Recommendations for Further work

Any further work within analyses the load characteristics of guide vane end seals should include the following:

- Comparison of additional parameters and estimate probability for leakage from the results calculated.
- Use of hyperelastic material models.
- Conduct new experimental load versus displacement tests and compare to the numerical results from this master thesis. Experimental friction testing can also be conducted for verification.
- Model in three dimensional working environment for comparison reasons. The three dimensional approach may differ compared to modelling in two dimensions due to contact definitions in three dimensions, but if it does not, it may be concluded that the contact modelling are correct for this master thesis.
- Preparation of Prony series. This is in order to determine the time dependent stress-strain state in a linear viscoelastic material, under an arbitrary loading process. It is necessary to consider the deformation history for hyperelastic materials. The time dependent constitutive equations of a solid viscoelastic material include these history effects. The load (stress) and displacement (strain) history, the loading rate (displacement rate), and time of load application on the specimen are all needed to determine the constants in the constitutive equations. A common form for these constitutive equations employs a Prony series.
- Conduct new experimental tests of material properties for implementation of hyperelasticity in software.
- Set up implicit analyses using, the arc length method. This uses the load magnitude as an additional unknown; it solves simultaneously for loads and displacements.

Therefore, another quantity must be used to measure the progress of the solution; ABAQUS/Standard uses the “arc length,” <sup>1</sup>, along the static equilibrium path in load-displacement space. This approach provides solutions regardless of whether the response is stable or unstable.

- Temperature dependency - analyze the viscoelastic behaviour. Because viscoelastic materials have the viscosity factor, they have a strain rate dependent on time in which should be accounted for in numerical analyses. The Bergstrom-Boyce model was one of the first advanced material model developed. This model is presented in [4]. It is supposed to work well for predicting the non-linear viscoelastic response of rubbers despite being a simple model and should may be tested.
- Capture Mullins effect, which is the damage criteria for elastomeric materials<sup>1</sup>.

---

<sup>1</sup>ABAQUS provides a material model to capture Mullins effect.

# Bibliography

- [1] Ismail J Abubakar, Peter Myler, and Erping Zhou. Constitutive modelling of elastomeric seal material under compressive loading. *Modeling and Numerical Simulation of Material Science*, 6(02):28, 2016.
- [2] Donald R. Askeland, Pradeep P. Fulay, Wendelin J. Wright, and D. K. Bhattacharya. *The science and engineering of materials*. Cengage Learning, Stamford, Conn, 6th ed., si-ed. prepared by d.k. bhattacharya. edition, 2011.
- [3] Kolbein Bell. *An engineering approach to finite element analysis of linear structural mechanics problems*. Akademika Publ., Trondheim, 2013.
- [4] JS Bergstrøm and MC Boyce. Constitutive modeling of the large strain time-dependent behavior of elastomers. *Journal of the Mechanics and Physics of Solids*, 46(5):931–954, 1998.
- [5] Kenneth G Budinski. Incipient galling of metals. *Wear*, 74(1):93–105, 1981.
- [6] Zhi Chen, Tinchao Liu, and Jianming Li. The effect of the o-ring on the end face deformation of mechanical seals based on numerical simulation. *Tribology International*, 97:278–287, 2016.
- [7] E. Dragoni and A. Strozzi. Analysis of an unpressurized, laterally restrained, elastomeric o-ring seal. *Journal of Tribology*, 110(2):193, 1988.
- [8] E. Dragoni and A. Strozzi. Theoretical analysis of an unpressurized elastomeric o-ring seal inserted into a rectangular groove. *Wear*, 130(1):41–51, 1989.
- [9] Carlos A Felippa. Error analysis of penalty function techniques for constraint definition in linear algebraic systems. *International Journal for Numerical Methods in Engineering*, 11(4):709–728, 1977.
- [10] Carlos A Felippa. Chapter 1: Overview. Web page, September 2012. <http://www.colorado.edu/engineering/CAS/courses.d/NFEM.d/NFEM.Ch01.d/NFEM.Ch01.index.html>.

- [11] Carlos A Felippa. Chapter 8: Multifreedom constraints 1. Web page, October 2016. <http://www.colorado.edu/engineering/CAS/courses.d/IFEM.d/IFEM.Ch08.d/IFEM.Ch08.index.html>.
- [12] Carlos A Felippa. Chapter 9: Multifreedom constraints 2. Web page, September 2016. <http://www.colorado.edu/engineering/CAS/courses.d/IFEM.d/IFEM.Ch09.d/IFEM.Ch09.index.html>.
- [13] Robert Flitney and Melvin W. Brown. *Seals and sealing handbook*. Elsevier, Amsterdam, 5th ed. edition, 2007.
- [14] Alan N Gent. On the relation between indentation hardness and young's modulus. *Rubber Chemistry and Technology*, 31(4):896–906, 1958.
- [15] A. George, A. Strozzi, J. Rich, and A. George. Stress fields in a compressed unconstrained elastomeric o-ring seal and a comparison of computer predictions and experimental results. *Tribol. Int*, 20(5):237–247, 1987.
- [16] Itzhak Green and Capel English. Stresses and deformation of compressed elastomeric o-ring seals. In *14th international conference on fluid sealing, Firenze, Italy*, volume 4, pages 6–8. Citeseer.
- [17] F. J. Harewood and P. E. McHugh. Comparison of the implicit and explicit finite element methods using crystal plasticity. *Computational Materials Science*, 39(2):481–494, 2007.
- [18] Werner Hofmann. *Rubber technology handbook*. Kautschuk-Technologie. Hanser, Munich, 1989.
- [19] William F. Hosford. *Mechanical behavior of materials*. Cambridge University Press, Cambridge, 2005.
- [20] Imecanica.org. Advanced topics overview of abaqus 2005. Web page, September 2013. <http://imechanica.org/node/15260>.
- [21] Kamal K Kar, Mukesh Rawat, and Joshua U Otaigbe. Finite element analysis of hyperelastic materials: Elastomeric seal. In *ANTEC... conference proceedings*, volume 2, pages 2277–2281. Society of Plastics Engineers.
- [22] Beomkeun Kim, Seong Lee, Jayone Lee, Sehyun Cho, Hyungmin Park, Sanghoon Yeom, and Sung Park. A comparison among neo-hookean model, mooney-rivlin model, and ogden model for chloroprene rubber. *International Journal of Precision Engineering and Manufacturing*, 13(5):759–764, 2012.

- [23] Hyung-Kyu Kim, Jeong-Hwan Nam, Jai-Sug Hawong, and Young-Ho Lee. Evaluation of o-ring stresses subjected to vertical and one side lateral pressure by theoretical approximation comparing with photoelastic experimental results. *Engineering Failure Analysis*, 16(6):1876–1882, 2009.
- [24] Kent Larson. Can you estimate modulus from durometer hardness for silicones? Web page, 2016. [http://www.dowcorning.com/content/publishedlit/11-3716-01\\_-durometer-hardness-for-silicones.pdf](http://www.dowcorning.com/content/publishedlit/11-3716-01_-durometer-hardness-for-silicones.pdf).
- [25] Jaroslav Mackerle. Rubber and rubber-like materials, finite-element analyses and simulations, an addendum: a bibliography (1997? 2003). *Modelling and Simulation in Materials Science and Engineering*, 12(5):1031, 2004.
- [26] Moan.T. Lecture, 2003. Lecture notes of Advanced Structural analysis - Chapter 12 - Nonlinear analysis.
- [27] NTNU. Guide vanes in francis turbines. Lecture, March 2017. <http://www.ivt.ntnu.no/ept/fag/tep4195/innhold/Forelesninger/forelesninger>
- [28] Joshua Pelleg. *Mechanical Properties of Materials*, volume 190 of *Solid Mechanics and Its Applications*. Springer Netherlands, Dordrecht, Dordrecht, 2013.
- [29] Rainpower. General technical description. PDF, December 2008.
- [30] Rainpower. Rainpower.no - home. Web page, March 2017. <http://rainpower.no/>.
- [31] ResearchGate. Comparison of implicit and explicit procedures. Web page. <https://www.researchgate.net/file.PostFileLoader.html?id=587d09e55b4952b76c2fabbb3&assetKey=AS>
- [32] Wilhelm Rust. *Non-Linear Finite Element Analysis in Structural Mechanics*. Springer International Publishing: Cham, Cham, 2015.
- [33] Ebbe Smith. E-mail correspondance. E-mail correspondance with application specialist, PLM Technology, 2017.
- [34] Dassault Systèmes. *Abaqus Analysis User's Guide*, 6.14 edition, April 2014. <http://129.97.46.200:2080/v6.14/books/usb/default.htm>.
- [35] Dassault Systèmes. *Abaqus Theory Guide*, 6.14 edition, April 2014. <http://ivt-abacusdoc.ivt.ntnu.no:2080/v6.14/books/stm/default.htm>.
- [36] Dassault Systèmes. *Abaqus/CAE User's Guide*, 6.14 edition, April 2014. <http://129.97.46.200:2080/v6.14/books/usi/default.htm>.

- [37] Dassault Systèmes. Modeling rubber and viscoelasticity with abaqus. Internet Lecture, February 2017. <https://academy.3ds.com/en/learn/modeling-rubber-and-viscoelasticity-abaqus-1>.
- [38] Max Tillberg. E-mail correspondance. E-mail correspondance with application engineer, Trelleborg Sealing Solutions Norway AS, 2017.
- [39] Nikolaos Vasios. Nonlinear analysis of structures - the arc length method: Formulation, implementation and applications. Web page, 2015. <https://scholar.harvard.edu/files/vasios/files/ArcLength.pdf>.
- [40] Åge Ø Waløen. Del 2: Elementmetoden. en innføring. Kompendium, January 1995.
- [41] Di Wu, Shaoping Wang, and Xingjian Wang. A novel stress distribution analytical model of o-ring seals under different properties of materials. *Journal of Mechanical Science and Technology*, 31(1):289–296, 2017.
- [42] Si-wei Zhang and Si-Wei Zhang. *Tribology of Elastomers*. Tribology and Interface Engineering. Elsevier Science, Burlington, 2004.
- [43] Yunus A. Çengel and John M. Cimbala. *Fluid mechanics : fundamentals and applications*. McGraw-Hill, Boston, 3rd ed. in si units. edition, 2014.
- [44] Petter T.K. Østby. Personal communication. Personal communication with Turbine designer at Rainpower AS, 2017.

# Appendix

**A** Technical description

**B** Original experimental tests sheet

**C** FEA - Procedure notes

**D** Dassault Systemes - ABAQUS 6.14-1

**E** Stress and strain

**F** Material

**G** Experimental tests

**H** Implicit results

**I** Plane strain results

**J** Plane stress results

**K** Model development


**L** Risk analysis





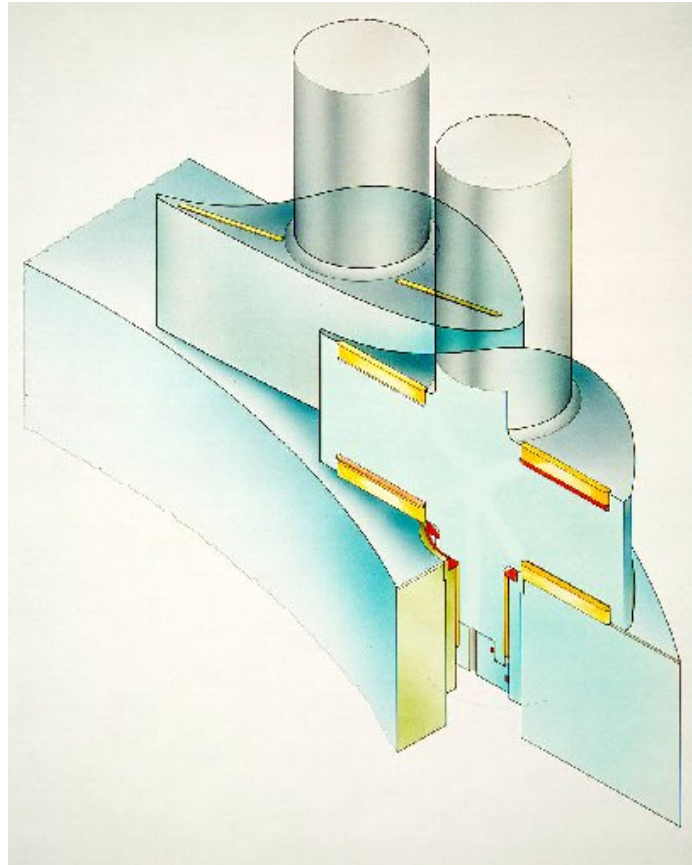
# Appendix A

## Technical description of guide vanes end seals

 <b>RAINPOWER</b>	<b>DESCRIPTION</b>
<p align="center"><b>Francis- and Pump Turbines</b> Guide vane end seals</p>	Document no.: 17560 KH doc. no.: Revision No.: 1 Page 1 of 2
Subject: <b>General Technical Description</b>	First issued date: 2008-04-12
<p><small>Retten til utnyttelse av denne beskrivelse tilhører Rainpower Norway AS og må ikke kopieres, utleveres eller forelegges uvedkommende uten tillatelse fra Rainpower. This document and the design is the property of Rainpower Norway AS and must not be used nor disclosed to any part without Rainpower's permission.</small></p>	

**1 GENERAL**

The Rainpower Guide Vane End Seals are incorporated in the guide vanes in order to minimize leakage water between guide vane ends and the mating surfaces on head- and bottom covers. This is especially important on high head units, where the leakage will reduce turbine efficiency and may contribute to increased sand erosion. The seals are active in closed and open guide vane positions, which is normally not the case with sealing elements located in the head- and bottom cover surfaces.




**2 DESIGN DETAILS**

The sealing elements are made of wear- and corrosion resistant material. The material properties and seal geometry are optimized to minimize wear and avoid galling on the mating surfaces on head- and bottom covers.

The sealing elements are located in accurately machined slots in the guide vanes. The necessary sealing force is obtained by elastic spring elements in the slots.

1	2012-02-02	Updated section 4	Wka	331	BA
0	2008-04-12	Issued for use	Wka	373	MGL
Rev	Date	Description	Written by	Dept	Appr

 <b>RAINPOWER</b>	<b>DESCRIPTION</b>
<b>Francis- and Pump Turbines</b> Guide vane end seals	Document no.: 17560 KH doc. no.: Revision No.: 1 Page 2 of 2
Subject: <b>General Technical Description</b>	First issued date: 2008-04-12
<small>Retten til utnyttelse av denne beskrivelse tilhører Rainpower Norway AS og må ikke kopieres, utleveres eller forelegges uvedkommende uten tillatelse fra Rainpower.  This document and the design is the property of Rainpower Norway AS and must not be used nor disclosed to any part without Rainpower's permission.</small>	

### 3 ADVANTAGES

The main advantages of the guide vane end seals are:

- Increased turbine efficiency. Leakage water between guide vanes and head-/bottom cover will reduce turbine efficiency, especially at part load and especially on high head units.
- Reduction of sand erosion. For units exposed to sand erosion, it is regarded especially important to reduce the leakage water across the guide vanes and to avoid sealing elements in the head- and bottom covers.
- Centering of the guide vanes. The spring characteristics of the end seals contribute to exact centering of the guide vanes between the head- and bottom covers, which will reduce the risk for galling.

### 4 REFERENCES

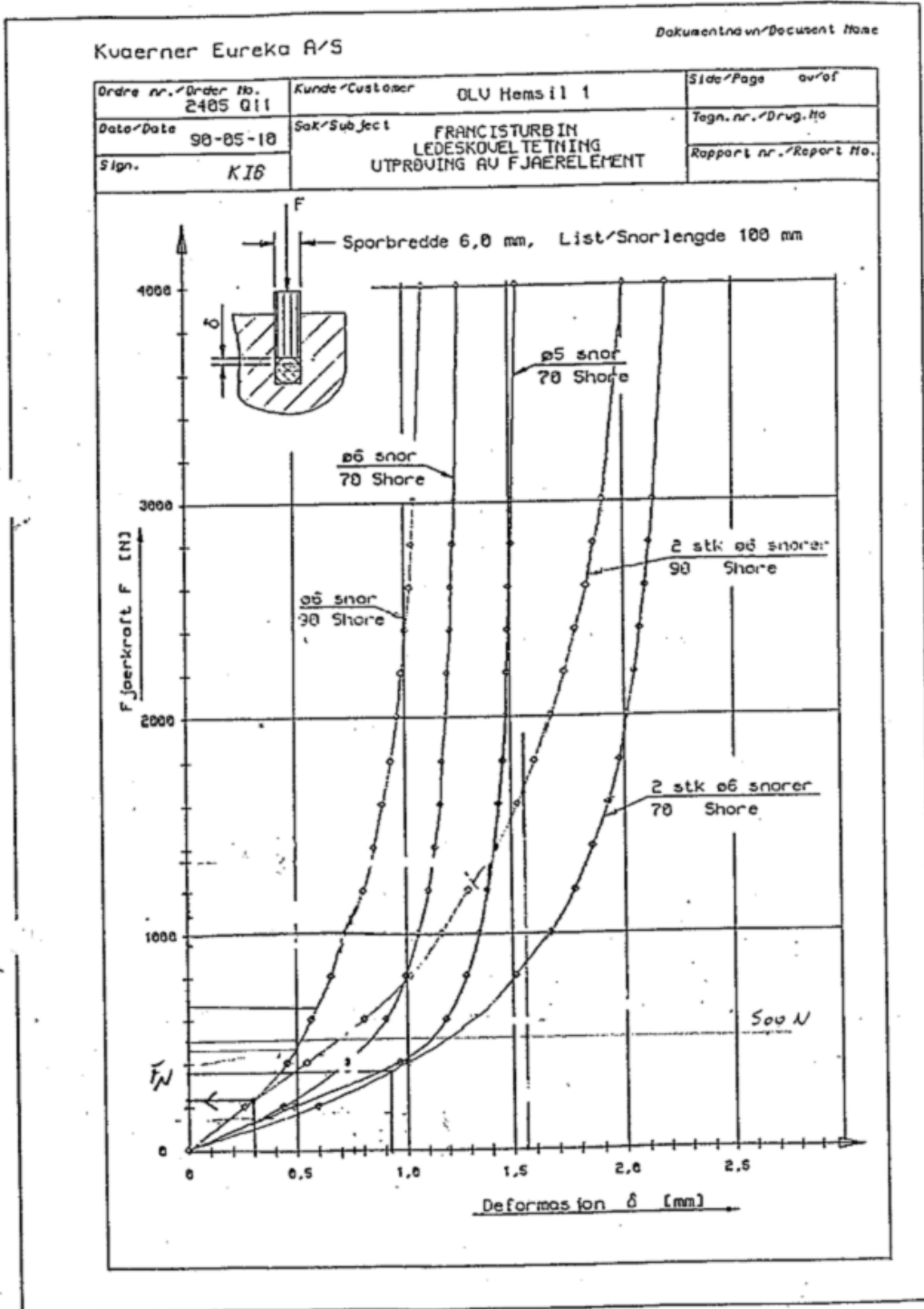
The following are examples of units equipped with Rainpower Guide Vane End Seals

<b>Year ordered</b>	<b>Plant</b>	<b>Country</b>	<b>No. of units</b>	<b>Head M</b>	<b>Output MW</b>	<b>Speed rpm</b>
2010	Nedre Roessaaga	Norway	2	238	46.6	428.6
2009	Rendalen	Norway	1	185	100	333.3

# Appendix B

## Original experimental tests sheet

323/950510



95-03-14 atg.

# Appendix C

## Procedure notes

## General

This appendix is made in order to disseminate experiences from the process. A selection of the procedure notes is retrieved directly from ABAQUS User Manuals, articles or lectures.

## Finite Element Methods

Mackerle [25] stated: "The finite-element method is based originally on small strain, linear elasticity theory and this formulation is not suitable for the analysis of rubber and rubber-like materials". This applies mainly to pure material testing. The possibility of recreating the exact trend for the load deflection curves from the experimental tests provided by Rainpower should be present. However, when modelling in ABAQUS there is a variety of challenges which should be notified. Several attempts were made using both implicit solver; static, general and the explicit solver; dynamic, explicit for the linear-elastic approach. When this only partly works for recreation, new ways of solving this was investigated. When applying load instead of displacement turned out to be as challenging as it was; is there any way to treat both the force and the displacement as unknown and use the incrementation to control the compression. The arc length method treat both force and displacement as unknowns. This is a implicit solver alternative which can be controlled by defining either load or displacement. In addition, if it does not achieve the given displacement it will still finish the incrementation and increase the load. In ABAQUS this is called the Riks Method and is mostly used in buckling and collapse analysis. After several attempts it turned out that since this is, as the static, general solver an implicit solver it kept on experience trouble due to interaction conditions.

As a result of varying displacement for the experimental tests, while the force intend to increase towards infinity, but stopped at 4000, attempts applying a force instead of an enforced displacement where conducted. Keeping the force constant, while the displacement is the unknown was considered as a option. Unfortunately, this turned out to be challenging, even though it sounds easy. Speculating; when an enforced displacement are applied, only one degree of freedom, DOF, is free, the other are fixed or constraint in certain directions. When applying loads, only one DOF is fixed, while others are free to move, requiring more constraints for the simultaneous movement of the upper wire and the O-ring.

Furthermore, when applying a load, the load is only working on the part it is assigned to, statically, meaning no movement is specified in comparison to the case of enforced displacement. When applying an enforced displacement, the part is assigned a movement in a specific direction, for instance a movement of 2 mm downwards in the Y-direction. In this case, ABAQUS understand the associated interaction for the components relative to one another. Unfortunately, this is not the case when applying a load. The need for additional constraints or connectors defining the connection between the

O-ring and the upper wire is present to allow the upper wire and the O-ring to move simultaneously. When applying connectors and constraints, ABAQUS require penalty contact algorithm, which is not the default option for contact pairs. By using penalty contact; penetration is allowed to happen, probably leading to cluttered force versus displacement curves. The only connector that seemed to work were the coupling-constraint between a reference point on the wire coupled with a reference point on the ring. No result worth mentioning were obtained from these attempts.

## Arc Length Method

For the general Newton-Raphson iterations, force or displacement is known. When neither force or displacement are known, the Arc Length Method of iteration can be useful. The Arc Length Method, or the Riks Method <sup>1</sup>, are used in order to follow the equilibrium path beyond critical points. For this method both displacement,  $\Delta D$  and load  $\Delta\lambda$  increments are controlled simultaneously. The basic idea behind arc length methods is that instead of keeping the load or the displacement fixed during an incremental step, both the load and displacement increments are modified during iterations [39]. Both the load and the displacement are treated as unknowns. The general non-linear system equilibrium equation [39]:

$$F^{int}(u) - F^{ext} = 0 \Rightarrow F^{int}(u) - \lambda q = 0 \quad (C.1)$$

Where  $F^{ext}$  are external forces,  $F^{int}$  are internal forces,  $\lambda$  is scalar quantity to control the load vector and  $q = F^{ext}$ .

The Arc Length Method equation [39]:

$$(\Delta u + \delta u)^T(\Delta u + \delta u) + \psi^2(\Delta\lambda + \delta\lambda)^2(q^T q) = \Delta l^2 \quad (C.2)$$

Where  $\Delta u$  is the variation in displacements,  $\Delta\lambda$  is the load vector coefficient and  $q$  is the increased load solution. The Riks method uses, as mentioned, the load magnitude as an additional unknown; it solves simultaneously for loads and displacements. This means that no solution can be obtained at a given displacement or a given load. Since both these are unknowns; another quantity must be defined. The Riks method use the Arc Length,  $l$ , along the static equilibrium path to progress the simulation. This approach provides solutions regardless of whether the response is stable or unstable. If the Riks step is a continuation of a previous history, any loads that exist at the beginning of the step and are not redefined are treated as “dead” loads with constant magnitude. A load whose magnitude is defined in the Riks step is referred to as a “reference” load. All prescribed

---

<sup>1</sup>Arc Length Method and Riks Method are used interchangeably. E.Riks presented this method in 1979.



loads are ramped from the initial (dead load) value to the reference values specified. The loading during a Riks step is always proportional. The current load magnitude,  $P_{total}$ , is defined by:

$$P_{total} = P_0 + \lambda(P_{ref} - P_0) \quad (C.3)$$

where  $P_0$  is the dead load,  $P_{ref}$  is the reference load vector, and  $\lambda$  is the load proportionality factor. The load proportionality factor is found as part of the solution. Abaqus/Standard prints out the current value of the load proportionality factor at each increment. You provide an initial increment in arc length along the static equilibrium path,  $l_{in}$ , when you define the step. The initial load proportionality factor,  $\lambda_{in}$ , is computed as:

$$\Delta\lambda_{in} = \frac{\Delta l_{in}}{l_{period}} \quad (C.4)$$

where is a user-specified total arc length scale factor (typically set equal to 1). This value of  $\Delta\lambda_{in}$  is used during the first iteration of a Riks step. For subsequent iterations and increments the value of is computed automatically, so you have no control over the load magnitude. The value of is part of the solution. Minimum and maximum arc length increments,  $\Delta l_{min}$  and  $\Delta l_{max}$ , can be used to control the automatic incrementation.

Since the loading magnitude is part of the solution, it is required to specify a method when the step is completed. It is possible specify a maximum value of the load proportionality factor,  $\lambda_{end}$ , or a maximum displacement value at a specified degree of freedom. The step will terminate when either value is crossed. If neither of these finishing conditions is specified, the analysis will continue for the number of increments specified in the step definition.

”The Riks method works well in snap-through problems - those in which the equilibrium path in load-displacement space is smooth and does not branch. It can also be used to solve postbuckling problems, both with stable and unstable postbuckling behavior.” ABAQUS Analysis Users Guide [34] section 6.2.4.

## **Additional attempts of curve fitting**

Prior to the plane stress and plane strain discovery, several attempts were conducted struggling to get the curves fit the best way possible. One attempt proposed of recreating the curves was by use of bilinear material curve to define a plasticity criteria. Using the curves provided by Trelleborg Sealing Solutions the true stress and true strain were calculated from the engineering stress and engineering strain. The formulas used is attached in Appendix E. This turned out to be difficult as the curves does not have a distinct limit between linear region and plasticity region. Assuming a bilinear material curve, the yield stress and corresponding strains could have been defined in the material module in ABAQUS. Unfortunately, this did not work and no results were obtained. The curves from Trelleborg can be found in Appendix L. It was difficult to define a clear yield point from these curves, making the bilinear material approach not sufficient. Additionally, the use of strain measure were also investigated as a potential cause for the deviation.

Another attempt was applying an even higher enforced displacement than 2 mm, as for instance 3 mm and 4 mm, to obtain the wanted curves, but the simulation for plane stress conditions did not seem to have reached its maximum displacement and could be compressed even further. This is clearly not rare when the O-ring is allowed to expand in the z-direction. As seen from the experimental test results, it was rare to obtain around 2 mm displacement before the force went towards infinity.

## Rigid parts

When modeling contact including rigid bodies, the definition of the rigid body geometry is essential. It is recommended that contact interactions should be formed with surfaces of equal geometry. For instance if a planar analytical rigid body is used (as in this master thesis) to model contact with a two dimensional deformable surfaces. Similarly, an axisymmetric rigid body is recommended when modeling contact with surfaces defined as axisymmetric elements. Three dimensional rigid bodies should be used to model contact either with surfaces formed by three dimensional element. It is important to notice that a rigid body have to contain only two- or three dimensional elements. It is not possible to model contact between two analytical rigid surfaces due to the fact that nodes cannot be shared between two rigid bodies [34] section 2.4.1 - Modelling contact with a rigid body.

According to the ABAQUS Analysis User's Guide [34] section 2.3.4, there are certain advantages and disadvantages using analytical rigid surfaces. The advantages of using Analytical rigid surfaces instead of defining element based(discrete) rigid surfaces is mainly limited to contact modelling:

- Several geometries can be modelled exactly by use of analytical rigid surfaces because of the ability to parameterize the surface with curved line segments. An analytical rigid surfaces can reduce contact noise and provide a better approximation to contact interaction because of a smoother surfaces.
- Due to a better approximation of the contact algorithm, using analytical rigid surfaces instead of rigid surfaces formed by element faces may result in decreased computational cost.

The disadvantages of using analytical rigid surfaces for contact modelling are:

- Contact cannot be modelled between two analytical surfaces. This is due to the fact that an analytical rigid surface is required to act as a master surface in a contact interaction.
- As a consequence of the fact that analytical rigid surfaces do not contain elements, neither contact forces or pressures can be contoured on the surface. However, contact forces and pressures can be contoured on the slave surface.
- An analytical rigid surface does not contribute to the mass and rotary inertia properties of the rigid body. If it is necessary to account for mass distribution on an analytical rigid surface, mass and rotary inertia properties must be defined for the rigid body. Alternatively, a discrete rigid surface can be used instead.
- The output for the reaction force in ABAQUS/Explicit for a analytical rigid surface is calculated only for the constraints active at the reference node (e.g. constraints

specified as boundary conditions). If it is desirable to calculate the net contact force on the rigid body corresponding to an unconstrained degree of freedom, this have to be calculated from the acceleration and the mass of the rigid body.

## Stability limit

According to IMechanica [20], the stability limit can be defined as: "the largest time increment that can be taken without the method generating large, rapidly growing errors". It is closely related to wave propagation (the time required for a stress wave to cross the smallest element dimension in the model). If the mesh contains small elements, or due to a very high wave speed, the time increment can be fairly small in an Dynamic, Explicit analysis. Most of the advantages of the explicit procedure work for quasi-static processes. Mass scaling can be used to reduce the wave speed. The stability criterion requires that  $E \geq 0$ ,  $G \geq 0$  and  $-1 \leq \nu \leq 0.5$ .

The stability limit in the explicit dynamics procedure can be expressed as [20]:

$$t = \left( \frac{L^e}{c_d} \right) \quad (\text{C.5})$$

Dilatational wave speed in a linear elastic material is defined as [20]:

$$c_d = \sqrt{\frac{E}{\rho}} \quad (\text{C.6})$$

# Appendix D

## Dassault Systèmes - ABAQUS 6.14-1

## ABAQUS interface

ABAQUS 6.14-1 consists of several modules providing the opportunity to model and conduct FEM-analysis of different mechanical challenges. The modules in ABAQUS are in a chronological order simplifying correct set up of analyses. Figure D.1 shows the modules interface menu in ABAQUS. The most essential ones are:

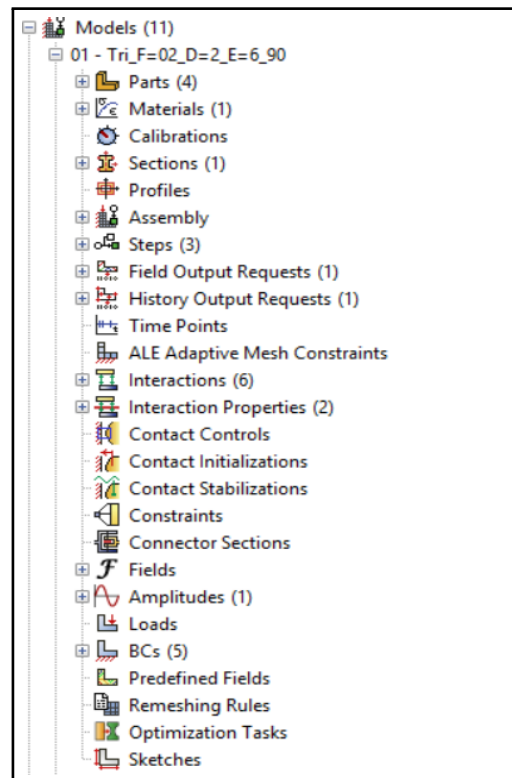


Figure D.1: ABAQUS modules

The **part** module is where the part is defined. The part is defined as either discrete rigid part, an analytical rigid part, Eulerian or a deformable part. Depending on the combination of modelling space (3D, 2D or axisymmetric). In general, ABAQUS provides available options for defining parts between solid, shell, wire and point. If a three dimensional deformable solid is defined, ABAQUS provides to choose between extrusion, revolution or sweep as type. These alternatives vary depending on the definitions and are limited for some cases such as 2D. Since the parts do not have any properties, geometry, section or material properties associated with it when finished in part module, these need to be defined in the property module.

In the **property** module, coinciding properties such as material properties, section, section assignments, layout of composites or material orientation are defined. Section definition contains information about the different properties of a part or a region of the part. Alternatively, editing material in terms of material properties, mechanical behaviour, thermal behaviour etc. is done in the property module. Section assignment

and defining category in terms solid, shell, beam, fluid or other is defined in property module [21].

In the **assembly** module various parts modelled is put together to represent the assembled mechanical component. Parts need to be defined as either independent parts or dependent parts. For meshing (in the mesh module) the parts needs to be defined as independent parts in the assembly module. This is were you create instances and assemble the instances together.

In the **step module** the different analysis steps are defined. After assembly module, the set up of the analysis begins with defining the sequence of steps. ABAQUS automatically creates a required initial step, where the initial BC 's is assigned. Consecutive steps, e.g. load steps, can be defined following the required initial step. Furthermore, there are two kinds of steps in ABAQUS: *Implicit* or *Explicit* which is described in detail in section 2.5.1. For each individual step, the step manager indicates whether ABAQUS will account for non-linear effects from large displacements and deformations. If the displacements due to loading are relatively small during a step, the effects may be small enough to be ignored. However, in cases where the load result in large displacements, non-linear geometric effects can become important. The Nlgeom setting for a step determines whether ABAQUS will account for geometric non-linearity in a step [36] section 14.3.2.

In the **interaction module**, contact and frictional behaviours are defined. This module is important in analyses where interaction between different instances in an assembly occur. The preferred contact algorithm is defined in this module, choosing between kinematic method or penalty method. Theory behind the interaction properties and definitions are described in detail in the theory chapter. If contact after separation is required, it can be defined in this module as well as the frictional coefficient. The definition of contact interactions is essential when analysing the material behaviour in highly confined environments.

The **load** module provides the opportunity to apply loading and boundary conditions. Boundary conditions is assigned in relation to their respective steps in the boundary condition manager. If one part of the model for instance is fixed at one step, but allowed to move in the next step, this is defined in the load manager. When creating a boundary conditions, it is necessary to assign it relative to the step where it is active. Furthermore, the properties of the BC 's is defined in terms of displacement, rotation, symmetric, antisymmetric or encastre/fixed or any other alternative relevant for the particular case.

In the **mesh** module the different parts are meshed and assigned element properties. In the mesh module the element type such as quad, tri, or hybrid are defined in addition to the element size which are defined as seed size. This is were the geometry are approximated by a finite element mesh. In the mesh module you define, depending on the geometry if it is a hexahedron, tetrahedron, quadrilateral, triangle or which element types



that should be assigned. In addition you define if it should be, for instance, a structured mesh or swept mesh. You also assign seeds in the mesh module which describe the size of the elements of the mesh generated.

In the **job** module the assembly are analysed and the result files are generated. This module is where you submit your model for analysis. When analysis is completed, you access the result tab and can retrieve curves, stresses and deformation pictures in addition to animations of the simulation.

## Additional reading in ABAQUS

### Contact interactions

Useful section in the ABAQUS Analysis User's Guide when modelling contact can be:

- 36.1 - Overview
- 36.2 - Defining general contact in Abaqus/Standard
- 36.3 - Defining contact pairs in Abaqus/Standard
- 36.4 - Defining general contact in Abaqus/Explicit
- 36.5 - Defining contact pairs in Abaqus/Explicit
- 2.3.4 - Analytical rigid surface definition
- 2.4.1 - Rigid body definition (Paragraph modeling contact with a rigid body)
- Lecture 4 – Imechanica

### Material

Recommended reading associated with elastic material behaviour compared to hyperelastic behaviour in ABAQUS are:

- Abaqus Analysis User's Guide - Section 22.1.1 - Elastic behavior overview
- Abaqus Analysis User's Guide - Section 22.5.1 - Hyperelastic behavior of rubberlike materials

# Appendix E

## Stress and strain

## Calculation procedure

Stress and strain calculations, and measure for the respective quantities is an important aspect to consider when conduction numerical analyses. Following are the equations that can be used for calculating strains:

True stress equation according to [19]:

$$\sigma = \frac{F}{A} \quad (\text{E.1})$$

True strain equation according to [19]:

$$\epsilon = \ln\left(\frac{L}{L_0}\right) \quad (\text{E.2})$$

Engineering stress equation according to [19]:

$$s = \frac{F}{A_0} \quad (\text{E.3})$$

Engineering strain equation according to [19]:

$$e = \frac{\Delta L}{L_0} \quad (\text{E.4})$$

Calculating true tress and true strain from the engineering quantities:

Engineering strain equation according to [19]:

$$\sigma = s(1 + e) \quad (\text{E.5})$$

Engineering strain equation according to [19]:

$$\epsilon = \ln(1 + e) \quad (\text{E.6})$$

## Stress and strain measure

There are several possible parameters affecting the results of the numerical analysis. Which strain measure do ABAQUS use? ”The stress measure used in ABAQUS is Cauchy or “true” stress, which corresponds to the force per current area” [34] section 1.2.2 - Conventions.

Green strain equation E.7:

$$\epsilon_G = \frac{1}{2} \left( \frac{l^2 - L^2}{L^2} \right) \quad (\text{E.7})$$

Almansi strain equation E.8:

$$\epsilon_E = \frac{1}{2} \left( \frac{l^2 - L^2}{l^2} \right) \quad (\text{E.8})$$

Logarithmic strain equation E.9:

$$\epsilon_E = \ln \frac{l}{L} = \ln(\lambda) \quad (\text{E.9})$$

$\lambda$  = Stretch ratio. L is the initial length while l is the final length. The following information mainly refer to ABAQUS Theory Guide [35] section 1.4.2 and ABAQUS Analysis Guide section 1.2.2.

- The stress measure defined in ABAQUS is true stress, which corresponds to the force per current area. Unlike the stress measure, there is no clearly defined true strain.
- The preferable choice of strain measure depends on analysis type, material behavior, and personal preference.
- The default strain output in ABAQUS/Standard is the integrated total strain (E). This strain is composed of the elastic strain (EE), the inelastic strain (IE) and the thermal strain (TE).
- For large-strain shells, membranes, and solid elements in ABAQUS/Standard two other measures of total strain can be requested: logarithmic strain (LE) and nominal strain (NE).
- The default strain output in ABAQUS/Explicit is Logarithmic strain (LE) due to the fact that total strain is not available in ABAQUS/Explicit.
- Logarithmic strain is the most appropriate for elastic-plastic or elastic-visco-plastic materials as a result of very small elastic strains (because the yield stress is small compared to the elastic modulus). As a result, it is not advantageous to use Green’s strain.

# Appendix F

## Material

## Additional equations

Additionally, a second model provided by Gent for calculating Young's modulus from the hardness number is:

$$E = 3G \quad (\text{F.1})$$

Where  $G$  is the shear modulus

Finally, the third model that will be presented for converting shore hardness to Young's modulus is the Reuss model:

$$\text{Log}_{10} * E = 0.0235 * S - 0.6403 \quad (\text{F.2})$$

Where  $S$  is the hardness number.

## Hyperelastic Material Models

Note; the information presented in this section does mainly refer to the online course: "Lesson 2 - Introduction to Hyperelastic models - Modeling Rubber and Viscoelasticity with Abaqus" at 3ds Academy website [37].

### General

Hyperelastic material models are mainly used for FEM-analysis where parts are assigned materials properties associated with elastomer and rubber-like materials. These materials is characterized by an instantaneous elastic response (in which persists even at large strains/deformations) when force is applied. The hyperelastic material models in ABAQUS 6.14-1 is by default isotropic, non-linear and incompressible. The mechanical response separates into shear behavior and a volumetric behaviour.

ABAQUS provides several hyperelastic material models in which can be used for simulating nearly incompressible materials. Each model defines the strain energy function ( $W$ ) in a different way. In general, there are two types of (overall) models when considering hyperelastic material models:

- Physically-motivated models: These models consider the material response from the viewpoint of the microstructure.
- Phenomenological models: These models consider the problem from the viewpoint of continuum mechanics.

### Neo-Hookean and Mooney-Rivlin

As presented in the online lecture at 3ds academy there are several hyperelastic materials in which will be presented. Neo-Hookean and Mooney-Rivlin model are hyperelastic material models where the strain energy density function,  $W$ , is built from invariants of the left Cauchy-Green deformation tensor. Another hyperelastic model is the Ogden model, which is a hyperelastic model where its strain density function,  $W$ , is expressed by principal stretch ratio. Another model which can be used to predict the stress strain behaviour of hyperelastic material is the Neo-Hookean. This model can partly be compared to Hooke's Law. Generally, this model is one of the simplest (and one of the first hyperelastic material models) models for an hyperelastic, incompressible material. Neo-Hookean provides a good approximation at smaller strains, but cannot capture upturns in the stress-strain curve [22]. The model describes the strain energy density function,  $W$ , as follows:

$$W_1 = C_1(I_1 - 3) \tag{F.3}$$

Another widely known hyperelastic material model is the; Mooney-Rivlin model. Instead of describing the strain density function,  $W$ , by use of just one combination of the invariants, the Mooney-Rivlin model describes the strain energy density function,  $W$ , as a linear combination of two of the invariants. This models provides a good approximation to moderate strains [22]. The model is as follows:

$$W = C_1(I_1 - 3) + C_2(I_2 - 3) \quad (\text{F.4})$$

### Additional hyperelastic material models

In general, reduced polynomial models does not include any dependence on stress-invariant  $I_2$ . This factor can be eliminated from the strain energy function because of the following arguments:

- Generally, the sensitivity of the strain energy functions to variations in  $I_2$  is significantly smaller than the sensitivity to variations in  $I_1$ .
- It may be preferable to avoid introducing coefficientents calibrated from data which is potentially inaccurate due to the fact, that measuring the influence of  $I_2$  to the strain energy function is quite difficult.
- By eliminating the terms where  $I_2$  is present from the strain energy function improves the ability to better predict behaviour for complex deformation states. This is valid when test data for only one single deformation state is available.

The **Yeoh model** is a third-order reduced polynomial model. The Yeoh model provides a high level of accuracy over a large strain range. Unlike the Neo-Hookean, this model can capture the "upturn" in the stress-strain curve. As mentioned it can be used for limited test data.

The **Ogden model** is a phenomenological model using principal stretches instead of invariants. As an alternative to use of integer power, this models use real powers which allows a great model accuracy. This model depends on full test data and is not applicable with limited test data, for instance just uniaxial tension.

The **Arruda-Boyce model and the Van der Walls model** is two most commonly used physically-motivated models. In general, the Van der Walls model contains four material parameters, while the Arruda-Boyce contains just two material parameter. The Arruda-Boyce model is a two-parameter model, based on only  $I_1$ . The oefficients ability to change change is limited, which makes this model applicable for limited test data.



# Appendix G

## Experimental tests

## General

As a part of further work for this master thesis it is recommended to conduct experimental tests to survey the material properties. This section present standards used for experimental testing of rubber-like materials and some test data guidelines retrieved from the learn online course at 3ds academy. Pictures of uniaxial, biaxial planar and volumetric test is retrieved from Abaqus Analysis User Guide [34], section 22.5.1.

Usually, the physical tests of the elastomeric rubber are conducted prior to final processing of the actual product. It is tested on so called "batches". The experimental tests needs to be conducted according to the given standards [37]:

- ASTM D575 - Standard test methods for rubber properties in compression.
- ASTM D412 - Standard test methods for vulcanized rubber and thermoplastic elastomers - tension

Through 3ds academy course "Modelling Rubber and Viscoelasticity in ABAQUS" there are several tutorials for modelling hyperelastic materials. This course provides one set of examples for uniaxial tension, biaxial tension, planar tension and volumetric test data with basis in experimental testing. Using this course in addition to conduct experimental tests may be useful in terms of comparing the results of the linear-elastic approach to a hyperelastic approach.

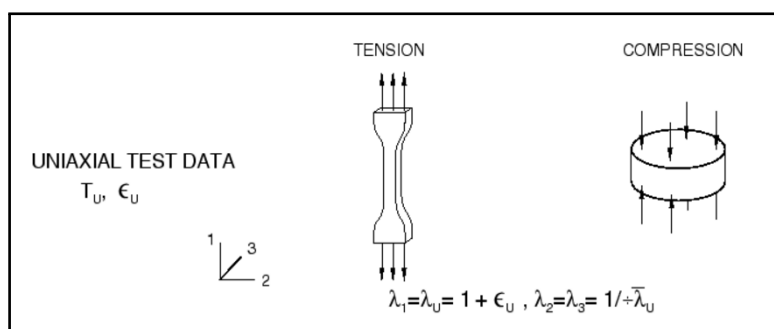


Figure G.1: Uniaxial Test

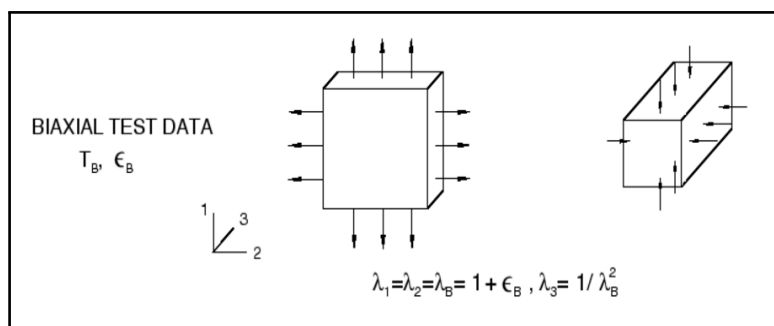


Figure G.2: Biaxial Test

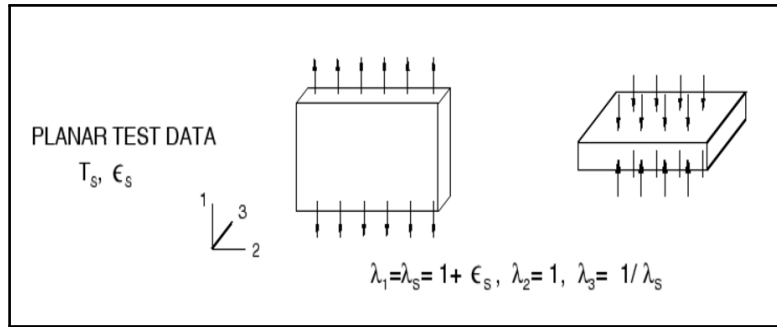


Figure G.3: Planer test

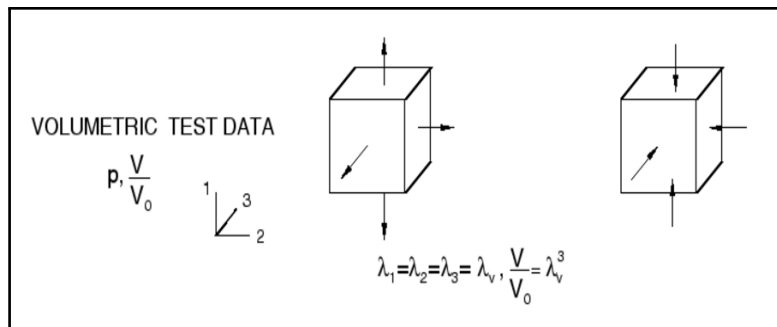


Figure G.4: Volumetric test

## Test Data Guidelines

The course "Modeling Rubber and Viscoelasticity with ABAQUS" at 3ds Academy [37] points out the importance of experimental tests for defining hyperelastic material properties. The most significant factor when choosing a rubber material model is the availability of sufficient and accurate test data. As a result, it is important to collect data from as many modes of deformation as possible:

- Uniaxial tension and/or compression
- Planar tension and/or compression
- Equibiaxial tension and/or compression
- Shear - Only used for hyperelastic foam

If compressibility is important, as it is for the case of compressed elastomeric O-ring seals, volumetric data is important and must be collected. It is preferable to perform all tests on the same batch to characterize a given material. Using test specimens from the same batch of material is recommended. Additionally, it may be necessary to validate the test specimen by cutting small uniaxial specimens from real components for comparison. In terms of achieving the most accurate material model it may be necessary to use data from more than one mode of deformation (e.g. uniaxial tension) to achieve the most accurate material model [37].

# Appendix H

## Implicit results

## Shore70 A

Figure H.1 illustrate the difference between the experimental curve, the implicit curve and the explicit curve for a single O-ring in Shore 70A material hardness with tangential side walls.

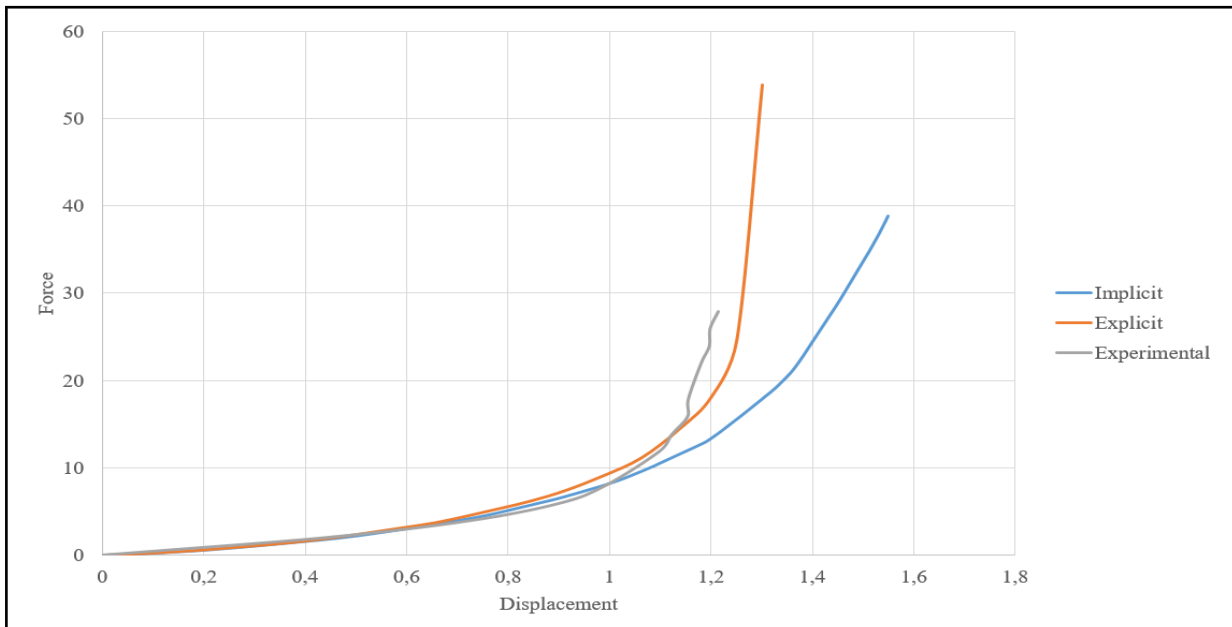


Figure H.1: Explicit vs Implicit vs Experimental - Shore 70 - Ø6

Table H.1 illustrates the numerical curves from analyses with a single O-ring in Shore 70A material hardness and cross-sectional diameter of 6 mm with. The side walls are contributing to pre-tension indicating a groove too small compared to the seal diameter.

Table H.1: Parameters - Shore 70A -  $\text{Ø}6$  - One sealing element - Groove too small

Hardness	Cross section	Offset side walls	$\mu$	Test
Shore 70A	$\text{Ø}6$	0.00 mm	0.5	Numerical
Shore 70A	$\text{Ø}6$	-0.025 mm	0.5	Numerical
Shore 70A	$\text{Ø}6$	-0.05 mm	0.5	Numerical
Shore 70A	$\text{Ø}6$	-0.10 mm	0.5	Numerical
Shore 70A	$\text{Ø}6$	-0.15 mm	0.5	Numerical

Figure H.2 illustrates the numerical curves from analyses with the parameters from Table H.1:

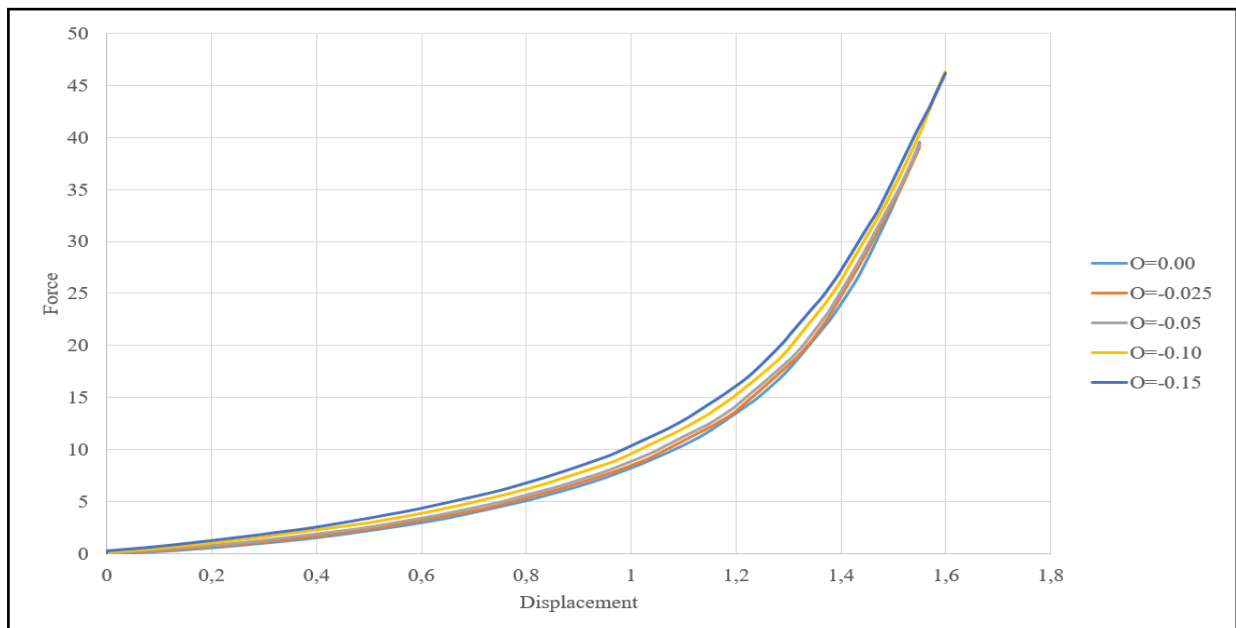


Figure H.2: Shore 70 -  $\text{Ø}6$  -  $F=0.5$  - Implicit

Table H.2 illustrates the numerical curves from analyses with a single O-ring in Shore 70A material hardness and cross-sectional diameter of 5 mm with. The side walls are contributing to pre-tension indicating a groove too small compared to the seal diameter.

Table H.2: Parameters - Shore 70A -  $\varnothing 5$  - One sealing element - Groove too small

Hardness	Cross section	Offset side walls	$\mu$	Test
Shore 70A	$\varnothing 6$	0.00 mm	0.5	Numerical
Shore 70A	$\varnothing 6$	-0.025 mm	0.5	Numerical
Shore 70A	$\varnothing 6$	-0.05 mm	0.5	Numerical
Shore 70A	$\varnothing 6$	-0.10 mm	0.5	Numerical
Shore 70A	$\varnothing 6$	-0.15 mm	0.5	Numerical

Figure H.3 illustrates the numerical curves from analyses with the parameters from Table H.2:

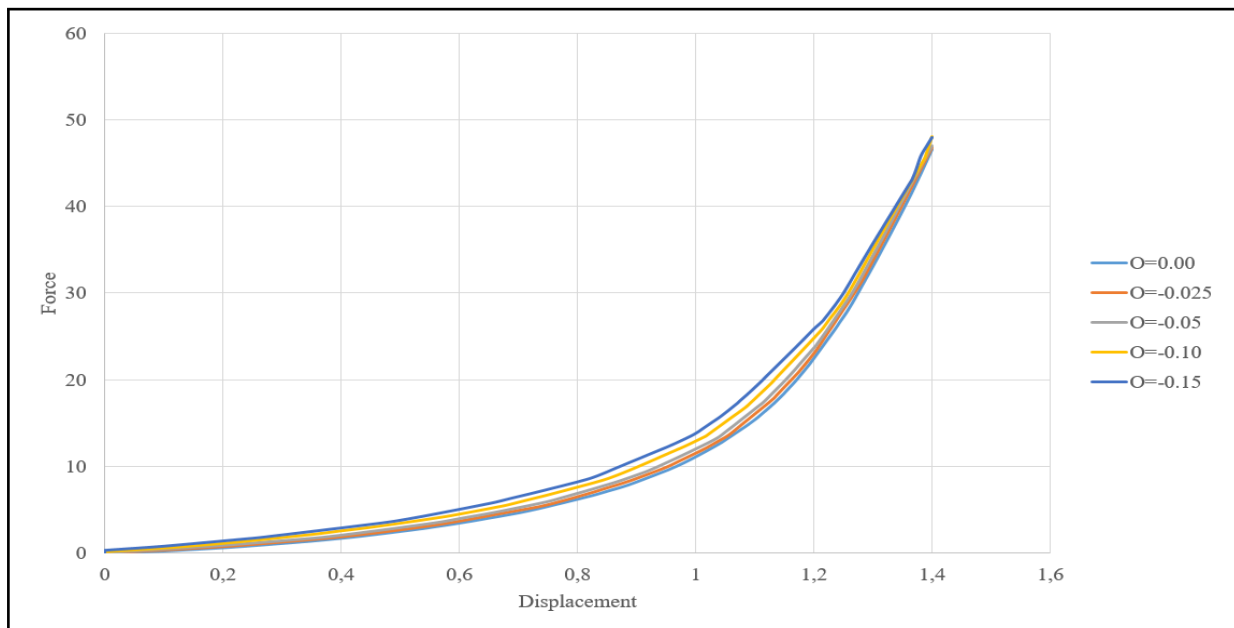


Figure H.3: Shore 70 -  $\varnothing 5$  -  $F=0.5$  - Implicit



# Appendix I

## Plane strain results

## Numerical compression of one O-ring

This section presents the numerical analysis for a single sealing element compared to each other with varying tolerances of the groove. Following situations will be presented:

- Shore 70A with offset of side walls equal to 0.00 mm, -0.025 mm, -0.05 mm, -0.10 mm and -0.15 mm representing situation when the rectangular groove is too small compared to a sealing element with cross sectional diameter of 6 mm.
- Shore 70A with offset of side walls equal to 0.00 mm, 0.05 mm, 0.10 mm, 0.15 mm and 0.20 mm representing situation when the rectangular groove is too wide compared to a sealing element with cross sectional diameter of 6 mm.
- Shore 70A with offset of side walls equal to 0.00 mm, -0.025 mm, -0.05 mm, -0.10 mm and -0.15 mm representing situation when the rectangular groove is too small compared to a sealing element with cross sectional diameter of 5 mm.
- Shore 70A with offset of side walls equal to 0.00 mm, 0.05 mm, 0.10 mm, 0.15 mm and 0.20 mm representing situation when the rectangular groove is too wide compared to a sealing element with cross sectional diameter of 5 mm.
- Shore 90A with offset of side walls equal to 0.00 mm, -0.025 mm, -0.05 mm, -0.10 mm and -0.15 mm representing situation when the rectangular groove is too small compared to a sealing element with cross sectional diameter of 6 mm.
- Shore 90A with offset of side walls equal to 0.00 mm, 0.05 mm, 0.10 mm, 0.15 mm and 0.20 mm representing situation when the rectangular groove is too wide compared to a sealing element with cross sectional diameter of 6 mm.
- Shore 90A with offset of side walls equal to 0.00 mm, -0.025 mm, -0.05 mm, -0.10 mm and -0.15 mm representing situation when the rectangular groove is too small compared to a sealing element with cross sectional diameter of 5 mm.
- Shore 90A with offset of side walls equal to 0.00 mm, 0.05 mm, 0.10 mm, 0.15 mm and 0.20 mm representing situation when the rectangular groove is too wide compared to a sealing element with cross sectional diameter of 5 mm.

## Shore 70A

Table I.1 presents parameters for analysis where the side walls contribute to pre-tension when the cross-sectional diameter of the sealing element is 6 mm.

Table I.1: Parameters - Shore 70A - 6 mm - One sealing element - Groove too small

Hardness	Cross section	Offset side walls	$\mu$	Test
Shore 70A	6 mm	0.00 mm	0.5	Numerical
Shore 70A	6 mm	-0.025 mm	0.5	Numerical
Shore 70A	6 mm	-0.05 mm	0.5	Numerical
Shore 70A	6 mm	-0.10 mm	0.5	Numerical
Shore 70A	6 mm	-0.15 mm	0.5	Numerical

Figure I.1 illustrates a single sealing element compressed in vertical direction with parameters from table I.1.

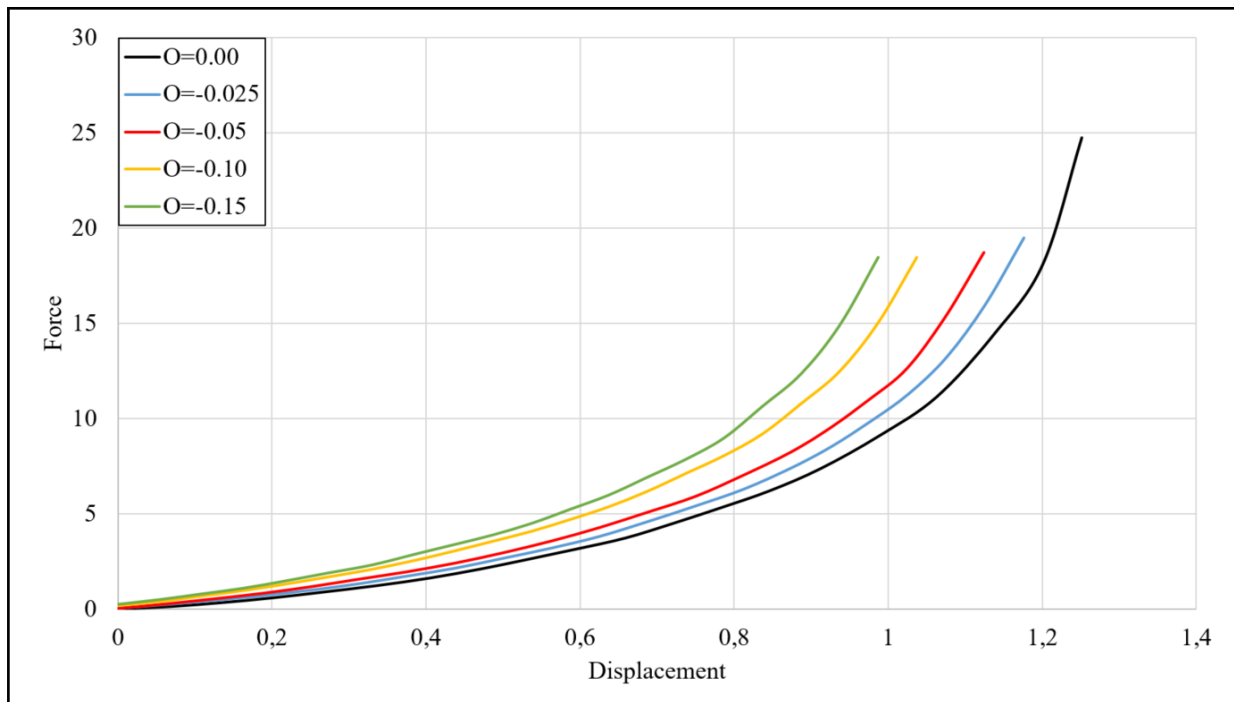


Figure I.1: Shore 70A - 6 mm - One sealing element - Groove too small

Table I.2 presents the parameters for the analysis where the side walls are offset from the sealing element illustrating a groove too wide when the cross-sectional diameter of the seal is 6 mm.

Table I.2: Parameters - Shore 70A - 6 mm - One sealing element - Groove too wide

Hardness	Cross section	Offset side walls	$\mu$	Test
Shore 70A	6 mm	0.00 mm	0.5	Numerical
Shore 70A	6 mm	0.05 mm	0.5	Numerical
Shore 70A	6 mm	0.10 mm	0.5	Numerical
Shore 70A	6 mm	0.15 mm	0.5	Numerical
Shore 70A	6 mm	0.20 mm	0.5	Numerical

Figure I.2 illustrates one sealing element compressed in vertical direction with parameters from Table I.2.

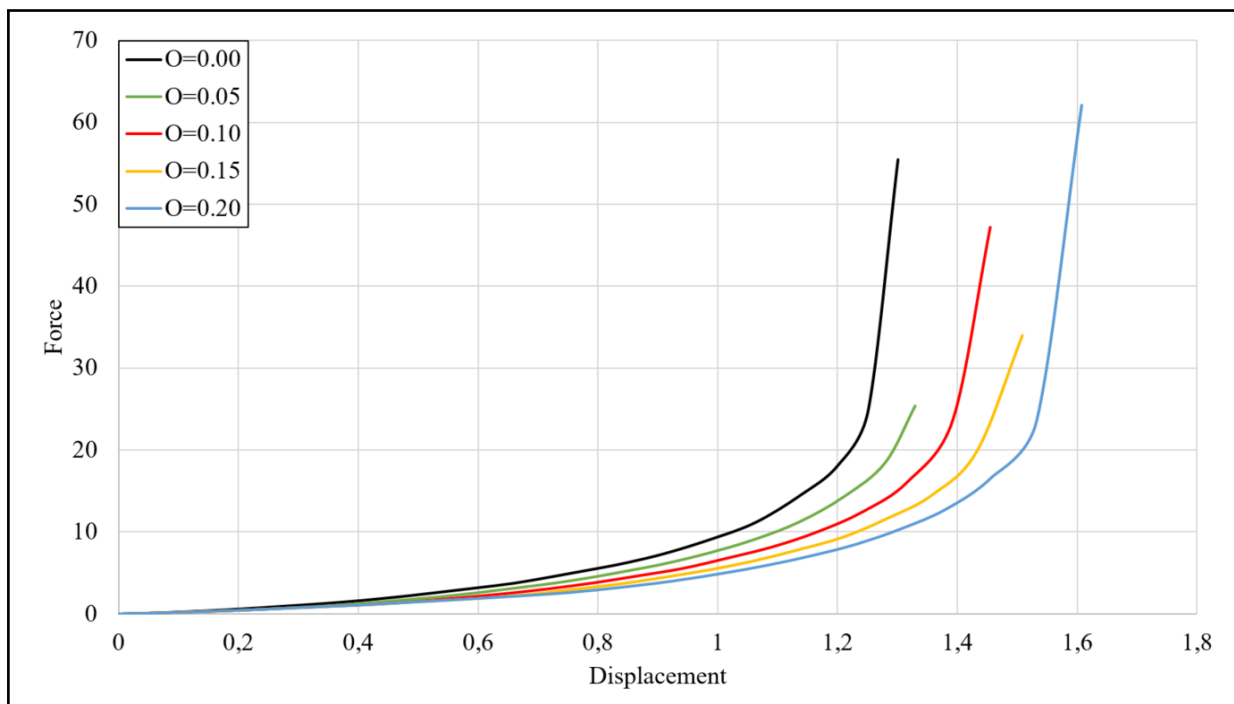


Figure I.2: Shore 70A - 6 mm - One sealing element - Groove too wide

Table I.3 presents the parameters for the analysis where the side walls contribute to pre-tension when the cross-sectional diameter of the sealing element is 5 mm.

Table I.3: Parameters - Shore 70A - 5 mm - One sealing element - Groove too small

Hardness	Cross section	Offset side walls	$\mu$	Test
Shore 70A	5 mm	0.00 mm	0.5	Numerical
Shore 70A	5 mm	-0.025 mm	0.5	Numerical
Shore 70A	5 mm	-0.05 mm	0.5	Numerical
Shore 70A	5 mm	-0.10 mm	0.5	Numerical
Shore 70A	5 mm	-0.15 mm	0.5	Numerical

Figure I.3 shows one sealing element compressed in vertical direction with parameters from Table I.3.

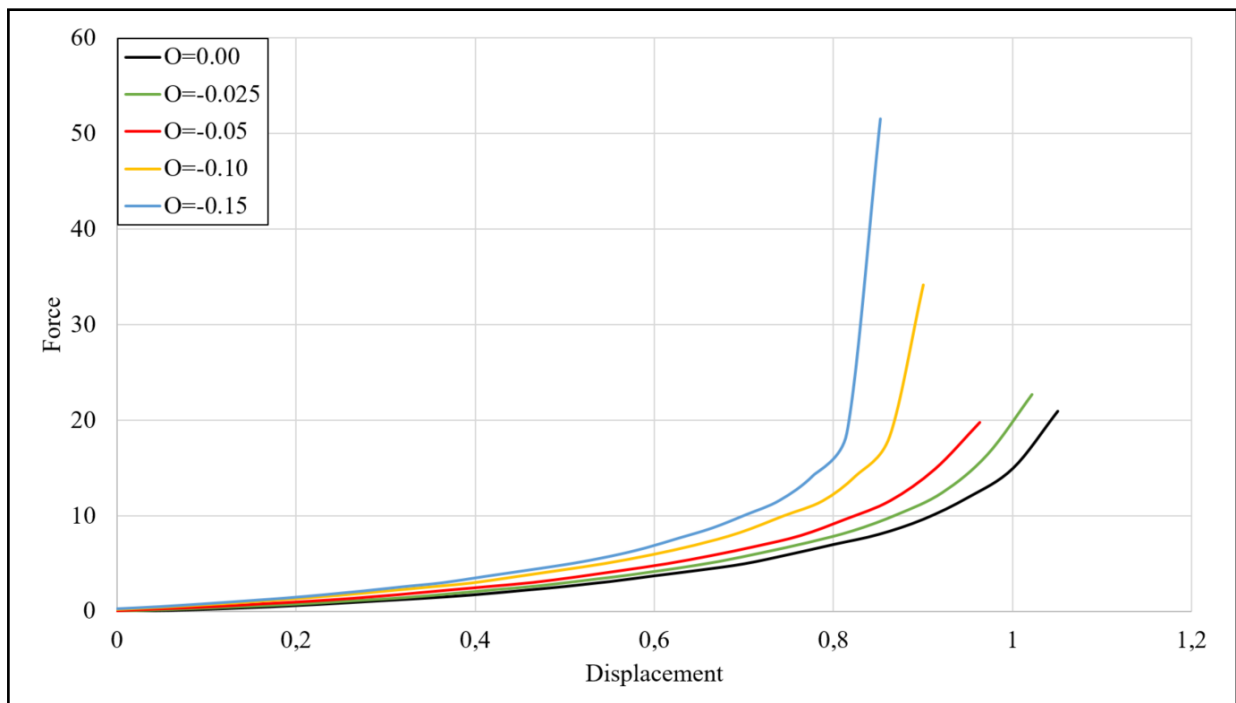


Figure I.3: Shore 70A - 5 mm - One sealing element - Groove too small

Table I.4 presents the parameters for the analysis where the side walls are offset from the sealing element illustrating a groove too wide when the cross-sectional diameter of the seal is 5 mm.

Table I.4: Parameters - Shore 70A - 5 mm - One sealing element - Groove too wide

Hardness	Cross section	Offset side walls	$\mu$	Test
Shore 70A	5 mm	0.00 mm	0.5	Numerical
Shore 70A	5 mm	0.05 mm	0.5	Numerical
Shore 70A	5 mm	0.10 mm	0.5	Numerical
Shore 70A	5 mm	0.15 mm	0.5	Numerical
Shore 70A	5 mm	0.20 mm	0.5	Numerical

Figure I.4 illustrates one sealing element compressed in vertical direction with parameters from Table I.4.

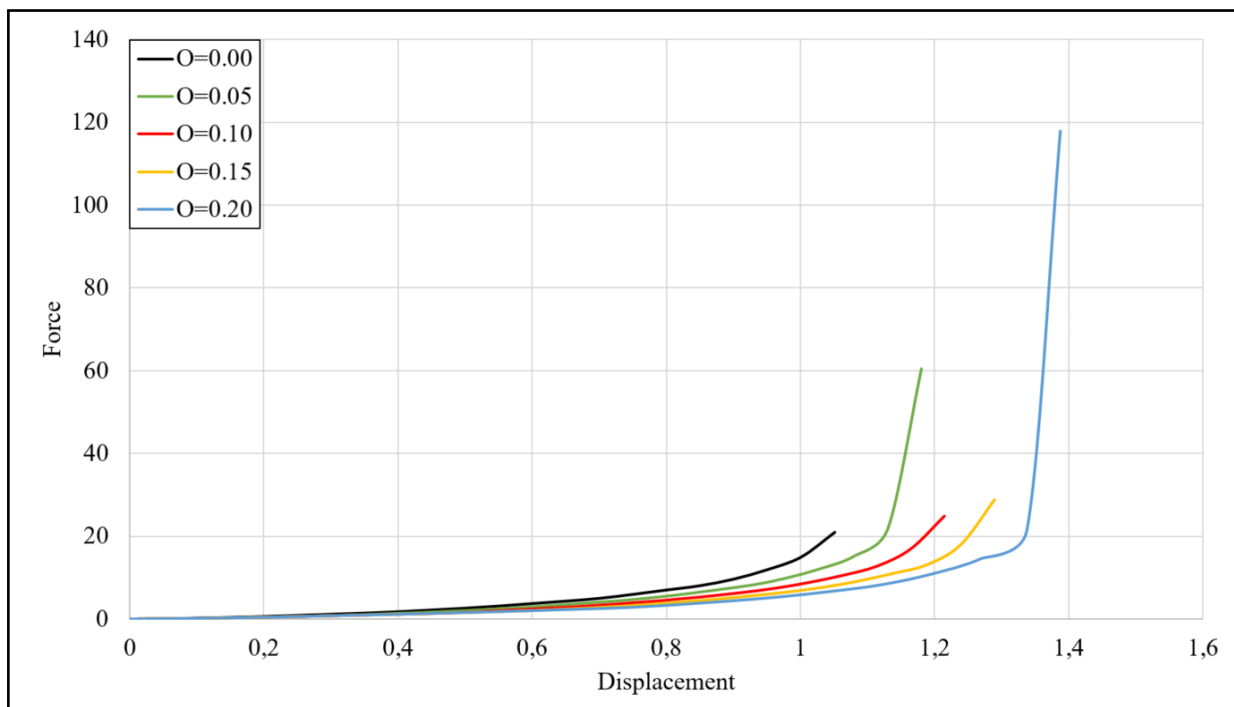


Figure I.4: Shore 70A - 5 mm - One sealing element - Groove too wide

## Shore 90A

Table I.5 presents the parameters for the analysis where the side walls contribute to pre-tension in the sealing element when material hardness is Shore 90A and cross sectional diameter of the seal is 6 mm.

Table I.5: Parameters - Shore 90A - 6 mm - One sealing element - Groove to small

Hardness	Cross section	Offset side walls	$\mu$	Test
Shore 90A	6 mm	0.00 mm	0.5	Numerical
Shore 90A	6 mm	-0.025 mm	0.5	Numerical
Shore 90A	6 mm	-0.05 mm	0.5	Numerical
Shore 90A	6 mm	-0.10 mm	0.5	Numerical
Shore 90A	6 mm	-0.15 mm	0.5	Numerical

Figure I.5 illustrates one sealing element compressed in vertical direction with parameters from Table I.5.

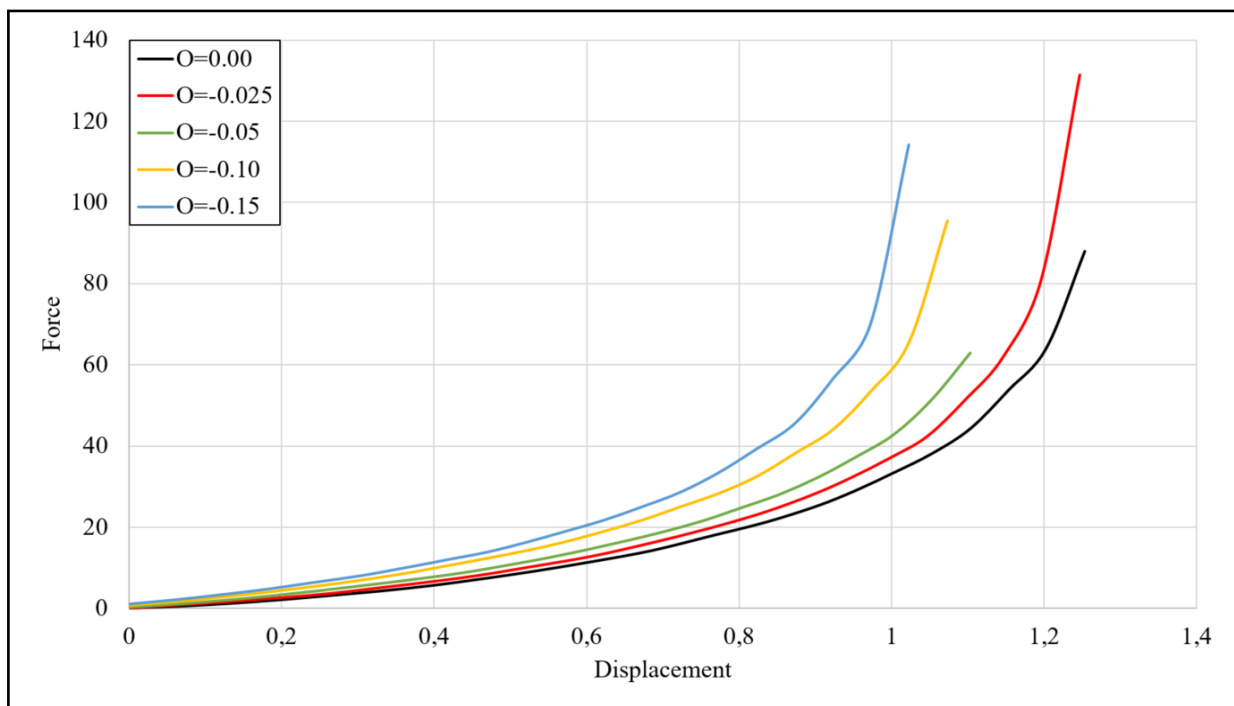


Figure I.5: Shore 90A - 6 mm - One sealing element - Groove to small

Table I.6 presents the parameters for the analysis where the side walls are offset from the sealing element illustrating a groove too wide when the material hardness is Shore 90A and cross sectional diameter of the seal is 6 mm.

Table I.6: Parameters - Shore 90A - 6 mm - One sealing element - Groove too wide

Hardness	Cross section	Offset side walls	$\mu$	Test
Shore 90A	6 mm	0.00 mm	0.5	Numerical
Shore 90A	6 mm	0.05 mm	0.5	Numerical
Shore 90A	6 mm	0.10 mm	0.5	Numerical
Shore 90A	6 mm	0.15 mm	0.5	Numerical
Shore 90A	6 mm	0.20 mm	0.5	Numerical

Figure I.6 illustrates one sealing element compressed in vertical direction with parameters from Table I.6.

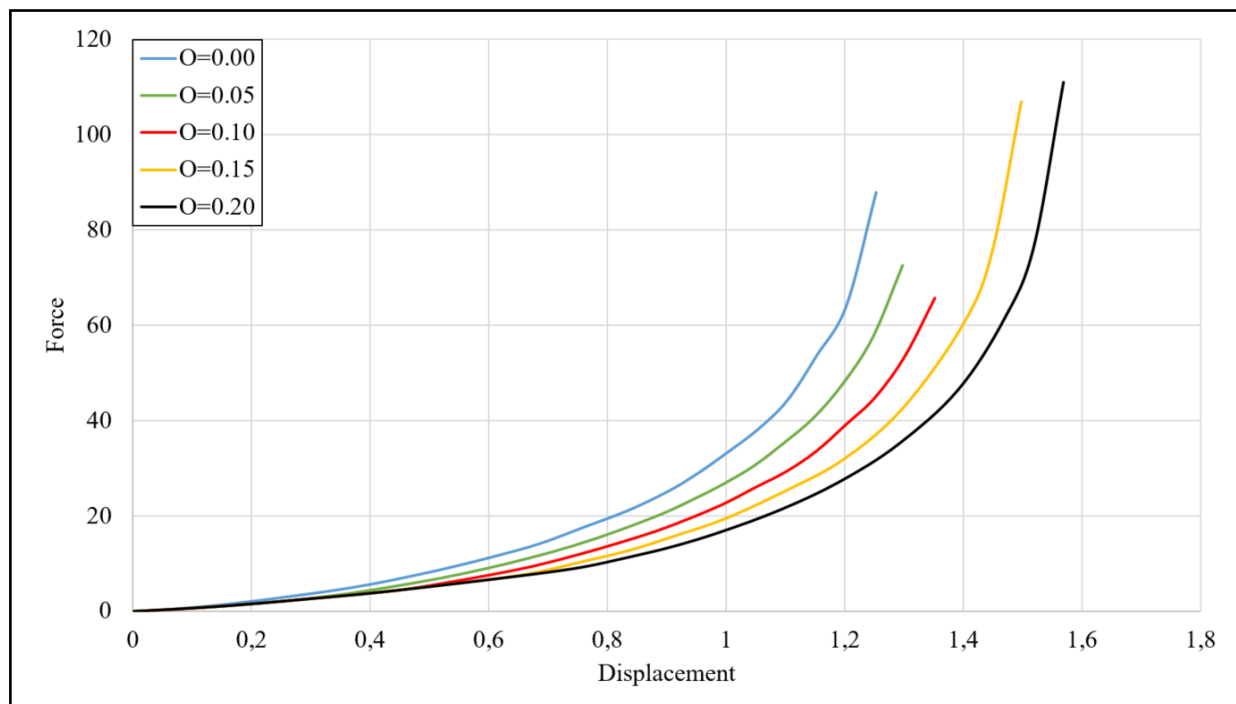


Figure I.6: Shore 90A - 6 mm - One sealing element - Groove too wide



Table I.7 presents the parameters for the analysis where the side walls contribute to pre-tension in the sealing element when the cross-sectional diameter of the seal is 5 mm.

Table I.7: Parameters - Shore 90A - 5 mm - One sealing element - Groove too small

Hardness	Cross section	Offset side walls	$\mu$	Test
Shore 90A	5 mm	0.00 mm	0.5	Numerical
Shore 90A	5 mm	-0.025 mm	0.5	Numerical
Shore 90A	5 mm	-0.05 mm	0.5	Numerical
Shore 90A	5 mm	-0.10 mm	0.5	Numerical
Shore 90A	5 mm	-0.15 mm	0.5	Numerical

Figure I.7 shows one sealing element compressed in vertical direction with parameters from Table I.7.

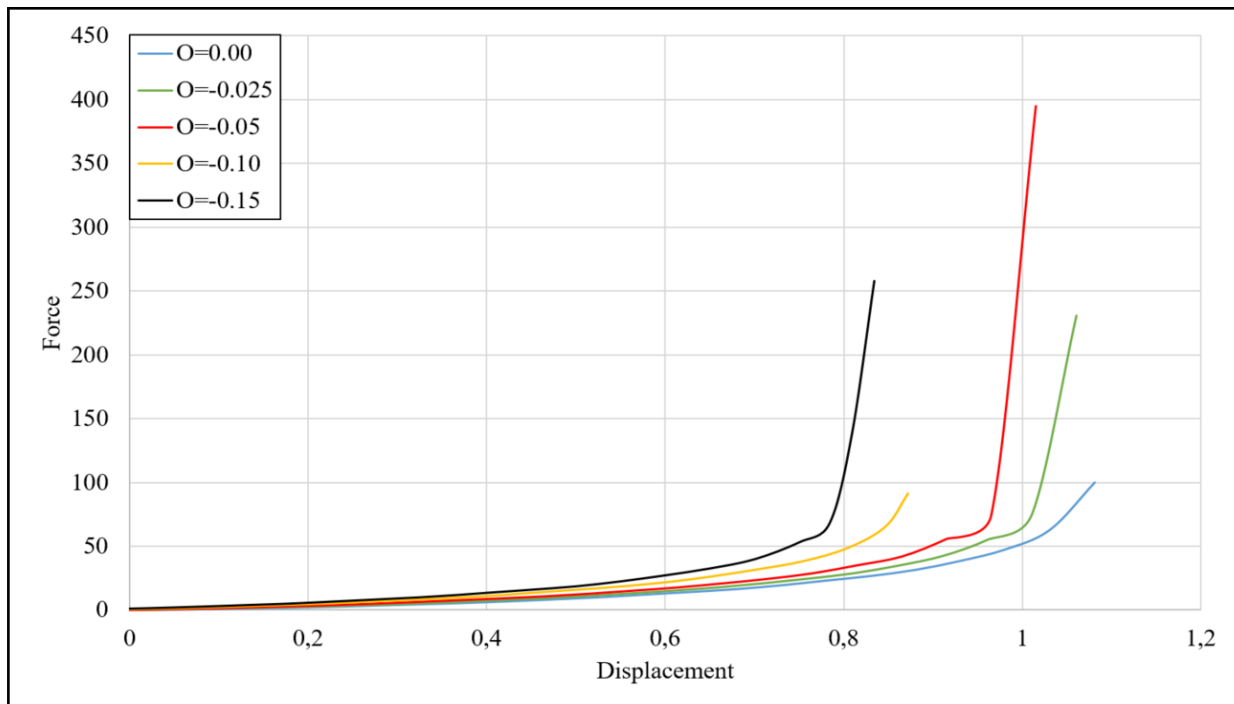


Figure I.7: Shore 90A - 5 mm - One sealing element - Groove too small

Table I.8 presents the parameters for the analysis where the side walls are offset from the sealing element illustrating a groove too wide when the cross section diameter of the seal is 5 mm.

Table I.8: Parameters - Shore 90A - 5 mm - One sealing element - Groove too wide

Hardness	Cross section	Offset side walls	$\mu$	Test
Shore 90A	5 mm	0.00 mm	0.5	Numerical
Shore 90A	5 mm	0.05 mm	0.5	Numerical
Shore 90A	5 mm	0.10 mm	0.5	Numerical
Shore 90A	5 mm	0.15 mm	0.5	Numerical
Shore 90A	5 mm	0.20 mm	0.5	Numerical

Figure I.8 illustrates a single sealing element compressed in vertical direction with parameters from Table I.8.

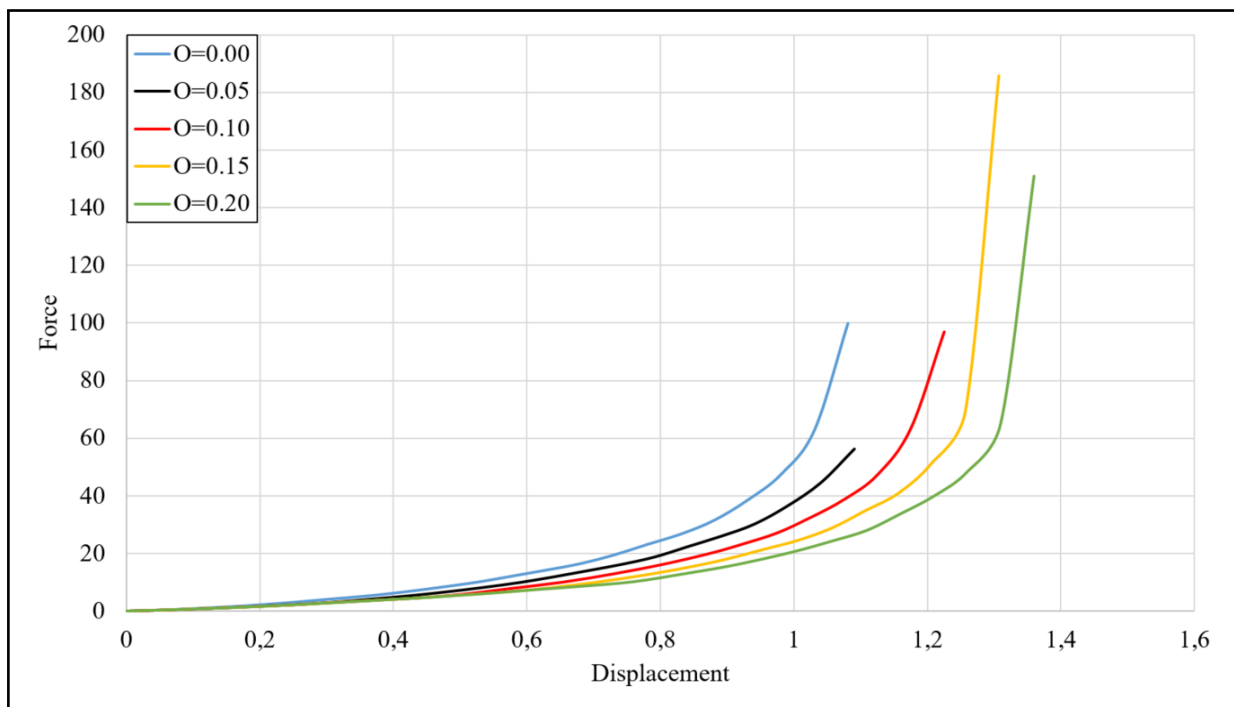


Figure I.8: Shore 90A - 5 mm - One sealing element - Groove too wide

## Numerical compression of two O-rings

This section presents the numerical analysis for two sealing elements compared to each other without comparing to experimental tests. Following situations will be presented:

- Two sealing elements in Shore 70A with offset of side walls equal to 0.00 mm, -0.025 mm, -0.05 mm, -0.10 mm and -0.15 mm representing situation when the rectangular groove is too small compared to the two seal cross sectional diameter of 6 mm.
- Two sealing elements in Shore 70A with offset of side walls equal to 0.00 mm, 0.05 mm, 0.10 mm, 0.15 mm and 0.20 mm representing situation when the rectangular groove is too wide compared to the two seals cross sectional diameter of 6 mm.
- Two sealing elements in Shore 70A with offset of side walls equal to 0.00 mm, -0.025 mm, -0.05 mm, -0.10 mm and -0.15 mm representing situation when the rectangular groove is too small compared to the two seals cross sectional diameter of 5 mm.
- Two sealing elements in Shore 70A with offset of side walls equal to 0.00 mm, 0.05 mm, 0.10 mm, 0.15 mm and 0.20 mm representing situation when the rectangular groove is too wide compared to the two seals cross sectional diameter of 5 mm.
- Two sealing elements in Shore 90A with offset of side walls equal to 0.00 mm, -0.025 mm, -0.05 mm, -0.10 mm and -0.15 mm representing situation when the rectangular groove is too small compared to the two seals cross sectional diameter of 6 mm.
- Two sealing elements in Shore 90A with offset of side walls equal to 0.00 mm, 0.05 mm, 0.10 mm, 0.15 mm and 0.20 mm representing situation when the rectangular groove is too wide compared to the two seals cross sectional diameter of 6 mm.
- Two sealing elements in Shore 90A with offset of side walls equal to 0.00 mm, -0.025 mm, -0.05 mm, -0.10 mm and -0.15 mm representing situation when the rectangular groove is too small compared to the two seals cross sectional diameter of 5 mm.
- Two sealing elements in Shore 90A with offset of side walls equal to 0.00 mm, 0.05 mm, 0.10 mm, 0.15 mm and 0.20 mm representing situation when the rectangular groove is too wide compared to the two seals cross sectional diameter of 5 mm.

## Position 1 - Shore 70 A

Table I.9 presents the parameters for the analysis where the offset of the side walls represent a groove too wide compared to the cross-sectional diameter of the sealing elements.

Table I.9: Parameters - Shore 70A - 6 mm - Two rings - Groove too wide

Hardness	Cross section	Offset side walls	$\mu$	Test
Shore 70A	6 mm	0.00 mm	0.5	Numerical
Shore 70A	6 mm	0.05 mm	0.5	Numerical
Shore 70A	6 mm	0.10 mm	0.5	Numerical
Shore 70A	6 mm	0.15 mm	0.5	Numerical
Shore 70A	6 mm	0.20 mm	0.5	Numerical

Figure I.9 illustrates the numerical test results for two sealing elements with the parameters presented in Table I.9 is presented.

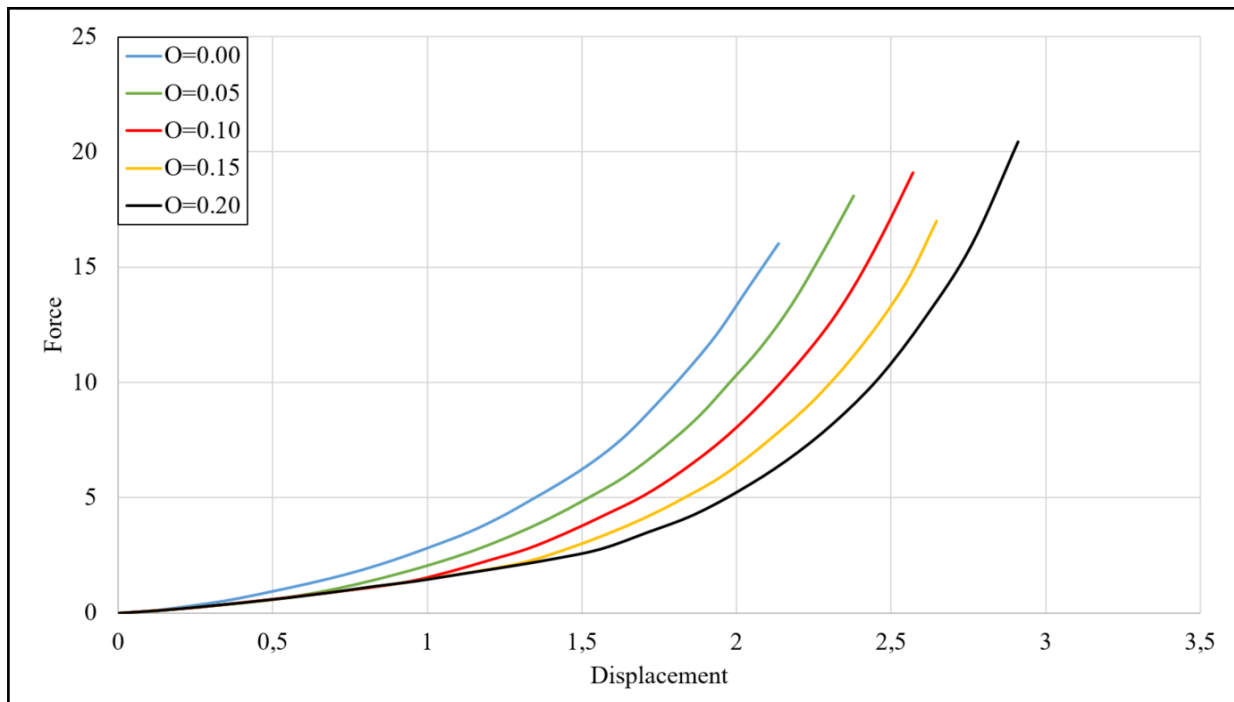


Figure I.9: Shore 70A - 6 mm - Two rings - Groove too wide

Table I.10 presents the parameters for the analysis where the side walls contribute to pre-tension in the sealing elements, illustrating a groove too small compared to the cross-sectional diameter of the seals.

Table I.10: Parameters - Shore 70A - 6 mm - Two rings - Groove too small

Hardness	Cross section	Offset side walls	$\mu$	Test
Shore 70A	6 mm	0.00 mm	0.5	Numerical
Shore 70A	6 mm	-0.025 mm	0.5	Numerical
Shore 70A	6 mm	-0.05 mm	0.5	Numerical
Shore 70A	6 mm	-0.10 mm	0.5	Numerical
Shore 70A	6 mm	-0.15 mm	0.5	Numerical

In Figure I.10 the numerical tests for two O-rings with the parameters presented in Table I.10 is presented.

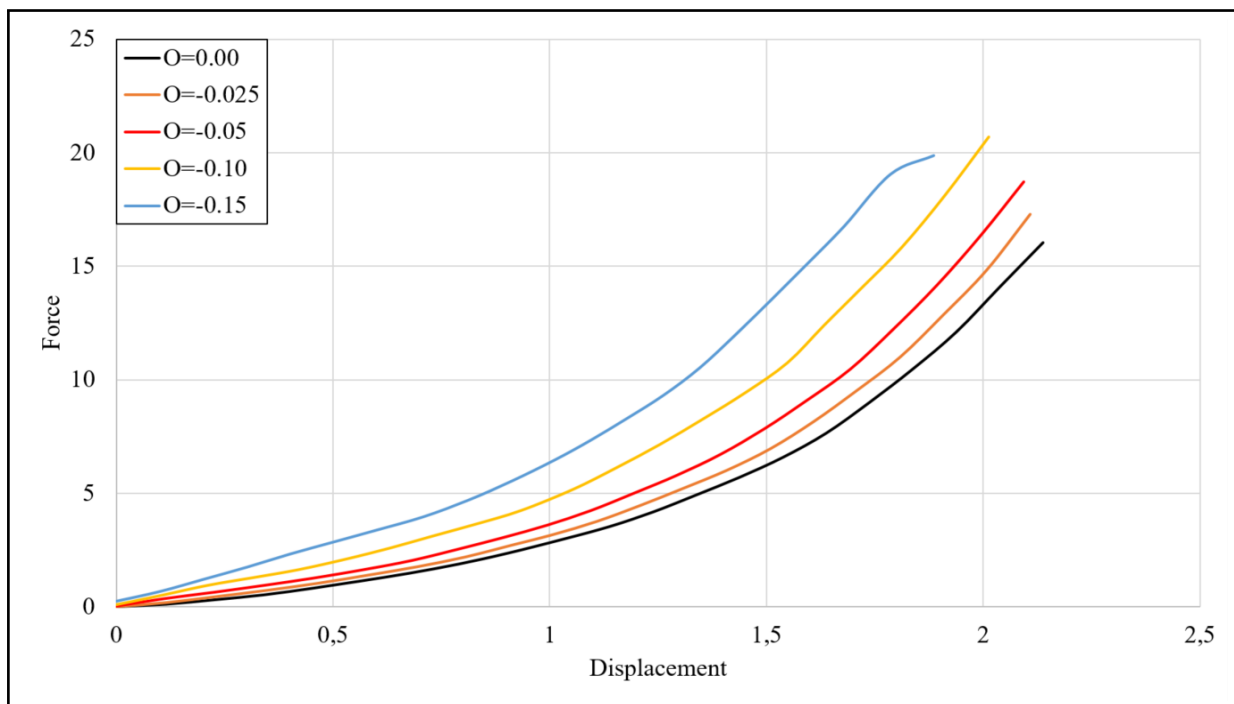


Figure I.10: Shore 70A - 6 mm - Two rings - Groove too small

Table I.11 presents the parameters for the analysis where the offset of the side walls represent a groove too wide compared to the cross-sectional diameter of the sealing elements.

Table I.11: Parameters - Shore 70A - 5 mm - Two rings - Groove too wide

Hardness	Cross section	Offset side walls	$\mu$	Test
Shore 70A	5 mm	0.00 mm	0.5	Numerical
Shore 70A	5 mm	0.05 mm	0.5	Numerical
Shore 70A	5 mm	0.10 mm	0.5	Numerical
Shore 70A	5 mm	0.15 mm	0.5	Numerical
Shore 70A	5 mm	0.20 mm	0.5	Numerical

Figure I.11 illustrates the numerical test results for two sealing elements with the parameters presented in Table I.11 is presented.

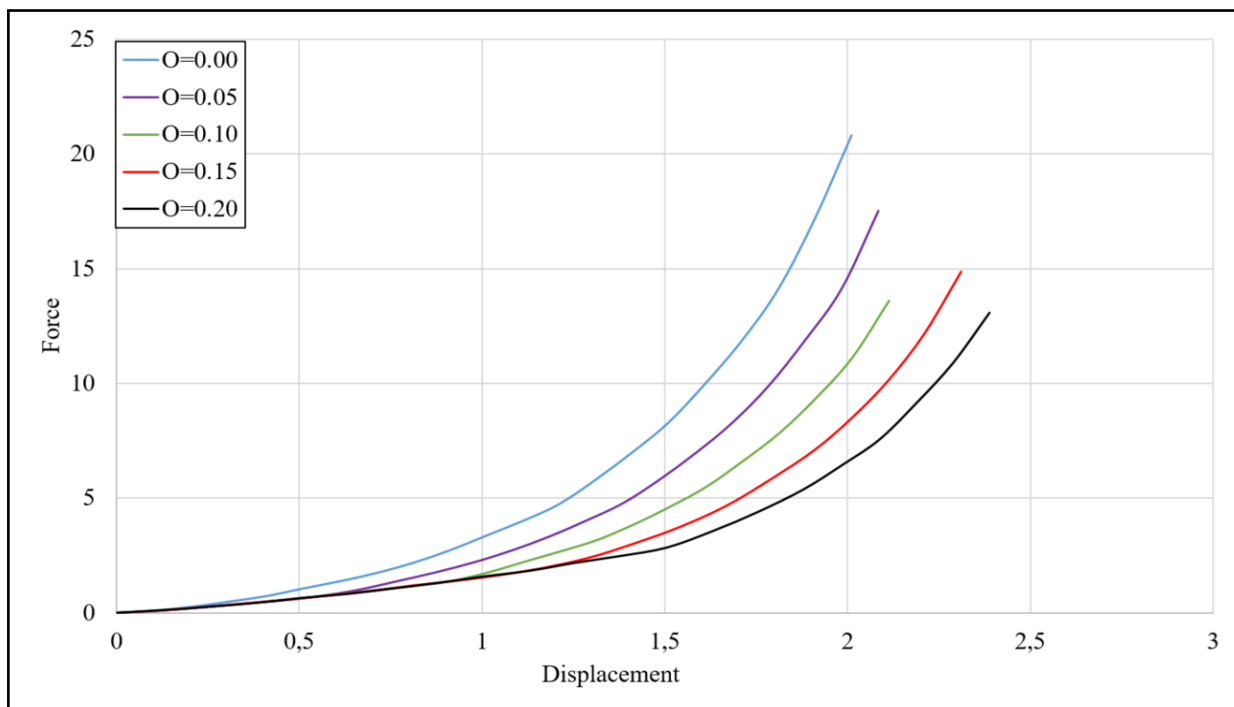


Figure I.11: Shore 70A - 5 mm - Two rings - Groove too wide

Table I.12 presents the parameters for the analysis where the side walls contribute to pre-tension in the sealing elements, illustrating a groove too small compared to the cross-sectional diameter of the seals.

Table I.12: Parameters - Shore 70A - 5 mm - Two rings - Groove too small

Hardness	Cross section	Offset side walls	$\mu$	Test
Shore 70A	5 mm	0.00 mm	0.5	Numerical
Shore 70A	5 mm	-0.025 mm	0.5	Numerical
Shore 70A	5 mm	-0.05 mm	0.5	Numerical
Shore 70A	5 mm	-0.10 mm	0.5	Numerical
Shore 70A	5 mm	-0.15 mm	0.5	Numerical

Figure I.12 illustrates the numerical test results for two sealing elements with the parameters presented in Table I.12.

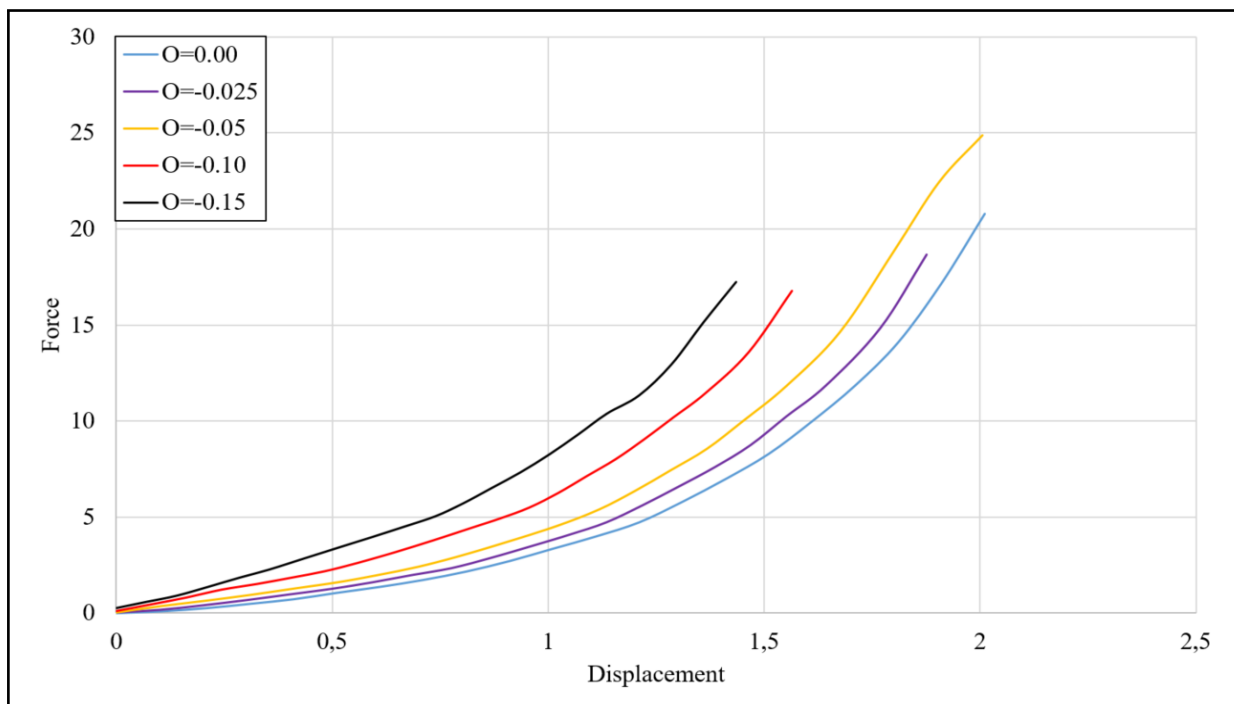


Figure I.12: Shore 70A - 5 mm - Two rings - Groove too small

## Position 1 - Shore 90 A

Table I.13 presents the parameters for the analysis where the offset of the side walls represent a groove too wide compared to the cross-sectional diameter of the sealing elements.

Table I.13: Parameters - Shore 90A - 6 mm - Two rings - Groove too wide

Hardness	Cross section	Offset side walls	$\mu$	Test
Shore 90A	6 mm	0.00 mm	0.5	Numerical
Shore 90A	6 mm	0.05 mm	0.5	Numerical
Shore 90A	6 mm	0.10 mm	0.5	Numerical
Shore 90A	6 mm	0.15 mm	0.5	Numerical
Shore 90A	6 mm	0.20 mm	0.5	Numerical

Figure I.13 illustrates the numerical test results for two sealing elements with the parameters presented in Table I.13.

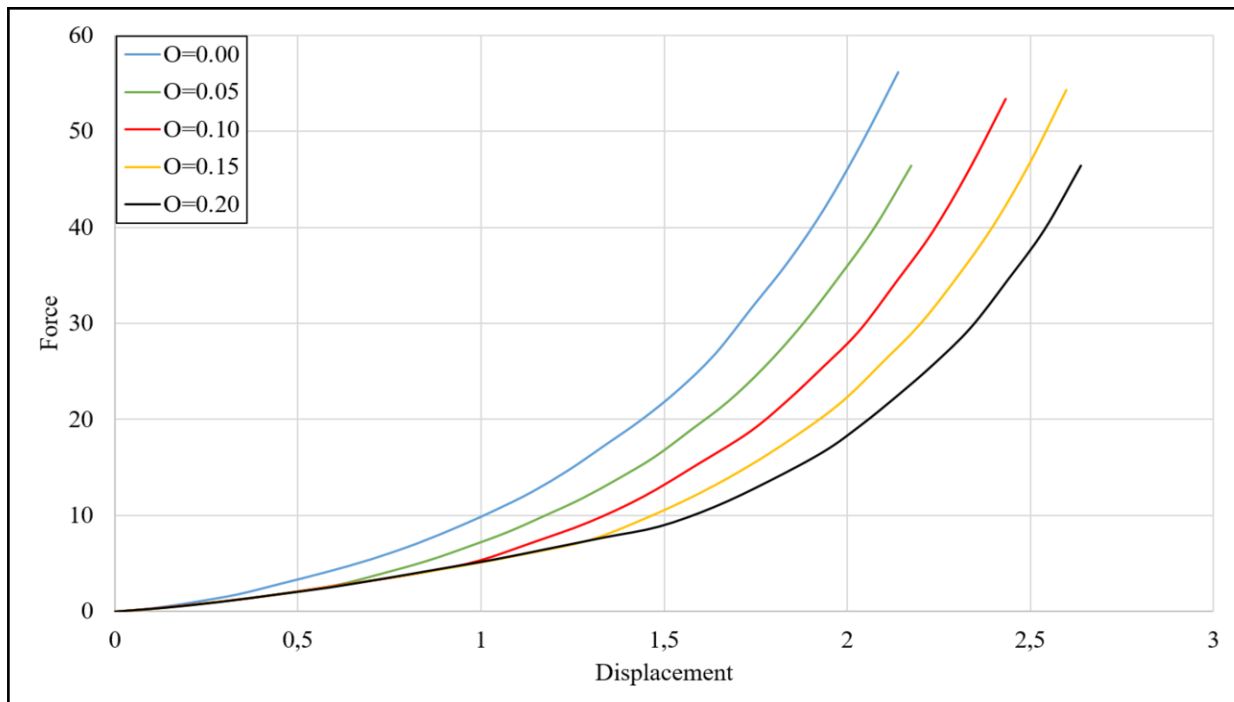


Figure I.13: Shore 90A - 6 mm - Two rings - Groove too wide



Table I.14 presents the parameters for the analysis where the side walls contribute to pre-tension in the sealing elements, illustrating a groove too small compared to the cross-sectional diameter of the seals.

Table I.14: Parameters - Shore 90A - 6 mm - Two rings - Groove too small

Hardness	Cross section	Offset side walls	$\mu$	Test
Shore 90A	6 mm	0.00 mm	0.5	Numerical
Shore 90A	6 mm	-0.025 mm	0.5	Numerical
Shore 90A	6 mm	-0.05 mm	0.5	Numerical
Shore 90A	6 mm	-0.10 mm	0.5	Numerical
Shore 90A	6 mm	-0.15 mm	0.5	Numerical

Figure I.14 illustrates the numerical test results for two sealing elements with the parameters presented in Table I.14.

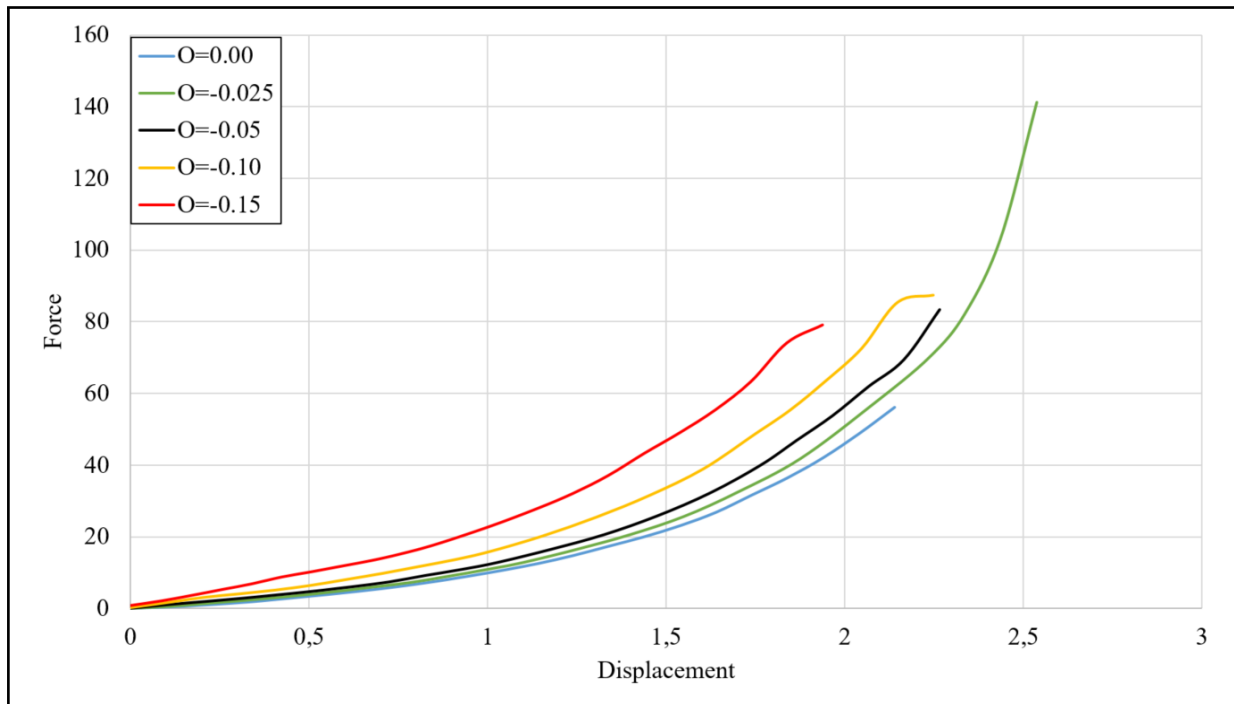


Figure I.14: Shore 90A - 6 mm - Two rings - Groove too small

Table I.15 presents the parameters for the analysis where the offset of the side walls represent a groove too wide compared to the cross-sectional diameter of the sealing elements.

Table I.15: Parameters - Shore 90A - 5 mm - Two rings - Groove too wide

Hardness	Cross section	Offset side walls	$\mu$	Test
Shore 90A	5 mm	0.00 mm	0.5	Numerical
Shore 90A	5 mm	0.05 mm	0.5	Numerical
Shore 90A	5 mm	0.10 mm	0.5	Numerical
Shore 90A	5 mm	0.15 mm	0.5	Numerical
Shore 90A	5 mm	0.20 mm	0.5	Numerical

Figure I.15 illustrates the numerical test results for two sealing elements with the parameters presented in Table I.15.

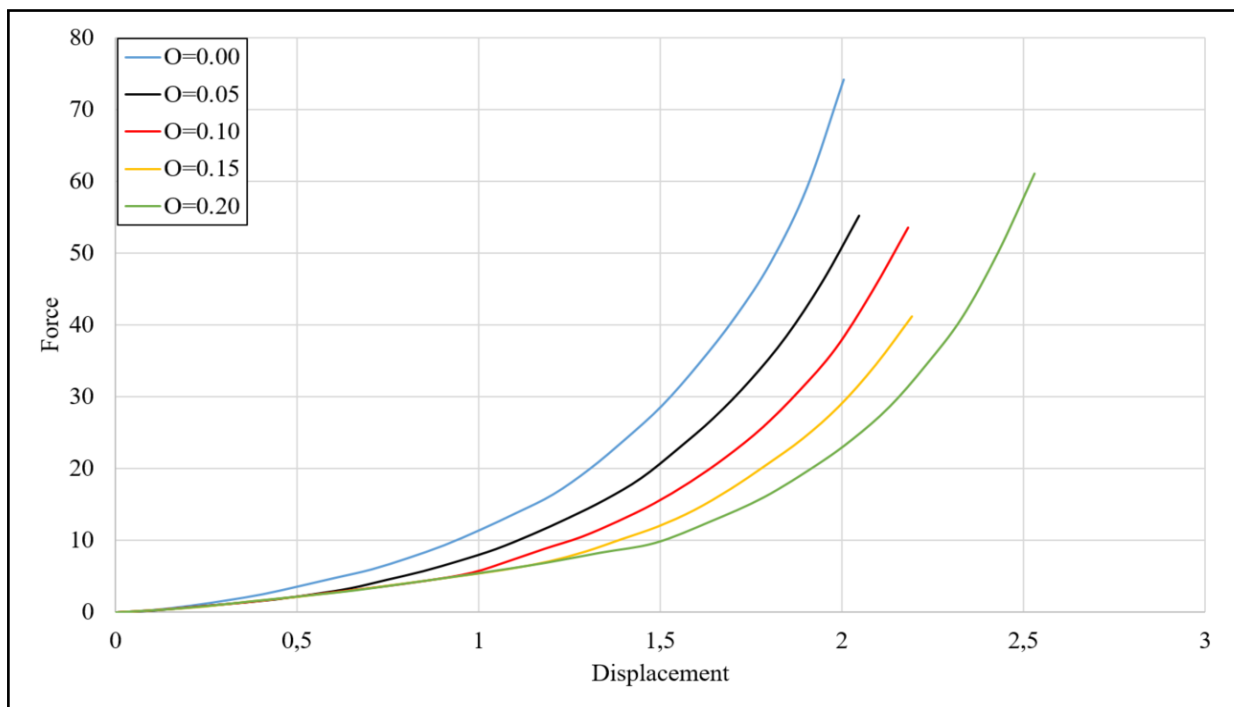


Figure I.15: Shore 90A - 5 mm - Two rings - Groove too wide

Table I.16 presents the parameters for the analysis where the side walls contribute to pre-tension in the sealing elements, illustrating a groove too small compared to the cross-sectional diameter of the seals.

Table I.16: Parameters - Shore 90A - 5 mm - Two rings - Groove too small

Hardness	Cross section	Offset side walls	$\mu$	Test
Shore 90A	5 mm	0.00 mm	0.5	Numerical
Shore 90A	5 mm	-0.025 mm	0.5	Numerical
Shore 90A	5 mm	-0.05 mm	0.5	Numerical
Shore 90A	5 mm	-0.10 mm	0.5	Numerical
Shore 90A	5 mm	-0.15 mm	0.5	Numerical

Figure I.16 illustrates the numerical test results for two sealing elements with the parameters presented in Table I.16.

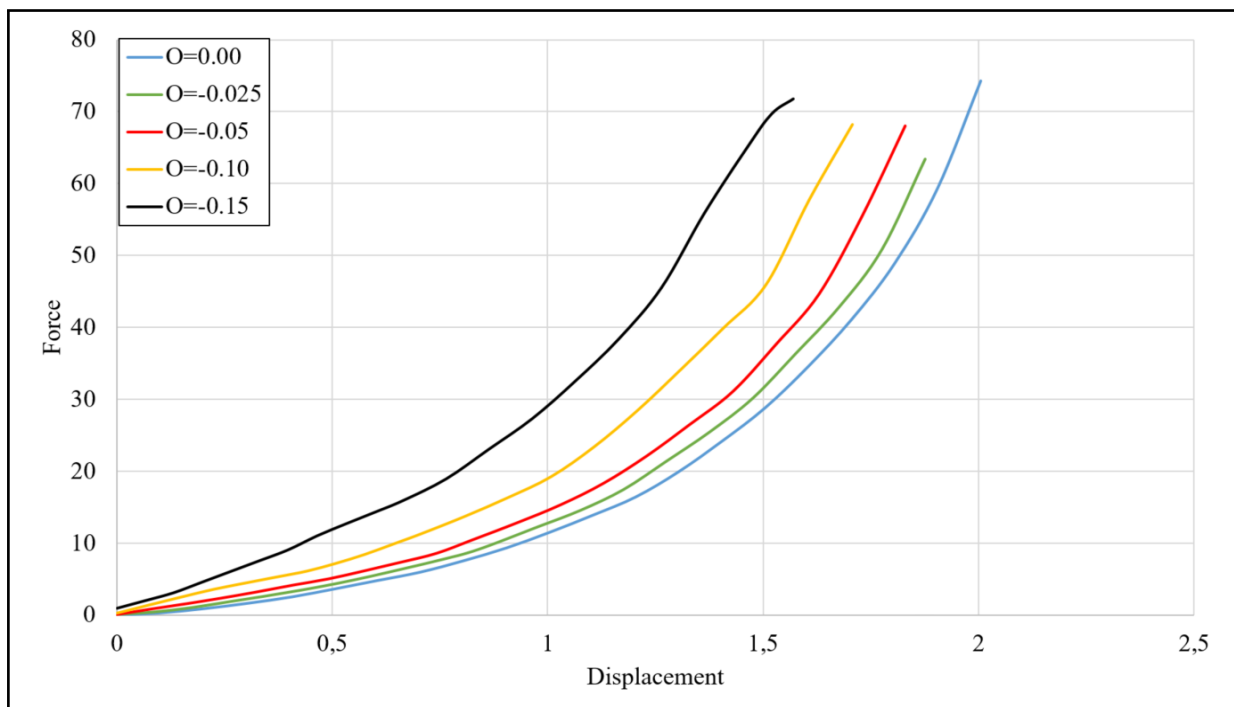


Figure I.16: Shore 90A - 5 mm - Two rings - Groove too small

## Comparison of curves

### Material hardness comparison

Table I.17 presents the parameters for the analysis where the side walls contribute to the opposite of pre-tension in the a single sealing element, illustrating a groove too wide compared to the cross-sectional diameter of the seal.

Table I.17: Parameters - Shore 70A and 90A - 6 mm - One seal - Groove too wide

Hardness	Cross section	Offset side walls	$\mu$	Test
Shore 70A and 90A	6 mm	0.00 mm	0.5	Numerical
Shore 70A and 90A	6 mm	0.05 mm	0.5	Numerical
Shore 70A and 90A	6 mm	0.10 mm	0.5	Numerical
Shore 70A and 90A	6 mm	0.15 mm	0.5	Numerical
Shore 70A and 90A	6 mm	0.20 mm	0.5	Numerical

Figure I.17 illustrates the numerical test results for one sealing element with the parameters presented in Table I.17.

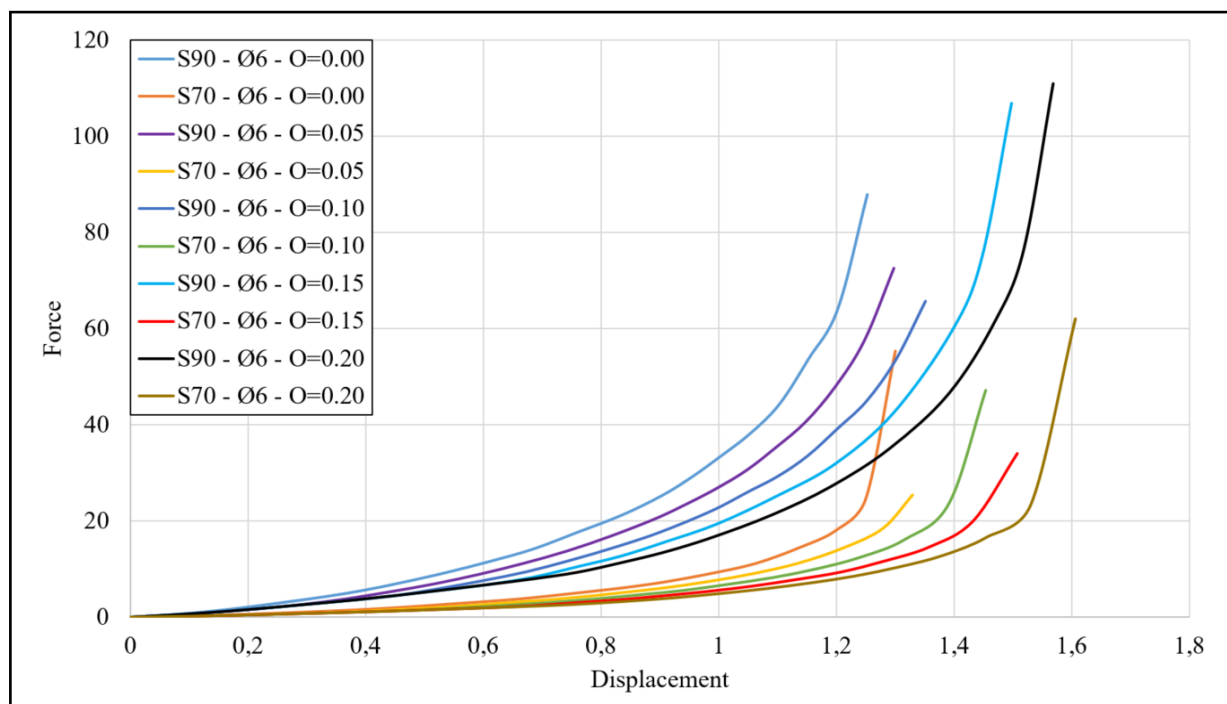


Figure I.17: Shore 70A and 90A - 6 mm - One seal - Groove too wide

Table I.18 presents the parameters for the analysis where the side walls contribute to the opposite pre-tension in the sealing elements, illustrating a groove too wide compared to the cross-sectional diameter of the seals.

Table I.18: Parameters - Shore 70A and 90A - 6 mm - Two seals - Groove too wide

Hardness	Cross section	Offset side walls	$\mu$	Test
Shore 70A and 90A	6 mm	0.00 mm	0.5	Numerical
Shore 70A and 90A	6 mm	0.05 mm	0.5	Numerical
Shore 70A and 90A	6 mm	0.10 mm	0.5	Numerical
Shore 70A and 90A	6 mm	0.15 mm	0.5	Numerical
Shore 70A and 90A	6 mm	0.20 mm	0.5	Numerical

Figure I.18 illustrates the numerical test results for two sealing elements with the parameters presented in Table I.18.

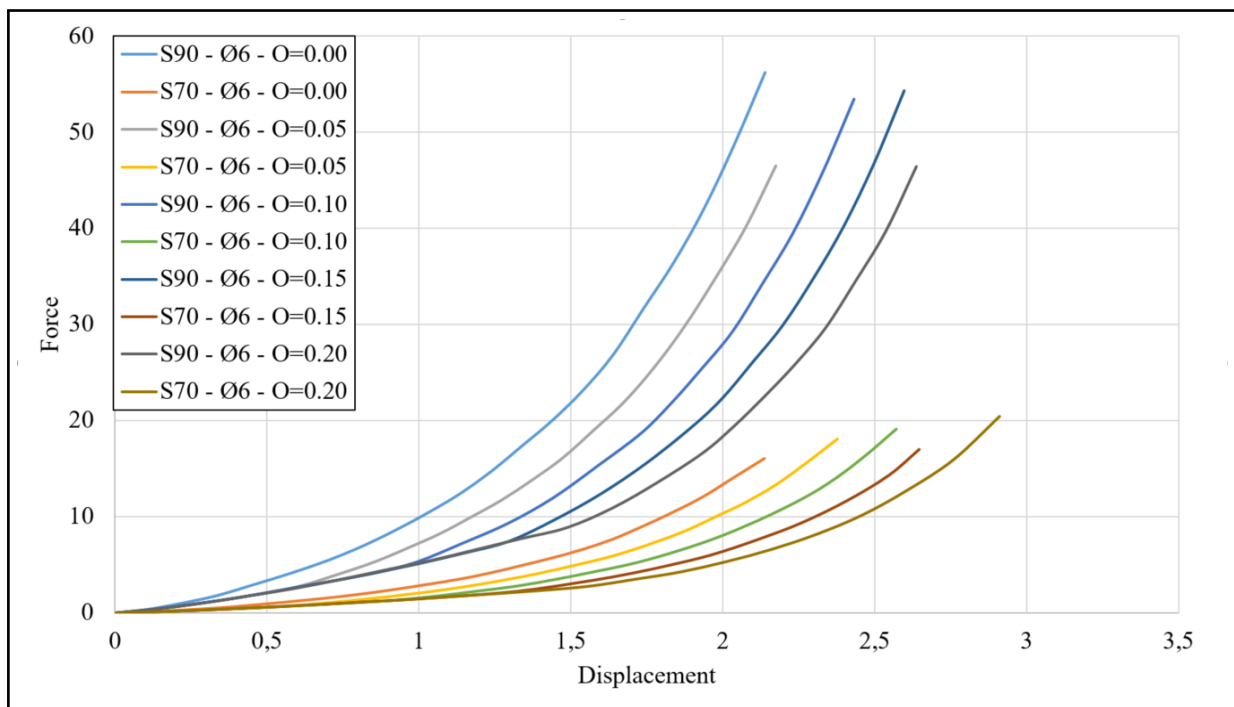


Figure I.18: Shore 70A and 90A - Ø6 - Two rings - Groove too wide

## Cross-sectional diameter compared - One seal

Table I.19 presents the parameters for the analysis where the side walls contribute to pre-tension in the sealing element, illustrating a groove too small compared to the cross-sectional diameter of the seal.

Table I.19: Parameters - Shore 90A - 5 mm and 6 mm - One seal - Groove too small

Hardness	Cross section	Offset side walls	$\mu$	Test
Shore 90A	5 mm and 6 mm	0.00 mm	0.5	Numerical
Shore 90A	5 mm and 6 mm	-0.025 mm	0.5	Numerical
Shore 90A	5 mm and 6 mm	-0.05 mm	0.5	Numerical
Shore 90A	5 mm and 6 mm	-0.10 mm	0.5	Numerical
Shore 90A	5 mm and 6 mm	-0.15 mm	0.5	Numerical

Figure I.19 illustrates the numerical test results for one sealing element with the parameters presented in Table 4.10.

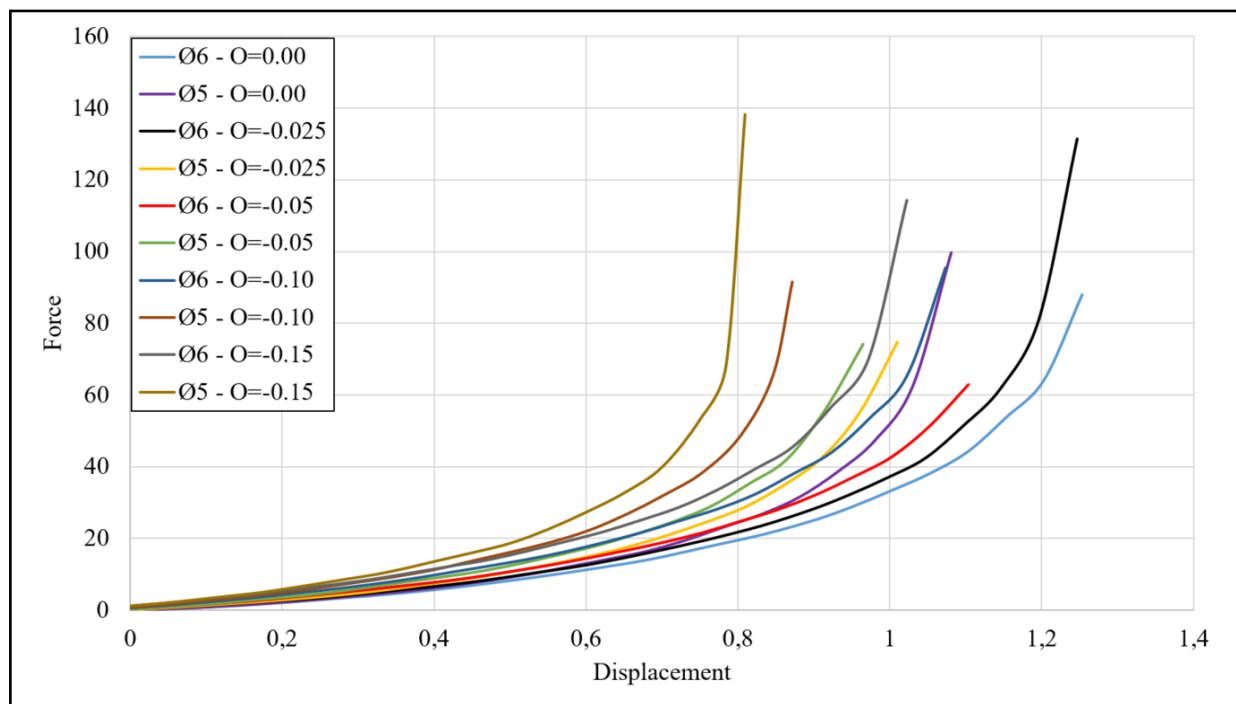


Figure I.19: Shore 90A - 5 mm and 6 mm - One seal - Groove too small

Table I.20 presents the parameters for the analysis where the offset of the side walls represent a groove too wide compared to the cross-sectional diameter of the sealing element.

Table I.20: Parameters - Shore 90A - 5 mm and 6 mm - One ring - Groove too wide

Hardness	Cross section	Offset side walls	$\mu$	Test
Shore 90A	5 mm and 6 mm	0.00 mm	0.5	Numerical
Shore 90A	5 mm and 6 mm	0.05 mm	0.5	Numerical
Shore 90A	5 mm and 6 mm	0.10 mm	0.5	Numerical
Shore 90A	5 mm and 6 mm	0.15 mm	0.5	Numerical
Shore 90A	5 mm and 6 mm	0.20 mm	0.5	Numerical

Figure I.20 illustrates the numerical test results for two sealing elements with the parameters presented in Table I.20.

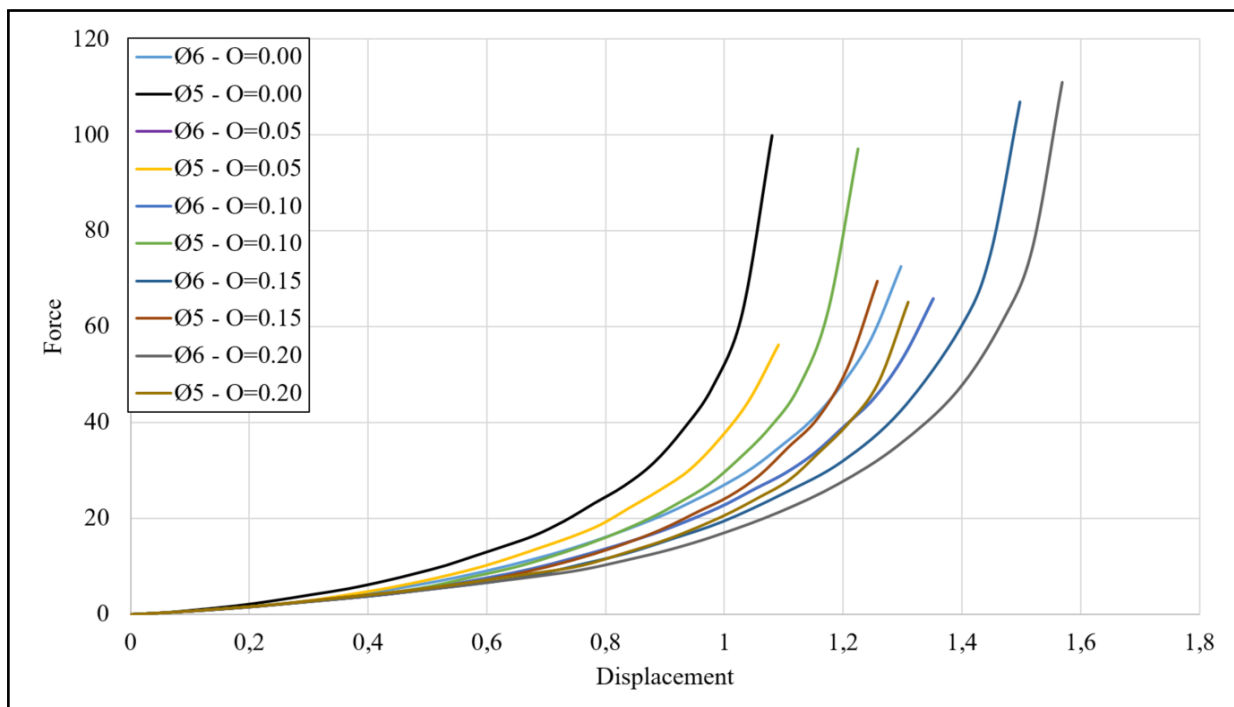


Figure I.20: Shore 90A - 5 mm and 6 mm - One seal - Groove too wide

## One ring compared to two O-rings

Table I.21 presents the parameters for the analysis where the side walls contribute to pre-tension in the sealing elements, illustrating a groove too small compared to the cross-sectional diameter of the seals.

Table I.21: Parameters - Shore 70A - 5 mm - One compared to two - Groove too small

Hardness	Cross section	Offset side walls	$\mu$	Test
Shore 70A	5 mm	0.00 mm	0.5	Numerical
Shore 70A	5 mm	-0.025 mm	0.5	Numerical
Shore 70A	5 mm	-0.05 mm	0.5	Numerical
Shore 70A	5 mm	-0.10 mm	0.5	Numerical
Shore 70A	5 mm	-0.15 mm	0.5	Numerical

Figure I.21 illustrates the numerical test results for the sealing elements with parameters presented in Table I.21.

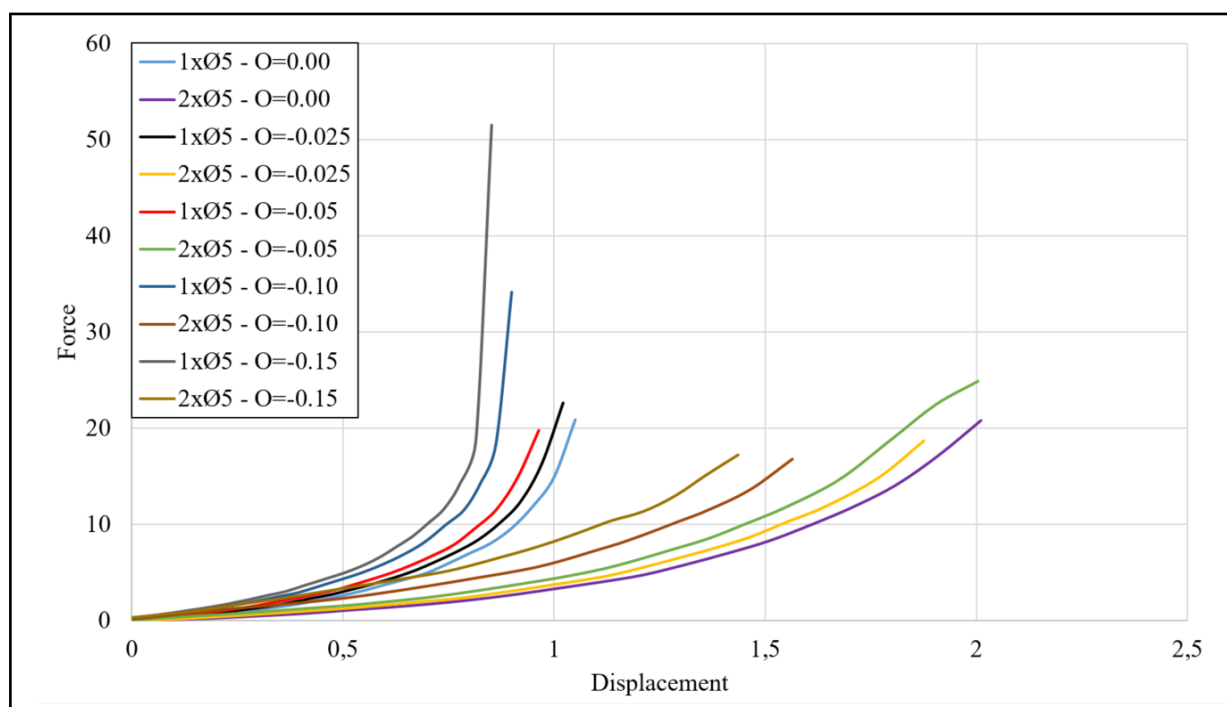


Figure I.21: Shore 70A - 5 mm - One and two rings - Groove too small



Table I.22 presents the parameters for the analysis where the side walls contribute to pre-tension in the sealing elements, illustrating a groove too small compared to the cross-sectional diameter of the seals.

Table I.22: Parameters - Shore 90A - 5 mm - One compared to two - Groove too small

Hardness	Cross section	Offset side walls	$\mu$	Test
Shore 90A	5 mm	0.00 mm	0.5	Numerical
Shore 90A	5 mm	-0.025 mm	0.5	Numerical
Shore 90A	5 mm	-0.05 mm	0.5	Numerical
Shore 90A	5 mm	-0.10 mm	0.5	Numerical
Shore 90A	5 mm	-0.15 mm	0.5	Numerical

Figure I.22 illustrates the numerical test results the sealing elements with parameters presented in Table I.22.

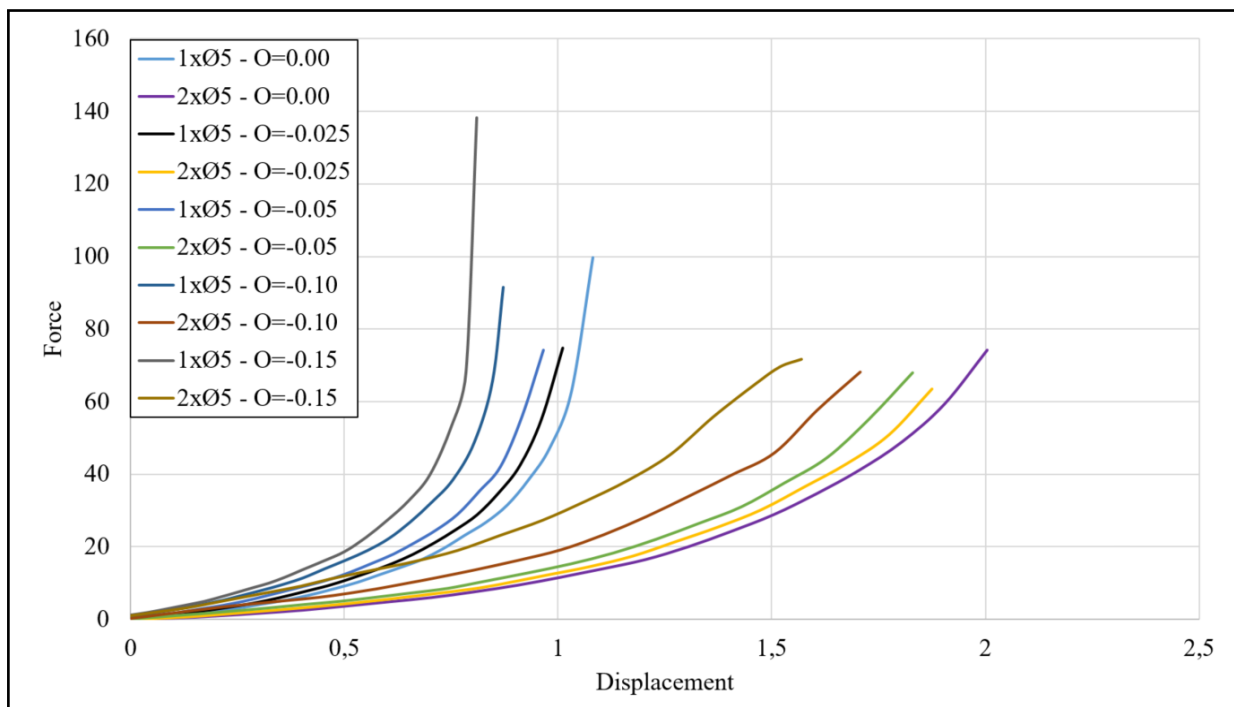


Figure I.22: Shore 90A - Ø5 - One and two rings - Groove too small

Table I.23 presents the parameters for the analysis where the offset of the side walls represent a groove too wide compared to the cross-sectional diameter of the sealing elements.

Table I.23: Parameters - Shore 70A - 5 mm - One compared to two - Groove too wide

Hardness	Cross section	Offset side walls	$\mu$	Test
Shore 70A	5 mm	0.00 mm	0.5	Numerical
Shore 70A	5 mm	0.05 mm	0.5	Numerical
Shore 70A	5 mm	0.10 mm	0.5	Numerical
Shore 70A	5 mm	0.15 mm	0.5	Numerical
Shore 70A	5 mm	0.20 mm	0.5	Numerical

Figure I.23 illustrates the numerical test results for the sealing elements with parameters presented in Table I.23.

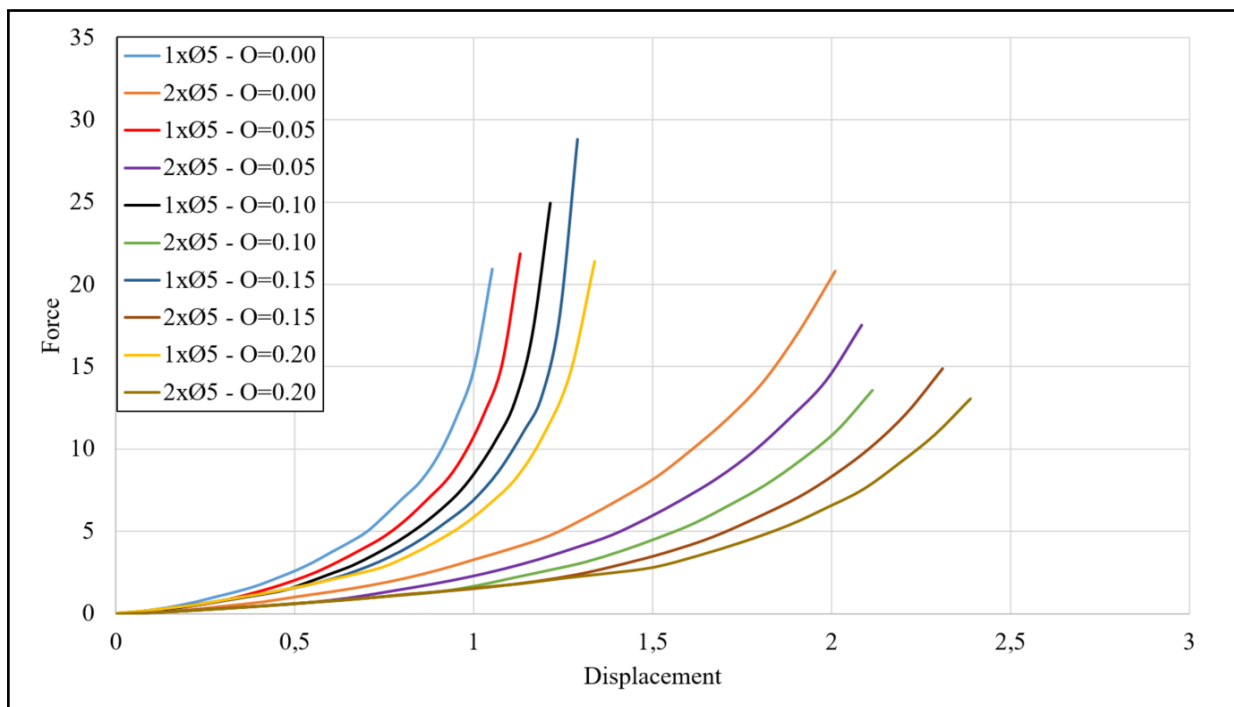


Figure I.23: Shore 70A - 5 mm - One and two rings - Groove too wide

Table I.24 presents the parameters for the analysis where the offset of the side walls represent a groove too wide compared to the cross-sectional diameter of the sealing elements.

Table I.24: Parameters - Shore 90A - 5 mm - One compared to two - Groove too wide

Hardness	Cross section	Offset side walls	$\mu$	Test
Shore 90A	5 mm	0.00 mm	0.5	Numerical
Shore 90A	5 mm	0.05 mm	0.5	Numerical
Shore 90A	5 mm	0.10 mm	0.5	Numerical
Shore 90A	5 mm	0.15 mm	0.5	Numerical
Shore 90A	5 mm	0.20 mm	0.5	Numerical

Figure I.24 illustrates the numerical test results for the sealing elements with parameters presented in Table I.24.

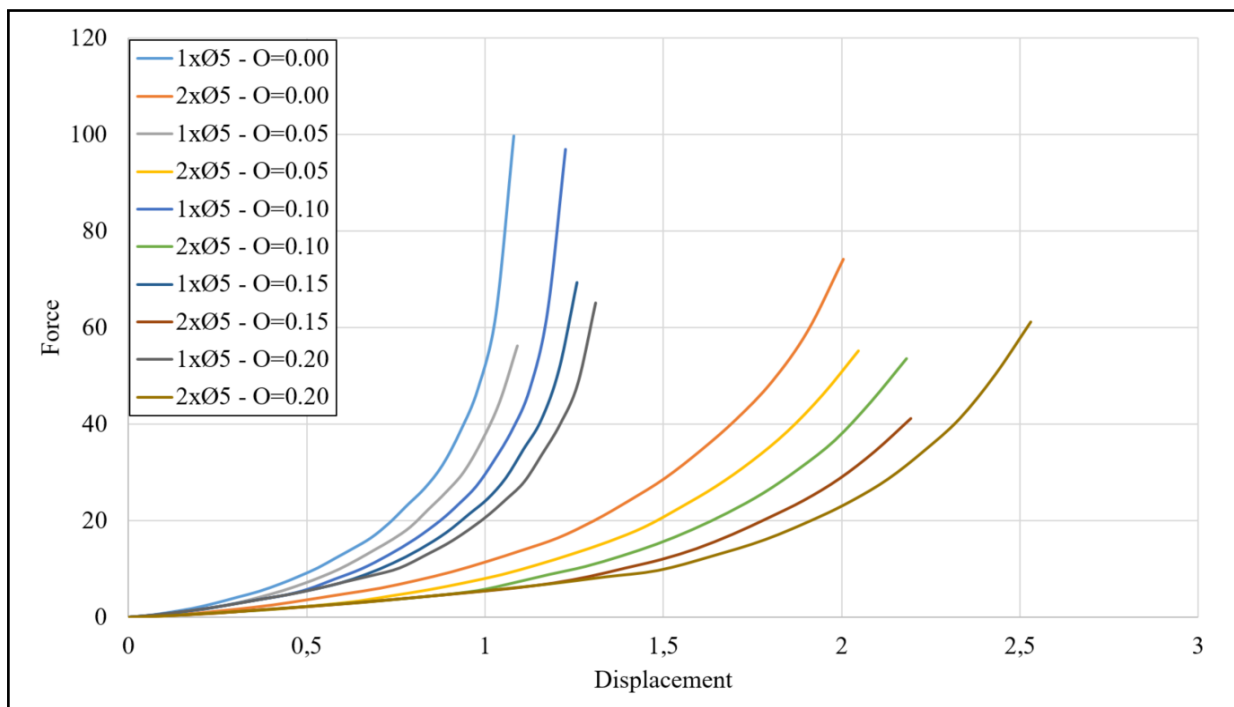


Figure I.24: Shore 90A - 5 mm - One and two rings - Groove too wide

## Two rings compared

Table I.25 presents the parameters for the analysis where the side walls contribute to pre-tension in two sealing elements, illustrating a groove too small compared to the cross-sectional diameter of the seals.

Table I.25: Parameters - Shore 90A - 5 mm and 6 mm - Two rings compared - Groove too small

Hardness	Cross section	Offset side walls	$\mu$	Test
Shore 90A	5 mm and 6 mm	0.00 mm	0.5	Numerical
Shore 90A	5 mm and 6 mm	-0.025 mm	0.5	Numerical
Shore 90A	5 mm and 6 mm	-0.05 mm	0.5	Numerical
Shore 90A	5 mm and 6 mm	-0.10 mm	0.5	Numerical
Shore 90A	5 mm and 6 mm	-0.15 mm	0.5	Numerical

Figure I.25 illustrates the numerical test results for two sealing elements with parameters presented in Table I.25.

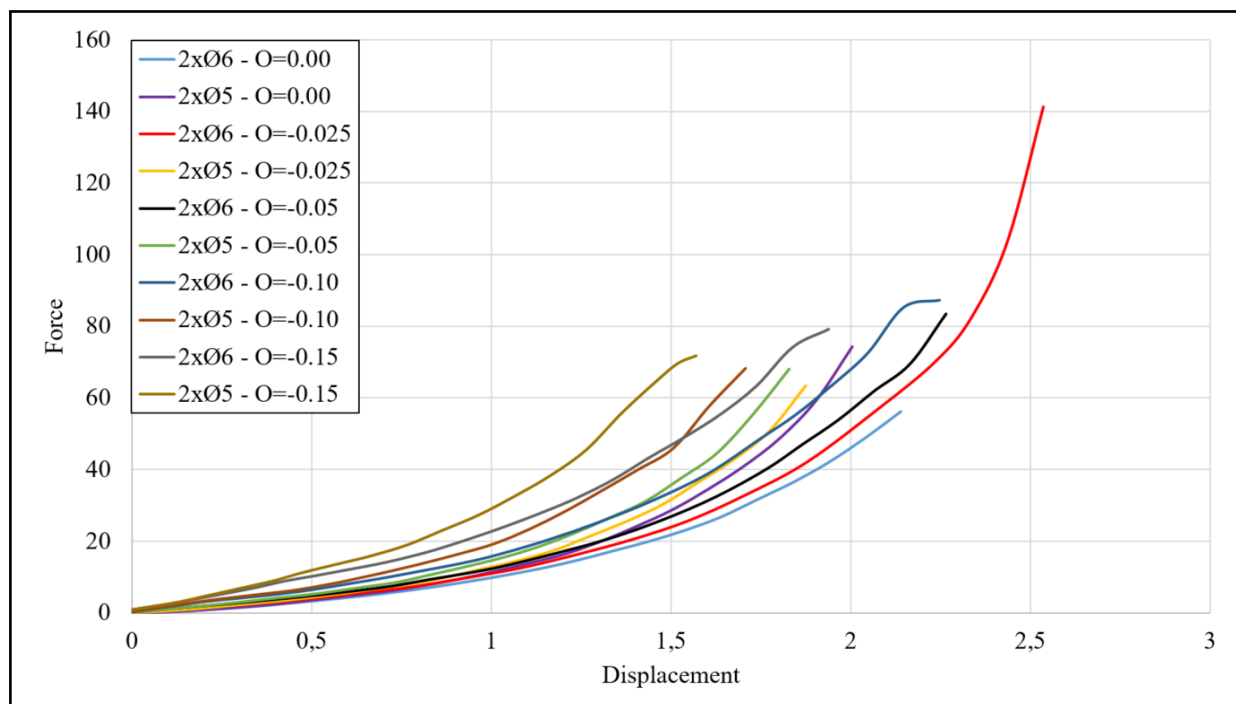


Figure I.25: Shore 90A - 5 mm and 6 mm- Two rings - Groove too small

Table I.26 presents the parameters for the analysis where the side walls contribute to pre-tension in the sealing elements, illustrating a groove too small compared to the cross-sectional diameter of the seals.

Table I.26: Parameters - Shore 90A - 5 mm and 6 mm - Two rings compared - Groove too wide

Hardness	Cross section	Offset side walls	$\mu$	Test
Shore 90A	5 mm and 6 mm	0.00 mm	0.5	Numerical
Shore 90A	5 mm and 6 mm	0.05 mm	0.5	Numerical
Shore 90A	5 mm and 6 mm	0.10 mm	0.5	Numerical
Shore 90A	5 mm and 6 mm	0.15 mm	0.5	Numerical
Shore 90A	5 mm and 6 mm	0.20 mm	0.5	Numerical

Figure I.26 illustrates the numerical test results for two sealing elements with parameters presented in Table I.26.

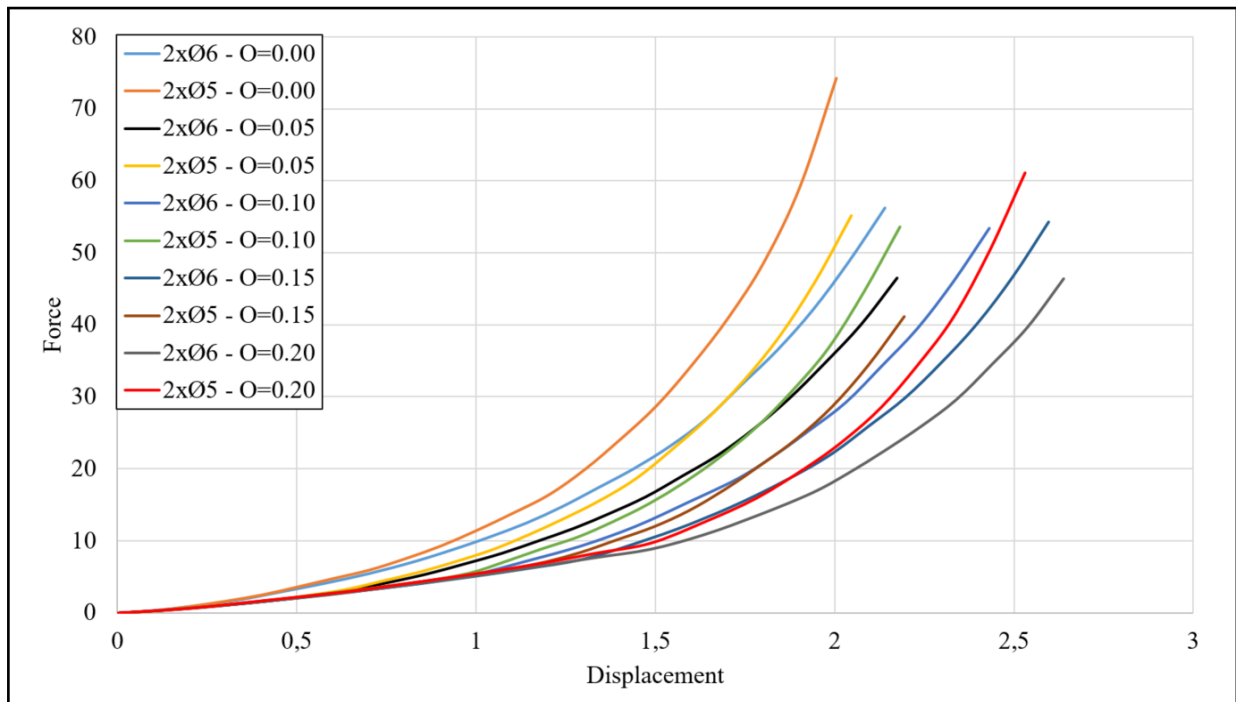


Figure I.26: Shore 90A - 5 mm and 6 mm - Two rings - Groove too wide

## Three positions

Figure I.27 is similar to Figure 4.25 but with displacement of side walls equal -0.10mm.

Table I.27: Parameters - Shore 70A - 6 mm - Two rings - 3 positions - Pretension

Hardness	Cross section	Offset side walls	Friction	Test	Position
Shore 70A	6 mm	-0.10 mm	0.5	Numerical	1
Shore 70A	6 mm	-0.10 mm	0.5	Numerical	2
Shore 70A	6 mm	-0.10 mm	0.5	Numerical	3

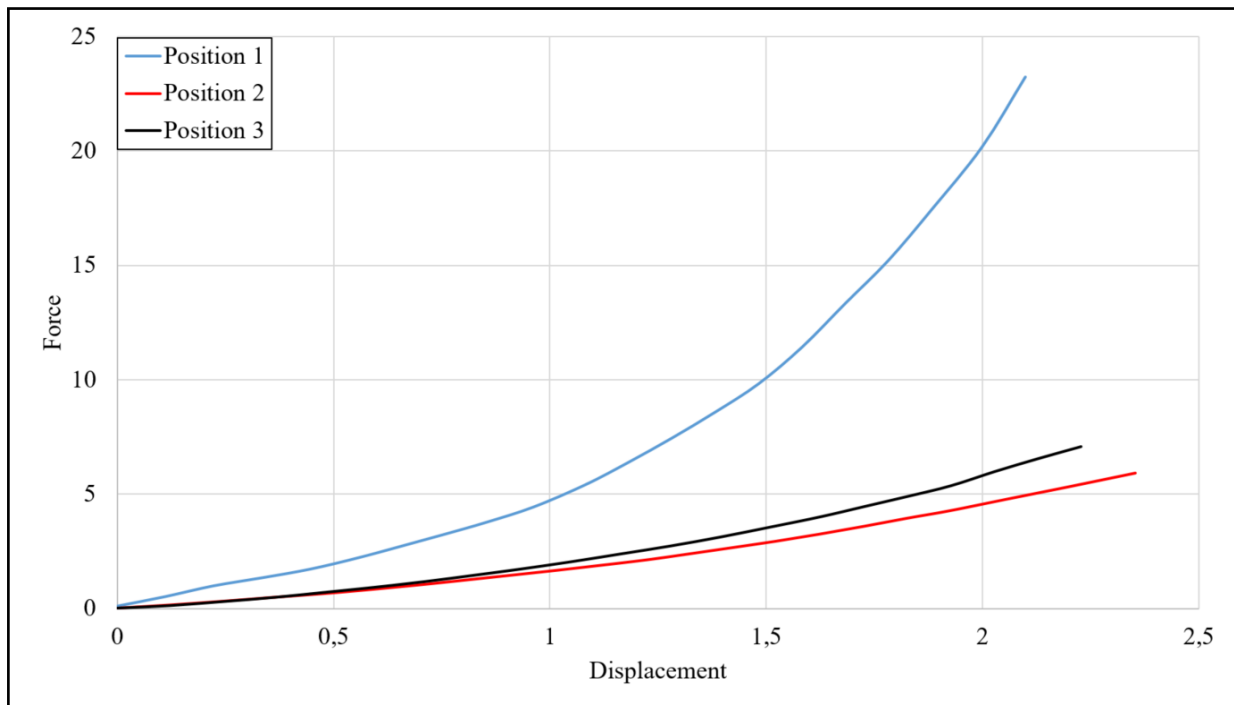


Figure I.27:  $\text{Ø}6$  -  $\mu=0.5$  - Groove too small - 3 positions

# Hysteresis

## Groove too small

Analyses with multiple loading and unloading step is conducted. Two O-rings in position 1 with a groove too small compared to the cross-sectional diameter of the seal is analyzed. The sequence of steps are as follows:

1. The simulation start with the required initial step
2. Load step of the side walls of -0.1 mm from both sides which gives a pre-tension
3. Load step from upper wire in negative vertical direction
4. Unload step from upper wire in positive vertical direction
5. Load step from upper wire in negative vertical direction
6. Unload step from upper wire in positive vertical direction
7. Load step from upper wire in negative vertical direction
8. Unload step from upper wire in positive vertical direction

The simulation are conducted with friction coefficient,  $\mu$ , 0.5. The shore 90A hardness is shown in Figure I.28:

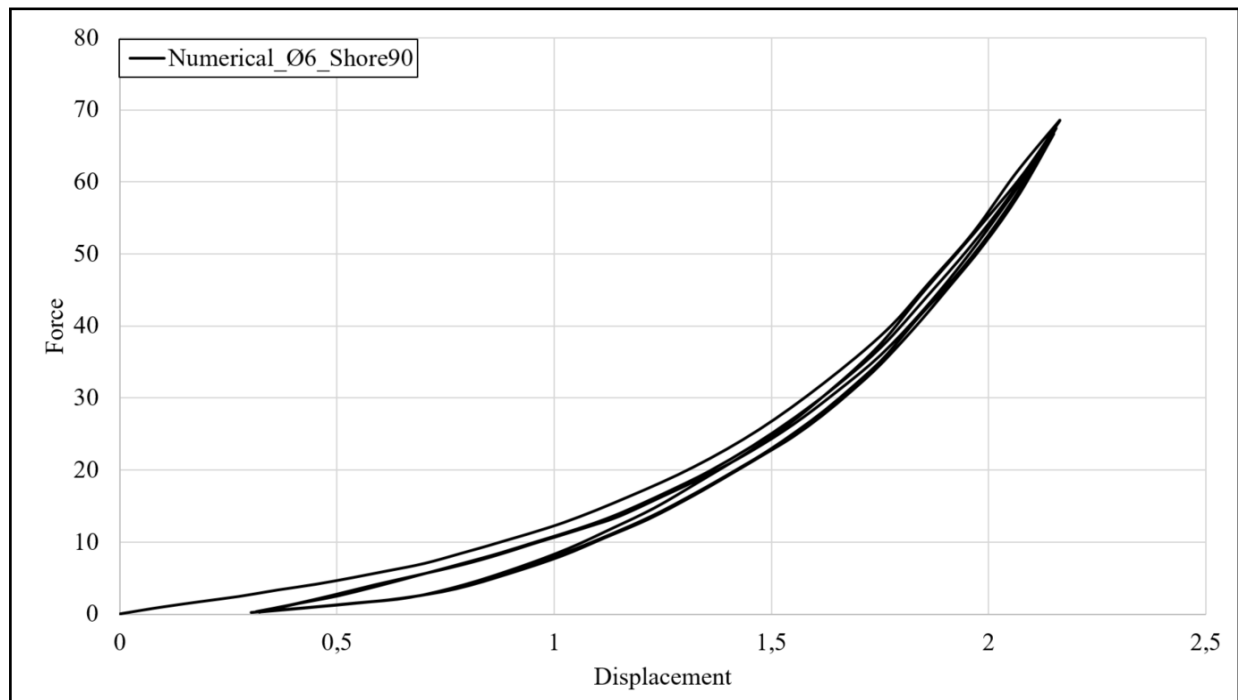


Figure I.28: Multiple steps - Hysteresis - Shore 90A -  $\mu=0.5$  - 6 mm

## Groove tangential

Two O-rings in position 1 with tangential side walls of the O-rings. The sequence of steps are as follows:

1. The simulation start with the required initial step
2. Load step from upper wire in negative vertical direction
3. Unload step from upper wire in positive vertical direction
4. Load step from upper wire in negative vertical direction
5. Unload step from upper wire in positive vertical direction
6. Load step from upper wire in negative vertical direction
7. Unload step from upper wire in positive vertical direction

Shore 90A is shown in Figure I.29.

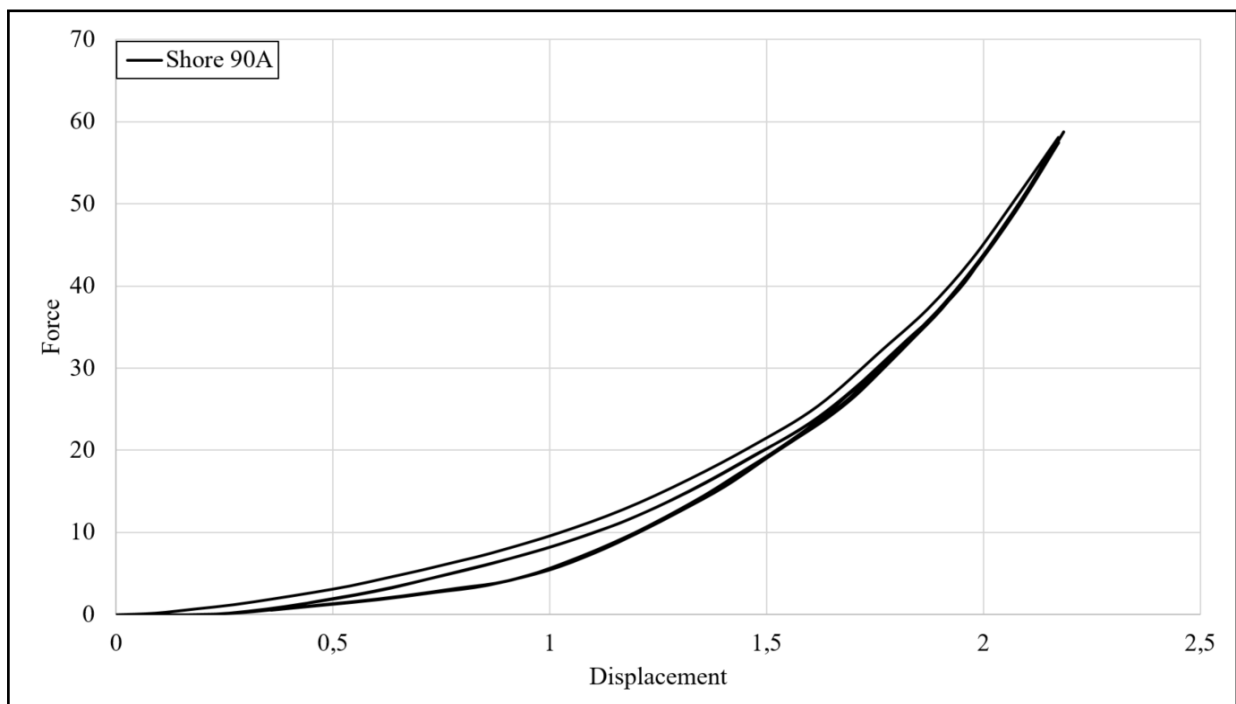


Figure I.29: Multiple steps - Hysteresis - Shore 90A -  $\mu=0.5$  - 6 mm



The next simulations are similar to the simulations in Figure 4.23 and Figure I.29 but are conducted with friction coefficient,  $\mu$ , 1.0. The shore 70A hardness is shown in Figure I.30 while the Shore 90A hardness is shown in Figure I.31

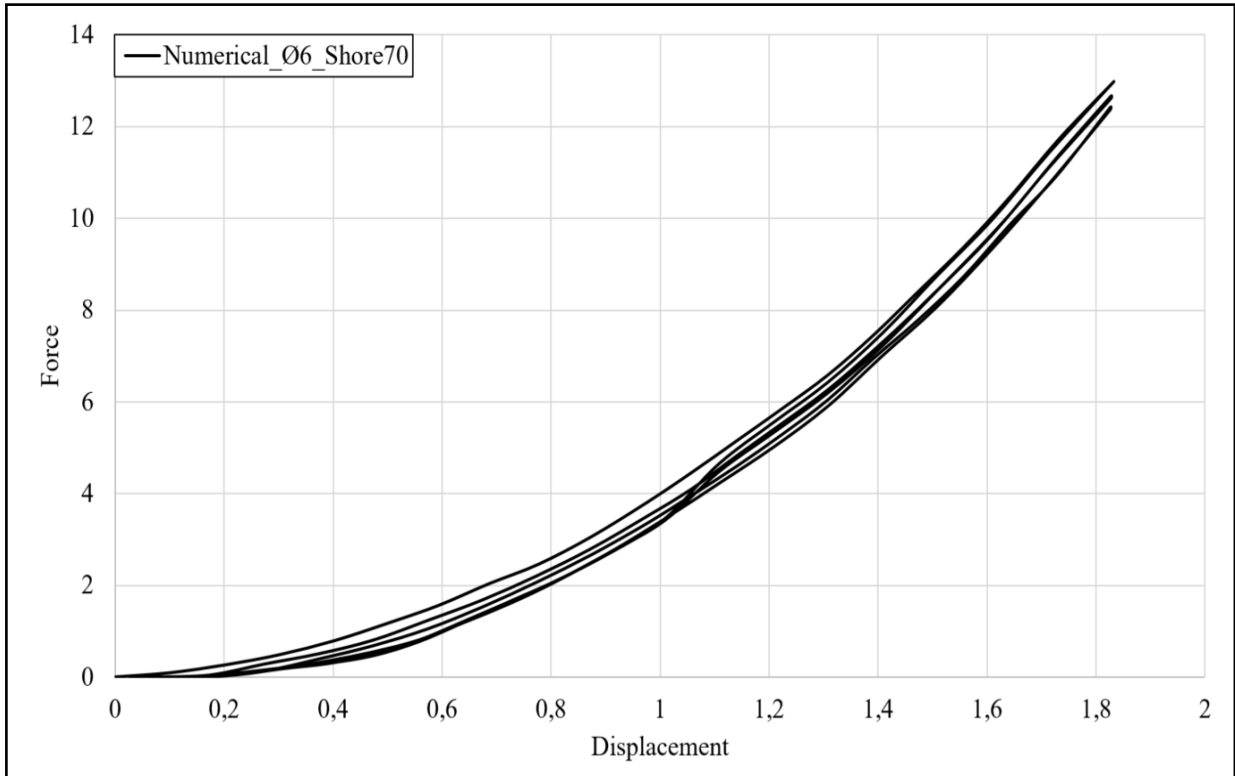


Figure I.30: Multiple steps - Hysteresis - Shore 70A -  $\mu=1.0$  - 6 mm

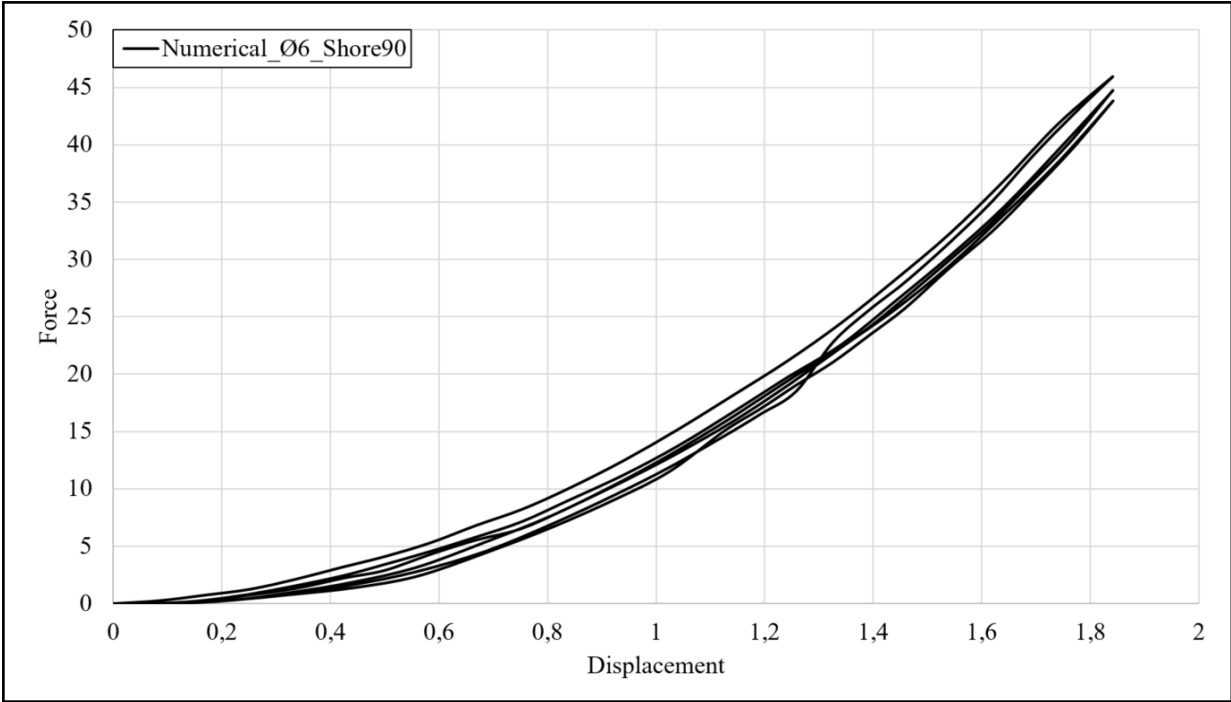


Figure I.31: Multiple steps - Hysteresis - Shore 90A -  $\mu=1.0$  - 6 mm

## Groove too wide

Analyses with multiple loading and unloading step is conducted. Two O-rings in position 1 with a groove too wide compared to the cross-sectional diameter of the sealing element is analyzed. The sequence of steps are as follows:

1. The simulation start with the required initial step
2. Load step from upper wire in negative vertical direction
3. Unload step from upper wire in positive vertical direction
4. Load step from upper wire in negative vertical direction
5. Unload step from upper wire in positive vertical direction
6. Load step from upper wire in negative vertical direction
7. Unload step from upper wire in positive vertical direction

The next simulations are conducted with side walls 0.10 offset fra the tangent of the O-rings, using a coefficient of friction,  $\mu$ , equal to 0.5. The shore 70A hardness is shown in Figure 4.24. Shore 90A is shown in Figure I.32:

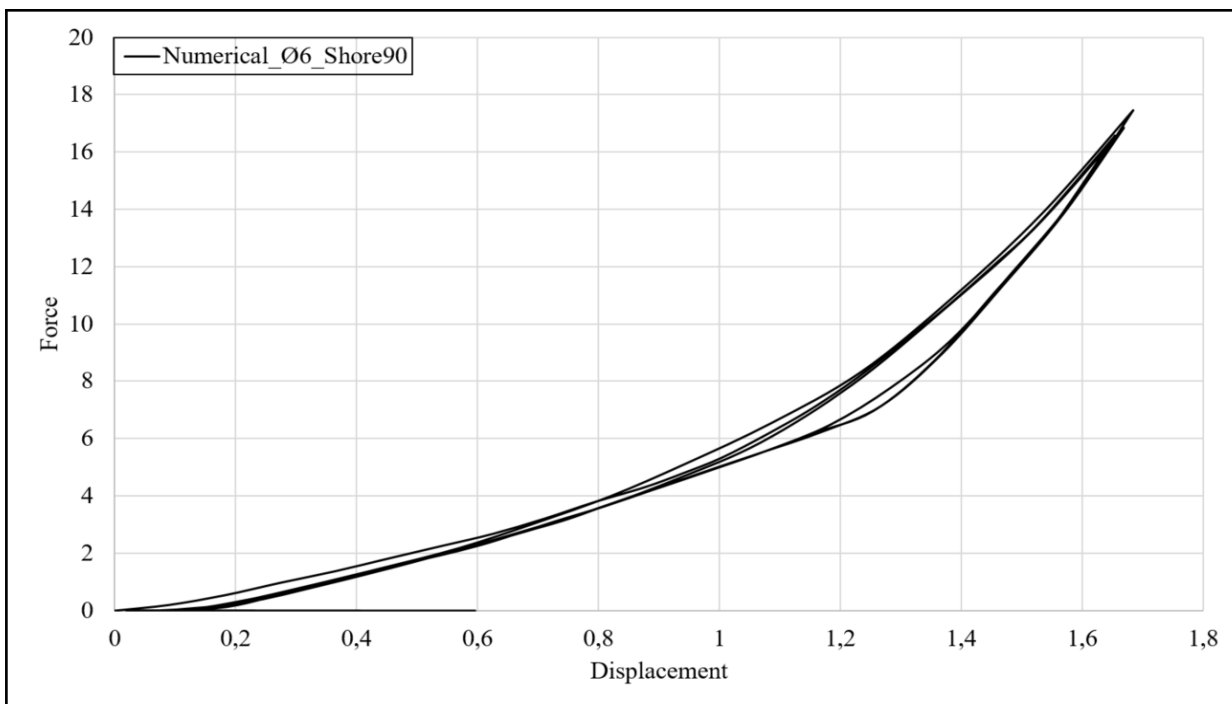


Figure I.32: Multiple steps - Hysteresis - Shore 90A -  $\mu=0.5$  - 6 mm

## Two steps hysteresis

The following curves shows the hysteresis behaviour for one O-ring when only three steps are conducted:

1. The simulation start with the required initial step
2. Load step from upper wire in negative vertical direction
3. Unload step from upper wire in positive vertical direction

Figure I.33 illustrates a single O-ring in Shore 70A material hardness with cross-sectional diameter of 6 mm, and tangential side walls which undergoes one load cycle. The friction coefficient between mating surfaces is assumed to be 0.5.

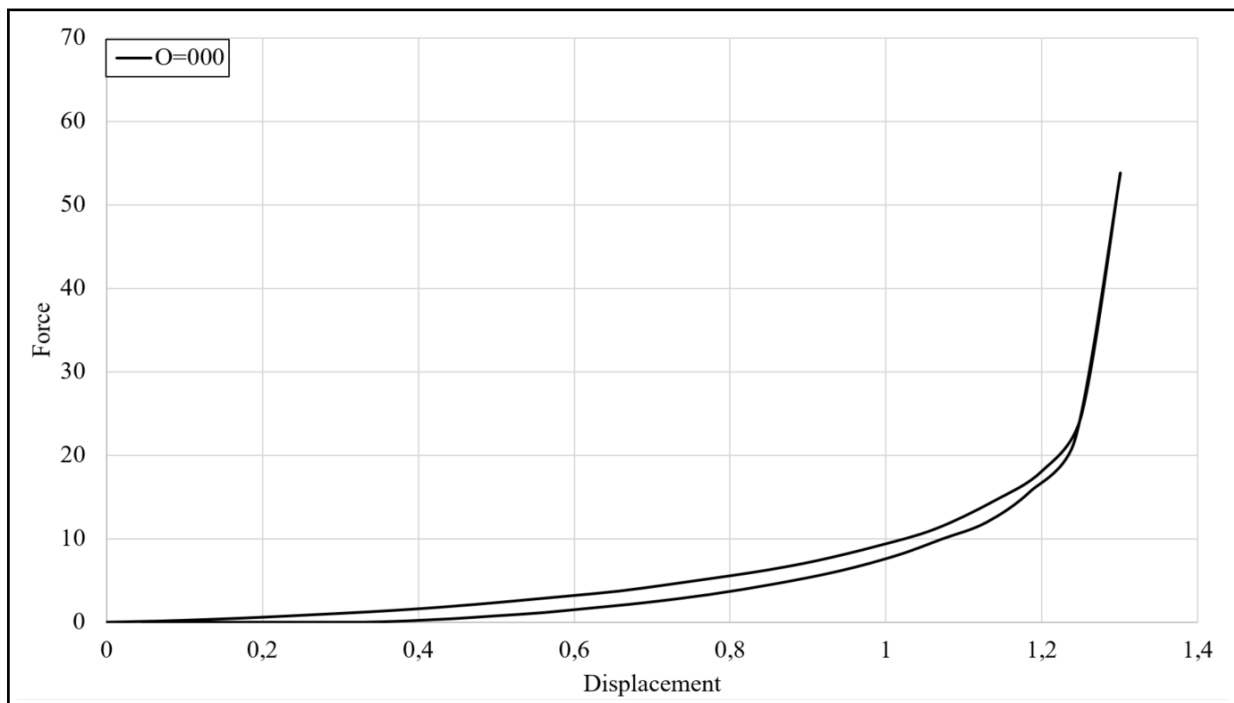


Figure I.33: Hysteresis - 6 mm -  $\mu=0.5$  - One ring

Figure I.34 illustrates a single O-ring in Shore 70 A material hardness with cross-sectional diameter of 6 mm, and tangential side walls which undergoes one load cycle. The friction coefficient between mating surfaces is assumed to be 1.0.

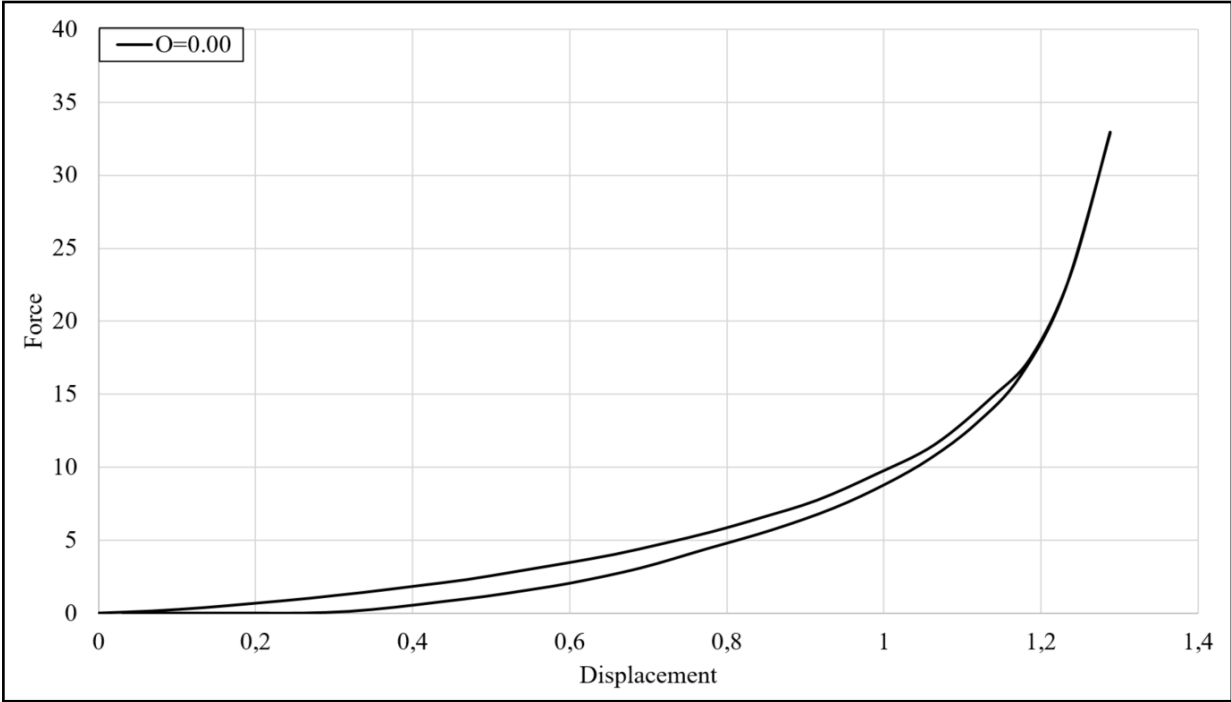


Figure I.34: Hysteresis - 6 mm -  $\mu=1.0$  - One ring

## Two O-rings compression

Figure I.35 shows the results of two O-rings in Shore 70A material hardness with cross-sectional diameter 6 mm with offset 0.00 mm and -0.10 mm in position 1 compared:

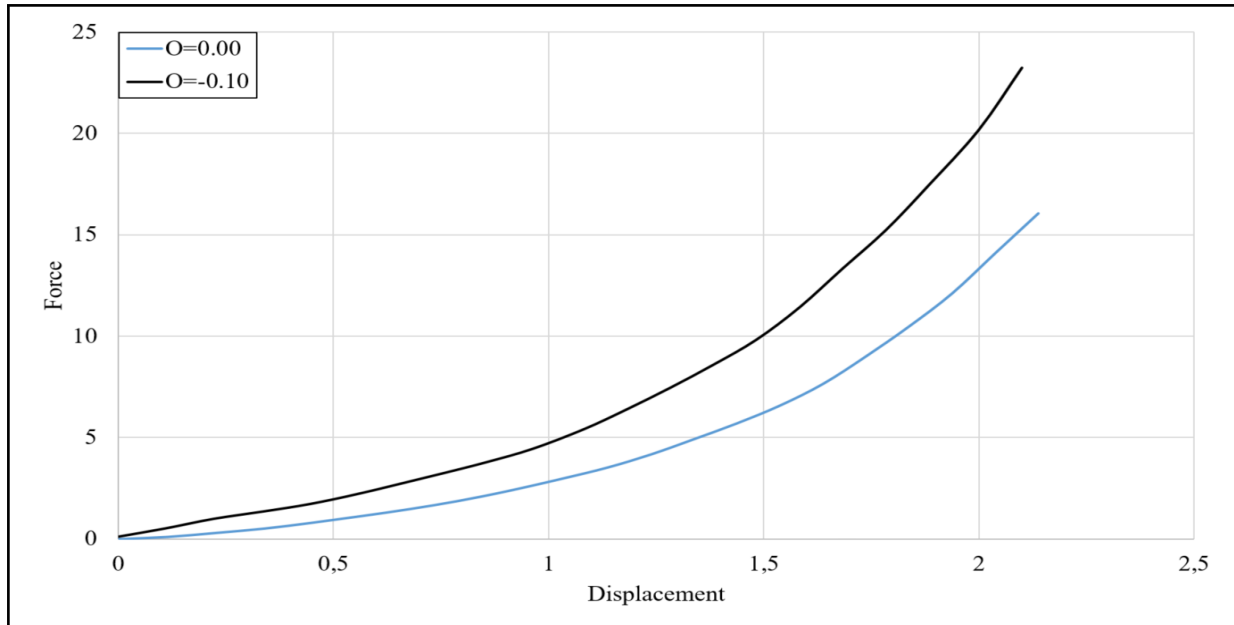


Figure I.35: 6 mm -  $\mu=0.5$  - Shore 70A - Position 1

Figure I.36 shows the results of two O-rings in Shore 70A material hardness with cross section diameter 5 mm with offset 0.00 mm and -0.10 mm in position 1 compared:

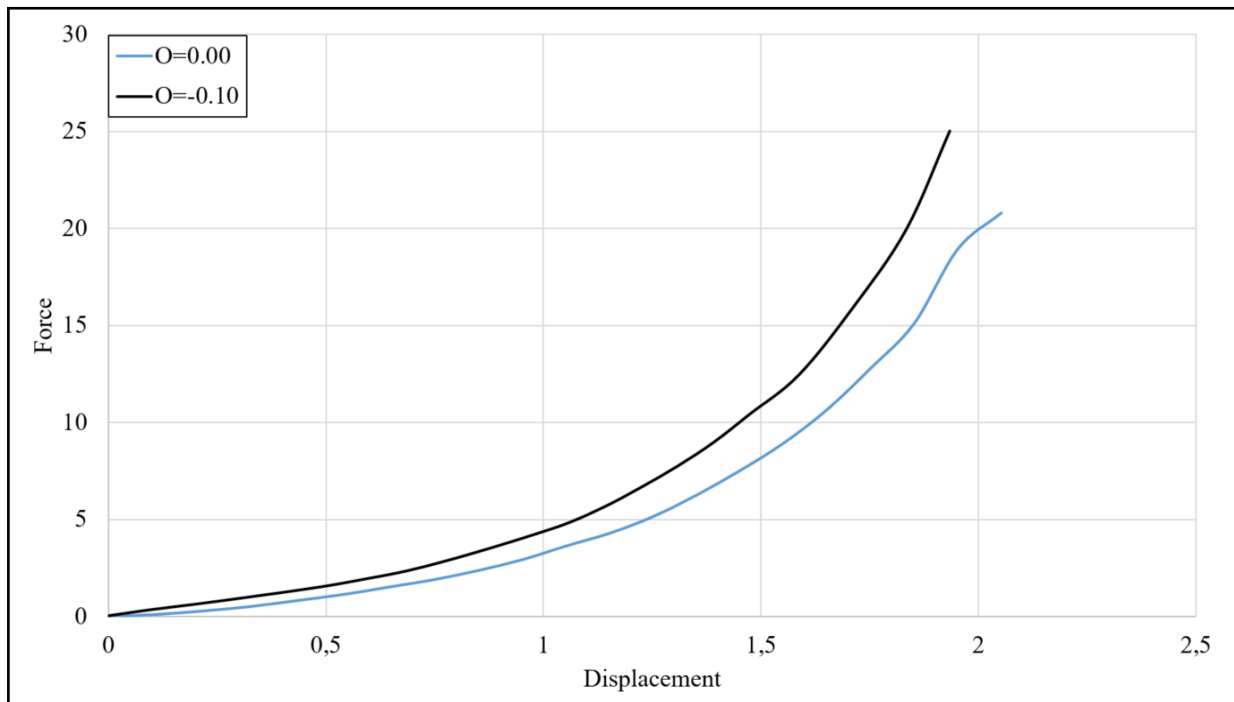


Figure I.36: 5 mm -  $\mu=0.5$  - Shore 70A - Position 1

Figure I.37 shows the results of two O-rings in Shore 70A material hardness with cross section diameter 6 mm with offset 0.00 mm and -0.10 mm in position 2 compared:

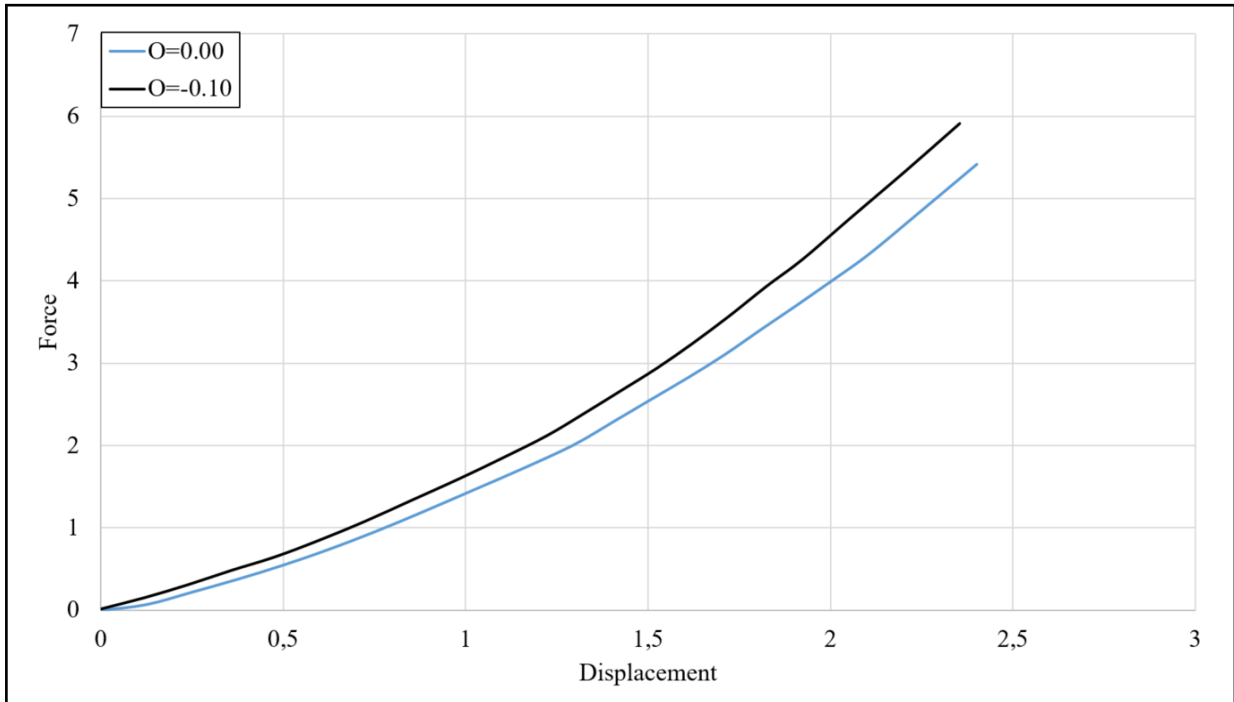


Figure I.37: 6 mm -  $\mu=0.5$  - Shore 70A - Position 2

Figure I.38 shows the results of two O-rings in Shore 70A material hardness with cross section diameter 5 mm with offset 0.00 mm and -0.10 mm in position 2 compared:

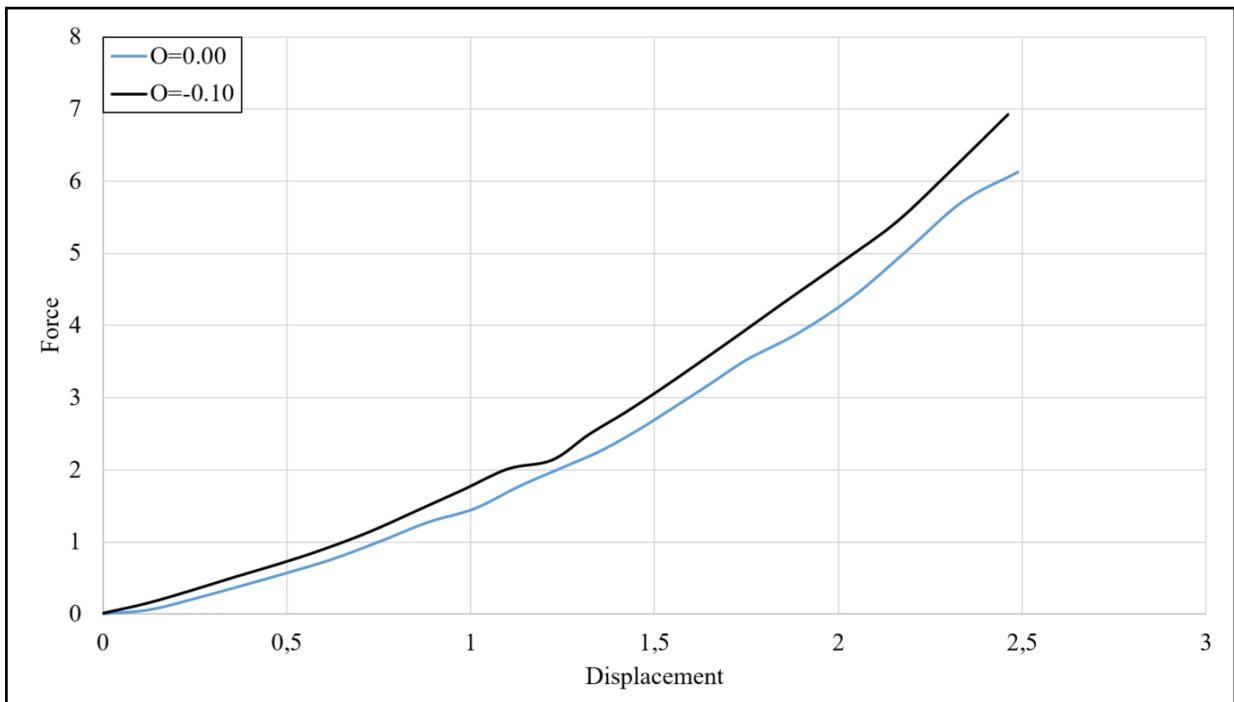


Figure I.38: 5 mm -  $\mu=0.5$  - Shore 70A - Position 2

Figure I.39 shows the results of two O-rings in Shore 70A material hardness with cross section diameter 6 mm with offset 0.00 mm and -0.10 mm in position 3 compared:

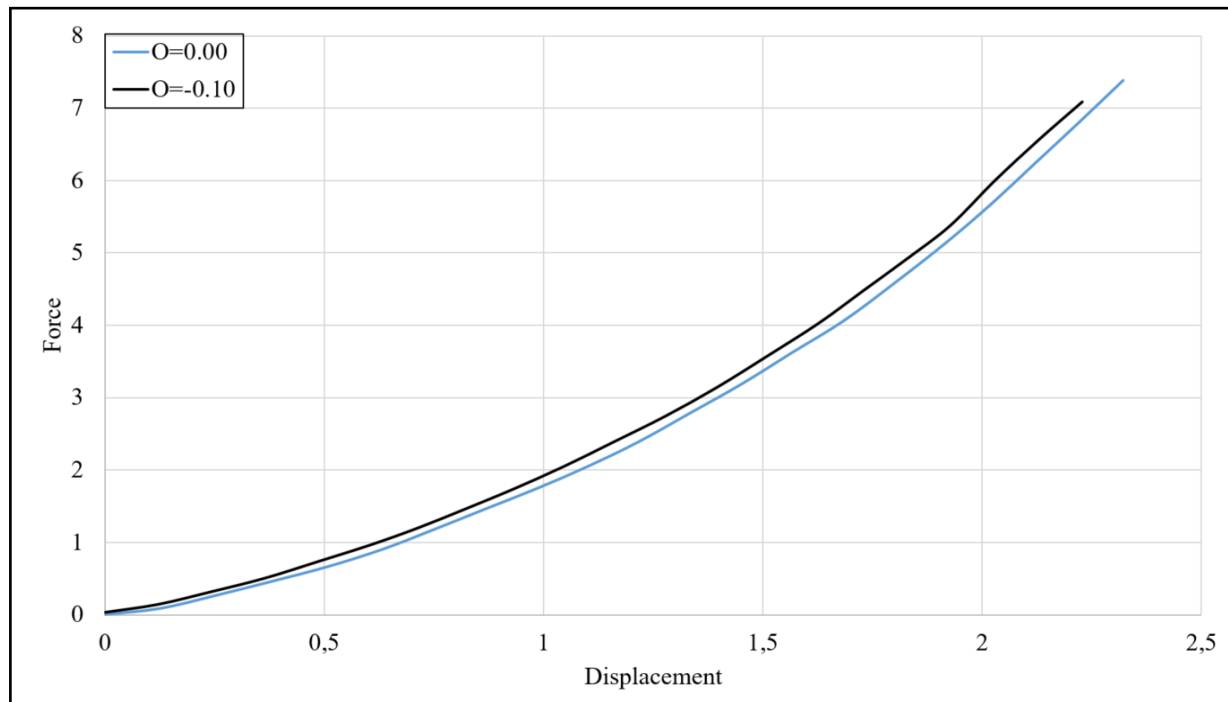


Figure I.39: 6 -  $\mu=0.5$  - Shore 70A - Position 3

Figure I.40 shows the results of two O-rings in Shore 70A material hardness with cross section diameter 5 mm with offset 0.00 mm and -0.10 mm in position 3 compared:

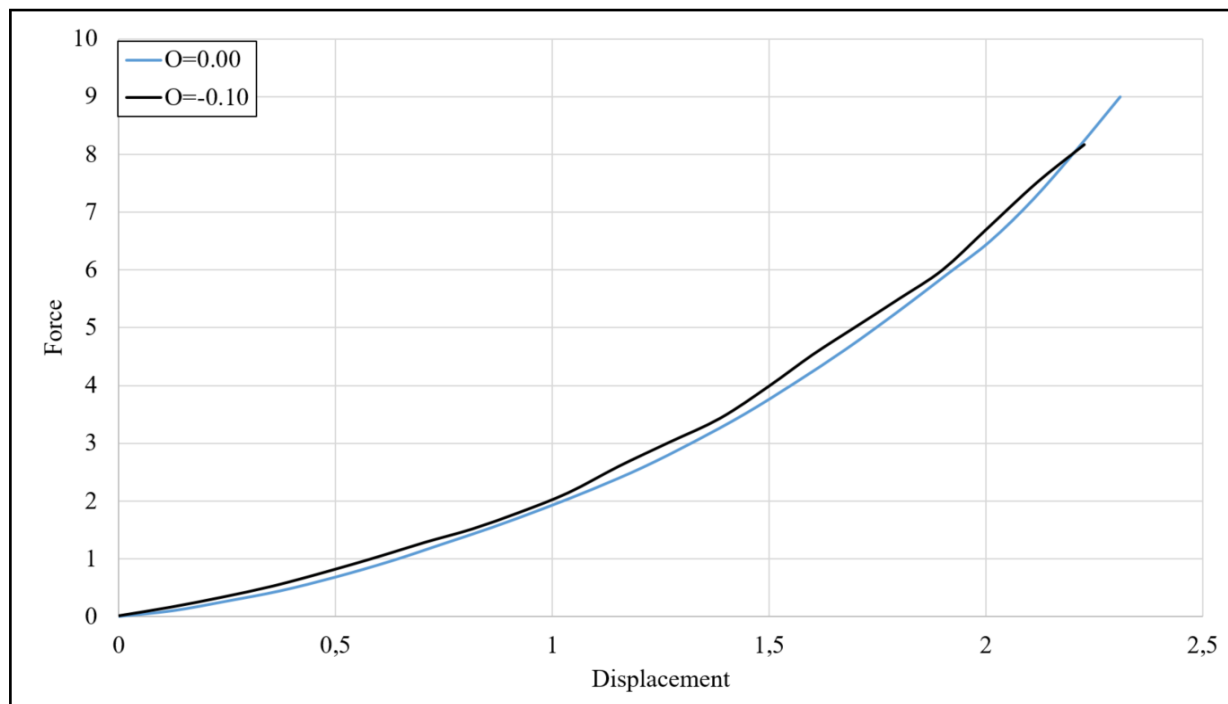


Figure I.40: 5 mm -  $\mu=0.5$  - Shore 70A - Position 3



# Appendix J

## Plane stress results

## Experimental tests compared to numerical tests

Figure J.1 shows the results of one O-ring in Shore 70A hardness with cross-sectional diameter 6 mm compared to experimental tests. The Young's modulus is varying as an attempt to fit the curves:

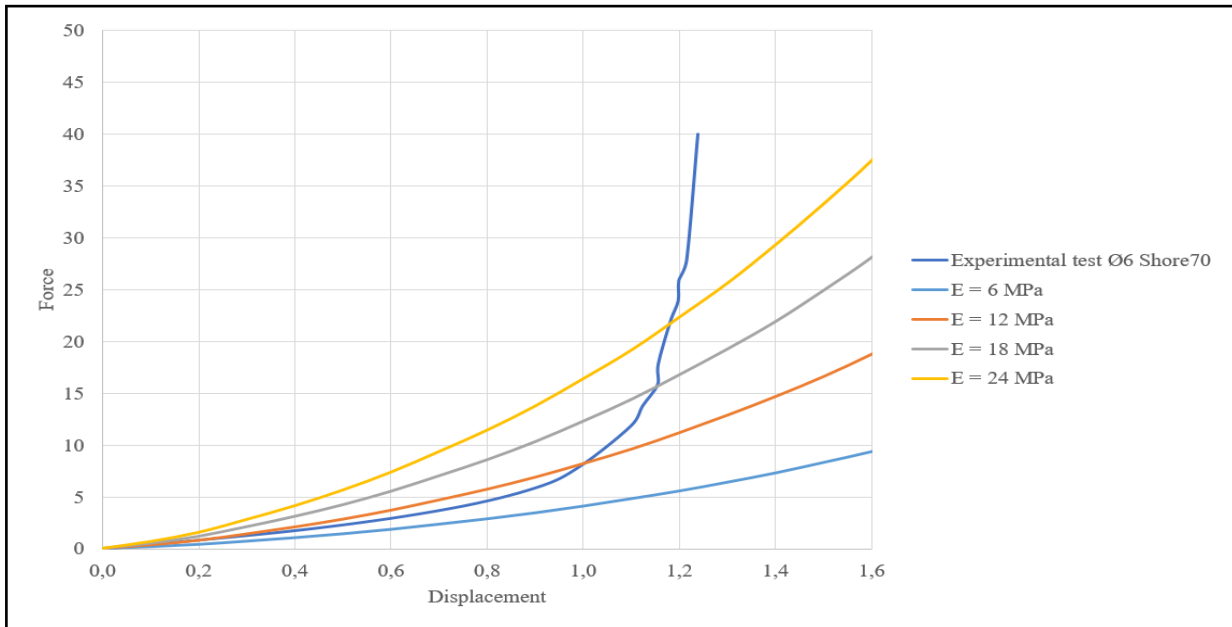


Figure J.1: 6 mm -  $\mu=1$  - Shore 70A

Figure J.2 shows the results of one O-ring in Shore 70A hardness with cross sectional diameter 5 mm compared to experimental tests. The Young's modulus for the numerical test is 6 MPa:

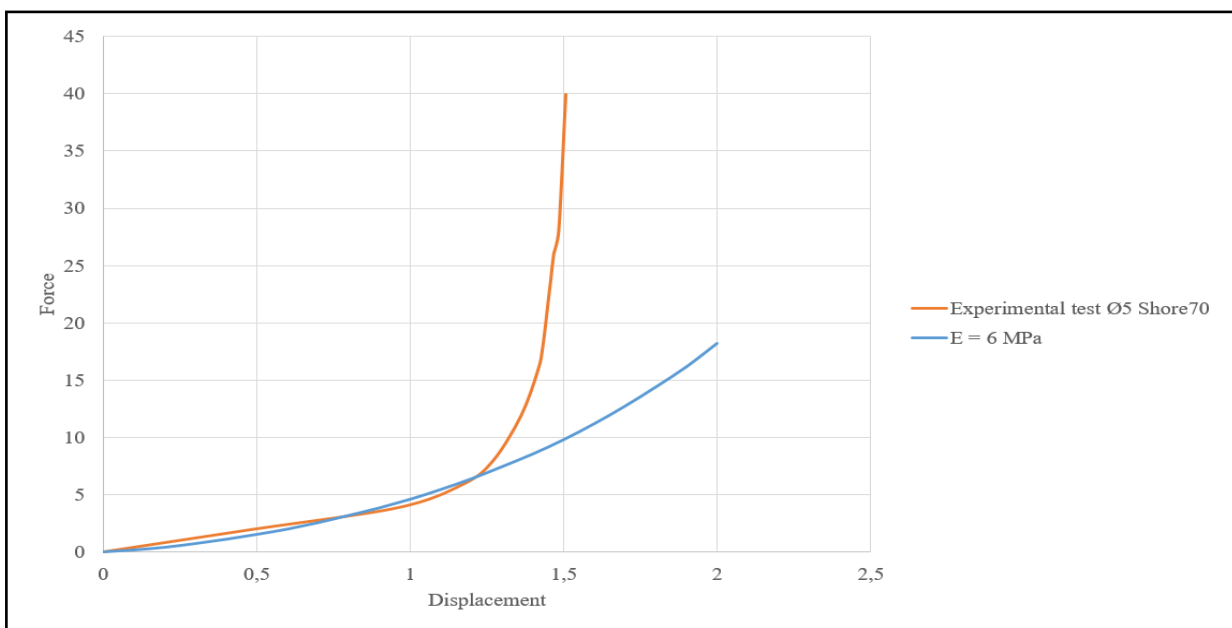


Figure J.2: 5 mm -  $\mu=1$  - Shore 70A

Figure J.3 shows the results of one O-ring in Shore 90A hardness with cross sectional diameter 6 mm compared to experimental tests. The Young's modulus is varying as an attempt to fit the curves:

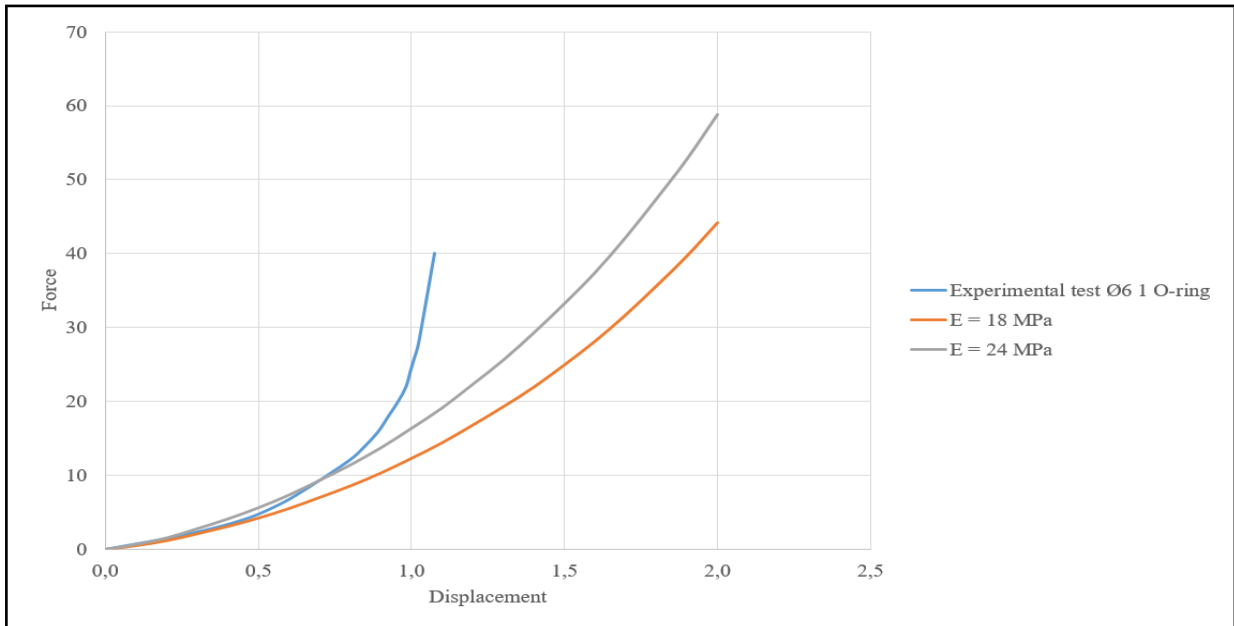


Figure J.3: 6 mm -  $\mu$  - Shore 90A

Figure J.4 shows the results of two O-rings in Shore 70A hardness with cross sectional diameter 6 mm compared to experimental tests. The Young's modulus is varying as an attempt to fit the curves:

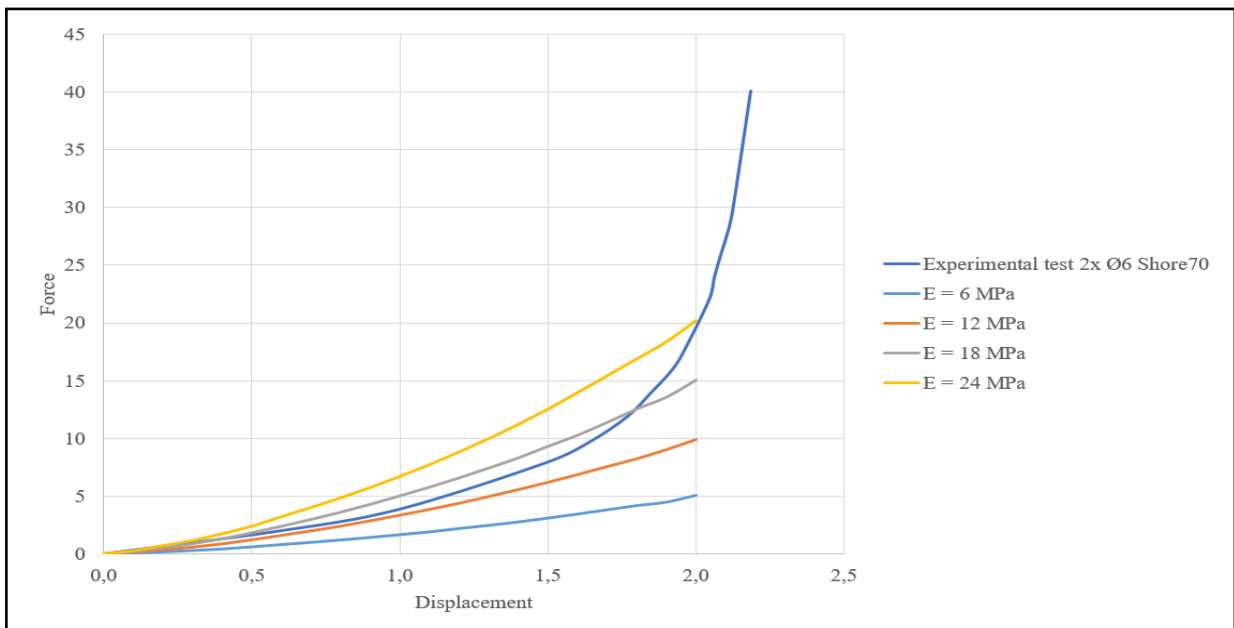


Figure J.4: 2x 6 mm -  $\mu$  - Shore 70A

Figure J.5 shows the results of two O-rings in Shore 90A hardness with cross

sectional diameter 6 mm compared to experimental tests. The Young's modulus is varying as an attempt to fit the curves:

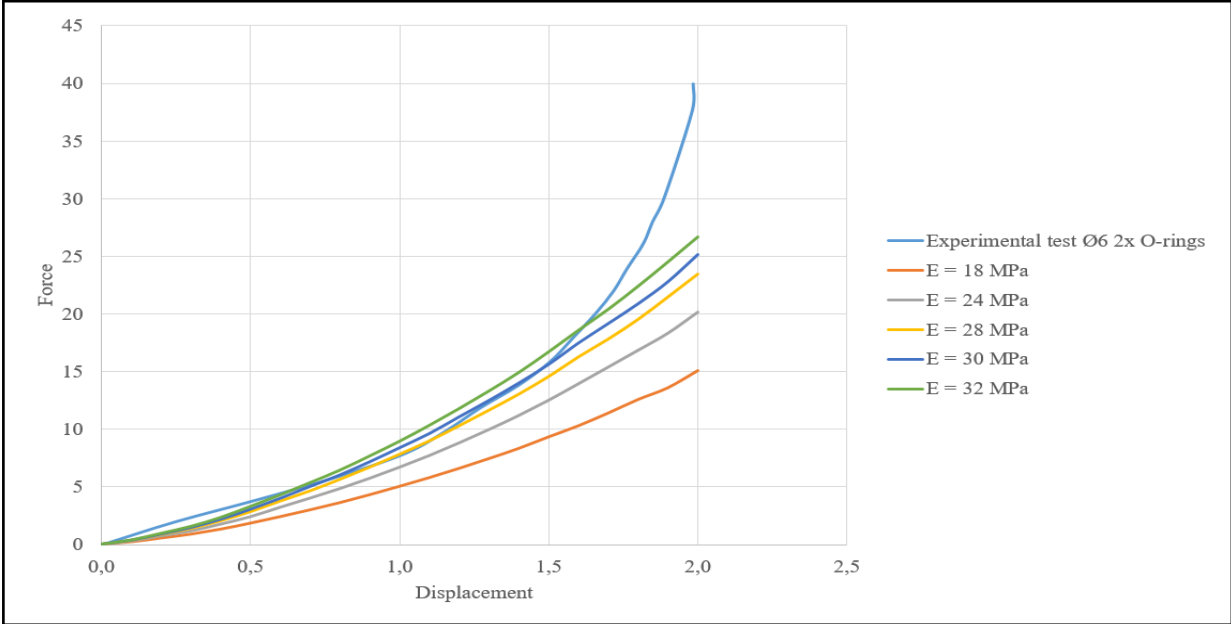


Figure J.5: 2x 6 mm -  $\mu=1$  - Shore 90A

# Appendix K

## Model development

This section presents the model development throughout the process starting with Figure K.1 which illustrates the first model:

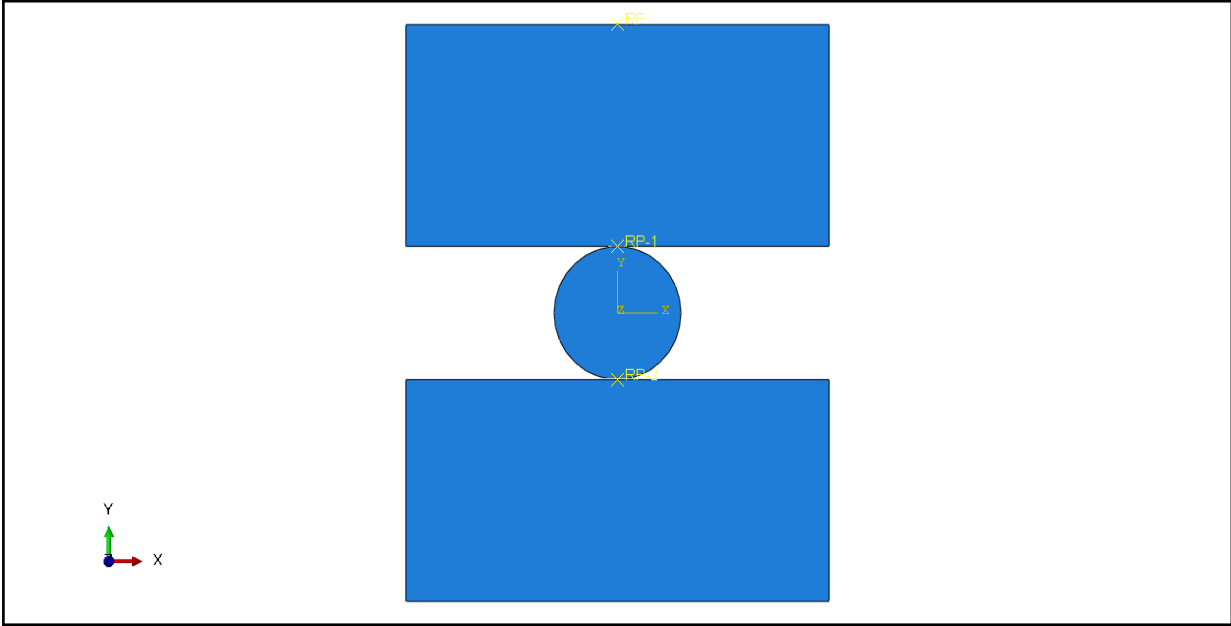


Figure K.1: The first model

Figure K.2 shows the second model:

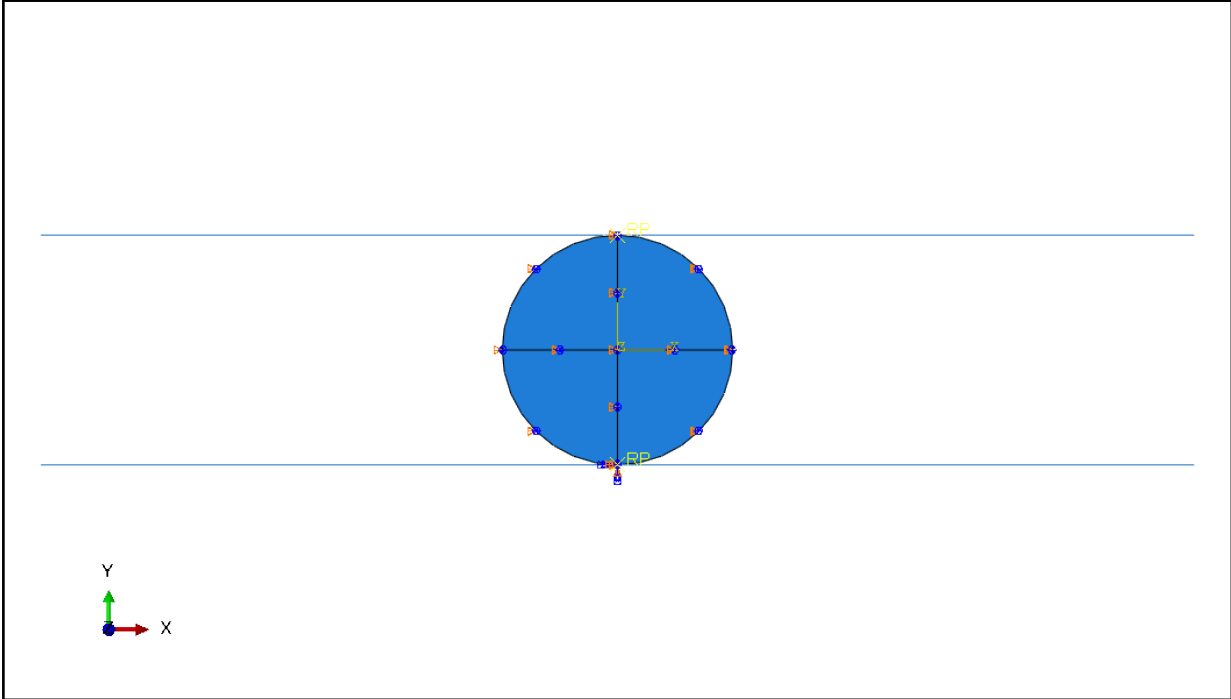


Figure K.2: The second model

Figure K.3 shows the third model.

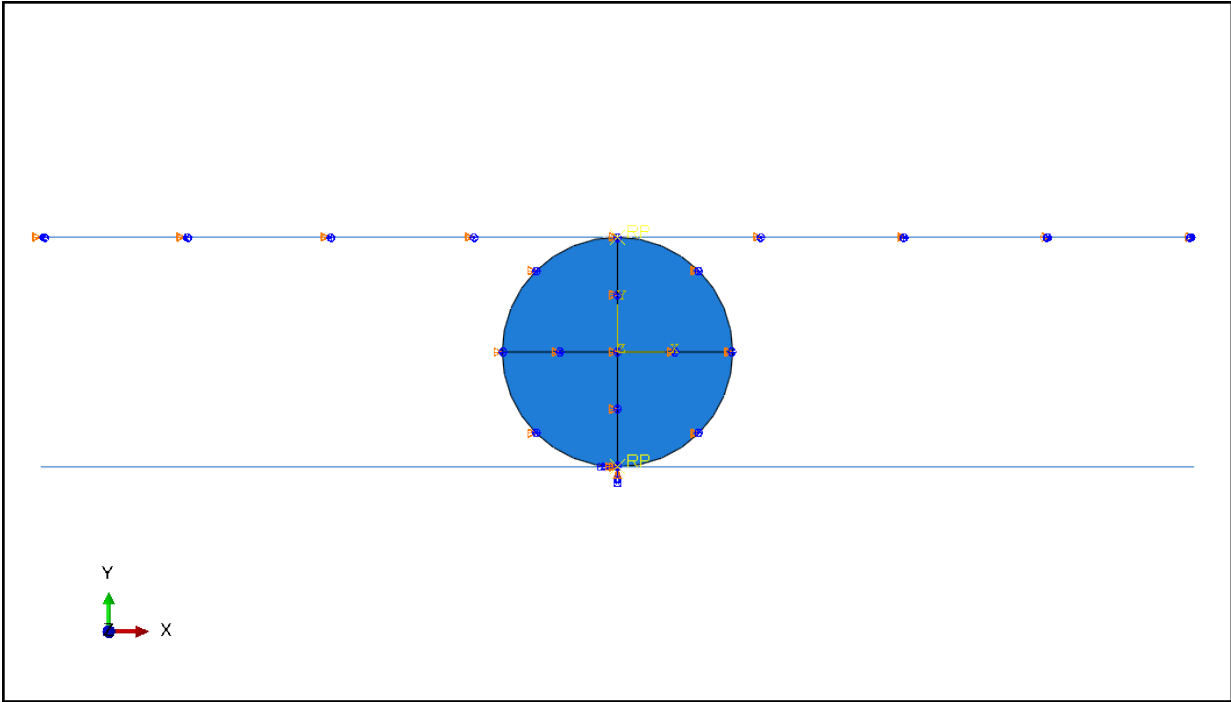


Figure K.3: The third model

Figure K.4 shows the fourth model:

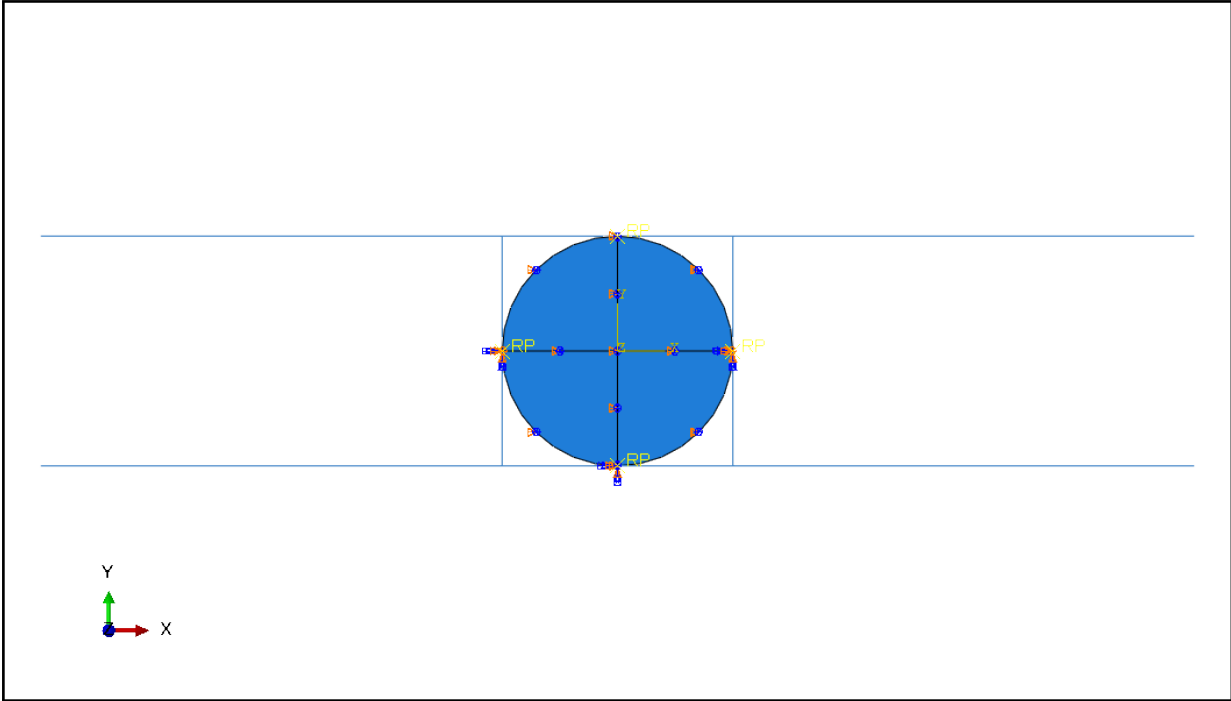


Figure K.4: The fourth model

Figure K.5 shows the fifth model.

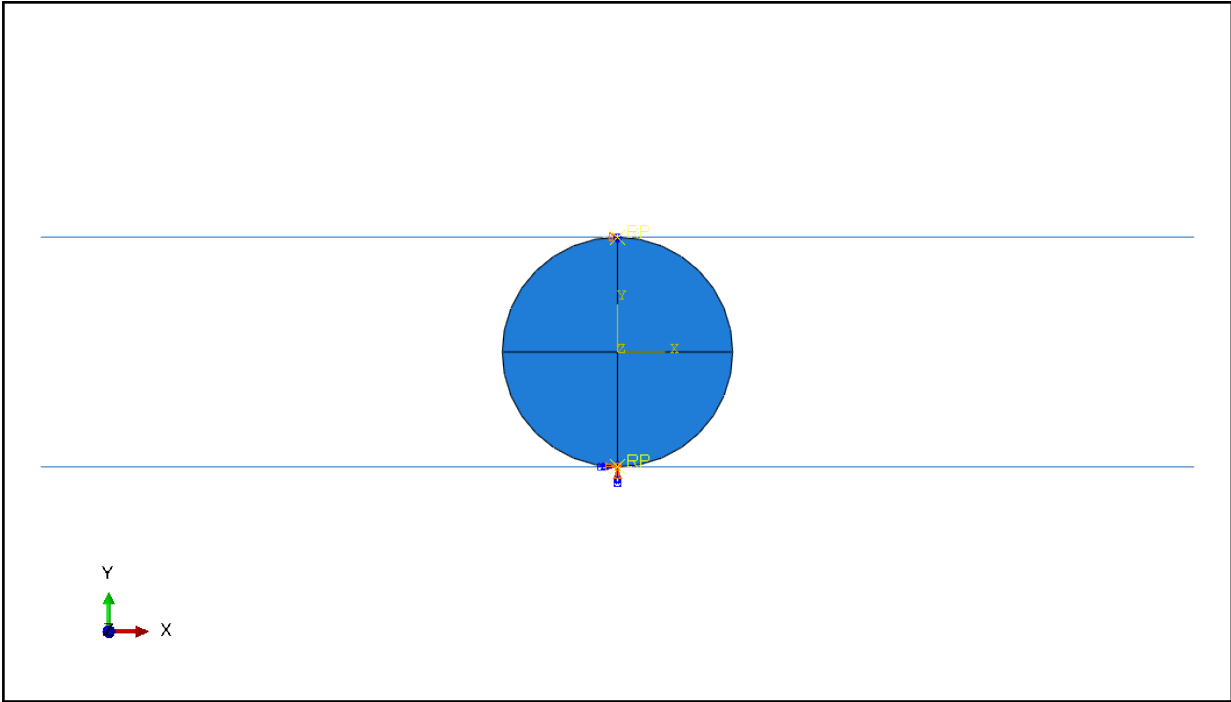


Figure K.5: The fifth model

Figure K.6 shows one the final model, which is the one used for analyses:

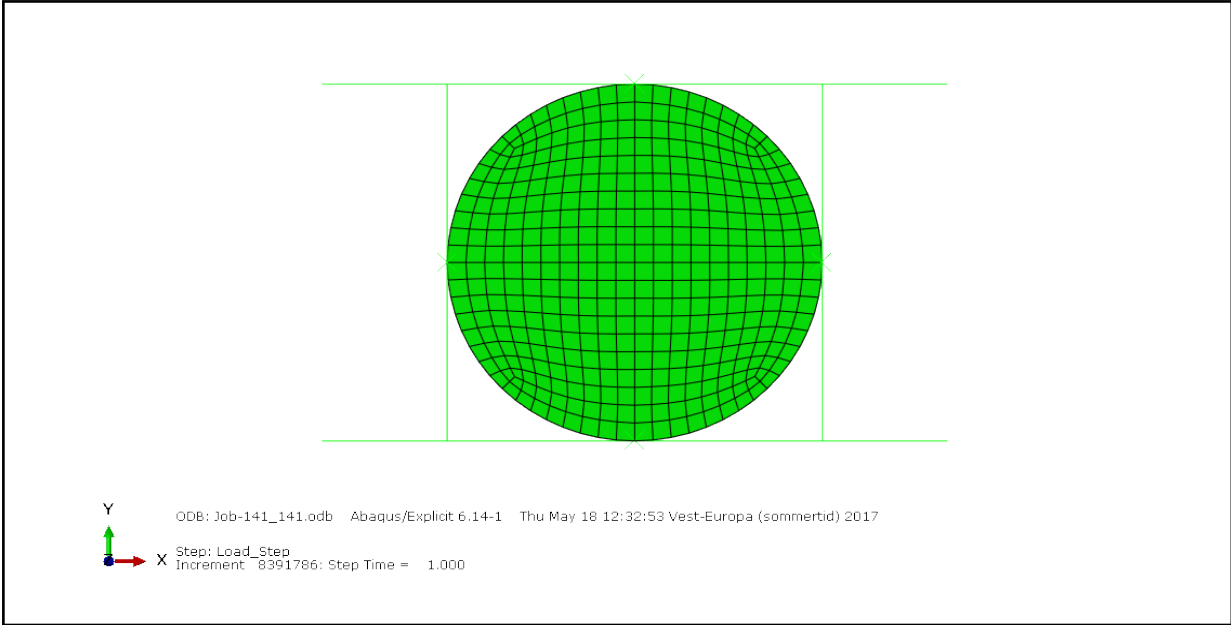


Figure K.6: Final model



# Appendix L

## Risk analysis



**Enhet: Institutt for Maskinteknikk og produksjon**      **Dato: 02.02.2017**

**Linjeleder: Torgeir Welo**


**Deltakere ved kartleggingen (m/ funksjon): Hans Kristian Hofsrud - Student**  
*(Ansv. veileder, student, evt. medveiledere, evt. andre m. kompetanse)*

**Kort beskrivelse av hovedaktivitet/hovedprosess: Masteroppgave student Hans Kristian Hofsrud: Load Deflection Characteristics of Guide Vane End Seals of Francis Turbines**

**Er oppgaven rent teoretisk? (JA/NEI): JA**      «JA» betyr at veileder innestår for at oppgaven ikke inneholder noen aktiviteter som krever risikovurdering. Dersom «JA»: Beskriv kort aktivitetene i kartleggingskjemaet under. Risikovurdering trenger ikke å fylles ut.

**Signaturer: Ansvarlig veileder: Bjørn Haugen**      *Bjørn Haugen*      **Student: Hans Kristian Hofsrud**      *Hans Kristian Hofsrud*

ID nr	Aktivitet fra kartleggings-skjemaet	Mulig uønsket hendel	Vurdering av sannsynlighet (1-5)	Vurdering av konsekvens:				Risiko-Verdi (menneske)	Kommentarer/status Forslag til tiltak
				Menneske (A-E)	Ytre miljø (A-E)	Øk/ materiell (A-E)	Om-dømme (A-E)		
1	Undersøkelse: Regler, krav og ønsker	- Ryggproblemer - Senebetennelse - Søvnproblemer - Underskudd på viktige vitaminer	3	A	A	A	A	A3	- God kontorstol - Regelmessige pauser - Spise godt - Trene regelmessig - God kroppsholdning
2	Utarbeidet prosjektrapport	- Ryggproblemer - Senebetennelse - Søvnproblemer - Underskudd på viktige vitaminer	3	A	A	A	A	A3	- God kontorstol - Regelmessige pauser - Spise godt - Trene regelmessig - God kroppsholdning
3	Kontorarbeid med litteraturstudie, analyser i Abaqus og eventuelle utregninger	- Ryggproblemer - Senebetennelse - Søvnproblemer - Underskudd på viktige vitaminer	3	A	A	A	A	A3	- God kontorstol - Regelmessige pauser - Spise godt - Trene regelmessig - God kroppsholdning

NTNU	Risikovurdering		Utarbeidet av	Nummer	Dato
			HMS-avd.	HMSRV2601	22.03.2011
HMS			Godkjent av		Erstatter
			Rektor		01.12.2006

### Sannsynlighet vurderes etter følgende kriterier:

Svært liten 1	Liten 2	Middels 3	Stor 4	Svært stor 5
1 gang pr 50 år eller sjeldnere	1 gang pr 10 år eller sjeldnere	1 gang pr år eller sjeldnere	1 gang pr måned eller sjeldnere	Skjer ukentlig

### Konsekvens vurderes etter følgende kriterier:

Gradering	Menneske	Ytre miljø Vann, jord og luft	Øk/materiell	Omdømme
E Svært Alvorlig	Død	Svært langvarig og ikke reversibel skade	Drifts- eller aktivitetsstans > 1 år.	Troverdighet og respekt betydelig og varig svekket
D Alvorlig	Alvorlig personskaade. Mulig uførhet.	Langvarig skade. Lang restitusjonstid	Driftsstans > ½ år Aktivitetsstans i opp til 1 år	Troverdighet og respekt betydelig svekket
C Moderat	Alvorlig personskaade.	Mindre skade og lang restitusjonstid	Drifts- eller aktivitetsstans < 1 mnd	Troverdighet og respekt svekket
B Liten	Skade som krever medisinsk behandling	Mindre skade og kort restitusjonstid	Drifts- eller aktivitetsstans < 1 uke	Negativ påvirkning på troverdighet og respekt
A Svært liten	Skade som krever førstehjelp	Ubetydelig skade og kort restitusjonstid	Drifts- eller aktivitetsstans < 1 dag	Liten påvirkning på troverdighet og respekt

### Risikoverdi = Sannsynlighet x Konsekvens

Beregn risikoverdi for Menneske. Enheten vurderer selv om de i tillegg vil beregne risikoverdi for Ytre miljø, Økonomi/materiell og Omdømme. I så fall beregnes disse hver for seg.

### Til kolonnen "Kommentarer/status, forslag til forebyggende og korrigerende tiltak":

Tiltak kan påvirke både sannsynlighet og konsekvens. Prioriter tiltak som kan forhindre at hendelsen inntreffer, dvs. sannsynlighetsreducerende tiltak foran skjerpet beredskap, dvs. konsekvensreducerende tiltak.



